A global perspective of the secondary organic aerosol lifecycle in the present-day and future

Jamie Michael Kelly

Doctor of Philosophy

School of GeoSciences

August 2018

Declaration

I declare that this thesis has been composed solely by myself and that it has not been submitted, either in whole or in part, in any previous application for a degree. Except where otherwise stated, the work presented is entirely my own.

Jamie Michael Kelly
August 2018

Abstract

Secondary organic aerosol (SOA) is a major component of aerosol. Aerosol affect the radiation budget of the Earth and are detrimental to human health. Robust assessments of the impact of SOA on air quality and climatic are hindered by uncertainties in the SOA lifecycle.

There are approximately 37 million unique organic compounds in the atmosphere. With such a large number of potential sources of SOA, representing the SOA lifecycle in a global model is challenging. SOA schemes within models vary in several ways, including: the emissions source types considered, and how volatile organic compound (VOC) physicochemical processing is treated. As a result, estimates of the global SOA production rate from models and observations range several orders of magnitude. Furthermore, simulated SOA concentrations from global models are typically lower than observed. The objectives of this study are to (i) quantify the impact of biogenic, anthropogenic and biomass burning VOC emissions on the global SOA budget and model agreement with observations, (ii) explore the sensitivity of the global SOA budget and model agreement with observations to variations in the physicochemical processing of VOCs, and (iii) examine how future changes in climate and emissions influence the SOA lifecycle. Throughout this study, a global chemistry-climate model (UKCA) is used, developed, and tested against a suite of surface and aircraft observations

Firstly, the impact of biogenic, anthropogenic and biomass burning VOC emissions on the global SOA budget and model agreement with observation is quantified. This is achieved by introducing new VOC emission source types, whilst maintaining a fixed VOC oxidation mechanism. As

source of SOA, monoterpene ($C_{10}H_{16}$) has been studied under laboratory conditions extensively. This VOC is commonly included in SOA schemes and, in many cases, is the only source of SOA. In this study, when monoterpene is the only source of SOA, the simulated global SOA production rate is 20 Tg (SOA) a^{-1} and the normalised mean bias (NMB) with respect to observed SOA is -91 %. In response to the addition of new emission source types, isoprene (C_5H_8), a lumped anthropogenic VOC (VOC_{ANT}) and a lumped biomass burning VOC (VOC_{BB}), to the SOA scheme the global SOA production rate increases by 275 % (to 75 Tg (SOA) a^{-1}), and model agreement with observations improves (NMB = -51 %). The improvement in agreement between simulated and observed SOA is primarily due to the inclusion of VOC_{ANT}, as opposed to isoprene or VOCBB. These results demonstrate that, under a single-step oxidation scheme, with a fixed yield of SOA, biogenic, anthropogenic, and biomass burning VOC emissions account for around half of the observed SOA abundance.

With the new SOA scheme which considers all major VOC sources of SOA, the next objective is to explore the sensitivity of the SOA budget and model agreement with observations to variations in the physicochemical processing of VOCs. This is achieved by performing simulations with varying VOC deposition and oxidation mechanisms, whilst maintaining fixed VOC emissions. In light of recent field and explicit modelling studies, the sensitivity of SOA to VOC deposition is quantified. By including both dry and wet deposition of all VOC precursors of SOA, the global SOA production rate from all VOC sources reduces by 37 % (to 47 Tg (SOA) a^{-1}) and model agreement with observations worsens (NMB = -66 %). Hence, neglecting VOC deposition can have significant impacts on SOA formation.

According to chamber and field studies, VOCs form SOA after several generations of oxidation, and with yields which are sensitive to nitrogen oxide (NO_X) concentrations. Therefore, for the anthropogenic and biomass burning VOC precursors of SOA ($VOC_{ANT/BB}$), model simulations are performed

varying (a) the parent VOC reactivity, (b) the number of reaction intermediates, and (c) accounting for the influence of NO_X on SOA yields. Both variations in parent VOC reactivity and accounting for the NO_X-sensitive SOA yields have a substantial impact on simulated SOA, whereas SOA is mostly unaffected by the introduction of the reaction intermediate. In response to these variations in oxidation, the global SOA production rate from $VOC_{ANT/BB}$ ranges from 18 Tg (SOA) a^{-1} to 45 Tg (SOA) a^{-1} (+150 %) and the NMB with respect to observed SOA ranges from -46 to -71 %. SOA is extremely sensitive to variations in parent VOC reactivity and accounting for the NO_X-sensitive SOA yields, but is unaffected by the introduction of the reaction intermediate. These simulations highlight how the use of simplified VOC oxidation mechanisms within SOA schemes can have profound impacts on the global SOA budget and model agreement with observations.

Finally, the impact of future changes in climate and emissions on the SOA lifecycle is quantified. This is achieved by driving the UKCA model with the Intergovernmental Panel on Climate Change (IPCC) Representative Concentration Pathway (RCP) 8.5 for the 2090s and the present-day (2000s). Compared to the present-day, climate change alone results in a 23 % increase in the global SOA burden due to increases in both SOA production (10 %) and the SOA lifetime (12 %). This climate-induced increase in SOA production is driven by an 82 % increase in monoterpene emissions due to the warming associated with RCP8.5 (4.6 °C). Global isoprene emissions reduce by 1 % under future climate change due to the opposing effects of warming and rising carbon dioxide concentrations which suppress isoprene synthesis ('CO_2 inhibition'). Projected changes in anthropogenic and biomass burning emissions alone result in a 3 % decrease in the global SOA load compared to the present-day due to a reduction in the SOA production rate (-6 %) and an increase in the SOA lifetime (4 %). This emissions-driven reduction in global SOA production is driven by a projected 11 % decrease in anthropogenic and biomass burning

VOCs. When future changes in climate and emissions are combined, the global SOA burden increases by 20 % in the future compared to the present-day, which is due to increases in SOA production (4 %) and a lengthening of the SOA lifetime (15 %). Therefore, these results imply a growth in the global SOA burden due to rising biogenic VOC emissions and a lengthening of the SOA lifetime, despite reductions in anthropogenic and biomass burning emissions.

This thesis contributes to the understanding of the SOA lifecycle in the present-day and the future. In relation to uncertainty in SOA and the impacts of SOA on air quality and climate, greater observational constraints on VOC emissions, deposition and oxidation mechanisms are required. Furthermore, these results imply a growing importance of natural sources of SOA in the future.

Lay Abstract

The Earth's atmosphere mostly consists of gases, such as nitrogen and oxygen. In addition to these gases, there are liquid and solid particles, referred to as aerosol. Aerosol are extremely small, with diameters less than that of human hair. The amount of aerosol in the atmosphere is very low in comparison to oxygen and nitrogen, yet their existence have profound impacts on many aspects of the Earth system. For example, aerosol can affect radiation which, in-turn, affects climate. Also, these particles can be inhaled by humans and cause health problems.

One type of aerosol which is measured in large quantities across the Earth's surface is secondary organic aerosol (SOA). SOA is formed from gaseous organic compounds (precursors), which are released from a variety of sources, including human activity (i.e. burning of fossil fuels), biomass burning (i.e. natural forest fires and human-made fires) and plants. These emitted gaseous organic compounds undergo a range of chemical reactions, leading to the production of SOA. SOA is washed out of the atmosphere by rainfall (wet deposition), and by sedimentation onto the Earth's surface due to the effects of gravity (dry deposition). The amount of SOA in the atmosphere (burden) is controlled by a delicate balance between SOA production and SOA removal.

The objectives of this thesis are to (i) investigate how human activity, biomass burning and plants influence the production of SOA, (ii) explore how chemical reactions of precursor gases influence the production of SOA, and (iii) quantify how future changes in climate and emissions over the 21st century will affect the amount of SOA in the atmosphere. Throughout this study, a model is used. This model represents many processes, including

weather (e.g. temperature, rainfall, etc.), emissions of gaseous organic compounds, and chemical reactions.

The first objective is to investigate how precursor emissions from humans, plants and forest fires influence the production of SOA in the atmosphere. Results from this thesis indicate that every year, 75 Tg of SOA is formed in the atmosphere. Around half (53 %) of the SOA formed every year originates from plants, with human activity and biomass burning accounting for the remaining 32 and 15 %, respectively. Hence, this harmful pollutant is a stems from of both natural and non-natural sources.

The next objective is to explore how the chemical reactions of precursor gases control the amount of SOA formed. This is achieved by analysing the reaction pathways of gases, with a particular focus on the gases emitted from human activities. These results reveal how the emitted organic gases have a number of potential reaction pathways. Also, the reaction pathways are influenced by chemical conditions, such as the amount of nitrous oxide present. When the precursor is emitted from human activities, if there is lots of nitrous oxide present, the precursor gases react, but only lead to a small amount of SOA formed. By contrast, if the precursor is emitted into a region devoid of nitrous oxide, the organic gases react and lead to a large amount of SOA produced. Hence, not only is the amount of organic gases emitted into the atmosphere important, but so too is the environment. The importance of this is that industrialised and urban regions contain high nitrous oxide levels, whereas clean, remote regions contrail low nitrous oxide levels. Hence, when organic gases from human activity are released into urban and industrialised regions, the high nitrous oxides levels supress SOA formation. However, when the organic gases from human activity are released into clean, remote regions, the low levels of oxide enhance the formation of SOA.

The final objective is to determine if the amount of SOA in the atmosphere will change in the future. Results from these simulations suggest that by the year 2100s, the global-average surface air temperature will increase by 4.6 °C. This increased temperature stimulates the amount of organic gases released from plants. Hence, climate changes increases the production of SOA in the future. At the same time, the efficiency of SOA removal from the atmosphere, reduces in the future. Hence, in the future, SOA will last longer in the atmosphere. Therefore, future increases in SOA production are compounded by reductions in SOA removal, such that the amount of SOA in the atmosphere increases by 20 % in the future.

“Our crown has already been paid for. All we have to do is wear it”

- James Baldwin

Acknowledgements

Firstly, Ruth and Fiona, you gave me the opportunity to start this journey, and you patiently guided me through to the finish line. In-between, there were some tough times. Like when I spent months trying to close the SOA budget, only to find I didn't have all the diagnostics required. Or when I found out all my model simulations had used emissions that were upside down. Or when I spent months trying to implement the two-product scheme, only to find out it was near impossible. The two of you picked me after each of these challenges, and you inspired me to not give up.

My fellow friends in Crew, Pedro, Paula, Rosa, Michael, and Zhenze, thank you all for keeping me company. Someone who really helped me out, the one who I started this with, who I wouldn't have been able to finish this without, Sara. You have given me an endless supply of cake, cheese, satsumas, chocolate, someone to laugh with, someone to laugh at, and friendship. Together, we got through those endless days, evenings, and weekends of work. I will cherish our time together.

Fraser, Paul and Arron, I have you all to thank for the escape you offered me over the past four years. Running with Edinburgh Frontrunners, going to yoga and meditation classes, cycling through the Hebrides, and trips to bothys. They were the perfect escape from my PhD. Equally as therapeutic were our all-night drinking and dancing in The Street, or worse, The Planet. Yes, Saturday nights will never be the same again.

Suzy, Amber and Mariann, you've provided me a long-distance supply of drama that's kept me entertained and distracted. You also gave me some magical times in Paris, Milan, and Marrakesh (and Northampton!). Rachel,

you kept me sane with your insane humour mostly centred on nuts, lemons, Nutella and buses. My original study buddy, and long-term buddy, Eleanor, thank you for always supporting me.

Mum and Dad, not only have you supported me, but you have actively encouraged every single one of my decisions, giving me the confidence to be the person I am today. Emma, you are my sister, my spiritual guidance councillor and my friend, thank you for empowering me. And to the rest of the family, Lewis, Amy, Frankie, Ashley, Nan, Pap, Auntie Jo, Uncle Rick, Amber, Georgia and Casey - I am truly blessed to have you all surrounding me.

And finally, Johannes, I apologise for dragging you along with me on my marathon training runs all through the winter, and to library at the weekends during the summer, and to the badminton and basketball courts. You have supported me since the day we met. I only hope I can return some of this to you over the rest of our lives together.

Contents

List of Figures

List of Tables

Chapter 1 **Introduction**

The composition of the atmosphere is inter-connected to many other components of the Earth system. This section begins with the motivation of this thesis, which is the role of atmospheric composition in the Earth system (Section 1.1). Following this, gas-phase tropospheric chemistry (Section 1.2) and aerosol chemistry (Section 1.3) are discussed. Next, the interactions within and between organic compounds are described (Section 1.4) – these interactions play a crucial role in determining if SOA is formed or not. Next, SOA is introduced (Section 1.5). Following this, SOA precursor emissions (Section 1.6), SOA production (Section 1.7) and SOA properties and processing (Section 1.8) are described – these descriptions focus on SOA at the molecular level. Next, global perspectives of SOA in the present-day (Section 1.9) and future (Section 1.10) are discussed. This section then concludes with research questions of this thesis (Section 1.11).

1.1 The health and climate impacts of atmospheric composition

The World Health Organisation (WHO) undertake periodic reviews of the research on the detrimental effects of exposure to air pollution on human health and identify particulate matter (PM), ozone (O_3) and nitrogen dioxide (NO_2) to be the most important (WHO, 2013). Increases in surface O_3 and $PM_{2.5}$ (PM with an aerodynamic diameter < 2.5 μm) driven by human activities since the pre-industrial time have are estimated to lead to 0.7 (± 0.3) million annual respiratory mortalities and 3.5 (± 0.9) million annual cardiopulmonary mortalities, respectively (Anenberg et al., 2011) . Legislation

developed by the European Union establishes health based standards for a number of air pollutants, which are shown in Table 1.1. When the concentrations shown in Table 1.1 are breached, the period is referred to as an exceedance or an episode.

Table 1.1 - EU health based standards for pollutants. $PM_{2.5}$ and PM_{10} refer to particulate matter with aerodynamic diameters of less than 2.5 and 10 µm, respectively, and are discussed in more detail in Section 1.3.1. Benzene and polycyclic aromatic hydrocarbons are organic compounds, which are described in Section 1.4.

Pollutant	Averaging period	Concentration / µg m^{-3}	Permitted exceedances each year
$PM_{2.5}$	1 year	25	-
PM_{10}	1 year	40	-
Benzene	1 year	5	-
Polycyclic aromatic hydrocarbons	1 year	0.001	-
O_3	Maximum daily 8 hour running mean	120	25 days averaged over 3 years
NO_2	1 hour	200	18

Air pollution affects the ecosystem. For example, air pollution alters radiation (Mercado et al., 2009), and can be toxic towards plants (Ainsworth, 2017;Ainsworth et al., 2012). In addition, air pollution can affect visibility (Davidson et al., 2005).

Both PM and O_3 are associated with climate change as they can interact with radiation and perturb the energy balance of the Earth. Figure 1.1 displays how aerosol can interact with radiation and cloud. Aerosols can

interact with radiation, either directly by scattering or absorbing (aerosol-radiation interactions), or indirectly, by altering cloud properties (aerosol-cloud interactions), as shown schematically in Figure 1.1 (Boucher et al., 2013). The aerosol climate forcing is the difference between radiative fluxes of the present-day and preindustrial times due to anthropogenic changes. Some of the largest sources of uncertainty in aerosol climate forcing are the aerosol-cloud interactions (Stocker et al., 2013) and of the state of the preindustrial atmosphere (Carslaw et al., 2013).

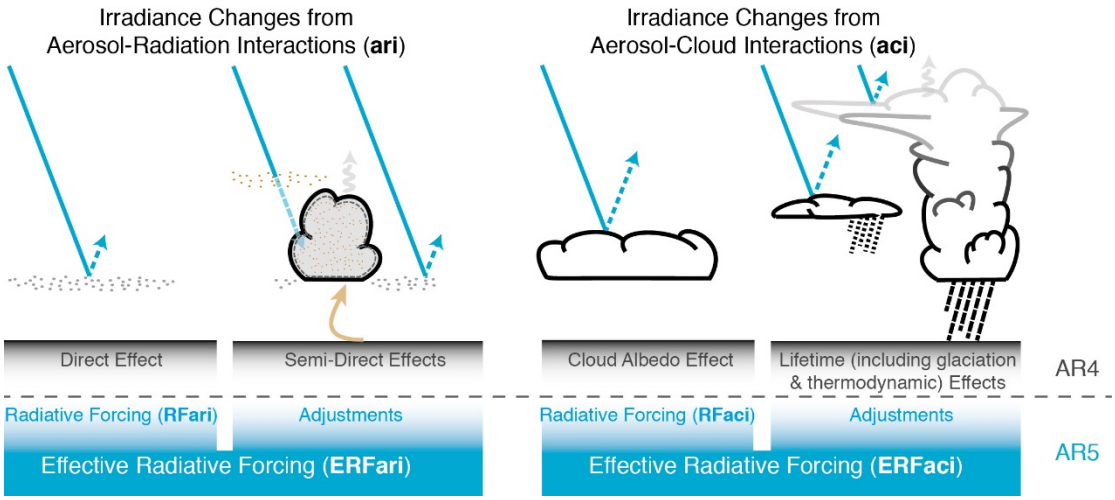

Figure 1.1 – Schematic diagram showing direct and indirect effects of aerosol on radiation, taken from (Boucher et al., 2013)

Many aerosol component have natural sources, which are sensitive to climate. Therefore, human-induced changes in climate can in-turn lead to climate feedbacks via changes in natural aerosol emissions (Kulmala et al., 2004;Carslaw et al., 2010). These feedbacks contribute to uncertainties in the projections of the climate, via variations in climate sensitivity. Overall, the composition of the atmosphere is highly coupled to several components of the Earth system. Understanding these interactions can help reduce the

detrimental impacts of air pollution on human health, and aid in providing robust climate change projections.

1.2 Tropospheric gas-phase chemistry

A variety of chemicals are released into the troposphere. In the presence of oxidants, reaction cascades of these chemicals leads to the production of a plethora of gaseous, liquid and solid products. In this section, key tropospheric gas-phase chemistry that provides the foundation for this thesis is discussed.

1.2.1 The hydroxyl radical

The hydroxyl radical (OH) is formed in the atmosphere by ozone in presence of ultra-violet (UV) radiation

$$O_3 + h\nu \rightarrow O_2 + O(^1D) \quad \text{(R1.1)}$$

$$O(^1D) + M \rightarrow O + \text{M} \quad \text{(R1.2)}$$

$$O(^1D) + H_2O \rightarrow 2OH \quad \text{(R1.3)}$$

The hydroxyl radical is a powerful oxidant, controlling the degradation of many atmospheric components. These include carbon monoxide (CO), methane (CH_4) and a variety of other organic compounds.

The global-average annual-average lifetime of a species is defined as the global-total annual-average burden of that species, divided by the global-total annual-total removal rate of that species. Hence, the lifetime can be

considered analogues to the duration of time the species spend in the atmosphere before being removed. Also, the lifetime can be considered as how efficiently the species is removed – a low lifetime is analogous to efficient removal, whereas a long lifetime is analogous to less-efficient removal. The reactivity of a species is the inverse of the lifetime. A high reactivity indicates a fast chemical removal – i.e. a short lifetime. Conversely, a low reactivity indicates a slow chemical removal – i.e. a long lifetime.

Figure 1.2 shows the global OH reactivity with respect to various species. The global annual OH reactivity is distributed across a range of species, some of which are discussed in detail in this thesis. The lifetime and reactivity are dependent on the temperature-dependent reaction coefficient between the two species, and the relative abundances. For example, the temperature dependent reaction coefficient for $OH+CH_4$ is substantially lower than OH+isoprene, yet the abundance of CH_4 exceeds the abundance of isoprene, hence, the reactivity of OH towards these two species is comparable.

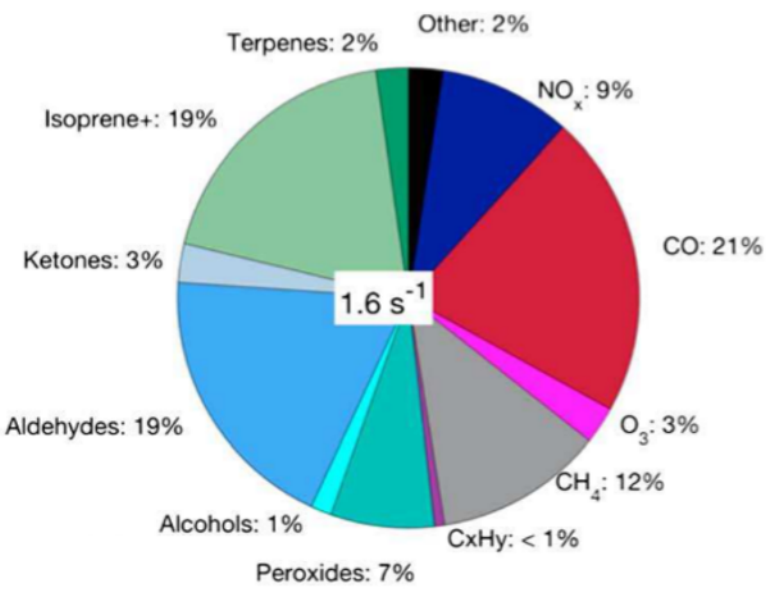

Figure 1.2– Global reactivity of the hydroxyl radical, taken and adapted from Safieddine et al. (2017)

1.2.2 **Carbon monoxide**

Carbon monoxide (CO) is emitted from a number of sources, including anthropogenic activities and biomass burning (Lamarque et al., 2010), and from phytoplankton (Swinnert. et al., 1970). CO oxidation affects a number of atmospherically relevant components. The oxidation of CO by OH (photooxidation) accounts for 21 % of the OH reactivity (Figure 1.2). This reaction cascade is initiated by the donation of an oxygen atom to CO, leading to the formation of carbon dioxide (CO_2) and a hydrogen atom

$$CO + OH \rightarrow CO_2 + H \quad \text{(R1.4)}$$

The hydrogen atom is unstable, and therefore reacts quickly with molecular oxygen (O_2), forming the hydroperoxyl radical (HO_2)

$$H + O_2 \rightarrow HO_2 \quad \text{(R1.5)}$$

In the absence of nitric oxide (NO), the hydroperoxyl radical then reacts with itself, forming hydrogen peroxide (H_2O_2)

$$HO_2 + HO_2 \rightarrow H_2O_2 \quad \text{(R1.6)}$$

Hydrogen peroxide can be removed through several pathways. This species is soluble so can be scavenged. Alternatively, H_2O_2 can be removed via photolysis, leading to the regeneration of OH through:

$$H_2O_2 + hv \rightarrow 2\,OH \quad \text{(R1.7)}$$

Alternatively, H_2O_2 can consume OH, forming another HO_2 racial and water vapour.

$$H_2O_2 + OH \rightarrow HO_2 + H_2O \quad \text{(R1.8)}$$

However, in the presence of NO, the HO_2 radical generated in R1.5 can lead to the production of nitrogen dioxide (NO_2)

$$HO_2 + NO \rightarrow OH + NO_2 \quad \text{(R1.9)}$$

NO_2 can then be photolysed, leading to the production of ozone (the production of ozone is discussed in further detail in Section 1.2.6).

$$NO_2 + hv \xrightarrow{O_2} O_3 \quad \text{(R1.10)}$$

Therefore, the formation of O_3 from CO and O_2 is a chain reaction, catalyzed by the HO_X family (HO_X = H + OH + HO_2) and by NO, with the net reaction being

Net: $CO + 2O_2 \rightarrow CO_2 + O_3 \quad \text{(R1.11)}$

1.2.3 **Methane**

Methane is released into the atmosphere from a number of different sources (discussed further in Sections 1.4 and 1.6.2). Once emitted, methane undergoes photooxidation in a similar fashion to CO, and accounts for 12 % of the OH reactivity (Figure 1.2). Methane photooxidation is initiated by hydrogen abstraction, resulting in the formation of a methyl radical (CH_3)

$$CH_4 + OH \rightarrow CH3 + H_2O \quad \text{(R1.12)}$$

Molecular oxygen then combines with the methyl radical to form the methyl peroxy radical (CH_3O_2), which can be considered analogous to HO_2 (R1.3)

$$CH_3 + O_2 \rightarrow CH_3O_2 \quad \text{(R1.13)}$$

CH_3O_2 reacts further, with HO_2 to form methylhydroperoxide (CH_3OOH), or with NO to form a methoxy radical (CH_3O)

$$CH_3O_2 + HO_2 \rightarrow CH_3OOH + O_2 \quad \text{(R1.14)}$$

$$CH_3O_2 + NO \rightarrow CH_3O + NO_2 \quad \text{(R1.15)}$$

Methylhydroperoxide, CH_3OOH, is further oxidized by OH (R1.16 – R1.17) or undergoes photolysis (R1.16)

$$CH_3OOH + OH \rightarrow CH_2O + OH + H_2O \quad \text{(R1.16)}$$

$$CH_3OOH + OH \rightarrow CH_3O_2 + H_2O \quad \text{(R1.17)}$$

$$CH_3OOH + hv \rightarrow CH_3 + OH \quad \text{(R1.18)}$$

The methoxy radical generated in R1.17 then rapidly reacts with O_2, to generate formaldehyde (CH_2O)

$$CH_3O + O_2 \rightarrow CH_2O + HO_2 \quad \text{(R1.19)}$$

Formaldehyde is either oxidized by OH (R1.20), or can photolyse in one of two possible positions (R1.21 – R1.22)

$$CH_2O + OH \rightarrow CHO + H_2O \quad \text{(R1.20)}$$

$$CH_2O + hv \xrightarrow{O_2} CHO + HO_2 \quad \text{(R1.21)}$$

$$CH_2O + hv \xrightarrow{O_2} CO + H_2 \quad \text{(R1.22)}$$

The CHO radical generated in R1.20 and R1.21 then reacts rapidly with molecular oxygen, yielding CO and HO_2

$$CHO + O_2 \rightarrow CO + HO_2 \quad \text{(R1.23)}$$

CO generated in the oxidation of methane (R1.22 – R1.23), then undergo further reactions, as described in Section 1.2.2. The overall net reaction of methane oxidation strongly depends on the conditions. Devoid of NO_x, the net reaction of methane oxidation would be the formation of ozone

Net: $CH_4 + 10O_2 \rightarrow CO_2 + H_2O + 5O_3 + 2OH \quad \text{(R1.24)}$

By contrast, in the presence of NO_X, the net reaction of methane oxidation would be the consumption of hydroxyl radicals

Net: $CH_4 + 3OH + 2O_2 \rightarrow CO_2 + 3H_2O + HO_2$ (R1.25)

Evidently, the amount of NO in the atmosphere has a strong influence on both methane and carbon monoxide reaction cascades.

1.2.4 **Other organic compounds**

In addition to CO (Section 1.2.2) and CH_4 (Section 1.2.3), several other organic compounds control the reactivity of OH (Figure 1.2). Isoprene and terpenes account for 19 and 2 %, respectively, of the global OH reactivity (Figure 1.2) The oxidation of these two species leads to the formation of SOA, which is discussed in greater detail later (Sections 1.71-1.7.3). Briefly, organic compounds are released from a number of different natural and anthropogenic sources. These species can react in a similar fashion to CO (Section 1.2.2) and CH_4 (Section 1.2.3), but the oxidation pathways are much more complex. Generally, these organic compounds lead to the production of peroxy radicals (RO_2). These peroxy radicals then undergo further oxidation. Crucially, the chemical conditions control the fate the proxy radical, which has implication for the amount of SOA formed. These organic compounds control the lifetime of OH, which in turn controls the lifetime of CH_4 and CO. In addition, organic compounds oxidation can lead to the production or removal of ozone, and also the formation of aerosol.

1.2.5 **Nitrogen oxides**

Nitric oxide (NO) and nitrogen dioxide (NO_2) are collectively referred to as NO_X. NOX accounts for 9 % of the global OH reactivity (Figure 1.2). NO_X is emitted form fossil fuel combustion and biomass burning (Lamarque et al., 2010), soil (Yienger and Levy, 1995), and lightning (Price and Rind, 1992). NO_X is primarily released in the form of NO. During the daytime at the surface, the timescale for NOx cycling is of the order of minutes.

$$NO + O_3 \rightarrow NO_2 + O_2 \quad \text{(R1.26)}$$

$$NO_2 + h\nu \xrightarrow{O_2} NO + O_3 \quad \text{(R1.27)}$$

This cycling between NO and NO_2 is a null cycle, with no net changes in NOx, O_2 or O_3. The mechanism for NO_2 removal depends on the time of day. During the day, when OH is present, NO_2 undergoes photooxidation leading to the production of nitric acid (HNO_3).

$$NO_2 + OH \rightarrow HNO_3 \quad \text{(R1.28)}$$

Nitric acid is extremely soluble and is therefore scavenged efficiently. At nighttime, NOx exists exclusively as NO_2. At nighttime, the removal of NO_2 is dominated by ozone, leading to the production of an extremely important oxidant, the nitrate radical (NO_3)

$$NO_2 + O_3 \rightarrow NO_3 + O_2 \quad \text{(R1.29)}$$

The nitrate radical is photolysed back to NO_2 during the daytime, hence, this species peaks during nighttime.

NO can also react with OH, to form nitrous acid (HONO)

$$OH + NO \rightarrow HONO \quad \text{(R1.30)}$$

HONO is then removed from the atmosphere either by photolysis or reaction with OH

$$HONO + hv \rightarrow OH + NO \quad \text{(R1.31)}$$

$$HONO + OH \rightarrow H_2O + NO_2 \quad \text{(R1.32)}$$

Hence, HONO can regarded as an OH reservoir, releasing OH in the presence of sunlight. Indeed, HONO is identified as the principal OH source in the early morning (Lee et al., 2016)

1.2.6 **Ozone**

Ozone is a precursor to the hydroxyl radical (R1.1). Ozone is transported into the troposphere from the stratosphere, as well as chemically produced within the troposphere. Tropospheric ozone is chemically produced by the cycling of NOx and reactions with peroxy radicals.

$$HO_2 + NO \rightarrow OH + NO_2 \quad \text{(R1.33)}$$

$$CH_3O_2 + NO \rightarrow CH_3O + NO_2 \quad \text{(R1.34)}$$

Following this, ozone is formed from NO_2 in the presence of sunlight

$$NO_2 + hv \xrightarrow{O_2} NO + O_3 \quad \text{(R1.35)}$$

Ozone is removed from the troposphere via dry deposition and reaction of $O(^1D)$ and water vapour (R1.1-1.3). These oxidants, together with CO, CH_4 and other organic compounds, play a crucial role in the formation of aerosol, as discussed below.

1.3 Aerosol-phase chemistry

Aerosol refers to small solid or liquid particles that are suspended in a gas. Whilst this term refers to both the particles and the gas, the term is generally used to describe the particle only. Alternatively, aerosol can be described as particulate matter (PM). The terms PM and aerosol are often used interchangeably. Natural sources of aerosol include volcanoes, windborne dust, sea spray, and vegetation. Anthropogenic sources include combustion (industry, residential and traffic) and solvent use. Biomass burning is another source of aerosol, and includes both intentional fires and natural fires. The size of these particles ranges from a few nanometers (nm) to tens of micrometers (μm). Particles released into the atmosphere in the aerosol phase are primary, whereas particles formed within the atmosphere are termed secondary. Particles are removed from the atmosphere via dry deposition, wet deposition, and evaporation (followed by chemical removal or deposition). The global-mean lifetime for an aerosol particle is of the order of days. This short lifetime creates strong spatial gradients in aerosol concentrations, leading to challenges in quantifying the aerosol distribution.

Due to the dependence on meteorology and chemical conditions, the abundance and properties of aerosol vary with location and season. In the following sub-sections, the main aerosol features are described.

1.3.1 The aerosol size distribution

Particles are commonly classified according to size, and this is illustrated by Figure 1.3. Fine particles range from 0.005 to 1 μm, and are further sub-divided into the nucleation mode (0.005 – 0.1 μm) and the accumulation mode (0.1 - 1μm) (Figure 1.3). Particles within the nucleation mode are

formed by the clustering of extremely low-volatility gases in a processes known as nucleation, and by the condensation of low-volatility vapours – hence, particles in this size range are usually formed within the atmosphere, as opposed to emitted. Nucleation mode particles are lost by condensational growth or by collisional uptake by larger sized particles (coagulation), both of which transfer particles into the accumulation mode. In some cases, the nucleation mode is further sub-divided into the Aitken mode (Figure 1.3). Sources of accumulation mode particles include growth of nucleation mode particles and direct emissions – hence, particles in this size mode are both produced and emitted. Approaching 1 μm, the large size of the particle suppresses further growth by both condensation and coagulation. This is due to the large surface and the slow movement of particles this size. Hence, particles are said to ‘accumulate’ in this mode. For the 1 – 10 μm size range, particles are generally emitted (primary) as opposed to being chemically produced.

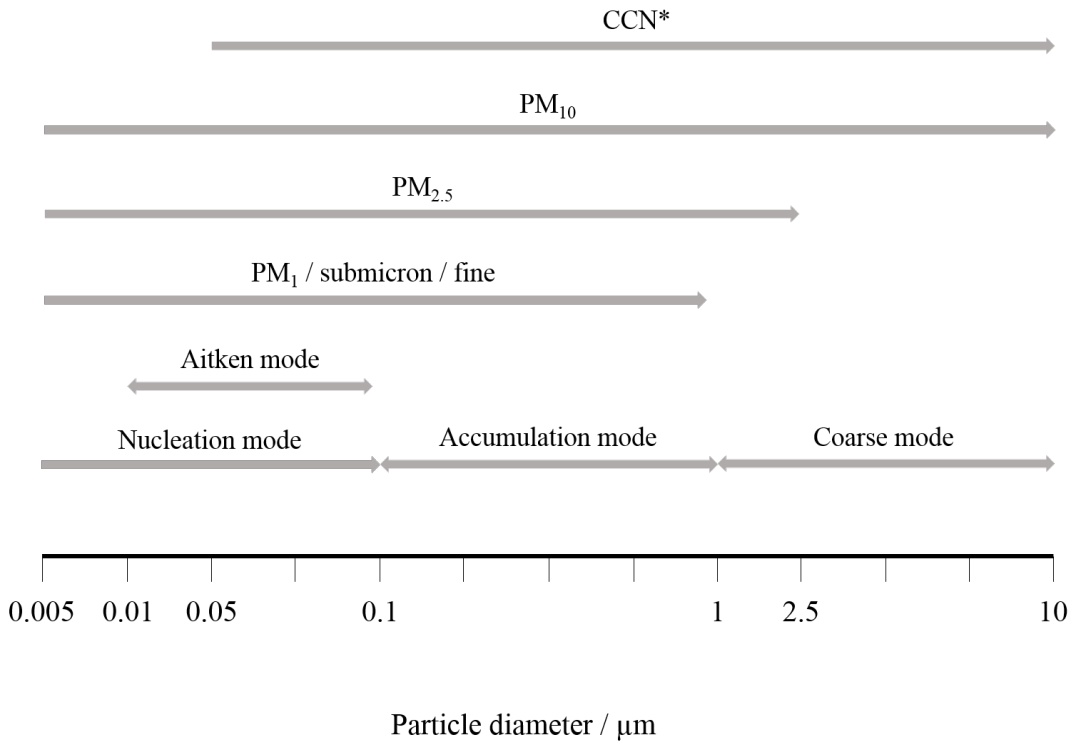

Figure 1.3 – Schematic diagram of aerosol size classification.

Aerosol deposition is influenced by both the particle size and its properties. For example, fine particles are too small to sediment, so are principally removed by wet deposition. Coarse particles are large enough to undergo significant dry deposition, as well as wet removal. In addition, the size of the particle also influences the health and climatic impacts. Soluble particles (hydrophilic) can be removed by wet deposition, whereas insoluble particles (hydrophobic) cannot.

In the absence of any aerosol, water vapour supersaturations of several hundred percent are required before nucleation can occur (i.e. cloud droplet formation). Aerosol can act as a nucleus for the growth of cloud and fog droplets. Cloud Condensation Nuclei (CCN) refer to a subset of aerosol,

with a diameter approximately greater than 0.05 μm (Figure 1.3). If aerosol did not exist, neither would clouds.

1.3.2 **The aerosol chemical composition**

Aerosols are composed of a variety of chemical species (components), including sulphate (SO_4^{2-}), nitrate (NO_3^-), ammonium (NH_4^+), organic aerosol (OA), elemental carbon (EC), crustal species, sea salt (SS), hydrogen ions (H^+), and water.

Global aerosol emissions are dominated by sea salt, with a global annual-total emission rate of 1,000 – 10,000 Tg a^{-1} (Winter and Chylek, 1997). Within sea-water, sea salt is approximately 55 % Cl and 31 % Na. Bursting bubbles and wind-induced waver breaking suspends sea-water into the air which, after evaporation, leaves sea salt aerosol. The chemical composition of sea salt aerosol is then modified by chemical transformations. For example, sodium chloride reacts with sulphuric acid vapour, forming sodium sulphate and hydrochloric acid vapour.

$$H_2SO_4(g) + 2NaCl \rightarrow Na_2SO_4 + 2HCl\,(g) \qquad \text{(R1.36)}$$

Dust emissions are also high, and are estimated between 500 and 4,400 Tg a^{-1} (Huneeus et al., 2011).

Note, carbon contains four valence electrons, and therefore has the capacity to form four covalent bonds. Graphene refers to one-dimensional carbon hexagonal lattices; each carbon atoms donates three valence electrons to neighbouring carbons atoms and the fourth valence electron is delocalised over the entire lattice. In graphene, these hexagonal structures can be laced with small quantities of other elements, such as oxygen and hydrogen.

Graphene can be formed upon combustion, whereby the one-dimensional structures combine, to form three-dimensional aggregates (usually spheres), which are termed soot particles. Soot carbon refers to the carbon component of soot particles.

The techniques for measuring soot can broadly be separated into one of two categories. Soot carbon measured using optical techniques is termed black carbon (BC). Soot carbon measured using thermal techniques is termed elemental carbon (EC). BC and EC do not correspond to a unique soot particle, but are instead proxies for soot carbon. The differences in these techniques for measuring soot carbon are non-negligible, often resulting in differing measurements of soot carbon (Andreae and Gelencser, 2006). Despite these discrepancies, the terms BC and EC are often used interchangeably within the literature.

OA refers to organic compounds (see section 1.4) in the aerosol phase. OA is further dived into primary OA (POA) and secondary OA (SOA). This split between these two fractions is extremely uncertain. Sources of POA include fossil fuel combustion and biomass burning, meat cooking, wood burning, and vegetation. SOA is formed in the atmosphere from a variety of sources (Section 1.7). Overall, the OA lifecycle is extremely uncertain, and is discussed in further detail in Section 1.9.

Sulphur dioxide (SO_2) is released from anthropogenic actvitites and volcanoes and dimethyl sulphide (DMS) is released from phytoplankton. Upon gas and aqueous phase oxidation, these gases lead to the production of sulphuric acid.

Gas-phase ammonia (NH_3) is released from agriculture, biomass burning and industrial activity. Once, emitted, ammonia can then interact with sulphur and other nitrogen containing species, leading to the formation of a variety of inorganic aerosol. The ammonia-nitric acid –sulphuric acid- water system, contains numerous species spanning gaseous, aqueous and solid

states. The chemical fate of ammonia depends on the relative concentrations of other species, temperature, humidity and acidity.

Ammonia can either form ammonium sulphate or ammonium nitrate. Sulphate has a lower vapour pressure (Section 1.4.4) than nitrate, so ammonia preferentially reacts with sulphate. Ammonia can react with sulphate, depending on the pH

Under very acidic conditions (low NH_3 relative to H_2SO_4)

$$NH_{3(g)} + H_2SO_{4(aq)} \rightarrow (NH_4)HSO_{4(s)} \quad \text{(R1.37)}$$

Under acidic conditions

$$3NH_{3(g)} + 2H_2SO_{4(aq)} \rightarrow (NH_4)_3H(SO_4)_{2(s)} \quad \text{(R1.38)}$$

If enough ammonia is present

$$2NH_{3(g)} + H_2SO_{4(aq)} \rightarrow (NH_4)_2SO_4 \quad \text{(R1.39)}$$

Any remaining ammonia can react with nitrate reversibly

$$NH_{3(g)} + HNO_{3(g)} \leftrightarrow NH_4NO_{3(s)} \quad \text{(R1.40)}$$

Samples of aerosol containing a mixture of chemical components can be heated (600 C). The components of aerosol which vapourise under these conditions are termed non-refractory. Most aerosol chemical components are non-refractory, except sea salt and mineral dust. Figure 1.4 shows the

location of sub-micron (PM_1; Figure 1.3) non-refractory aerosol mass concentrations, taken from Zhang et al. (2007). Across these sites, OA often dominates the aerosol composition, representing 18 – 70 % of the aerosol mass. To date, this study is one of the most geographically extensive chemically resolved aerosol measurement studies. At this same time, this study is clearly biased to northern hemisphere mid-latitudes. This database is publically accessible and is used for many studies on aerosol, including this thesis.

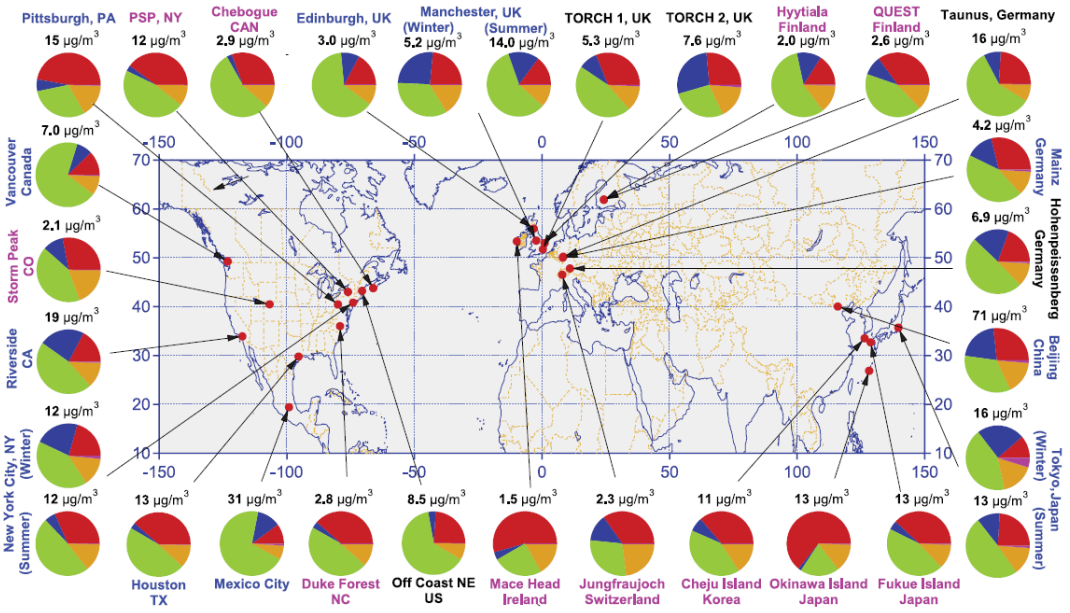

Figure 1.4 – Measurements of sub-micron aerosol mass concentrations, taken from Zhang et al. (2007). Points indicate locations of measurements. Pie charts show contribution of aerosol components: organic (green), sulphate (red), nitrate (blue), ammonium (orange), and chloride (purple).

1.4 Organic compounds: classifications, interactions, and properties

OA can be classified as POA, where it is emitted in the aerosol phase, or SOA, where it is formed within the atmosphere. In SOA formation, energetic gas-phase organic molecules must overcome an energy barrier in order to condense. This energetic barrier is dependent on the properties of the compounds, such as volatility, and by the external conditions, such as temperature. In this section, the theory of chemical boding (Section 1.4.1) is invoked to explain polarity (Section 1.4.2.), which in-turn explains the forces of attraction between molecules (Section 1.4.3). Finally, volatility is discussed (Section 1.4.4).

1.4.1 Intra-molecular interactions

There are more than 37 million known organic compounds in the atmosphere (Clayden et al 2001). These organic compounds can be grouped together according to their structural features. Members of a given family tend to have similar properties, such as chemical reactivity and volatility. In this section, the main organic compound families are discussed and used to explain their physicochemical behaviour.

Carbon contains 4 valence electrons. A covalent bond is shared pair of electrons. Carbon can covalently bond with from one to four other atoms. Organic compounds contain carbon atoms covalently bonded to at least one other atom. Hydrocarbons are a specific type of organic compound, where a carbon atom is covalently bonded to at least one hydrogen atom. Hence, CH_4 is an organic compound and a hydrocarbon, whereas CO is an organic compound.

Figure 1.5 shows some of the different hydrocarbon classifications. When all carbon atoms within a molecule share only single carbon-carbon bonds, the species is referred to as an alkane (or saturated hydrocarbon) (Figure 1.5). If a compound contains a pair of carbon atoms which share a carbon-carbon double bond, the molecule is an alkene (Figure 1.5). When a species shares a triple bond, the molecule is referred to as an alkyne (Figure 1.5). The strength of bonding decreases from alkane, to alkene to alkyne, hence, alkanes are least reactive, and alkynes are most reactive. Ring structures with bonding delocalized over the entire ring are referred to as aromatic.

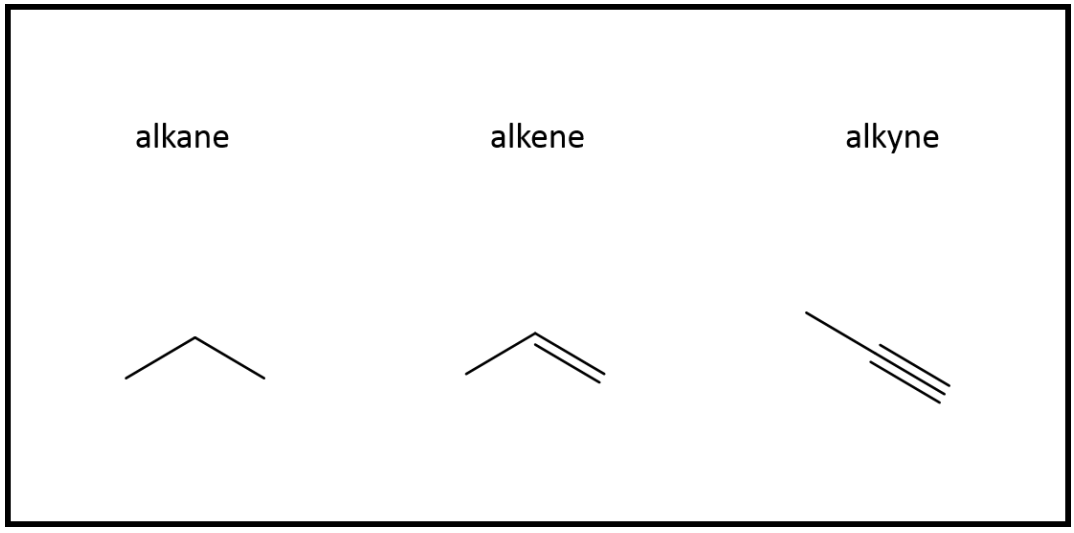

Figure 1.5– Example molecular structures of an alkane, alkene and alkyne. Note, these species contain carbon atoms covalently bonded to other atoms so can be classified as organic compounds. As the carbon atoms are bonded to hydrogen atoms, these species can also be classified as hydrocarbons.

The functional group of a molecule refers to a combination of atoms responsible for the characteristic reactions of a compound. The alkane group is a functional group (Figure 1.5), however, as it is so basic it is often omitted as a functional group. Instead, the alkane is often regarded as the scaffold, from which, functional groups are added to.

Figure 1.6 shows some example functional groups. The alkyl halide functional group has a carbon atom bonded to a halogen (-X; X = Cl, Br, F), the alcohol group has a carbon atom bonded to a hydroxyl group (-OH), and ethers have two carbon atoms bonded to the same oxygen atom (-O-) (Figure 1.6).

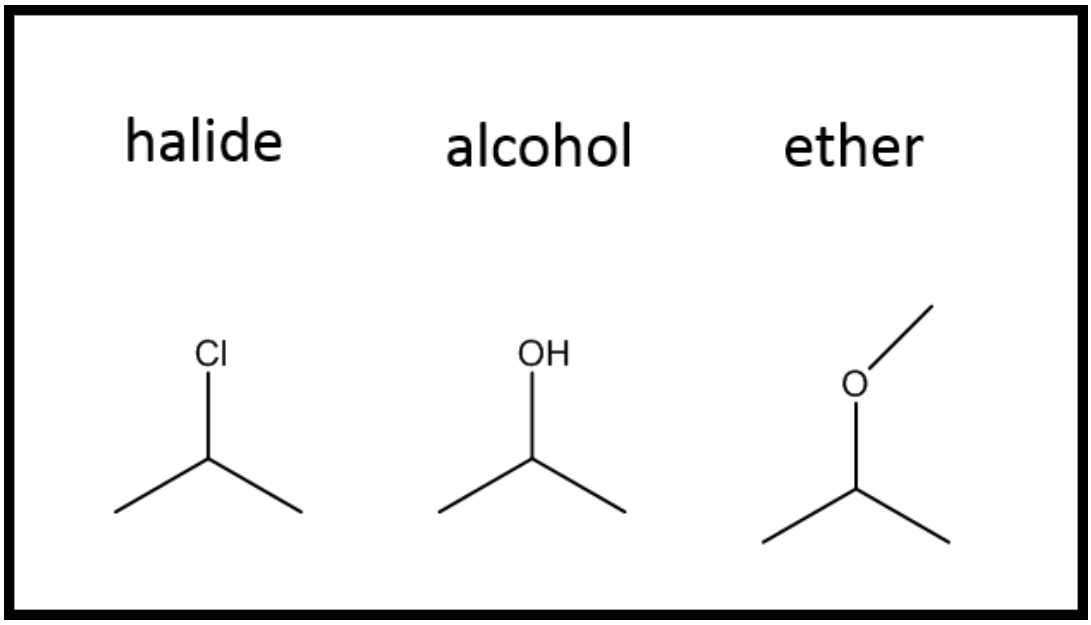

Figure 1.6 – Example molecular structures of a halide, alcohol and ether on the alkane backbone.

Carbon can also be bonded to atoms with double bonds. When a compound contains a carbon atom double bonded to an oxygen, the species is classified as a carbonyl (C=O). Figure 1.7 shows various carbonyl compounds. Carbonyls are further classified depending on what the carbonyl group is attached to. Carbonyls attached to a hydrogen are aldehydes, attached to no hydrogens are ketones, and attached to a hydroxyl group are carboxylic acids (Figure 1.7).

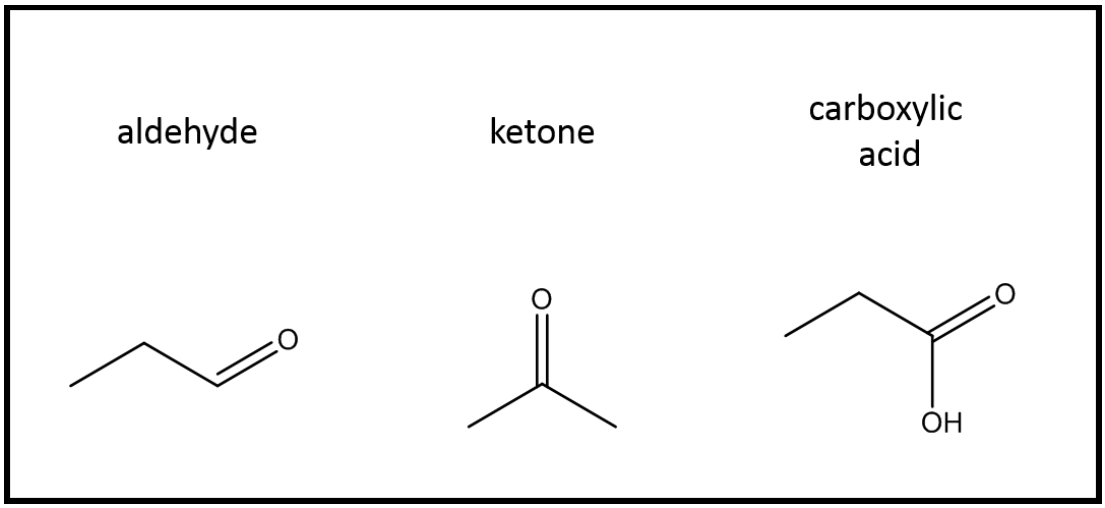

Figure 1.7– Example molecular structures of carbonyl organic compounds.

1.4.2 **Polarity**

Electronegativity is the tendency of an atoms to attract a pair of electrons. Figure 1.8 shows how a bonding pair of electrons are distributed between two identical atoms, and two different atoms. In the case where two different atoms are linked via a covalent bond, the shared pair of electrons is shared unequally between the atoms (Figure 1.8). This is due to differences in electronegativity. Atoms such as oxygen, sulphur, chlorine and nitrogen are electronegative, whereas hydrogen is electropositive (tendency of atoms to repel a proton).

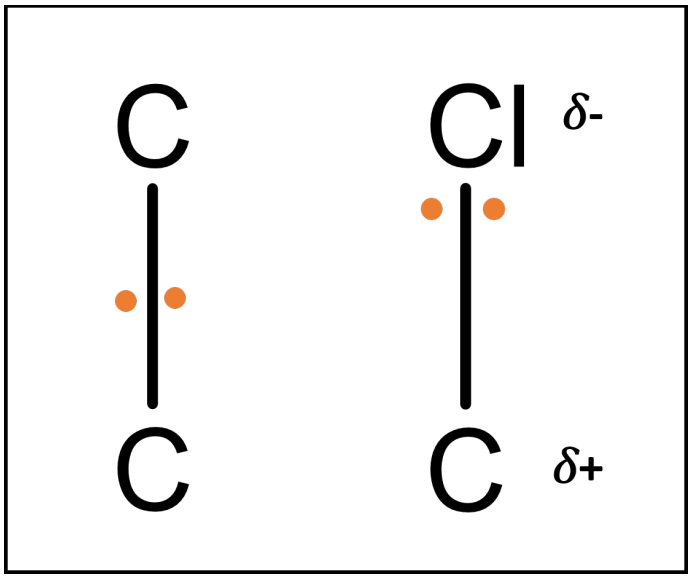

Figure 1.8 – (left) For a covalent bond between atoms of the same electronegativity, the shared pair of electrons (covalent bond) is equally distributed between the atoms, resulting in a non-polar bond. (right) For a covalent bond between atoms of different electronegativity, the shared pair of electrons (covalent bond) is not equally distributed between the atoms, resulting in a polar bond.

The shared pair of electrons between atoms with different electronegativity will therefore be closer to the more electronegative atom (Figure 1.8). This creates a partial negative charge on the electronegative atom and partial positive charge on the electropositive atom, thus, creating a dipole in electric charge (Figure 1.8). Conversely, a chemical bond between atoms with similar electronegativity is non-polar as the shared pair of electrons is equally distributed between the atoms (Figure 1.8).

1.4.3 **Inter-molecular interactions**

The interaction between molecules, known as the inter-molecular bonding, is determined by the polarity of the molecules. Inter-molecular bonding is shown schematically in Figure 1.9. As discussed above, compounds

containing atoms of different electronegativity are polar due to the unequal share of bonding electrons (Figure 1.8). Non-polar molecules are not charged, which suggest no interaction between these types of molecules. However, this is not the case. Within non-polar molecules, electrons are rotating around molecular orbitals, leading to the possibility of a transient partial electric charge. This partial charge can induce a partial charge in neighbouring non-polar molecule, leading to an interaction known as the Dispersion interaction (Figure 1.9). As this electric charge is only partial and temporary, intermolecular forces of this type are generally weak, with a typical bonding energy of 2 kJ mol^{-1}. However, the strength of this type of bonding is highly dependent on molecular mass. Examples of compounds with this type of inter-molecular bonding include methane, benzene and naphthalene.

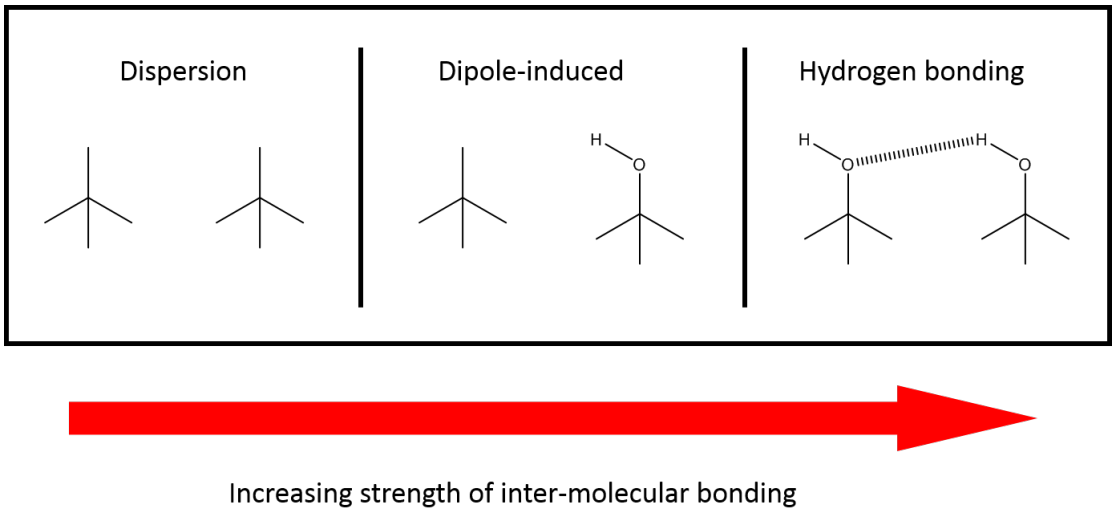

Figure 1.9 – Examples of dispersion, dipole-induced and hydrogen bonding inter-molecular forces.

Non-polar molecules can acquire a dipole in presence of a polar molecule. This attraction is referred to a dipole-induced-dipole interaction

(Figure 1.9). If two molecules both have dipoles, they can attract one another, with the interaction known as dipole-dipole. A sub-set of dipole-dipole interactions, Hydrogen bonding, are reserved for the interaction of the most electropositive atom (H) with an extremely electronegative atom (N, O, and F) (Figure 1.9). Hydrogen bonding is the strongest inter-molecular interaction for neutral species, with a typical bonding energy of 20 kJ mol^{-1}.

1.4.4 **Volatility**

A phase is a specific state of matter that is uniform throughout in composition and physical state. The gas phase is a totally random distribution of molecules, whereas the solid phase is a well-ordered structure of crystal. The liquid phase is somewhere between the two.

The phase of a substance or compound is partially controlled by the inter-molecular bonding. As the strength of inter-molecular bonding increases, the preference for the solid phase also increases. For example, consider the phase of water and methane at room temperature and pressure. Water molecules are attracted to one another by hydrogen bonding, which are extremely strong forces of attraction (Figure 1.9); hence, this substance is a liquid at room temperature. By contrast, methane molecules are non-polar and attracted to one another only by the weak dispersion forces (Figure 1.9), hence, this species is a gas at room temperature and pressure. However, benzene is also a non-polar molecule, but exists in the liquid phase at room temperature and pressure. Benzene is almost five times heavier than methane, hence, the dispersion forces of attraction are much higher.

For any given liquid, molecules are in dynamic equilibrium with both the liquid and gaseous state. The vapour pressure is the pressure of the gas phase substance whilst in equilibrium with the same condensed phase.

Another way of explaining this is in terms of volatility. The volatility is the tendency of a substance to vapourise. Note, low-volatility species condense more easily, hence, are more suitable precursors of SOA. Benzene and naphthalene are both non-polar molecules with weak dispersion inter-molecular bonding (Figure 1.9). Both of these species are large (in comparison to methane) and are liquid at room temperature and pressure. These substances are mainly in the liquid state, but are also in dynamic equilibrium with the gaseous state. Naphthalene is almost twice the size of benzene; hence, the inter-molecular bonding is much greater in comparison to benzene. Therefore, compared to benzene, naphthalene would have a lower vapour pressure and would be less volatile.

Similar to the vapour pressure, the Henry's law constant is also a measure of pressure of a gas, however, this is a measure of a gas in equilibrium with a liquid composed of another species. Hence, this is a measure of the condensation of a gas, followed by dissolution. Organic compounds that are also precursors of SOA have an effective Henry's constants (H_{eff}) ranging from 10^5 to 10^9 M atm^{-1} (Hodzic et al., 2014).

In addition to inter-molecular bonding, the phase of a substance is also affected by external conditions, such as temperature and pressure. Increased heat and pressure will drive phase transitions in the direction of gas to liquid to solid. For a liquid in equilibrium with a gas (vapour), increased temperature will increase the vapour pressure. Hence, SOA formation is favoured by (i) low temperatures, and (ii) high pressures.

Together, the size and functional group dictate the volatility of a species. Isomers refer to compounds with the same chemical formula (i.e. same number of carbon, hydrogen and oxygen atoms), but different structures. Figure 1.10 shows how the boiling point and number of possible structural isomers varies with increasing carbon chain length, ranging from methane (CH_4) to octadecane ($C_{18}H_{38}$). As the number of carbon atoms of

the alkane increases, the boiling point also increases. With increasing molecular mass, dispersion of attraction also increase. Hence, the molecular forces between octadecane molecules greatly exceeds those between methane molecules. The stronger interactions between octadecane molecules, therefore, explain why this species is a liquid at room temperature – i.e. it has a low volatility (tendency to vapourise). Conversely, dispersion forces of attraction between methane molecules are weak. Therefore, this species has a high volatility, and is a gas at room temperature and pressure.

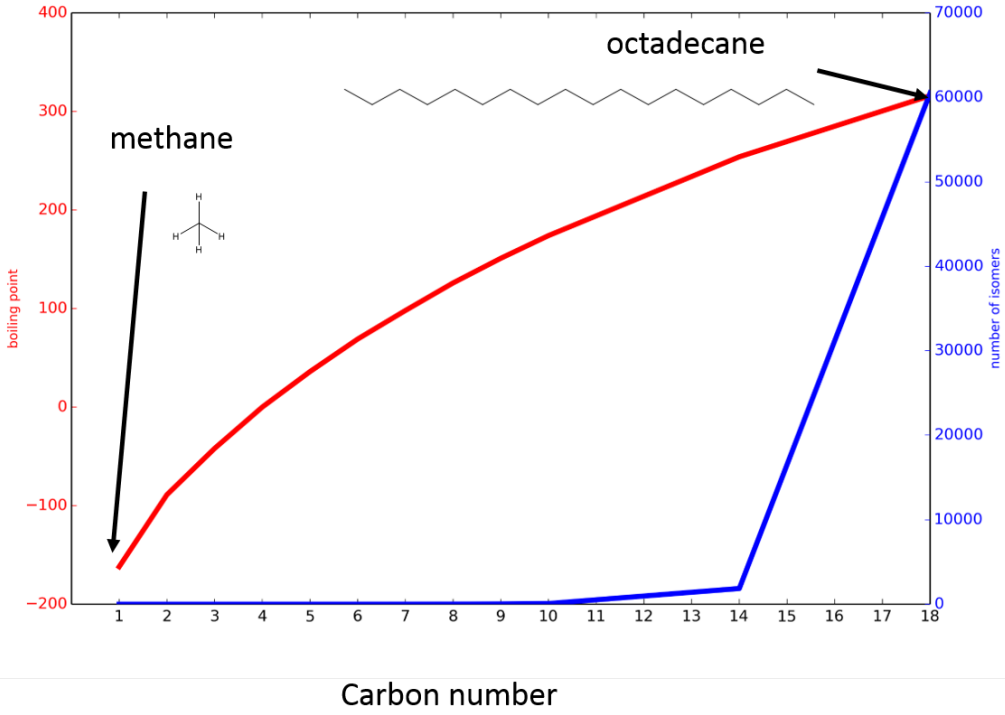

Figure 1.10 – Schematic diagram of relationship between molecular size and boiling point (red) and number of possible structural isomers (blue) for a series of alkanes.

The number of possible structural isomers increases exponentially with increasing carbon chain length (Figure 4). This explains the extremely high number of unique organic molecules in the atmosphere, of which, only a small fraction have been measured (Goldstein and Galbally, 2007).

1.5 Secondary organic aerosol

In this section, SOA and its lifecycle are briefly introduced. As previously shown in Figure 1.4, OA frequently dominates surface concentrations of non-refractory PM_1. Figure 1.11 shows the relative fraction of oxygenated OA, which is analogous to SOA, and hydrogen-like OA, which is analogous to POA, taken from (Zhang et al., 2007). The location of these measurements correspond to those shown in Figure 1.4. OA frequently dominates observed sub-micron aerosol mass (Figure 1.4), of which, OOA accounts for 63, 83, and 95 % across the urban, urban downwind, and remote sites, respectively (Figure 1.11). With the exception of densely populated cities, such as Beijing (China) and Mexico City (Mexico), observed OOA concentrations are comparable across all three environments types (Figure 1.11). By contrast, observed HOA is highest in urban regions. These results therefore suggest SOA has a mixture of urban and remote sources, whereas POA is predominantly urban.

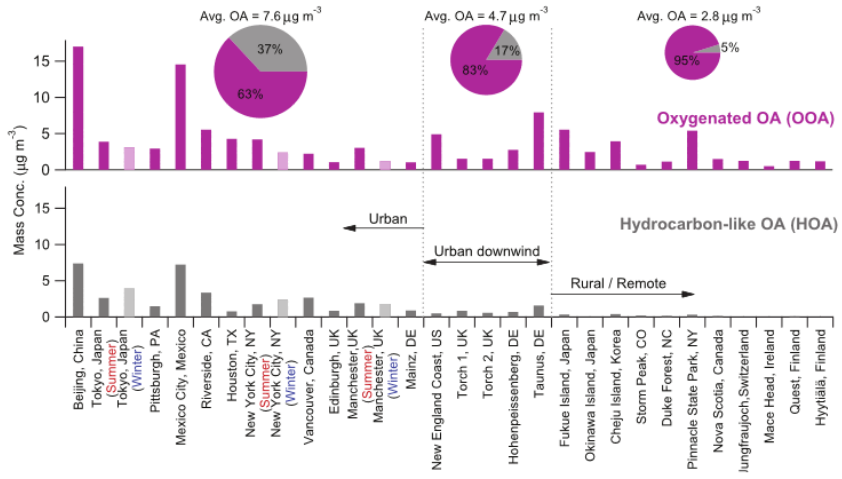

Figure 1.11– Average mass concentration of HOA and OOA for sites shown in Figure 1.4. Areas of the pie chart are scaled by the average concentration of total OA (HOA+OOA). Taken from (Zhang et al., 2007).

Figure 1.12 shows a schematic diagram of the SOA lifecycle. The SOA lifecycle begins with an emission of a gaseous organic compound. These gaseous organic compounds then undergo a range of psychical and chemical processing. Emitted gaseous hydrocarbons span a broad spectrum of volatility (Robinson et al., 2007;Robinson et al., 2010). Organic compounds can also undergo oxidation (e.g. Section 1.2.1-1.2.6). Whilst the majority of these oxidation products are small volatile species (i.e. CO_2), a small fraction of products are less volatile, which can then condense onto particles (Odum et al., 1996;Odum et al., 1997) or take part in the nucleation of particles (Ehn et al., 2014). Alternatively, gaseous organic compounds which are too volatile to condense but are polar, may condense into liquid water of cloud and aerosol. Within liquid water, the polar volatile organic compounds can oxidise, leading to reductions in volatility of the organics (Ervens, 2015). After liquid water evaporation, SOA is left. Finally, organic aerosol which has been emitted in the gas-phase (i.e. POA) can evaporate and re-condense, where it is then termed SOA (Robinson et al., 2007).

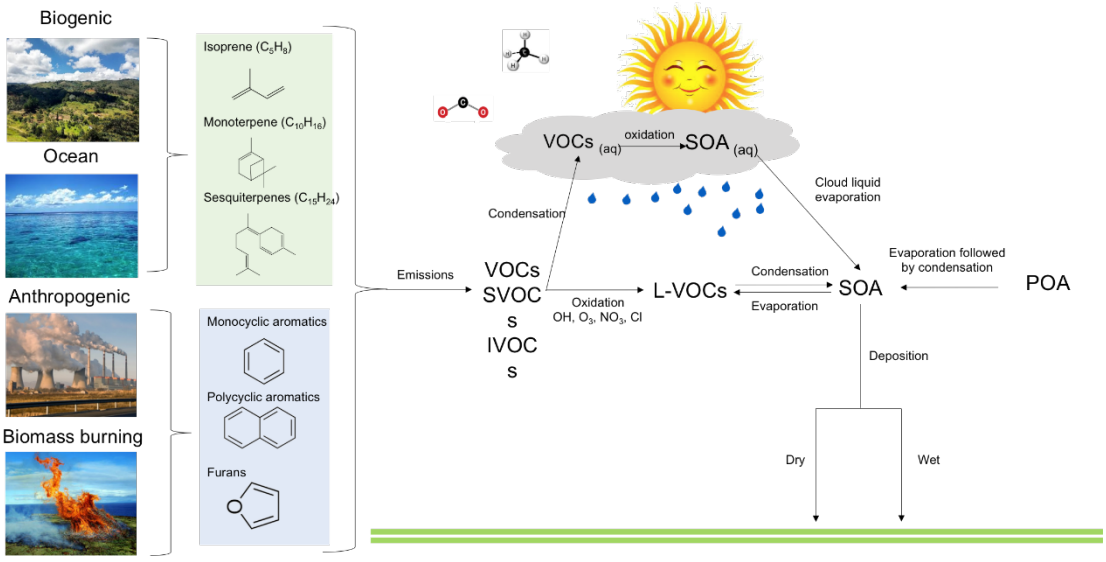

Figure 1.12– Schematic diagram of SOA lifecycle.

Once formed, SOA can interact with radiation and as a component of particulate matter affect human health. Also, within the aerosol phase, organic compounds can undergo further physical and chemical processing. Eventually, SOA is returned to the Earth's surface by wet or dry deposition. Hence, the SOA lifecycle begins with emissions of gaseous organic compounds, followed by SOA formation and SOA deposition.

In the following sub-sections, the SOA lifecycle is discussed. This begins with an overview of SOA precursor emissions (Section 1.6), followed by SOA production (1.7) and SOA particle processing and properties (Section 1.8).

1.6 Emissions of SOA precursors

The SOA lifecycle begins with emissions of organic compounds (Figure 1.12). Volatility (Section 1.4.4) is a critical aspect of both the precursor

emissions and of SOA. Hence, organic compound emissions are typically classified by volatility. This section on SOA precursor emissions begins with a brief explanation of how organic compound emissions are classified by volatility (Section 1.6.1), which is proceeded by analysis of the different sources (Section 1.6.2 – 1.6.3).

1.6.1 The volatility distribution of emitted organic compounds

A schematic diagram of the volatility distribution of organic compound emissions is shown in Figure 1.13. Organic compound emissions can be distinguished by volatility (Section 1.4.4). Volatile Organic Compounds (VOCs) exist exclusively in the gaseous state. Non-Volatile Organic Compounds (NVOCs) exist exclusively in the aerosol phase. The traditional concept of OA isolates organic compound emissions into two categories, with VOCs contributing to SOA formation, and NMVOCs being emitted as POA. This conceptual framework allows easy distinction between the two processes leading to SOA and POA. This distinction between VOC and NVOCs can be represented in both models and emissions databases relatively easy.

However, in reality, organic compounds are emitted spanning a broad spectrum, of volatility, which has led to the re-evaluation of the concept which neatly distinguishes NVOC/POA and VOC/SOA (Donahue et al., 2006;Robinson et al., 2007;Robinson et al., 2010;Donahue et al., 2011). As discussed in Sections 1.4.3 – 1.4.4, with increasing inter-molecular forces of attraction, the propensity for the solid/liquid phase is increased over the gas phase. Hence, these increasing in inter-molecular forces are synonymous to reductions in volatility. In the following sections, the emissions of each volatility class are discussed in more detail.

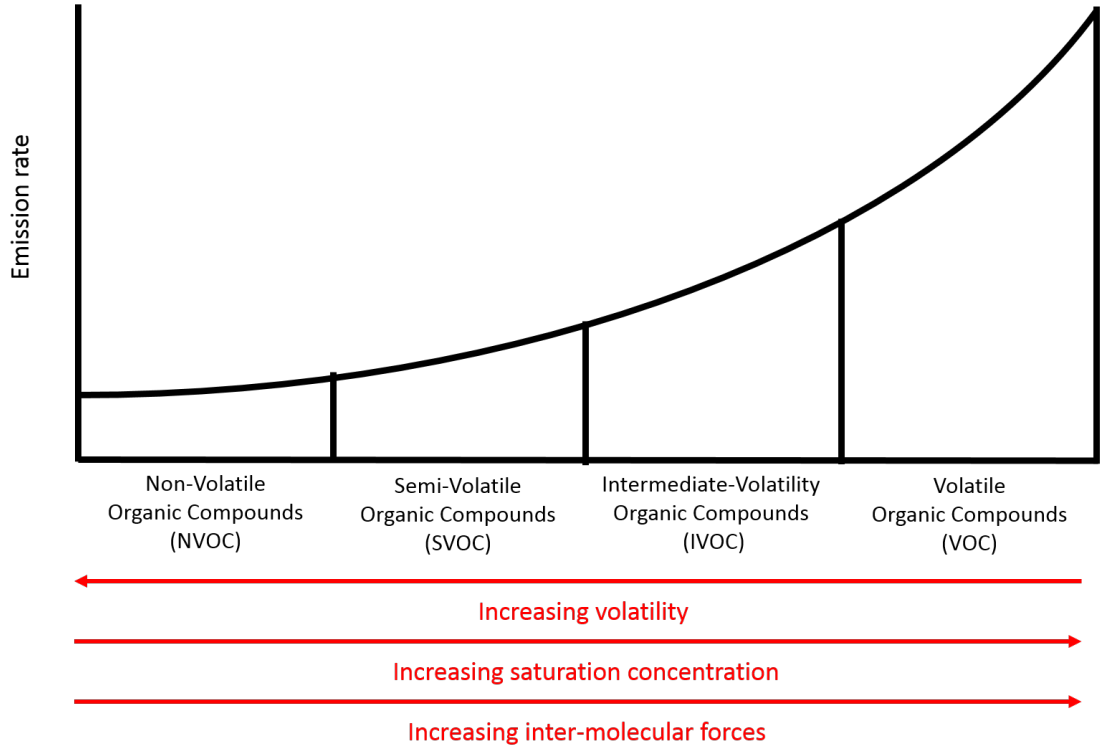

Figure 1.13– Volatility distribution of emitted organic compounds.

1.6.2 **Volatile organic compound emissions**

Volatile organic compounds (VOCs) are hydrocarbons with high vapour pressure/volatility, such that they exist exclusively in the gas-phase under atmospheric conditions. Methane (Section 1.2.3) is an example of a VOC. Methane is a small non-polar substance and is therefore classified as a VOC. Methane is released from both natural and anthropogenic sources, with a global annual total methane emission rate of 500 – 600 Tg a^{-1} (Kirschke et al., 2013).

With the exception of methane, VOCs are typically extremely reactive towards oxidation (Atkinson and Arey, 2003). This has led to the distinction between all VOCs, and non-methane VOCs (NMVOCs). Figure 1.14 shows estimates of NMVOC emissions from biogenic and from anthropogenic and biomass burning sources.

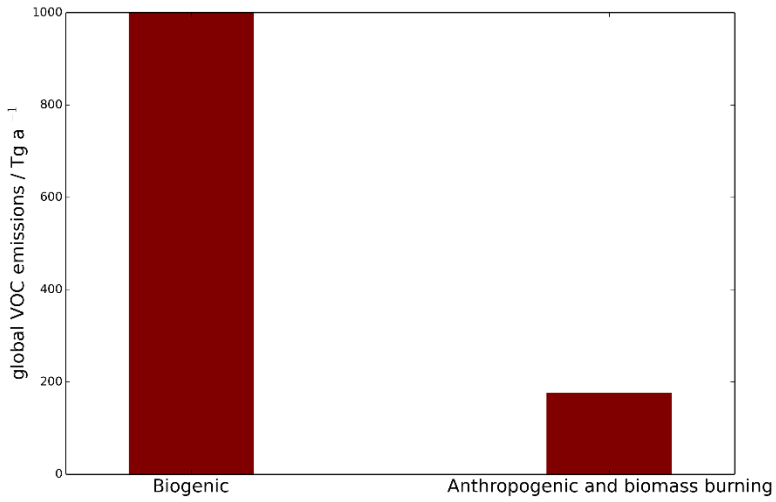

Figure 1.14 – Global annual-total NMVOC emissions from vegetation and anthropogenic and biomass burning activity. Biogenic VOC emissions estimate taken from Guenther et al. (2012), anthropogenic and biomass burning emissions estimate taken from Lamarque et al. (2010).

Vegetation is the single largest source of NMVOCs. Global annual-total VOC emissions from vegetation are estimated around 1,000 Tg a^{-1} (Guenther et al., 2012) and are predominantly alkenes, cyclic alkenes (cyloalkenes), and hydrocarbons with oxygenated functional groups. Many biogenic VOCs are unsaturated and/or polar, hence, they are oxidized relatively quickly. The dominant VOCs released from vegetation are shown in Figure 1.15. Isoprene (2-methyl-1,3-butadiene) accounts for around 50 % (500 Tg a^{-1}) of the total biogenic VOC emission rate (Figure 1.14), and for 19 % of the global OH reactivity (Figure 1.2). Terpenes, which include both monoterpene and sesquiterpenes are comprised of 2 and 3 isoprene units

respectively. Similarly, these species are also alkenes and therefore relatively reactive – they account for 2 % of the global OH reactivity (Figure 1.2). Isoprene, monoterpene and sesquiterpenes are all small non-polar alkenes. Therefore, these species interact via the dispersion forces of attraction.

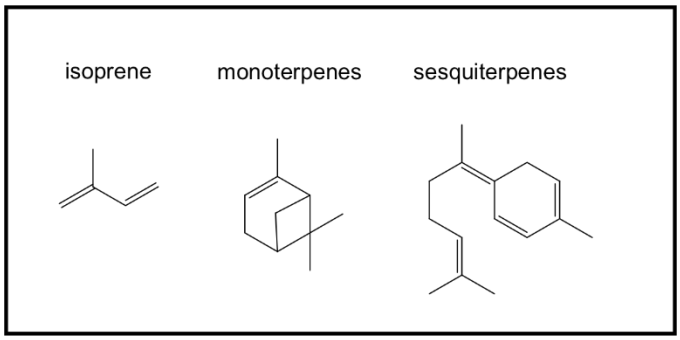

Figure 1.15 – Structure of VOCs associated with biogenic emissions. For each species, vegetation is the largest source, however, they are all also released in small quantities from soil (Bourtsoukidi et al., 2018), phytoplankton (Moore et al., 1994;Shaw et al., 2003) and humans (Fenske and Paulson, 1999).

Anthropogenic and biomass burning activities release a complex mixture of VOCs, including alkanes, alkenes, carbonyls, and aromatic compounds. Aromatic VOC emissions from anthropogenic and biomass burning activates are estimated at around 16 – 32 Tg a^{-1} (Henze et al., 2008;Pye and Seinfeld, 2010;Cabrera-Perez et al., 2016). These species are non-polar and are therefore, attracted to one another via dispersion forces of attractions, hence, they are classified as volatile. Figure 1.16 shows some typical aromatic VOCs released from anthropogenic and biomass burning activities. These include benzene (C_6H_6), toluene (C_7H_8) and xylene (C_8H_{10}).

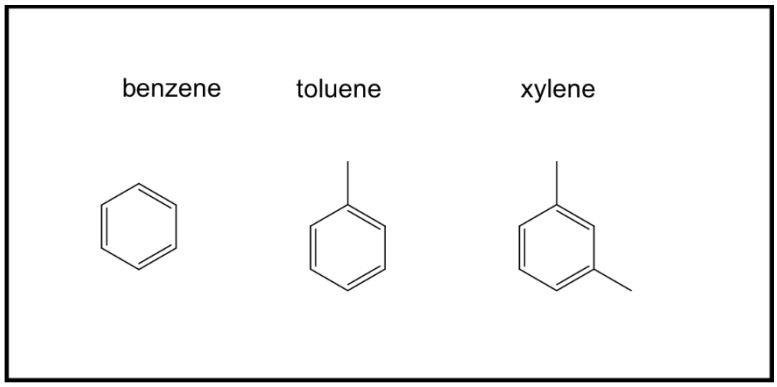

Figure 1.16 – Structure of typical VOCs related to anthropogenic and biomass burning activity.

1.6.3 Semi- and intermediate-volatility organic compound emissions

Semi-volatile organic compounds (SVOCs) and intermediate-volatility organic compounds (IVOC), when combined, are referred to as S/IVOCs. With increasing carbon length, the number of possible structural isomers increases exponentially (Figure 1.10). S/IVOC are is a complex mixture of extremely large hydrocarbons, hence, identifying individual compounds is challenging, but probably consist of large straight chain (aliphatic) alkanes and aromatic compounds with multiple rings (polycyclic) (Hu et al., 2013;Zhao et al., 2015). Figure 1.17 shows some typical S/IVOCs. Note, all these species are non-polar, yet the large size results in strong intermolecular forces of attraction. Naphthalene and n-hexadecane are smaller than floranthene and n-pentacosane, therefore, the former are classified as SVOCs (higher volatility) and the latter are classified as IVOCs (lower volatility).

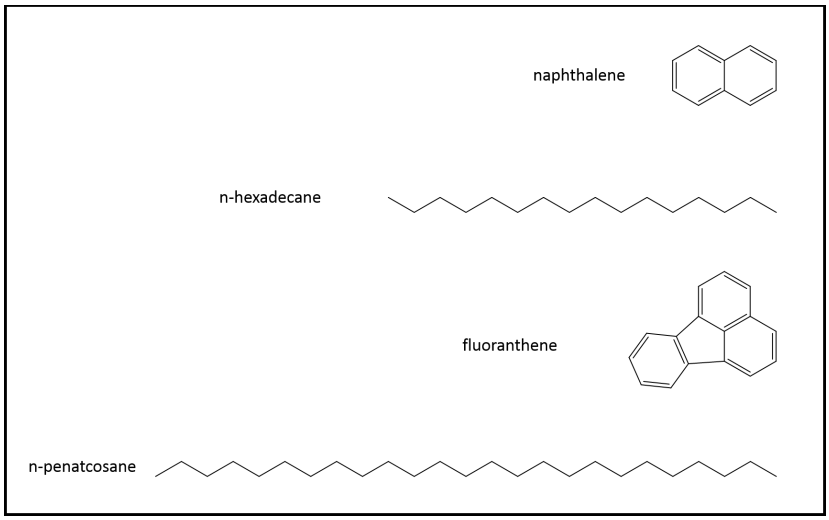

Figure 1.17 - Structure of example SVOCs (floranthene and n-penatacosane) and IVOCs (naphthalene and n-hexadecane).

Whilst the existence of S/IVOCs is widely accepted, the emission rate of these species is virtually unknown. S/IVOCs are not included in traditional emissions inventories. To calculate the amount of S/IVOC emissions, the volatility distribution of emissions from typical OA fuels is measured under chamber conditions. Figure 1.18 is an example of this, which shows the volatility distribution of emitted organic compounds from diesel exhaust. Note, non-volatile organic compounds have a saturation vapour pressure (C*) of less than 0.1 μg m^{-3}. Therefore, for this fuel type, all organic compound emissions between C* = 1 – 10^6 are not captured by traditional emissions inventories (Figure 1.18). For clarity, this implies that the magnitude or organic compound emissions missing from traditional emission inventories (S/IVCOs) is substantially greater than the amount of NVOCs (or POA) which are presently captured in emissions inventories. Hence, Robinson et al. (2007) reveals an extremely large fraction of organic compound emissions which are not included in traditional emission inventories.

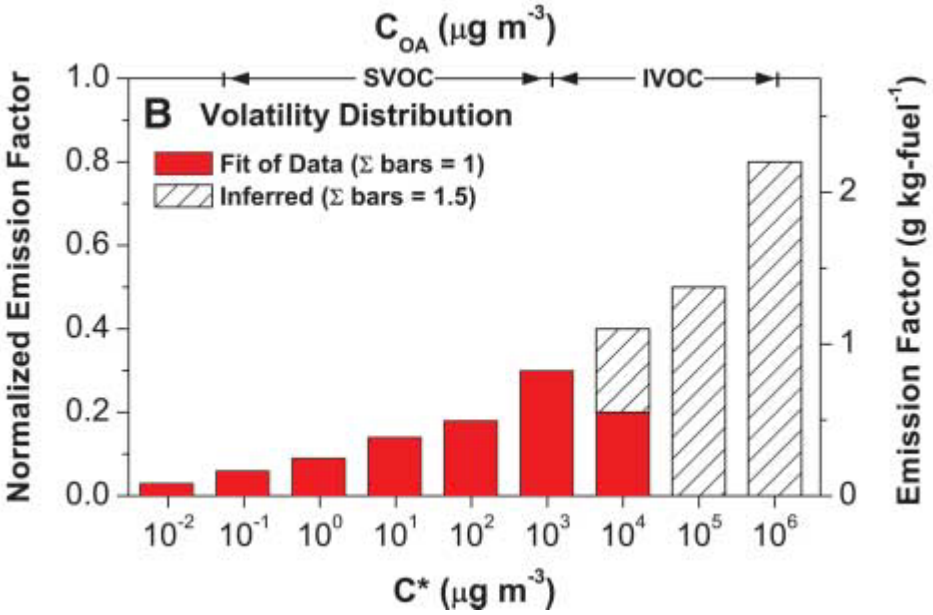

Figure 1.18 – Observed OA volatility distribution, taken from Robinson et al. (2007)

Using the distribution in Figure 1.18, it is possible to estimate the amount of S/IVOCs emissions for a corresponding POA emission rate. However, Figure 1.18 is taken from a single fuel type, so the validity of extrapolating these results to a global POA emissions inventory remains unclear. Using this method, the amount of missing S/IVOCs has been estimated to range from a factor of 0.25 to 2.8 of POA emissions (Robinson et al., 2010;Shrivastava et al., 2008). Estimated global annual-total S/IVOC emissions are shown in Figure 1.19, and range from 54 (Hodzic et al. (2016) to 450 Tg a^{-1} (Shrivastava et al., 2015) (Figure 1.19).

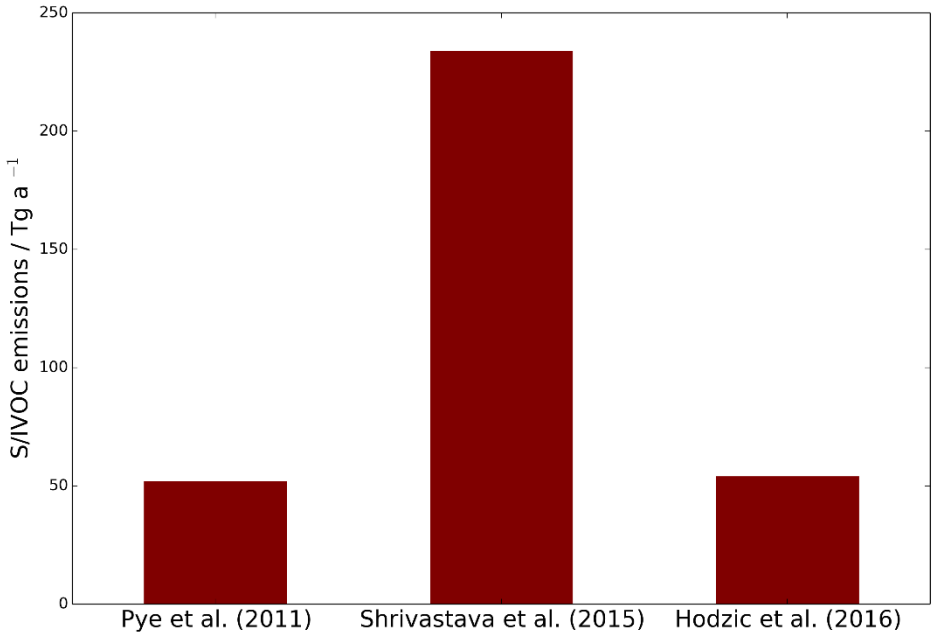

Figure 1.19 – Estimates of global annual-total S/IVOC emissions from the literature.

1.7 Production of SOA

The emitted hydrocarbons (Section 1.6) are now discussed in terms of their oxidation and propensity to form SOA. Note, the oxidation pathways and SOA production strength are known with varying degrees of certainty across these sources.

1.7.1 Production of SOA from isoprene

Isoprene is one of the most abundant VOCs in the atmosphere (Section 1.6.2) and is relatively reactive towards oxidation (Figure 1.2). Through its

abundance and high reactivity, isoprene affects may aspects of chemistry, such as methane (Safieddine et al., 2017) and ozone (Geng et al., 2011). Consequently, considerable effort has been invested into elucidating the oxidation of this species (Paulot et al., 2009;Peeters et al., 2009;Peeters and Nguyen, 2012). Early studies conclude that isoprene oxidation products are too volatile to condense, leading to isoprene being discarded as a potential source of SOA. However, today, isoprene is considered a major source of SOA, due to both low-volatility and soluble oxidation products.

Figure 1.20 shows a simplified version of isoprene photooxidation, taken and adapted from various studies (Carlton et al. (2009), Marais et al. (2016) and Shrivastava et al. (2017)). Note, within this reaction cascade, oxidation channels are known with varying degrees of certainty. Isoprene photooxidation is initiated by addition of the hydroxyl racial followed by rapid addition of molecular oxygen (O_2), resulting in the formation of the hydroxyl peroxy radical ($ISOPO_2$) (Figure 1.20). Under low-NOx conditions, $ISOPO_2$ can react with HO_2, leading to the production of a hydroxyl peroxide (ISOPOOH) (Figure 1.20). This species can then react with another HO_2 to form C5 LVOC (Krechmer et al., 2016), or with OH followed by isomerization to form C5 epoxydiol (IEXPOX) (Paulot et al., 2009), both of which, are key precursors of SOA formation under low-NOx conditions (Figure 1.20). Alternatively, under high-NOx conditions, $ISOPO_2$ can react with NO, leading to the formation of small volatile fragments, such as methyl vinyl ketone (MVK), methacrolein (MACR) (Carlton et al., 2009), as well as carbonyls and nitrates (Lockwood et al., 2010) (Figure 10). Further photooxidation of MACR leads to the formation of C5 hydroxyepoxides (MEXPOX), a key precursor to SOA formation under high-NOx conditions (Lin et al., 2013). Finally, if concentrations of both HO_2 and NO are low, $ISOPO_2$ can undergo unimolecular isomerization, leading to the production of hydroxyperoxy aldehyde (HPALD) (Figure 1.20), which is also an important precursor of SOA (Nguyen et al., 2010;Crounse et al., 2011).

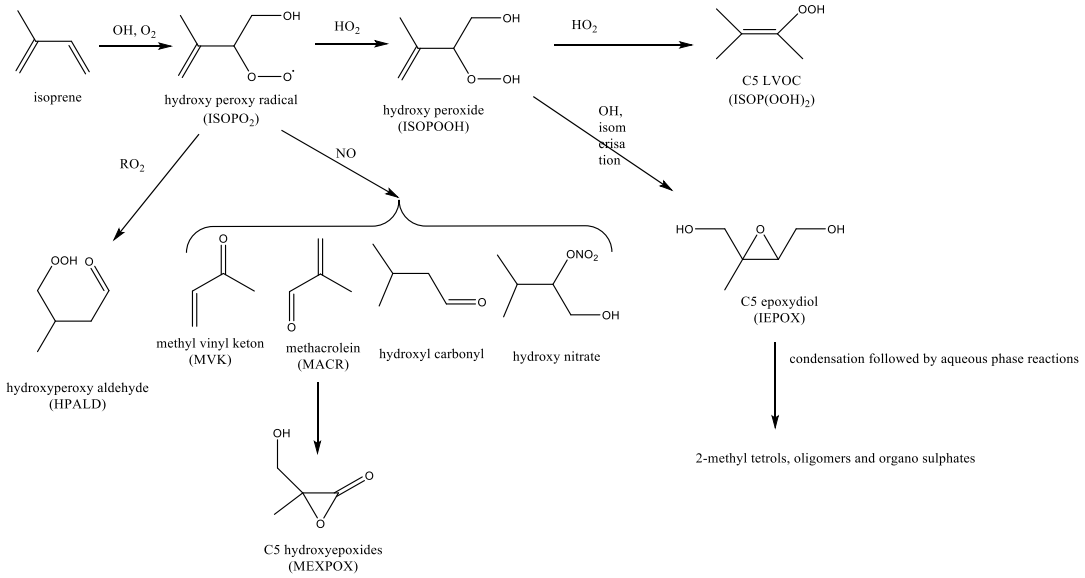

Figure 1.20 - Schematic diagram of isoprene oxidation, adapted from Carlton et al. (2009), Marais et al. (2016) and Shrivastava et al. (2017).

With environmental chambers, when a gas-phase species is subjected to oxidation, the amount of SOA formed relative to the amount of gas-phase organic that has reacted, is termed the ‘SOA yield’. This yield can either be expressed in terms of a mass or molarity (i.e. moles). Under laboratory conditions, at extremely high isoprene concentrations, an SOA yield of 0.8 % is observed from isoprene Pandis et al. (1991). This small SOA yield at unrealistically high isoprene concentrations implies isoprene is not a significant source of SOA in the atmosphere. Crucially, in this experiment, no pre-existing aerosol mass (‘aerosol seed’) is used. Also, at the time of this study, the identity of many isoprene photooxidation products were virtually unknown. However, later field studies over the Amazon reveal the importance of isoprene as a source of SOA (Claeys et al., 2004). This is due to the identification of 2-methyltetrol in ambient samples of SOA (Figure 1.20). 2-methyltetrol has a molecular structure that strongly resembles isoprene but is not directly emitted, hence, it is an ‘isoprene SOA tracer’.

Today, this tracers is now known to be a product of aqueous phase oxidation of IEPOX (Peeters et al., 2009;Peeters and Nguyen, 2012), as shown in Figure 1.20.

This new observational evidence motivates the re-evaluation of the strength of SOA formation from isoprene. More recent chamber-derived SOA yields from isoprene range from 0.2 to 23 % (Edney et al., 2005;Kroll et al., 2005, 2006;Dommen et al., 2006;Kleindienst et al., 2007;Ng et al., 2008), and are dependent on the initiating oxidant, seed particles, humidity and most notably, NO_x. In particular, SOA yields decrease with rising NO_x levels – however, the exact cause for this sensitivity is unknown (Kroll et al., 2005, 2006;Ng et al., 2007a).

1.7.2 **Production of SOA from monoterpenes**

Monoterpene consists of two isoprene units, and has the chemical formula $C_{10}H_{16}$ (Figure 1.15). This class of compound can be either linear (acyclic) or can contain rings (cyclic). Of all the monoterpene isomers, the cyclic species, α-pinene, is emitted in the largest quantities, representing ~50 % of the global annual-total monoterpene emission rate.

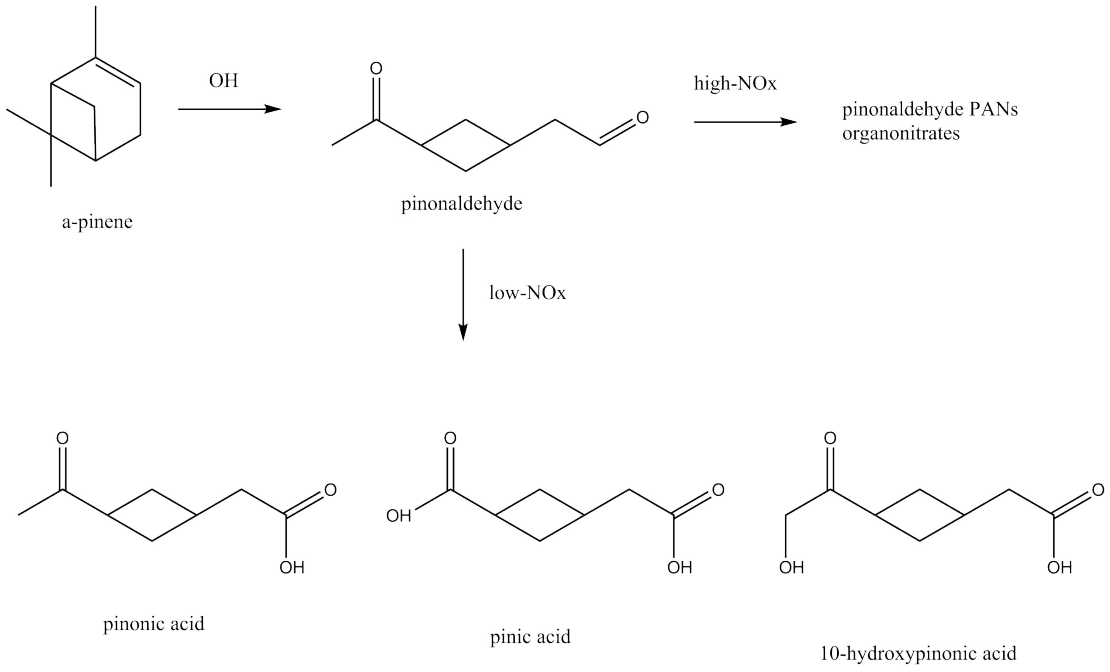

Figure 1.21 – Schematic diagram of oxidation of α-pinene by OH, taken and adapted from (Eddingsaas et al., 2012b;Eddingsaas et al., 2012a)

Figure 1.21 shows a simplified description of α-pinene photooxidation, adapted from Eddingsaas et al. (2012a) and Eddingsaas et al. (2012b). Irrespective of initial conditions, photooxidation of α-pinene leads to production of pinonaldehyde (Figure 11). This product is extremely important for SOA formation, yet the yield of this species from α-pinene is highly uncertain, ranging from 20 to 80 % (Arey et al., 1990;Noziere et al., 1999;Aschmann et al., 2002;Lee et al., 2006). The fate of pinonaldehyde governs the strength of SOA production. Under high-NOx conditions, pinonaldehyde peroxyacetyl nitrates and other organonitrates are formed (Figure 1.21). By contrast, under low-NOx conditions, carboxylic acids are formed, which are extremely polar and therefore have low vapour pressures (Figure 1.21). Examples of these low-volatility monoterpene photooxidatoin products include pinonic acid, 10-hydrooxypinoic acid and pinic acid (Figure 1.21), and have all been identified in ambient SOA samples (Kavouras et al., 1998, 1999;Anttila et al., 2005).

As an alternative to pinonaldehyde, under certain conditions, α-pinene can form extremely-low volatility organic compounds (ELVOC). In this case, the α-pinene peroxy radical undergoes numerous generations of autooxidation reactions (Ehn et al., 2014). This ELVOC formation is unique to monoterpene.

Overall, laboratory derived SOA yields from monoterpenes range considerably. This is due to differences in chamber conditions, such as temperature, humidity seed particles and initiating oxidant. For example, Eddingsaas et al. (2012a) find that the SOA yield from α-pinene varies from 8 – 37 %. Also, the measured SOA yield from monoterpenes reduce with increasing levels of NO_X (Eddingsaas et al., 2012a;Sarrafzadeh et al., 2016). The increasing SOA yield from α-pinene with decreasing NO_X concentrations is due to the effect of NO_X on pinonalehyde oxidation. However, the distribution of products from both these pathways are virtually unknown, both the identity and the corresponding volatility distribution.

1.7.3 **Production of SOA from sesquiterpenes**

Sesquiterpenes consist of three isoprene units (Figure 1.15). These species are extremely reactive and therefore oxidized on a timescale of minutes. Of all the sesquiterpenes, β-caryophyllene is one of the most abundant and well-studied, however, the oxidation mechanism is still relatively unclear (Lee et al., 2006;Ng et al., 2006;Chan et al., 2011). Overall, observed SOA yields from, β-caryophyllene range from 6 to 125 % (Hoffmann et al., 1997;Griffin et al., 1999;Ng et al., 2007a;Winterhalter et al., 2009;Alfarra et al., 2012;Chen et al., 2012;Jaoui et al., 2013). Note, an SOA yield which exceeds 100 % is possible when oxidation leads to the addition of functional groups, such as alcohols (Figure 1.16) and carboxylic acids (Figure 1.17). In contrast to isoprene (Section 1.7.1), monoterpene (Section 1.7.2) and aromatics

(Section 1.7.4), the SOA yield from sesquiterpenes increases with increasing levels of NOx (Ng et al., 2007a;Tasoglou and Pandis, 2015). However, the mechanistic description of β-caryophyllene oxidation which accounts for the influence of NO_X on the SOA yield is lacking from the literature.

1.7.4 **Production of SOA from aromatics**

Early estimates of SOA yields from aromatic compounds, which are conducted in relatively high NO_x concentrations, range between 5 and 10 % (Odum et al., 1997;Odum et al., 1996). However, more recent chamber studies suggest the SOA yields from aromatic compounds are strongly influenced by NO_x concentrations (Hurley et al., 2001;Song et al., 2005;Ng et al., 2007b;Chan et al., 2009). For example, in agreement with early estimates (Odum et al., 1996;Odum et al., 1997), Ng et al. (2007b) also observes an SOA yield from aromatic VOCs of 5 – 10 % under high-NO_X conditions. However, under lower NO_X concentrations, Ng et al. (2007b) measures substantially higher SOA yields of 37, 30 and 36 % for benzene (C_6H_6), toluene (C_7H_8) and xylene (C_8H_{10}), respectively. Under low-NO_X conditions, Chan et al. (2009) observes a much higher SOA yield of 73 % from naphthalene ($C_{10}H_8$).

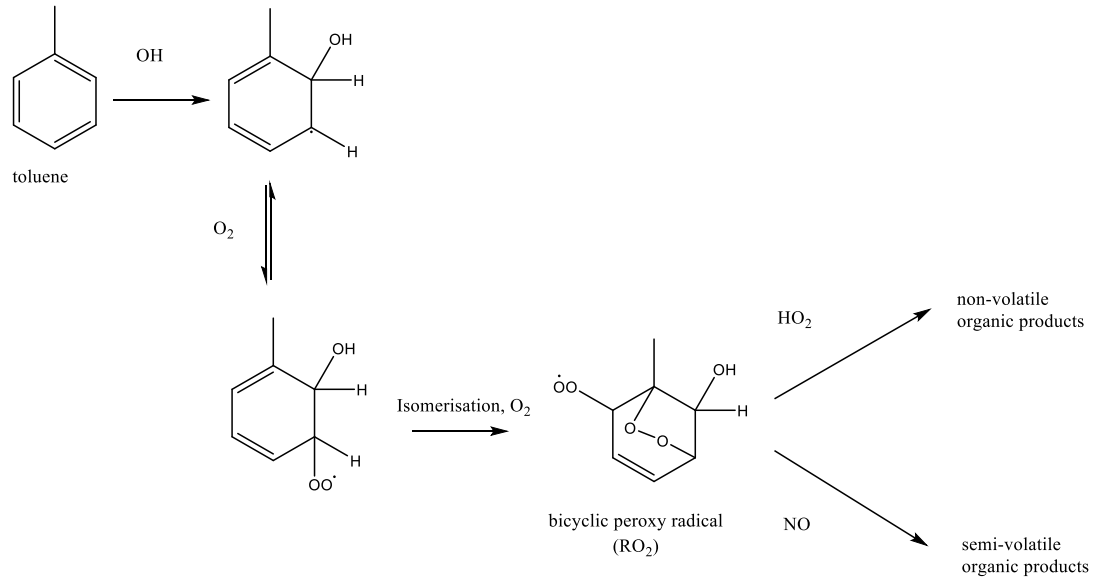

Figure 1.22 - Formation of lower volatility vapours (i.e. SOA precursors) from toluene photooxidation, as described in Ng et al. (2007b).

The exact mechanism describing aromatic oxidation is not yet fully understood, despite considerable progress to date (Kautzman et al., 2010;Li et al., 2016;Al-Naiema and Stone, 2017;Li et al., 2017b;Schwantes et al., 2017). Figure 1.22 shows a mechanistic description of SOA production from toluene, accounting for the influence of NOx on SOA production, adapted from Ng et al. (2007b). As aromatic oxidation is initiated by the hydroxyl radical (OH), the influence of NO_x on SOA production is probably due to reaction of NO with second or later generation oxidation products. Oxidation of the parent aromatic hydrocarbon by OH is followed by addition of molecular oxygen (O_2) and isomerization, forming a bicyclic peroxy radical, RO_2 (Johnson et al., 2004;Koch et al., 2007) (Figure 1.22). Under high-NO_X conditions, the peroxy radical reacts with the nitric oxide radical (NO) to form semi-volatile products, whereas, under low-NO_X conditions, the peroxy radical reacts with the hydroperoxyl radical (HO_2) to form non-volatile products (Ng et al., 2007b) (Figure 1.22). Hence, due to the difference in volatility of products, the RO_2+HO_2 yields a greater mass of SOA compared

to the RO_2+NO pathway. Water vapour may also be involved in the gas-phase oxidation of aromatic compounds (Hinks et al., 2018). However, as both positive (White et al., 2014) and negative (Cocker et al., 2001) correlations between aromatic SOA yields and relative humidity are observed in chamber studies, the role of water vapour in aromatic oxidation is not yet clear.

1.7.5 **Production of SOA from S/IVOC emissions**

Emitted S/IVOCs (Section 1.6.3) can also lead to production of SOA, either by directly partitioning or by oxidation followed by gas-to-particle partitioning. Several field and laboratory studies suggest SOA produced from S/IVOC emissions exceeds SOA produced from VOC emissions (Robinson et al., 2007;Gentner et al., 2012;Zhao et al., 2014). Note, SVOCs are less volatile than IVOCs (Figure 1.13). Subsequently, SVOCs can condense into the aerosol phase. By contrast, similar to VOCs, IVOCs require oxidation (and reductions in volatility) before condensation.

Upon emission, SIVOCs undergo a reaction cascade, leading to the formation of lower volatility products, including carboxylic acids, nitrates, and carbonyls (Pankow and Asher, 2008). Evidence of this mechanism is provided by both laboratory (Grieshop et al., 2009) and field studies (Lee et al., 2008).

Emitted IVOCs are too volatile to directly condense, hence, oxidation is mandatory before partitioning into the aerosol phase. Naphthalene, a polycyclic aromatic IVOC (Figure 1.17), undergoes photooxidation similar to monocyclic aromatic VOCs (e.g. toluene; Figure 1.16), as shown in Figure 1.22.

1.7.6 **Production of SOA from POA**

The traditional conceptual framework of OA assumes POA is non-volatile. In this case, after being emitted, POA would simply return to the surface of Earth via deposition. This conceptual framework has been redefined, now, POA is assumed to be semi-volatile (Robinson et al., 2007). If POA re-evaporates, generating gaseous organic compounds, these compounds may re-condense, where they would then be classified as SOA. Hence, moving away from a non-volatile approach, to a semi-volatile approach of SOA results in an additional source of SOA and an additional sink of POA.

1.7.7 **Production of SOA within the aqueous phase**

After several generations of oxidation, many organic gases lead to the production of small polar VOCs. For example, CO and CH_4 oxidation lead to the formation of formaldehyde (Section 1.2.2-1.2.3). Larger VOCs, like those discussed in this section (isoprene, monoterpene, aromatics), also lead to the production of small polar VOCs, including glyoxal, methylglyoxal, glycolaldehyde, pyruvic acid, and acetic acid and IEPOX (Eddingsaas et al., 2010;Surratt et al., 2010;Rossignol et al., 2014;El-Sayed et al., 2015;Sareen et al., 2016). The small size of these compounds prevents gas-to-particle partitioning (small size = volatile). However, the high polarity of these species allows dissolution in cloud and aerosol liquid water (Figure 1.12). Conditions within the aqueous phase are extremely different to the gas phase. Aqueous-phase oxidation of these carbonyls leads to the production of carboxylic acids such as oxalic acid, which have a low vapour pressure. After liquid water evaporation, these low-vapour pressure oxidized species remain in the

aerosol phase (Volkamer et al., 2007;Ervens, 2015). Hence, cloud and aerosol liquid water provide a medium for small polar species to be form SOA.

1.8 Processing and properties of SOA

Once formed, the fate and impacts of SOA are governed by the environmental conditions and the properties of the particles. However, the properties of the particle can continue to evolve via particle-phase processes (aging). In this section, the processing/aging (Section 1.8.1) and properties (volatility, state, hygroscopicity; Section 1.8.2- 1.8.4) of SOA are discussed.

1.8.1 Particle processing

Gas-phase and aqueous-phase oxidation of organic compounds can result in changes in volatility. For a given gas or aqueous-phase organic compound, it can condense into the aerosol phase. Within the aerosol phase, the organic compound can underdo further physical and chemical processing, otherwise known as heterogeneous reactions or aerosol ageing. The importance of aerosol aging is that this processing can continue to alter the volatility of a compound. Hence, once condensed, heterogeneous reactions further alter the fate of the organic compound, by either increasing or decreasing the volatility.

Figure 1.23 shows an example of an aerosol phase reaction of two identical organic species (monomers). These monomer units join in a process known as accretion (or oligomerization), to form an accretion product (or oligomer) (Figure 1.23). An infinite number of monomer units can join

together. In the case where two monomer unit join together, the process is referred to as dimerization, leading to the formation of a dimer.

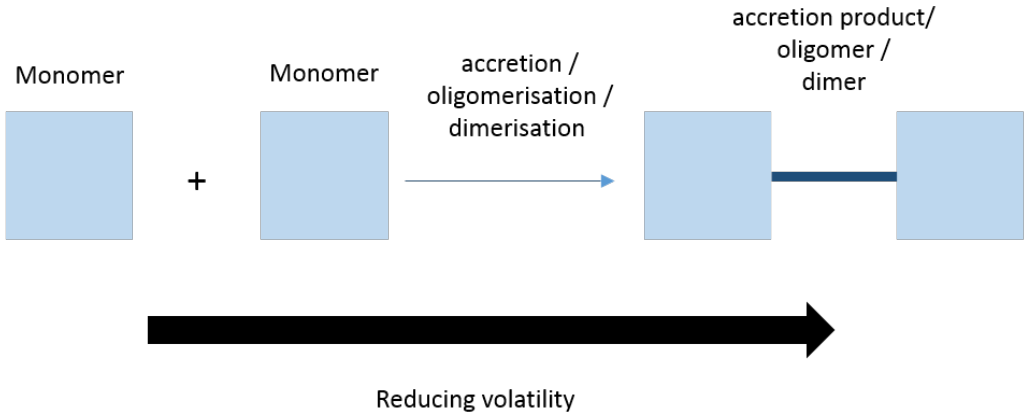

Figure 1.23 Schematic diagram showing how monomer units can combine, leading to reductions in volatility.

The density of organic compounds with an aerosol particle is higher than in the gas-phase. Hence, aerosol brings organic compounds into close contact with one another. This close contact within aerosol particles increases the probability of oligomerisation (Figure 1.23). Indeed, aerosol phase accretion reaction of organic compounds is observed (Gao et al., 2004;Cappa and Wilson, 2011;Lopez-Hilfiker et al., 2016). Oligomerisation is dependent on the structure of condensed phase organics and the environmental conditions, and leads to a variety of products including peroxyhemiacetals, esters, and hemiacetals (Shrivastava et al., 2017). Note, the products of oligomerization are larger than the monomer units, hence, overall, oligomerization leads to reductions in volatility of organic compounds. In addition, the presence of sulphate within the aerosol phase can lead to the production of organosulphates (Zhang et al., 2004;Wang et al., 2010) Organosulphates are more polar than the reacts (e.g. hydrocarbon + sulphur

compounds) and are, therefore, less volatile than pure hydrocarbons. Therefore, similar to oligomerisation, organosulphate production leads to the generation of lower volatility organic compounds.

1.8.2 **Particle volatility**

Volatility (section 1.4.4) is also an important aspect of OA. Figure 1.24 is a schematic diagram showing how semi-volatile and non-volatile SOA are formed. Note, for each pathway in Figure 1.24, the volatility of the parent hydrocarbon is undefined. In the first case (Figure 1.24 a), parent hydrocarbons are oxidized, leading to the generation of semi-volatile organic vapours. These semi-volatile vapours are in equilibrium with the aerosol phase. Hence, in this case, SOA is semi-volatile (Figure 1.24 a). Similarly, in the next case, hydrocarbons are oxidized to form semi-volatile compounds which are in equilibrium with the gas-phase (Figure 1.24 b). However, in this case, particle phase reactions lower the volatility (e.g. Section 1.8.1), leading to the production of non-volatile SOA (Figure 1.24 b). Finally, for some hydrocarbons, gas-phase oxidation can lead to the production of non-volatile gases (e.g. Crounse et al. (2013)) which condense into the aerosol phase, forming non-volatile SOA (Figure 1.24 c). Overall, the volatility of SOA is influenced by the parent hydrocarbon and the mechanisms of oxidation.

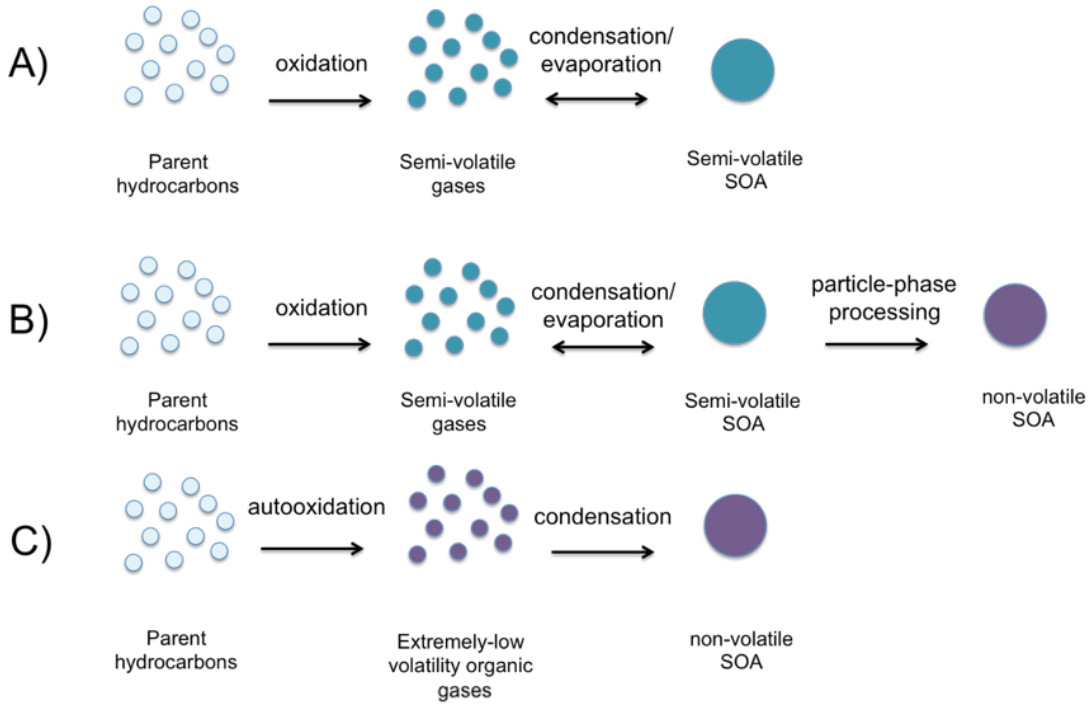

Figure 1.24 – Schematic diagram illustrating how the mechanism of SOA production partially governs the volatility of SOA.

Figure 1.25 shows the fraction of OOA which is semi-volatile (SV-OOA) and low-volatility (LV-OOA), taken from Jimenez et al. (2009). The variability in volatility observed across OOA (Figure 1.25) is dependent on the gas and particle phase processing that the organics have been subjected to (Figure 1.24). Oxidation products from monoterpenes are predominantly compounds with extremely low volatility, so-called ELVOCs, (e.g. Ehn et al. (2014)).However, combustion OA, either generated from gasoline (May et al., 2013c) or diesel (May et al., 2013b) within laboratory studies suggests OA is primarily semi-volatile. Also, analysis of OA emitted from the burning of vegetation within laboratory studies suggests OA is semi-volatile (May et al., 2013a). However, some specific cases suggest a proportion of OA is non-volatile (Jimenez et al., 2009;Cappa and Jimenez, 2010;Vaden et al., 2011).

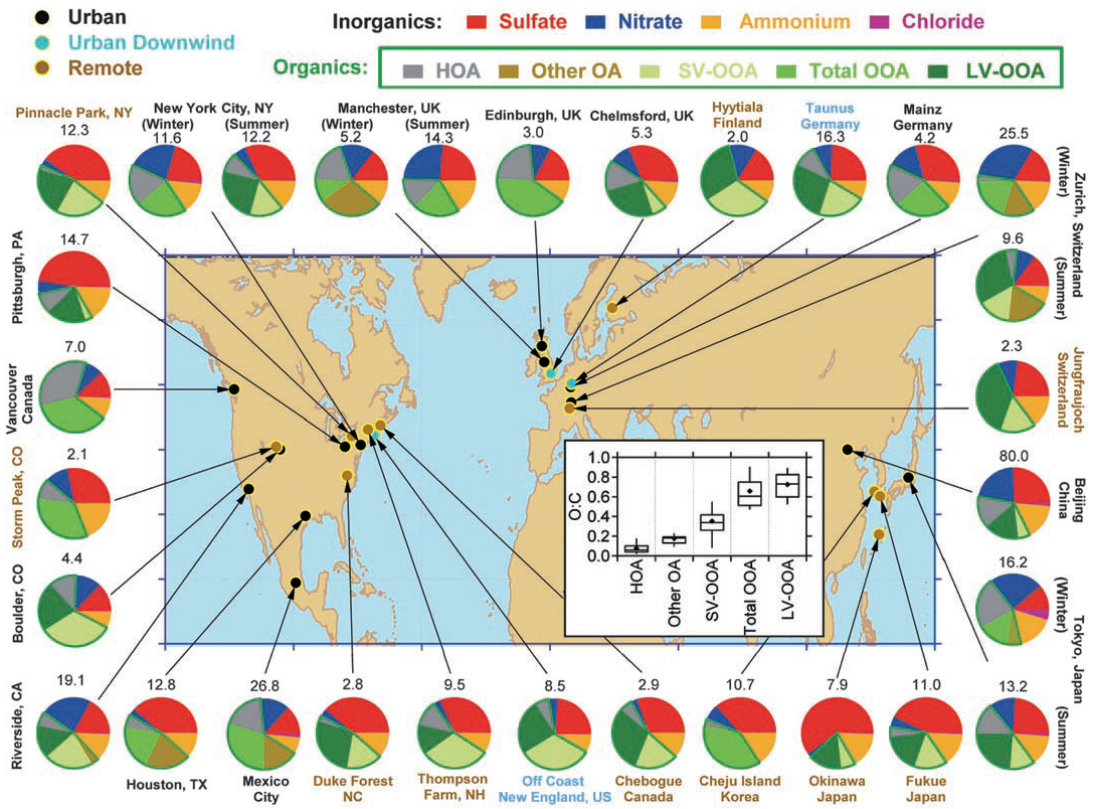

Figure 1.25 – Diagram showing submicron aerosol mass concentrations for the sites shown in Figure 1.4 (Zhang et al., 2007). OOA is further classify OA according to volatility; low-volatility OA (LV-OOA) and semi-volatile OA (SV-OOA) (Jimenez et al., 2009).

1.8.3 **Particle state and viscosity**

Figure 1.26 shows how particles can vary in state and viscosity. Traditional gas-to-particle partitioning theory (Pankow, 1994) assumes the particle is a well-mixed liquid-like solution, as shown for Figure 1.26 a. If a particle is semi-volatile, organic compounds partition between the aerosol and gaseous states in order to achieve equilibrium. Viscosity is a measure of the friction

between molecules of a liquid. The low viscosity of a liquid allows molecules to diffuse through the aerosol, achieving almost instantaneous equilibrium. However, according to chamber studies, SOA is solid-like (Virtanen et al., 2010). For a well-mixed semi-solid particle (Figure 1.26 b), gas-aerosol partitioning is dependent on the viscosity and size. As the viscosity of a well-mixed semi-solid particle increases, diffusion reduces, and therefore, increases the time required to reach equilibrium. Also, reaching equilibrium is delayed as the size of the particle increases. Finally, for some semi-solid particles, the various components within the particle can phase separate (Bell et al., 2017). For example, consider the example Figure 14 c, where the core and surface are separated. If the semi-volatile SOA were the core, then surface shell could prevent evaporation. Similarly, semi-volatile vapours may be prevented from condensing by the surface layer.

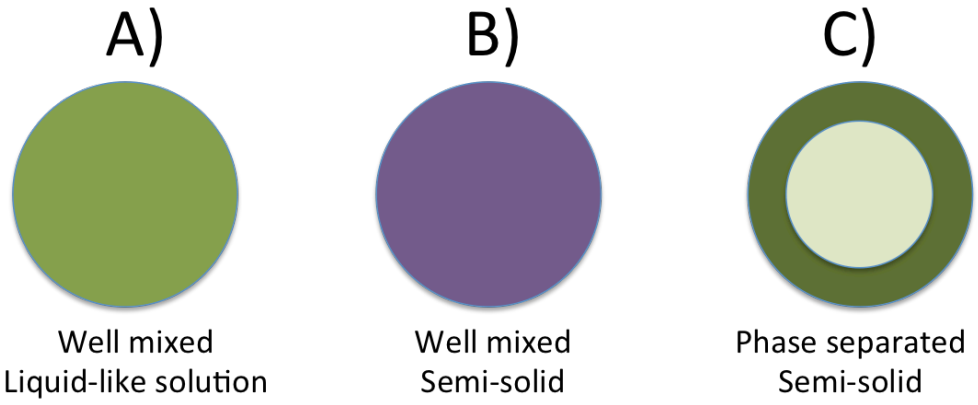

Figure 1.26 – Schematic diagram of SOA particles, illustrating importance of phase (i.e. viscosity) and morphology.

The viscosity of a particle is dependent on both relative humidity, and the chemical composition of organic molecules within the particle. Viscosity reduces with increasing relative humidity (Hinks et al., 2016). Also, oligomerisation and accretion reactions generate larger molecules, leading to increases in viscosity (Pfrang et al., 2011).

1.8.4 **Particle hygroscopicity**

The growth of nanometer sized particles to CCN (Figure 1.3) is primarily due to condensing organic vapours (Riipinen et al., 2011;Riipinen et al., 2012). Particles with a diameter less than 40 nm are too small to be active as CCN. Within the 40 – 200 nm size range, the hygroscopicity of the particle is a key parameter is determining if the particle can be activated as a CCN. Particles with diameters exceeding 200 nm are large enough to contain sufficient quantities of water such that they are activated as CCN. The hygroscopicity parameter is a dimensionless quantity, and defined as the volume-weighted hygroscopicity of the various components within the aerosol. Hence, in regions where SOA is a large fraction of aerosol, the hygroscopicity of SOA can influence the aerosol-cloud interactions.

The observed hygroscopicity parameter of SOA varies from 0 to 0.3 (Jimenez et al., 2009). Atmospheric aging of SOA may influence the hygroscopicity of the particle, however, some studies predict increased hygroscopicity with ageing (Pajunoja et al., 2015), whereas other studies suggest decreased hygroscopicity with SOA ageing (Cerully et al., 2015). For comparison, the observed hygroscopic parameter ranges 0.035 - 0.040 for black carbon (Peng et al., 2017), and 0.4 – 0.8 for inorganic aerosol (Tikkanen et al., 2018)

1.9 A global perspective of the SOA lifecycle in the present-day

All the previous discussion on the SOA lifecycle (sections 1.5 – 1.8) predominantly derives form laboratory and field studies (with the exception of global emission rates; Section 1.6). These studies provide insights into the SOA lifecycle at the molecular level. However, it is challenging to extrapolate these results to the global scale and to different time periods. Global models and satellites provide a global perceptive of the SOA lifecycle in the past, present and future. This section provides a summary of how the global SOA budget is estimated (1.9.1 and 1.9.2), how SOA formation can be parametrised (Section 1.9.3), and it's sources (1.9.4), the processing of precursors (1.9.5). This section then concludes with a discussion on how future changes in climate and emissions may influence the SOA lifecycle (Section 1.9.6).

1.9.1 The observed SOA budget (top-down methods)

There are several top-methods for estimating the global SOA budget. Firstly, the global SOA budget can be inferred from the sulphate budget, which is relatively well-established. This is achieved by measuring the ratio of sulphate to SOA in aerosol samples, and then applying this ratio to the global sulphate budget. Using this approach, Goldstein and Galbally (2007) estimate a global annual-total SOA production rate of between 280 and 1820 Tg (SOA) a^{-1}, but Hallquist et al. (2009) estimate a lower value at 230 Tg (SOA) a^{-1}. This top-down method for estimating the SOA budget is relatively crude (e.g. it assumes that the observed SOA to sulphate ratio is globally uniform).

Aerosol optical depth (AOD) is a measure of how much light transmission is prevented by aerosol due to the absorption and scattering of light. The AOD can be measured from satellites. AOD is a reflection of the optical properties of all aerosol components within a column. Using satellite AOD, Heald et al. (2010) estimates a global annual-total SOA production rate of 250 Tg (SOA) a^{-1}. The assumed optical properties of SOA are a major source of uncertainty in this method.

In situ observations of SOA mass concentrations can also be utilized to provide a top-down estimate of the SOA budget. For instance, observed SOA can be combined with a global model. The emissions of SOA precursors within the model can be varied until simulated and observed SOA concentrations agree, thus, providing an observationally-constrained top-down estimate of the global SOA budget. Using this very method, Spracklen et al. (2011) estimate a global annual-total SOA production rate ranging from 50 to 380 Tg (SOA) a^{-1}, with a best estimate of 140 Tg (SOA) a^{-1} . However, this method requires SOA observations, which are currently very sparse (Figure 1.4).

In summary, several top-down methods for estimating the global SOA budget are used. Considering all estimates from top-down studies, the global annual-total SOA production rate ranges from 50 to 1820 Tg (SOA) a^{-1}.

1.9.2 **The modelled SOA budget (bottom up methods)**

Models apply a process-based design to provide bottom-up estimates of the global SOA budget. A schematic diagram of an atmospheric model is presented in Figure 1.27. Within the atmosphere, the concentration of both gases and aerosol are controlled by emissions, chemistry (removal and production), transport (e.g. winds), and deposition. These processes can all

be parameterized within a model. Models which contain only chemical reactions are referred to as box-models or 1D-models. If chemistry, emissions, transport and deposition are all accounted for, the model is described as either a (i) chemistry transport model (CTM) if the meteorology is provided from off-line reanalyses, or (ii) a chemistry-climate model (CCM) or composition-climate model (CCM) if the model is able to provide the on-line calculation of meteorology. A chemistry-climate model is used in this thesis and is described in chapter 2. When CCMs calculate meteorological fields online, the model is described as free-running. If the meteorology (i.e. potential temperature and horizontal wind) is corrected towards re-analyses, the models is described as nudged. Models vary in many ways, including the horizontal and vertical resolution, the domain (i.e. global or regional), and how chemical process are treated.

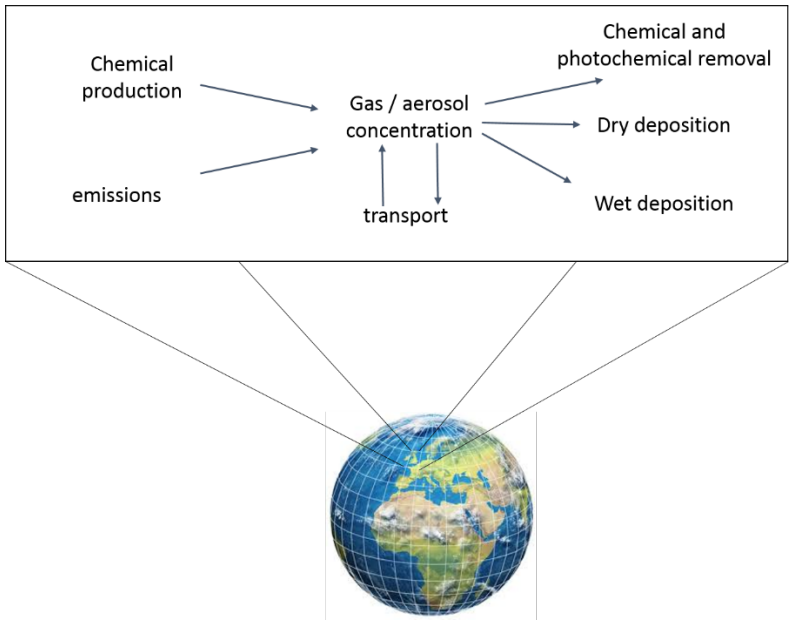

Figure 1.27 – Schematic diagram of an atmospheric model. Taken and adapted from Young et al. (2018).

The representation of gas-phase chemistry and aerosol-phase chemistry within atmospheric models is challenged by uncertainties in the physical and chemical processing of species within the atmosphere and by computational expense. For instance, treating aerosol populations is extremely challenging, which has led to a suite of parameterisations (Mann et al., 2014;Mann et al., 2010;Spracklen et al., 2005b, a). Of all the aerosol components, representing the SOA lifecycle in a model is particularly challenging.

Atmospheric models are widely used to examine the SOA budget. These bottom-up estimates of global annual-total SOA production range from 12 to 480 Tg (SOA) a^{-1} (Kanakidou et al., 2005;Heald et al., 2011;Tsigaridis et al., 2014;Shrivastava et al., 2015;Hodzic et al., 2016). Global chemistry transport models and general circulation model systematically underpredict observed OA concentrations in both urban (mean normalised bias = -62 %) and remote (mean normalised bias = -15 %) environments (Tsigaridis et al., 2014).

Global models also be used to estimate the climate impacts of SOA. For example, in a multi-model study, estimates of the increase in the global SOA burden since preindustrial times range from 0.09 to 0.97 Tg (SOA), which results in a direct radiative effect ranging from -0.21 to -0.01 W m^{-2} (Myhre et al., 2013). Treatment of SOA optical properties also varies between models and therefore contributes towards uncertainties in the climatic impacts of SOA (Tsigaridis et al., 2014). However, uncertainties in the climatic impacts of SOA appear to be dominated by uncertainties in the SOA budget, as opposed to the interaction between SOA and radiation (Rastak et al., 2017). Air quality and health impacts are also influenced by uncertainties in SOA concentrations which contribute to uncertainties in particulate matter levels.

The large inter-model spread in estimates of the SOA production rate could be due to differences in (i) how SOA formation is parameterized (Section 1.9.3), (ii) which sources of SOA are included and how they vary from one model to another (Section 1.9.4), and (iii) how the transformation of emitted hydrocarbons to SOA precursors is treated (Section 1.9.4). All of these are discussed in the following sub-sections.

1.9.3 **Modelling SOA formation**

Figure 1.28 shows a schematic representation of SOA formation. The processes displayed in Figure 1.28 are known with a varying degree of certainty. Firstly, the identity of dominant emitted hydrocarbons is uncertain (Section 1.7). Secondly, the certainty in the identity of oxidation products dramatically reduces with each successive generation of oxidation (Section 1.7). Hence, only a fraction of the species depicted in Figure 1.28 are known. This uncertainty is compounded by the fact that, of the identified species, only a fraction have laboratory derived data (e.g. rate constants, volatility, etc.). Finally, the sheer number organic compounds results in a large computational expense in treating the processes in Figure 1.28. As a result of these practical and scientific challenges, the formation of SOA within models requires parameterisations.

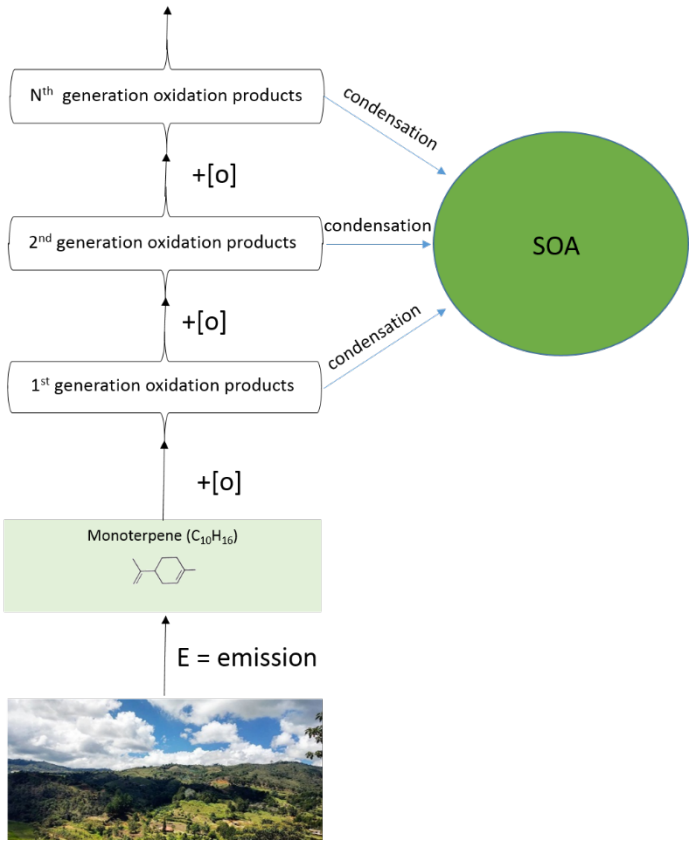

Figure 1.28 – Schematic diagram showing emissions of monoterpene, followed by multigenerational oxidation chemistry with simultaneous condensation into the aerosol phase.

In the simplest of schemes, production of SOA is calculated as a function of emissions, hence, SOA is 'emitted' as opposed to being formed in the atmosphere (Tsigaridis et al., 2014). For these schemes, a yield (α_E) is applied to the emission rate (E)

$$SOA\ production = E \times \alpha_E \qquad \text{(E1.1)}$$

In more sophisticated schemes, gas-phase oxidation of SOA precursors is treated, however, several simplifications are commonly made. For example, biogenic VOCs, such as isoprene and monoterpene, are known to have multigenerational oxidation mechanisms (Section 1.7.1-1.7.3), but the mechanisms are often reduced to less than two reaction steps when implemented in global models (Chung and Seinfeld, 2002;Heald et al., 2011;Scott et al., 2014;Scott et al., 2015). Similarly,

multigenerational oxidation mechanisms of aromatic compounds (Section 1.7.4) are often represented by less than two reaction steps (Tsigaridis and Kanakidou, 2003;Heald et al., 2011). Multigenerational oxidation mechanisms can be reduced to fewer reaction steps by adopting the fixed-yield approach, where a single yield (α) for oxidation of a VOC/HC is used to quantify the amount of low-volatility products (SOG).

$$HC + [O] \rightarrow \alpha SOG \xrightarrow{condensation} SOA \quad \text{(E1.2)}$$

In this case, $[O]$ represents oxidants, and SOG represents the entire population of multigenerational oxidation products that are condensable. Alternatively, multigenerational oxidation mechanisms can be simplified using the 2-products scheme (Odum et al., 1996;Odum et al., 1997). In this case, oxidation products are assigned to one of two surrogates (SOG_1 or SOG_2), with both condensing to form SOA

$$HC + [O] \rightarrow \alpha_1 SOG_1 \xrightarrow{condensation} SOA \quad \text{(E1.3)}$$

$$\rightarrow \alpha_2 SOG_2 \xrightarrow{condensation} SOA$$

In some schemes, organic compounds are lumped according to emissions types, such as anthropogenic or biomass burning (Spracklen et al., 2011;Hodzic et al., 2016), as is the case for this thesis (chapters 3 – 5). In other schemes, organic compounds are grouped according to volatility, such as the volatility basis set (VBS), (Donahue et al., 2006;Donahue et al., 2011). In this scheme, organic compounds are grouped either according to the volatility (one-dimensional), for volatility and O:C ration (two-dimensional). The volatility distribution is then modified according to environmental conditions, such as oxidants, and each volatility class is in equilibrium with both the gas and aerosol phase. The VBS scheme is used in several models (Tsimpidi et al., 2010;Jo et al., 2013;Hodzic et al., 2016;Shrivastava et al., 2015) .

By lumping organic species together, chemical ageing can be accounted for, even if the exact mechanism is not known. However, in grouping species together, molecular information is lost and it is therefore challenging to select the appropriate reaction coefficients and SOA yields from laboratory studies. In more complex SOA

schemes, gas-phase oxidation is treated explicitly (Lin et al., 2012;Lin et al., 2014;Khan et al., 2017), but this method is limited to SOA precursors with relatively well-known oxidation mechanisms. Overall, in terms of sophistication and level of detail, SOA formation parameterisations vary considerably across models (Tsigaridis et al., 2014). The sensitivity of SOA to these variations in oxidation mechanisms is unknown.

1.9.4 **SOA production from various sources**

Due to uncertainties in emissions (Section 1.6.2-1.6.3) and oxidation products (Sections 1.7), the sources of SOA considered in modelling studies also varies considerably. Global biogenic SOA production rate estimates (i.e. from vegetation) from global models range between 2.86 and 97.5 Tg (SOA) a^{-1} (Henze et al., 2008;Heald et al., 2008;Farina et al., 2010;Hodzic et al., 2016). Isoprene (Bonsang et al., 1992) and monoterpene (Yassaa et al., 2008) are also emitted from phytoplankton, leading to a global annual-total SOA production rate of 5 Tg (SOA) a^{-1} (Myriokefalitakis et al., 2010). Many global models only consider biogenic sources in their formation of SOA (Tsigaridis et al., 2014); other studies that include a number of different precursor types suggest that biogenic sources contribute 74 % (Hodzic et al., 2016) to 95 % (Farina et al., 2010) to the annual global total SOA production rate.

According to a number of laboratory studies, anthropogenic VOCs (e.g. aromatics) yield only a small amount of SOA (Odum et al., 1997). Therefore, the inclusion of anthropogenic SOA in global models based on such modest yields results with little SOA production (1.6 – 3.1 Tg (SOA) a^{-1}) and almost negligible SOA concentrations (Farina et al., 2010;Heald et al., 2011). However, over the NH mid-latitudes, observed SOA concentrations are highest in urban environments (Zhang et al., 2007). Indeed, in a top-down approach, where biogenic, biomass burning and anthropogenic SOA sources are scaled, Spracklen et al. (2011) finds that their simulated model bias is minimised when the global SOA budget is dominated by an anthropogenically--controlled source of ~100 Tg (SOA) a^{-1} and a biogenic SOA

production rate of 13 Tg (SOA) a^{-1}. The magnitude of anthropogenic SOA production as well as dominance over biogenic SOA production estimated in this top-down study is in contrast to bottom up estimates from global modelling studies. However, it remains unclear whether the anthropogenic dominance of global SOA production found in Spracklen et al. (2011) reflects the location of observations used to constrain this estimate since the observations are primarily located in the NH mid-latitudes where anthropogenic emissions are highest. Additionally, the reaction yield required to reach a production rate of 100 Tg (SOA) a^{-1} of anthropogenic SOA exceeds the reaction yield derived from earlier laboratory studies (Odum et al., 1997). Furthermore, a high SOA production rate from anthropogenic sources produces positive models biases compared to observed SOA concentrations in remote environments (Spracklen et al., 2011) and at higher altitudes (Heald et al., 2011). Hence, the magnitude of SOA production from anthropogenic sources remains unclear.

Using measurements, Cubison et al. (2011) estimates the global SOA production rate from biomass burning at 1 – 15 Tg (SOA) a^{-1}. This is consistent with Spracklen et al. (2011), who estimates a global SOA production rate from biomass burning of 3 – 26 Tg (SOA) a^{-1} using the same top-down approach described above. Anthropogenic and biomass burning emissions include S/IVOCs which, in addition to VOCs, can also contribute to SOA formation (Robinson et al., 2007), as discussed in Section 1.7.5. S/IVOCs are estimated to account for between 15 – 37 % of biomass burning carbonaceous emissions (Stockwell et al., 2015;Yokelson et al., 2013). Due to the limited knowledge of S/IVOCs emissions and chemistry, assumptions are required when implementing biomass burning S/IVOCs into global models. As a consequence biomass burning SOA production rate estimates from global models range substantially, from 15.5 Tg (SOA) a^{-1} (Hodzic et al., 2016) to 44 – 95 Tg (SOA) a^{-1} (Shrivastava et al., 2015). Therefore, biomass burning remains an additional highly uncertain and potentially important source of SOA.

The heterogeneous production of SOA may be an additionally important source of SOA, which is often not included in models (e.g., see Tsigaridis et al. (2014)). Soluble and polar organic vapours, which are too volatile to condense, may be taken up by the aqueous phase, either in aerosol liquid water or cloud liquid water

(Section 1.7.7). Within the aqueous phase, oxidation may lead to less volatile products which, after liquid evaporation, remain in the aerosol phase (Ervens, 2015). Recent estimates of the global annual-total SOA production rate within the cloud and aerosol phases are 13 – 47 and 0 – 13 Tg (SOA) a^{-1}, respectively (Lin et al., 2014;Lin et al., 2012). Thus aqueous production may be an important source of SOA, but several uncertainties remain, including the amount of cloud and liquid water in the atmosphere, and how to simulate the uptake of organic gases onto aqueous surfaces.

Overall, estimates of SOA production rates from individual sources ranges considerably from one modelling study to another. Furthermore, global models vary in terms of which sources are included. Together, these variations contribute to the overall uncertainty in the global SOA budget.

1.9.5 **Physical and chemical processing of SOA precursors**

Between emission and condensation into the aerosol phase, organic compounds undergo a range of complex multigenerational multiphase chemical and physical processes (Figure 1.12). Variations in the inclusion and treatment of these processes may contribute to the uncertainty in the SOA budget. Here, variations in SOA precursor deposition (Section 1.9.5.1) and oxidation (Section 1.9.5.2) are examined.

1.9.5.1 **Deposition of SOA precursors**

Deposition of organic compounds may prevent SOA formation. Recent field and modelling studies suggest several known SOA precursors are susceptible to deposition. For example, explicit modelling of the oxidation of terpene and aromatic VOCs identifies extremely soluble products, with effective Henry's constants (H_{eff}; Section 1.4.4) ranging from 10^5 to 10^9 M atm^{-1} (Hodzic et al., 2014). This suggests efficient wet removal of SOA precursors, considering H_{eff} for nitric acid (HNO_3) is ~2

$x10^5$ M atm^{-1} (Seinfeld and Pandis, 2006). However, the molecular-specific deposition parameters determined in field studies (Nguyen et al., 2015) can be difficult to apply to the lumped compounds used in global SOA schemes (Section 1.9.3). On a global scale, some modelling studies indicate a sensitivity of SOA to variations in precursor deposition (Henze and Seinfeld, 2006;Pye and Seinfeld, 2010;Hodzic et al., 2016). A few global modelling studies include both dry and wet deposition of SOA precursors, but the deposition parameters used vary across several orders of magnitude. For example, Shrivastava et al. (2015) use a value for H_{eff} of 7 $x10^3$ M atm^{-1}, whereas other studies use values ranging from 1 $x10^5$ to 5.3 $x10^9$ M atm^{-1} (Knote et al., 2015;Hodzic et al., 2016). In relation to dry deposition, field studies over forested regions of the USA observe significant dry deposition of highly oxygenated VOCs (Nguyen et al., 2015). The most rigorous studies on dry deposition have only been conducted using regional scale models. They find that dry removal of SOA precursors reduces modelled July-mean surface SOA concentrations by 20 – 40 % over Europe (Bessagnet et al., 2010), and reduces annual-average surface SOA concentrations by 46 % over the USA (Knote et al., 2015). Wet removal of SOA precursors reduces simulated annual-average surface SOA concentrations by 10 % over the USA, which reduces simulated positive biases in summertime SOA (Knote et al., 2015).

1.9.5.2 **Oxidation of SOA precursors**

The treatment of SOA precursor oxidation varies considerably from one model to another (Section 1.9.3). For instance, SOA is formed from aromatic VOCs only after several generations of oxidation (Section 1.7.4). However, this processes often simplified in global models.

As noted in Section 1.7.4, the SOA yields from aromatics is highly dependent on NOx conditions, as this influences the fate of the peroxy radical intermediate. For aromatic compounds, the peroxy radical reaction intermediate, together with competitive NO and HO_2 reactions with varying SOA yields (Figure 1.22) is incorporated in some SOA schemes. Benzene, toluene and xylene have been

incorporated into both global (Henze et al., 2008;Heald et al., 2011) and regional scale (Li et al., 2017a) models. Henze et al. (2008) uses the laboratory-derived yields from Ng et al. (2007b) for simulating aromatic VOC compounds (16 Tg (VOC) a^{-1}), which results in a global annual-total SOA production rate of 4 Tg (SOA) a^{-1}, with 61% of SOA being produced via the RO_2+HO_2 pathway (Fig 1.22). Peroxy radical chemistry is also applied to IVOC oxidation, which are a mixture of species emitted from both anthropogenic and biomass burning (Section 1.7.5). Pye and Seinfeld (2010) apply the laboratory-derived yields from Chan et al. (2009) to IVOCs (18 Tg (VOC) a^{-1}), which results in a global annual-total SOA production rate of 5 Tg (SOA) a^{-1}, with 75% of SOA being produced via the RO_2+HO_2 pathway. Despite peroxy radical chemistry being included in some SOA schemes (e.g. Henze et al. (2008) and Pye and Seinfeld (2010)), the influence on the global SOA budget and model agreement with observations has not been quantified.

To summarise, several aspects of the SOA lifecycle vary considerably from one modelling study to another, including how SOA production is parameterised (Section 1.9.3), which SOA precursor sources are included (Section 1.9.4.) and how these precursor are physically and chemically transformed (Section 1.9.5). The purpose of this section is to provide a brief summary of how SOA is represented in global models. The Aerosol Comparison between Observations and Models (AeroCOM) project includes a review of how OA is represented in CTMs and CCMs (Tsigaridis et al., 2014). Of the 31 models included in AEROCOM, 1 does not treat SOA production, but instead uses a climatology of aerosol concentrations. SOA production of the remaining models (30 models) is treated be either ‘pseudo emissions’ where an SOA yield is applied to biogenic emissions (13 models), a fixed yield approach where an SOA yield is applied to VOC oxidation (15 models), by explicitly treating multigenerational oxidation chemistry (1 model), or by representing multigenerational oxidation chemistry using the VBS (1 model). SOA production within the aqueous phase is treated by 4 models, and SOA production from S/IVOC emissions is treated by 1 model. Several (unquantified) members of the AEROCOM study do not include anthropogenic or biomass burring sources of SOA, assuming SOA is purely biogenic. In addition, whilst observational studies imply OA is mostly semi-volatile, only 13 models included in AEROCOM treat OA as non-volatile, with the remaining 17 models treating OA as non-volatile.

Earth system models (ESMs) are fully coupled climate models, including a GCM and other components of the Earth system, such as the ocean, biosphere, cryosphere and lithosphere. ESMs are used in the 5th phase of the Coupled Model Intercomparison Project (CMIP5), the output of which, contributes towards the Intergovernmental Panel on Climate Change (IPCC). The representation of the SOA lifecycle among these ESMs is even more limited than the CTM and CCMs counterparts (Tsigaridis et al., 2018)

1.9.6 **Projected changes in the SOA lifecycle**

The precursors of SOA are emitted from natural sources (e.g. vegetation (Guenther et al., 1995), soil (Bourtsoukidis et al., 2018) and phytoplankton (Moore et al., 1994)), and from biomass burning (van der Werf et al., 2010) and fossil fuel combustion (May et al., 2013c) (Section 1.6). Globally, modelling studies suggest 90 % of SOA is removed by wet deposition, with the remaining 10 % being removed by dry deposition (Tsigaridis et al., 2014). Both the sources and sinks of SOA are linked to meteorology, resulting in potential climate change impacts (Kulmala et al., 2004;Carslaw et al., 2010;Unger, 2014;Scott et al., 2018). In addition, since SOA is often a major component of particulate matter (Figure 1.4), future changes in SOA distributions influence air quality. Quantifying the extent to which the SOA lifecycle may change in the future is important for understanding future climate forcing by aerosols as well as for quantifying future air quality in terms of $PM_{2.5}$ concentrations.

Changes in climate affect oxidants, such as ozone (O_3) and the hydroxyl radical (OH) (Doherty et al., 2013;Voulgarakis et al., 2013), both of which control the volatility distributions of organic compounds. For semi-volatile SOA, organic compounds are in thermodynamic equilibrium between the aerosol phase and the vapour phase (Section 1.8.2). Therefore, the warming associated with climate change implies a decrease in the SOA burden since higher temperatures favour evaporation and disfavours condensation (Tsigaridis and Kanakidou, 2007). Projected changes in the hydrological cycle may also affect SOA distributions. Future changes in precipitation suggest modifications to the aerosol lifetime and burden (Allen et al. 2016; Hou et al., 2018). Global-average precipitation rates increase in the future (Collins et al., 2014). However, over the northern-hemisphere (NH)

mid-latitudes, large-scale precipitation reduces in the future, leading to a longer sulphate aerosol lifetime (Allen et al., 2016). Also, future changes in cloud droplets may affect aqueous phase SOA production (Lin et al., 2016).

Biogenic VOC emissions are affected by changes in climate, anthropogenic land-use and, for some compounds, atmospheric carbon dioxide (CO_2) concentrations. Isoprene and monoterpene account for ~65 % of the present-day global annual-total biogenic VOC emission rate (Guenther et al., 2012). These species are side products of leaf photosynthesis. Consequently, changes in light (Monson et al., 2007), temperature (Guenther et al., 1995) and water (Niinemets et al., 2010) can affect the emissions of these species by directly altering basal emission rates and by altering vegetation distributions (Schurgers et al., 2011). Above ambient CO_2 concentrations, the synthesis of isoprene and monoterpene may be inhibited ('CO_2 inhibition'). For several isoprene-emitting species, strong evidence of CO_2 inhibition is observed (Rosenstiel et al., 2003;Possell et al., 2005). In the case of monoterpene, CO_2 inhibition is only been observed in a limited number of monoterpene-emitting species (Llorens et al., 2009;Loreto and Schnitzler, 2010). Anthropogenic land-use can also affect biogenic VOC emissions (Unger, 2014). However, the plant species that emit isoprene and monoterpene are usually different. Generally, crops have low biogenic VOC emissions whereas woody vegetation has higher biogenic VOC emission rate. Therefore, agricultural expansion in forested regions may result in reduced biogenic VOC emissions (Rosenkranz et al., 2015).

Given SOA is potentially important from both air quality and climate perspectives, quantifying the SOA lifecycle in the present-day, and understanding how this may change in the future, is important. This can be achieved by using global chemistry-climate models and observations.

1.10 Research objectives of thesis

The overall aim of this thesis is to study the SOA lifecycle in detail. Specific objectives are to: quantify how variations in VOC emissions source type (Section 1.7.1-1.7.4) and VOC physical and chemical processing (Section 1.9.5) affect the SOA lifecycle (e.g. global SOA budget, SOA spatial distributions and model agreement with observations). The next objective is to quantify the sensitivity of the SOA lifecycle to future changes in climate and emissions (Section 1.9.6).

1.10.1 What is the impact of new biogenic, anthropogenic and biomass burning emissions on the SOA lifecycle?

Using a global chemistry-climate model, a number of VOC precursor source types of SOA are explored. In particular, isoprene, a lumped anthropogenic VOC, and a lumped biomass burning VOC are added to the existing model, which treats SOA formation from monoterpene only. A series of simulations are conducted to quantify how each new source of SOA affects (i) the global SOA budget, (ii) SOA spatial distributions, and (iii) model agreement with observations. Observations used to evaluate simulated OA concentrations are taken from surface and aircraft campaigns spanning urban, urban downwind and remote environments, as well as both hemispheres. Additional simulations are conducted to probe the sensitivity of SOA to VOC precursor reaction yields.

1.10.2 How do VOC deposition and oxidation mechanisms impact SOA production?

The SOA scheme in 1.8.1 is then used to explore the sensitivity of the SOA budget and model agreement with observations to uncertainties in precursor deposition and oxidation pathways. Firstly, gas-phase deposition is expanded to include all VOC precursors of SOA, with additional simulations testing the sensitivity of the SOA lifecycle to uncertainties in deposition parameters. Next, the oxidation pathway for anthropogenic and biomass burning VOC precursors of SOA are modified (accounting for the multigenerationsal chemistry described in Section 1.9.5.1). These modifications include (a) varying the parent hydrocarbon chemical reactivity, (b) varying the number of reaction steps, and (c) accounting for the influence of NOx on SOA yields.

1.10.3 How will projected changes in emissions and climate affect the SOA lifecycle?

Using the SOA scheme developed in 1.8.1, the effects of future changes in climate and emissions on the SOA lifecycle is quantified. This is done by conducting decadal time slice simulations, for the present-day (2000s) and the future (2090s) under the IPCC Representative Concentration Pathway (RCP) climate and emission scenarios. The relative roles of future changes in climate and emissions are quantified (i.e. climate change only versus emissions only).

Chapter 2 Description of model (HadGEM3-UKCA) and observations

The objectives if this thesis are to explore the SOA lifecycle in the present-day and future (Section 1.10). To achieve this, a global chemistry-climate model is used. Where necessary, biogenic VOC emissions are calculated interactively and simulated SOA and OA are compared to observations. This section includes a description of the chemistry-climate model, the observations used to constrain the model, and the modelling approaches used throughout this thesis.

For this thesis, the HadGEM3-UKCA chemistry-climate model is used, which is presented schematically in Figure 2.1. This chemistry-climate model comprises of atmospheric components: the Global Atmosphere 4.0 configuration (GA4.0; Walters et al. (2014)) of the Hadley Centre Global Environmental Model version 3 (HadGEM3; Hewitt et al., 2011) and the United Kingdom Chemistry and Aerosol (UKCA; Morgenstern et al., 2009; Mann et al., 2010; O'Connor et al., 2014) model and a land-surface component called the Global Land 4.0 (GL4.0) configuration of HadGEM3 (Walters et al., 2014) (Figure 2.1). Exchange between HAdGEM3 and UKCA at model timesteps allows gas and aerosol to be coupled to the atmospheric and land-surface components of the model.

This section is organised as follows. Firstly, the atmospheric (GA4.0) and land-surface (GL4.0) components of the climate model (HadGEM3) are described in Sections 2.1 and 2.2, respectively. Next, the stratosphere-troposphere gas-phase chemistry scheme (StratTrop; Section 2.3) and UKCA aerosol-scheme called GLOAMP-mode (Section 2.4) are discussed. Following this, the SOA lifecycle, which relies on a coupling between many components of the model, is described (Section 2.5). The suite of observations used to evaluate the model are then described in Section 2.6. This section then concludes with a brief overview of the various modelling approaches used across this thesis (Section 2.7).

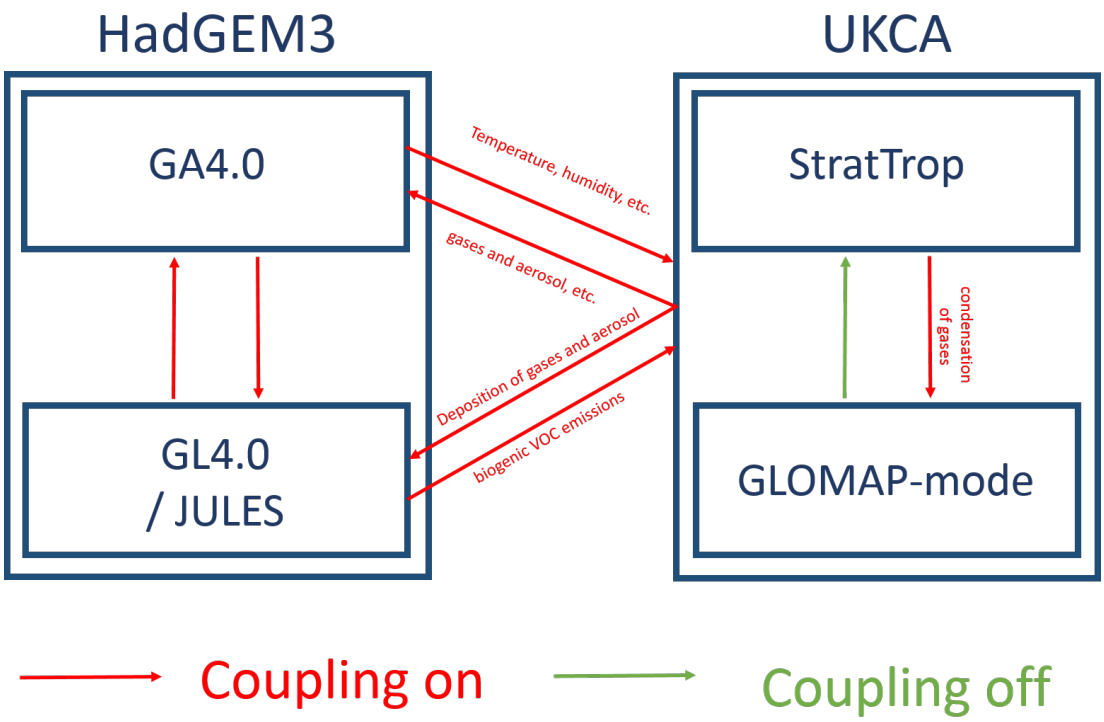

Figure 2.1 – Schematic diagram of HadGEM3-UKCA. Lines indicate how components of the model are coupled to one another, allowing exchange of variables (e.g. composition and dynamical processes).

2.1 Atmospheric component (GA4.0) of climate-model (HadGEM3)

In this section, the atmospheric component of the climate model is described. In this thesis, the Global Atmosphere 4.0 (GA4.0) configuration (Walters et al., 2014) of the Hadley Centre Global Environmental Model version 3 (HadGEM3; Hewitt et al. (2011)) is used (Figure 2.1). The horizontal resolution is 1.875° longitude by 1.25° latitude. The vertical dimension has 85 terrain-following hybrid-height levels distributed from the surface to 85 km. Sea-surface temperature (SST) and sea ice extent (SIE) fields are prescribed for all simulations. SST and SIE fields are then used to drive the meteorology. Hence, SST and SIE fields generally control the climate of the model. By varying the SST and SIE fields, different climate periods can be studied. In this set-up, where the meteorology and climate are driven by the SST

and SIE fields, the model is described as 'free running'. The HadGEM3-GA4.0 model has the option of 'relaxing (or 'nudging') the horizontal winds and potential temperature towards reanalyses data. This allows the simulated meteorology to closely match a given time period. In this set-up, where horizontal winds and potential temperature are being nudged towards reanalyses, the model is described as 'nudged'. Throughout this thesis, a combination of both nudged (Chapters 3 and 4) and free running (Chapter 5) simulations and performed.

Several different atmospheric dynamical processes relevant to the UKCA gas-phase (Section 2.3) and aerosol-phase (Section 2.4) tracers are calculated within GA4.0. In the HadGEM3-GA4.0 boundary layer scheme, atmospheric turbulent motion and tracer mixing is parametrised (Lock et al., 2000; Lock, 2001; Brown et al., 2008). Sub-grid scale transport of heat, moisture, momentum and UKCA tracers associated with cumulus clouds is treated within the convection scheme (Gregory and Rowntree, 1990). Large-scale advective transport follows Davies et al. (2005). Coupling between GA4.0 and UKCA (Figure 2.1) allows gases and aerosols to be incorporated into these dynamical processes. Note, although gases and aerosol can feedback onto climate via changes in radation, this feedback is off for all simulations performed in this thesis.

2.2 Land-surface component (GL4.0) of climate model (HadGEM3)

Emissions of isoprene (Section 1.6.2) and monoterpene (Section 1.6.2) can be calculated by the land-surface component of the model (Figure 2.1). The land surface component of HadGEM3 is the Global Land 4.0 (GL4.0) configuration of the Joint UK Land Environment Simulator (JULES; Best et al. (2011); Clark et al. (2011); Walters et al. (2014)). JULES simulates biogeophysical processes associated with land-atmosphere exchange. At the surface, there are 9 surface types. These are prescribed for all the simulations performed in this thesis. There are five plant functional types (PFT) (broadleaf trees, needleleaf trees, C_3 grass, C_4 grass, and shrubs) (see Section 2.5 for further details) and four non-vegetated surface types

(urban, inland water, bare soil, and ice). Photosynthesis within JULES is described by Cox et al. (1998)

Isoprene and monoterpene are mainly released from vegetation (Section 1.6.2). Emissions of these species can be calculated online within JULES and coupled to UKCA (Chapter 5). Alternatively, isoprene and monoterpene emissions can be prescribed (Chapters 3 and 4). Photosynthetic-based isoprene emission following Arneth et al. (2007b) are included in JULES following Pacifico et al. (2011). Here, isoprene emissions are linked to isoprene metabolism within plants (i.e. the supply of isoprene precursors). This method of calculating isoprene emissions is in contrast to semi-empirical approaches such as Model of Emissions of Gases and Aerosol from Nature (MEGAN), that are based on leaf-level relationships between isoprene emissions and temperature, light, etc. (Guenther et al., 2012). Simulated isoprene emissions under this photosynthetic-bases scheme has been evaluated extensively. Under present day conditions, simulated diurnal, day-to-day and seasonal variability in isoprene emissions are in reasonable agreement with observations over South America and East and South Asia (Pacifico et al., 2011). Isoprene emissions factors for each PFT are prescribed. An empirical factor, f_{CO2}, is used to account for CO_2 inhibition of isoprene production following Arneth et al. (2007b). Essentially, observed isoprene emissions are modified, accounting for changes in a number of factors, including photosynthetic rates and CO_2 concentration. Leaf-level isoprene emissions, I (kg C m^{-2} s^{-1}), are calculated following:

$$I = IEF \times s \times \frac{P+R}{P_{st}+ R_{st}} \times I_T \times I_{CO_2} \qquad \text{(E2.1)}$$

Where IEF is the PFT-specific isoprene emission factor (μg C gdw^{-1} h^{-1}), which is the isoprene emission rate under standard conditions (T = 303 K; photosynthetically active radiation (PAR) = 1000 μmol ,m^{-2} s^{-1}; atmospheric CO_2 concentration = 370 ppm). s is the specific density of leaf carbon (kg C m^{-2}), P is the net leaf photosynthesis (mol CO_2 m^{-2} s^{-1}) and R is dark respiration (mol CO_2 m^{-2} s^{-1}). The subscript 'st' denotes standard conditions. Hence, P_{st} represents net leaf photosynthesis at standard conditions (mol CO_2 m^{-2} s^{-1}) and R_{st} represents

respiration at standard conditions (mol CO_2 m^{-2} s^{-1}). I_T is an empirical factor (dimensionless), accounting for the influence of temperature on isoprene emission rate and is calculated following

$$I_T = \min\left[2.3; exp\left(\alpha(T - T_{st})\right)\right] \quad \text{(E2.2)}$$

Where α is an empirical constant (0.1 K^{-1}), T is the leaf temperature (K) and T_{st} is the leaf temperature at standard conditions (300.15 K).

I_{CO_2} is an empirical factor (dimensionless), accounting for the influence of CO_2 on isoprene emissions and is calculated following

$$I_{CO_2} = \frac{[CO_2]}{[CO_2]_{st}} \quad \text{(E2.3)}$$

Where $[CO_2]$ is the concentration of CO_2 within the leaf, and $[CO_2]_{st}$ is the concentration of CO_2 within the leaf under standard conditions.

Monoterpene emissions, M (kg C m^{-2} s^{-1}), are calculated following

$$M = MEF \times s \times M_T \quad \text{(E2.4)}$$

Where MEF is the PFT-specific monoterpene emission factor (μg C gdw^{-1} h^{-1}), s is the specific density of leaf carbon (kg C m^{-2}) and M_T is a temperature adjustment factor (dimensionless), calculated following

$$M_T = \exp\left(\beta(T - T_{st})\right) \quad \text{(E2.5)}$$

Where $\beta$is an empirical constant (0.09 K^{-1}), T is the leaf temperature (K) and T_{st} is the leaf temperature at standard conditions (300.15 K).

2.3 Gas-phase chemistry-scheme (StratTrop) of atmospheric composition component of the model (UKCA)

Atmospheric composition is simulated by the United Kingdom Chemistry and Aerosol (UKCA) model (Morgenstern et al., 2009; Mann et al., 2010; O'Connor et al. 2014) (Figure 2.1). The concentration of gas-phase species in UKCA is controlled through transport (Section 2.1), emissions (e.g. Section 2.2), chemical production, chemical removal, and deposition. The emissions used by UKCA vary throughout these thesis, so are discussed in relevant chapters. There are several different chemistry schemes which can be used by UKCA but here, 'StratTrop' chemistry scheme is selected; it combines the "TropIsop" tropospheric chemistry scheme from O'Connor et al. (2014) with the stratospheric chemistry scheme from Morgenstern et al. (2009). This chemistry scheme is used as the basis of this thesis, but evolves throughout the research chapters. StratTrop considers 75 species with 285 reactions. This includes odd oxygen (O_x), nitrogen (NO_y), odd hydrogen (HO_x = OH + HO_2), and carbon monoxide (CO). Hydrocarbons included are methane, C2 species (e.g. ethane), C3 species (e.g propane), and isoprene. Isoprene oxidation follows the Mainz Isoprene Mechanism (Poschl et al., 2000) which is described in detail by O'Connor et al. (2014). In addition to the aforementioned gas-phase species included in StratTrop, monoterpene and sulphur containing species (e.g. dimethyl sulfide) are also included, as these are precursors of aerosol. Photolysis rates are calculate online using the Fast-JX scheme (Neu et al., 2007). Unimoleuclar, bimolecular, trimolecular and termolecular reactions are all considered by UKCA-StratTrop. However, bimolecular reactions are most relevant for SOA precursors (Section 1.7.1-1.7.7). For bimolecular gas-phase reactions, rate constants are calculated following the Arrhenius expression

$$k = k_0 \left(\frac{T}{300}\right) exp\left(\frac{-\beta}{T}\right) \quad \text{(E2.6)}$$

where k_0 is the rate constant, β is the ratio of the activation energy over the universal gas constant (E_A/R), and T is temperature. The rate constant is then used to calculate the rate of reaction:

$$rate = k[A][B] \quad \text{(E2.7)}$$

where k is the rate coefficient, and [A] and [B] are concentrations of gases A and B, respectively. Table 2.1 lists kinetic data used in E2.6 for two species relevant to SOA forma, monoterpenes and isoprene.

Table 2.1 Kinetic parameters used to calculate rate coefficient (E2.6) for existing biogenic VOCs in UCKA model, taken from Atkinson and Arey (2003)

Reaction	k_0 / 10^{-12} x cm^3 $molecule^{-1}$ s^{-1}	B / K	k (298) / 10^{-12} x cm^3 $molecule^{-1}$ s^{-1}
monoterpene+ OH	12.0	-444.0	52.9
monoterpene+ O_3	0.00101	732.0	0.0000862
monoterpene+ NO_3	1.19	-925.0	6.12
isoprene + OH	27.0	-390.0	99.3
isoprene + O_3	0.01	1195.0	0.000180
isoprene + NO_3	3.15	450.0	0.692

Depending on the species, removal is controlled by oxidation (discussed above) and/or by deposition. Deposition of VOCs prevent SOA formation (Section 1.9.5). However, the identity of gas-phase SOA precursors is relatively unknown. Consequently, global models vary considerably in how, if

at all, SOA precursor deposition is treated. Indeed, one of the objectives of this thesis is to assess the sensitivity of SOA to variations in SOA precursor deposition (Section 1.10.2). For these reasons, the representation of gas-phase wet deposition (Section 2.3.1) and dry deposition (Section 2.3.2) in UKCA is outlined in the following sub-sections.

2.3.1 **Wet deposition of gases**

Within UKCA, wet deposition of gases is calculated as a first-order loss process as a function of precipitation, following Walton et al. (1988). For a detailed description of the wet deposition within UKCA, see O'Connor et al. (2014). Within each grid box, the scavenging rate, r, is calculated as follows:

$$r = S_j \times p_j(l) \quad \text{(E2.8)}$$

where S_j is the scavenging coefficient for precipitation type *j* and $p_j(l)$ is the precipitation rate for type j from model vertical level l. The two precipitation types, *j,* considered are convective and large-scale. For nitric acid (HNO_3), the scavenging coefficient is taken from Penner et al. (1991). For all remaining species, the scavenging coefficient is calculated by scaling the scavenging coefficient of HNO_3. This is done by calculating the fraction of each species in the aqueous phase as follows:

$$f_{aq} = \frac{L \times H_{eff} \times R \times T}{1 + L \times H_{eff} \times R \times T} \quad \text{(E2.9)}$$

Where L is the liquid water content, R is the universal gas constant and T is the temperature. H_{eff} is the species-specific effective Henry's coefficient (Section 1.4.4), which depends on the solubility and includes the effects of dissociation and complex formation. The species-specific effective Henry's coefficient is calculated as follows:

$$H_{eff} = k(298)exp\left(-\frac{\Delta H}{R}\left[\left(\frac{1}{T}\right)-\left(\frac{1}{298}\right)\right]\right)\times\left(1+\frac{k_{aq}}{[H^+]}\right) \quad \text{(E2.10)}$$

Where ΔH is the species-specific enthalpy of vaporisation and $k(298)$ is the rate coefficient at 298 K. $[H^+]$ is the hydrogen ion concentration (i.e pH). All cloud liquid water droplets are assumed to have a pH of 5.0 (Giannakopoulous, 1998). k_{aq} is calculated for species which dissociate upon dissolution, and is calculated as follows

$$k_{aq} = k_d(298)exp\left(-\frac{\Delta H_d}{R}\left[\left(\frac{1}{T}\right)-\left(\frac{1}{298}\right)\right]\right) \quad \text{(E2.11)}$$

Where k_d and ΔH_d are the rate coefficients and enthalpy of vapourisation for dissociation, respectively.

2.3.2 **Dry deposition of gases**

Dry deposition refers to the transfer of chemical species from the atmosphere to the surface in the absence of precipitation. Dry deposition of gas-phase species within UKCA is described in detail (O'Connor et al., 2014) so is only described briefly here. The dry deposition velocity (v_d) is calculated using a resistance-based approach (Wesely, 1989). This approach is analogous to an electrical circuit, where the transport of chemical species is dependent on three resistances, r_a, r_b, and r_c:

$$v_d = \frac{1}{r_a + r_b + r_c} \quad \text{(E2.11)}$$

Note, whereas r_c is species-specific, the remaining surface resistance terms are independent of the species. The aerodynamic resistance term, r_a, represents the resistance to transport of chemical species through the boundary layer to a thin layer of air just above the surface. This term is

calculated from the wind profile, taking into account the atmospheric stability and the surface roughness:

$$r_a = \frac{ln(z/z_0) - \Psi}{k \times u^*} \quad \text{(E2.12)}$$

where z is the height, z_0 is the roughness length, Ψ is the Businger dimensionless stability function, k is Karman's constant, and u^* is the friction velocity.

The quasi-laminar resistance term, r_b, refers to the resistance to transport though the thin layer of air close to the surface. The surface resistance term, r_c, otherwise known as the canopy resistance term, refers to resistance to uptake at the surface and is species specific. This term is dependent on the absorbing surface as well as the physical and chemical properties of the species. The canopy resistance term is related to surface conditions, time of day, and season. Within each grid box, the multiple resistances are calculated for each surface type, and then combined to provide a grid box mean deposition velocity and first-order loss rate.

Note, both monoterpene and isoprene are not included in dry or wet deposition. Some species included in the UKCA gas-phase chemistry scheme, such as monoterpene and sulphur-containing compounds, are also coupled to the aerosol phase chemistry, which is discussed next.

2.4 Aerosol-phase scheme (GLOMAP-mode) of atmospheric composition component of model (UKCA)

Aerosol schemes within global models vary in several ways (Section 1.9.2). The aerosol component of UKCA is the 2-moment modal version of the

Global Model of Aerosol Processes (GLOMAP-mode) (Mann et al., 2010). Both aerosol mass and number are transported in seven internally mixed log-normal modes (four soluble and three insoluble). Aerosol components (Section 1.3.2) considered are sulphate (SO_4), sea salt (SS), black carbon (BC), primary organic aerosol (POA) and secondary organic aerosol (SOA). Note, nitrate aerosol is not included, despite being an important fraction of PM (Figure 1.3.2).

Aerosol growth occurs via nucleation, coagulation, condensation, ageing, hygroscopic growth and cloud processing (Section 1.3.1). Condensation ageing refers to the coating of hydrophilic particles, resulting in transfer to the hydrophilic mode. Here, 10 monolayers of soluble particles are assumed sufficient for condensation ageing. Dry deposition and gravitational settling of aerosol follows Slinn (1982) and Zhang et al. (2012), respectively. Grid-scale wet deposition of aerosol occurs via nucleation scavenging and impact scavenging. Subgrid-scale wet removal occurs via plume scavenging (Kipling et al., 2013).

New particle formation from binary homogenous nucleation of sulphuric acid (H_2SO_4) follows that described by Kulmala et al. (2006). Gaseous sulphur compounds (sulphur dioxide, SO_2 and dimethyl sulphide, DMS) and VOCs are oxidised by the UKCA chemistry scheme, forming low volatility gases, which condense irreversibly onto pre-existing aerosol. Condensation of gases is calculated following Fuchs (1971) which is described in Mann et al. (2010). Mineral dust is also included in the model simulations, but treated in a separate aerosol module (Woodward, 2001).

2.5 Representation of the SOA lifecycle

This sections includes a description of the SOA lifecycle, followed by a more in-depth explanation of how SOA formation is formed in the UKCA-HAdGEM3 model. The SOA lifecycle is shown schematically in Figure 2.2. Simulating the SOA lifecycle requires multiple coupled competent of the UKCA-model. In the model, monoterpene is the only source of SOA considered. The emissions of this species can either be calculated online (JULES; Section 2.2) or prescribed. Once emitted, monoterpene undergoes both transport (HadGEM3-GA4.0; Section 2.1) and chemical oxidation (UKCA-StraTrop). Oxidation generates a secondary organic gas (SOG). SOG is non-volatile and therefore undergoes condensation, which is treated within the aerosol-phase component (UKCA-GLOMAP-mode; Section 2.4), to form SOA. Once, formed, SOA can undergo transport (HadGEM3-GA4.0; Section 2.1) and dry or wet deposition (UKCA-GLOMAP-mode; Section 2.4). A critical processes in the SOA lifecycle, and one of the focuses of this thesis, is how physical and chemical processing of emitted VOCs form SOA precursors, which is discussed in detail next.

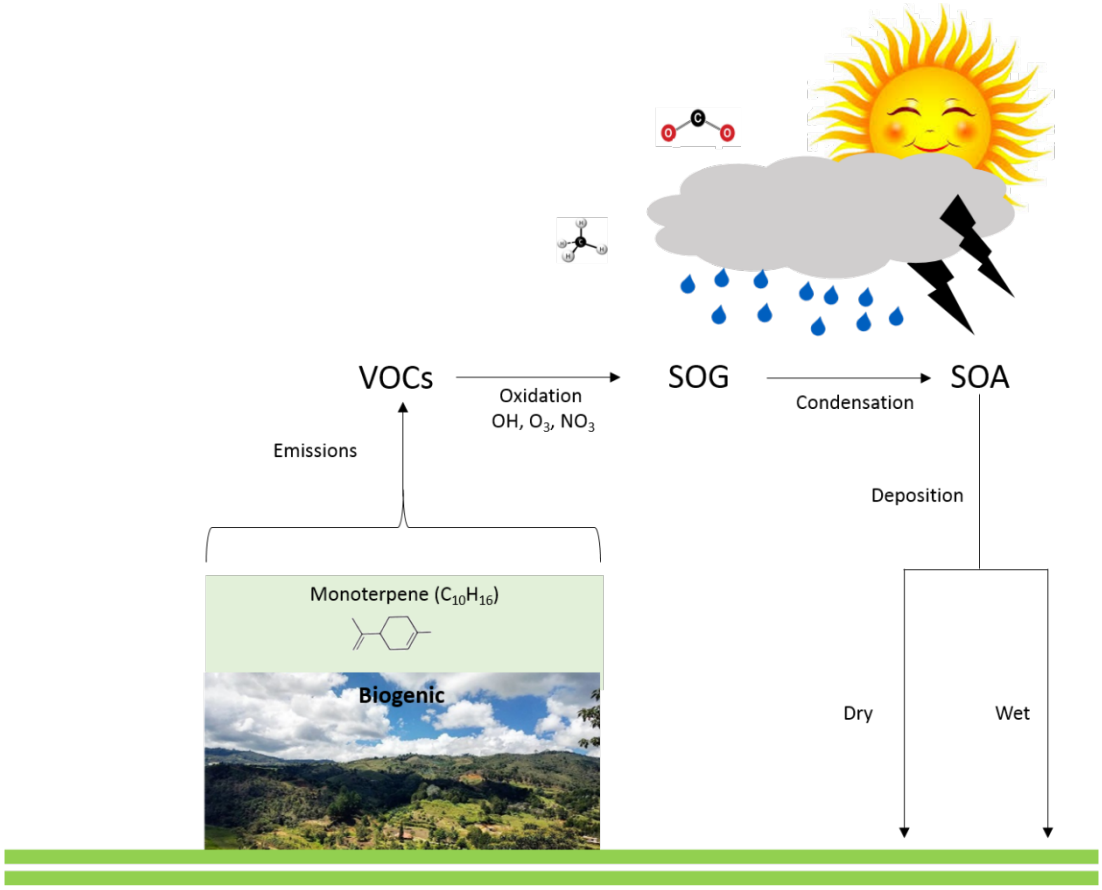

Figure 2.2 – Schematic diagram of SOA lifecycle within the UKCA model (Figure 2.1).

The formation of SOA is treated by a fixed-yield approach, analogous to E1.2. This is calculated as follows

$$VOC + [o] \xrightarrow{k_{VOC+[O]}} \alpha_{VOC+[O]} SOG \rightarrow SOA \qquad \text{(E2.13)}$$

where VOC is the concentration of an emitted VOC, [o] is the oxidant concentration, $k_{VOC+[O]}$ is the temperature-dependent rate coefficient (E2.6), $\alpha_{VOC+[O]}$ is the stoichiometric coefficient, and SOG is the secondary organic gas. SOG represents all multigenerational oxidation products that are assumed to be condensable (Figure 1.28; Chapter 1). SOG is treated as non-volatile, condensing irreversibly to form non-volatile SOA (Figure 1.24; Chapter 1). In addition to being non-volatile, SOA is also assumed to be

hydrophilic and is therefore susceptible to both dry and wet deposition. This combination of (i) a fixed yield SOA production pathway, and (ii) non-volatile SOA, and (iii) hydrophilic SOA, is adopted in several other modelling studies, using both the UKCA chemistry-climate model (Mann et al., 2010) and the GLOMAP chemical transport model (Scott et al., 2014;Scott et al., 2015;Scott et al., 2018;Spracklen et al., 2010;Spracklen et al., 2011).

Within this version of UKCA (vn8.4), the sole VOC considered in SOA formation is monoterpene. Monoterpene is predominantly a biogenic species (Section 1.6.2). Other VOC sources that are important for SOA formation, but are not considered in this version of the model are isoprene (Section 1.7.1), anthropogenic VOCs (Section 1.7.4) and biomass burning VOCs (Section 1.7.4). However, these VOC sources of SOA are added to the model in Chapter 3. Additional non-VOC sources of SOA that are not considered in the model are S/IVOCs (Section 1.7.5), POA (Section 1.7.6) and aqueous phase production (Section 1.7.7) – these sources are not implemented into the UCKA model in this thesis.

The emissions of monoterpene (which is included in SOA formation) and isoprene (which is added as a new source of SOA in chapter 3), can either be prescribed, or can be calculated on-line within the land-surface component of the model.

Overall, the HadGEM3-UKCA is able to represent several important aspects of the SOA lifecycle. Simulated SOA and OA concentrations can be compared against in-situ observations, allowing conclusion to be drawn an the model performance. The observations used to evaluate the model throughout this thesis are discussed next.

2.6 Observations used to constrain the model

The first two objectives of this thesis include quantifying how variations in the SOA scheme affect model agreement with observations (Sections 1.10.1-2). To achieve this, observed SOA and OA concentrations are compared to simulated concentration. The Aerosol Mass Spectrometer (AMS) measures non-refractory (Section 1.X) submicron (i.e. PM_1) aerosol mass concentrations (Jayne et al., 2000;Canagaratna et al., 2007). This instrument measures the mass of individual aerosol components; OA, sulphate, nitrate, ammonium, and chloride. Uncertainties associated with this method are estimated at +/-38 % (Bahreini et al., 2009),

OA spectra can be analysed further using factor analysis, classifying OA as either oxygenated OA (OOA) or hydrocarbon-like OA (HOA) (Section 1.5). OOA can be considered analogous to SOA, and HOA can be considered analogous to POA. This study uses a suite of OA observations, shown in Figure 2.3. These observations are a mixture of surface sites and aircraft campaigns but the majority of the observations are within the northern hemisphere mid-latitudes.

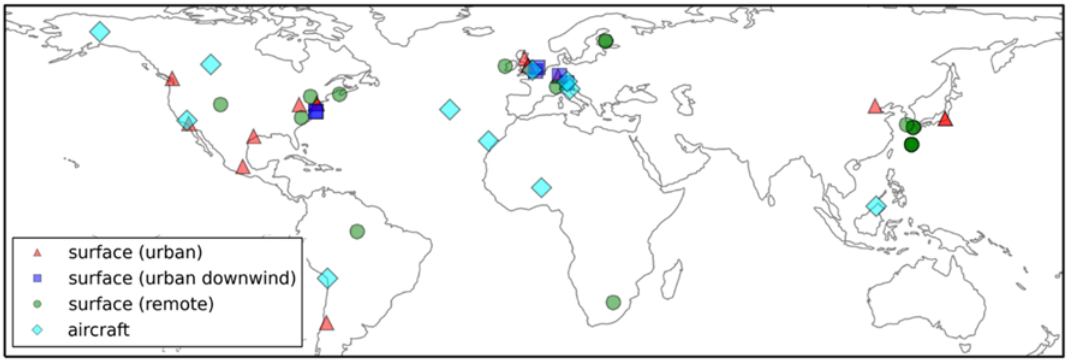

Figure 2.3 – Locations of the 40 surface AMS observations, originally compiled by Zhang et al. (2007) and subsequently updated on the AMS Global Database webs-site (https://sites.google.com/site/amsglobaldatabase/) and classified as urban (red triangles), urban downwind (blue squares) or remote (green circles). Of the surface observations, 37 are classified as hydrocarbon-like OA and oxygenated-OA. Observations from 10 aircraft campaigns, originally compiled by Heald et al. (2011), are also shown (light blue diamonds). Aircraft data remain as total OA.

2.6.1 **Surface sites**

Surface measurements, originally compiled by Zhang et al. (2007), span the time period 2000-2010. The 37 observed surface measurement locations are shown in Figure 2.3 and coloured according to the environment sampled: urban, urban downwind, or remote. With the exception of Manaus (Brazil) (Martin et al., 2010), and Welgegund (South Africa) (Tiitta et al., 2014), all surface OA spectra are analysed further using factor analysis, allowing classification as either OOA or HOA.

2.6.2 **Aircraft campaigns**

Observed OA from aircraft campaigns, originally compiled by Heald et al. (2011), are also used in this study. The locations of these aircraft observations are also shown in Figure 2.3. These campaigns span the period 2000 - 2010. Four campaigns are conducted in remote regions, which are located over the north Atlantic Ocean (TROMPEX and ITOP - Morgan et al. (2010)), Borneo (OP3 - Robinson et al. (2012)) and the tropical Pacific Ocean (VOCALS-UK - Morgan et al. (2010)). Three campaigns, EUCAARI, ADIENT and ADRIEX , sample polluted regions of Europe (Morgan et al., 2010). Three campaigns, ARCTAS-A, ARCTAS-B and ARCTAS-CARB, covering North America reflect remote regions which are sporadically influenced by biomass burning (Cubison et al., 2011). Measurements from the AMMA campaign over Western Africa are used (Capes et al., 2008;Capes et al., 2009). This campaign is also influenced by biomass burning.

2.8 Modelling approaches used in this thesis

There several different objectives to this thesis. This objectives are achieved using a variety of modelling approaches. Here, these approaches are briefly outlined. In Chapter 3, the impact of VOC emissions source types on the global SOA lifecycle is quantified. The chemistry-climate model already discussed (Sections 2.1–5) is used as a basis. New VOC sources of SOA are added to the model (Section 1.7.1-1.7.4). The impact of these new VOC emissions sources types on the SOA budget and distributions is quantified. Simulated SOA and OA are compared to observations (Section 2.6).

In Chapter 4, the sensitivity of the SOA lifecycle to variations in VOC psychical and chemical processing is assessed. This is achieved by using the SOA scheme (developed in Chapter 3), and further extending it by (i) including SOA precursors in deposition (Section 2.3.1-2.3.2), and by (ii) increasing the complexity of the oxidation scheme. Again, the impacts of these variations in VOC processing on the model to measurement agreement is assessed by using he observations described in Section 2.6.

For both chapters 3 and 4, which are based under present-day conditions and include comparing simulated SOA/OA with observed, the model is set-up such that meteorology and emissions are as close to the observed time period as possible. This is achieved by nudging the model (Section 2.1) and by using well-established biogenic VOC emissions of monoterpene and isoprene – not the interactive biogenic VOC emissions schemed in JULES which (Section 2.2).

In Chapter 5, the impacts of future changes in climate and emissions on the SOA lifecycle are examined. To capture the effects of climate change on natural components of the Earth system, the meteorology is free running

(Section 2.1) and the interactive biogenic VOC emissions scheme is utilised (Section 2.2).

All simulations in this study use the same prescribed surface type fractional cover (Section 2.1). Hence, future changes in vegetation composition in response to climate change or anthropogenic land use are not accounted for. Also, S/IVOCs, POA and aqueous phase SOA production are not considered in any model simulation of this thesis. In the following sections, the results from the research questions are addressed.

Chapter 3 **The impact of VOC emissions source types the on SOA lifecycle**

This chapter is published in an open-access journal called 'Atmospheric Chemistry and Physics' (ACP). The article is a collaboration with Professor Ruth Doherty, Dr Fiona O'Connor, and Dr Graham Mann. The article is available online (https://doi.org/10.5194/acp-18-7393-2018). Jamie Michael Kelly set-up, developed and performed all simulations – co-authors provided advice on all of these aspects. Jamie Michael Kelly performed the analysis and wrote the first draft of the manuscript. Co-authors provided feedback on subsequent manuscript drafts. The editor (Dr Konstantinos Tsigaridis) and reviewers provided additional feedback during the review process.

Jamie M. Kelly, Ruth M. Doherty, Fiona M. O'Connor, and Graham W. Mann (2018), The impact of biogenic, anthropogenic and biomass burning volatile organic compound emissions on regional and seasonal variations in secondary organic aerosol, Atmospheric Chemistry and Physics, 18, 7393–7422, https://doi.org/10.5194/acp-18-7393-2018

3.1 Introduction

Several aspects of the SOA lifecycle are highly uncertain. For instance, simulated SOA concentrations derived from global models are typically substantially lower than observed (Section 1.9.2). Estimated global annual-total SOA production rates, based on bottom-up approaches using global models, range from 12 to 480 Tg (SOA) a^{-1} (Kanakidou et al., 2005;Heald et al., 2011;Tsigaridis et al., 2014;Hodzic et al., 2016;Shrivastava et al., 2015). Estimates of the global SOA budget from top-down methods are even more uncertain. Global annual-total SOA production rates, estimated from scaling the sulphate budget (Goldstein and Galbally, 2007), or constraining the SOA budget using satellite data (Heald et al., 2010) or in-situ observations (Spracklen et al., 2011), range from 50 to 1820 Tg (SOA) a^{-1}).

Current global models represent a broad spectrum in chemical complexity, ranging from essentially no chemical-dependence on SOA production up to moderate-complexity SOA mechanisms with volatility basis set (VBS) (Donahue et al., 2006). Whether the systematic model negative bias with respect to observed SOA is due to either missing SOA sources or incomplete oxidation mechanisms is not yet clear. Although numerous studies investigate SOA production in global models, these mostly focus on individual sources, with an aim to reduce model biases. Very few studies include all major sources of SOA. Some studies suggest that the global SOA budget is dominated by biogenic sources (Hodzic et al., 2016), whereas others suggest it is dominated by biomass burning (Shrivastava et al., 2015) or anthropogenic activities (Spracklen et al., 2011). Quantifying the dominant sources of SOA is paramount for understanding air quality and climate impacts of SOA for both the present-day and future.

In this chapter, a global chemistry and aerosol model (UKCA; Chapter 2) is used to simulate SOA concentrations from all the VOC emission source

types: monoterpene (Section 1.7.2), isoprene (Section 1.7.1), anthropogenic and biomass burning activities (Section 1.7.4). Other sources of SOA production, such as from S/IVOCs (Section 1.7.5) and heterogeneous production (Section 1.7.7) may also be important, but in this chapter, the focus is on VOCs. The novelty of this chapter is that a global model is used to simulate SOA and POA from all major VOC emissions source types, evaluating simulated concentrations against a consistent set of observations to provide new insights into the seasonal influence of these different SOA precursor sources.

This chapter is organised as follows. Section 3.2 outlines the modelling approach used in this chapter. Next, the influence of VOC emissions source types on the simulated SOA lifecycle (Section 3.3-3.4) and model agreement with observations (Section 3.5) are quantified. Finally, concluding remarks are made (Section 3.6).

3.2 Chemistry-climate model description

In this section, the chemistry-climate model used in this chapter is briefly described. The chemistry-climate model used in this chapter has been described before (Chapter 2), hence, is only described here briefly. Simulations are performed with the United Kingdom Chemistry and Aerosol (UKCA) model (Morgenstern et al., 2009; Mann et al., 2010; O'Connor et al. 2014) coupled to the Global Atmosphere 4.0 (GA4.0) configuration (Walters et al., 2014) of the Hadley Centre Global Environmental Model version 3 (HadGEM3; Hewitt et al. (2011)). Horizontal winds and temperature in the model are nudged towards ERA-Interim reanalyses (Dee et al., 2011) using a Newtonian relaxation technique with a relaxation time constant of 6 hours (Telford et al., 2008). There is no feedback from the chemistry or aerosols

onto the dynamics of the model; this ensures identical meteorology across all simulations, so that differences in modelled SOA concentration are solely due to differences in SOA sources.

The United Kingdom Chemistry and Aerosol (UKCA) model used in this study combines the tropospheric chemistry scheme from O'Connor et al. (2014) with the stratospheric chemistry scheme from Morgenstern et al. (2009). There are 75 species with 285 reactions. Monoterpenes ($C_{10}H_{16}$), and isoprene (C_5H_8) are also included in this scheme, with reaction kinetics for these species presented in Table 3.1. The pre-existing isoprene reactions follow the Mainz Isoprene Mechanism (Poschl et al., 2000). Oxidation of isoprene by the nitrate or hydroxyl radicals generates only one initial product (ISON or ISO_2). Isoprene ozonolysis generates eight initial products (HO_2, OH, MACR, HCHO, $MACRO_2$, MeOO, HCOOH and CO). Within the UKCA model, the maximum number of products per reaction is four. Therefore, these eight products of isoprene ozonolysis are distributed over three parallel reactions. Under the pre-existing reactions, monoterpene is oxidised by OH, O_3 and NO_3 (Table 3.1).

Table 3.1 – Pre-existing and additional reaction kinetics for selected VOCs

Reaction	k_0 / 10^{-12} x cm^3 $molecule^{-1}$ s^{-1}	B / K	k (298) / 10^{-12} x cm^3 $molecule^{-1}$ s^{-1}
Pre-existing reactions			
$C_5H_8 + OH \rightarrow ISO_2$	27.0	-390.0	99.3
$C_5H_8 + NO_3 \rightarrow ISON$	3.15	450.0	0.692
$C_5H_8 + O_3 \rightarrow HO_2 + OH$	0.01	1195.0	0.000180
$C_5H_8 + O_3 \rightarrow MACR + HCHO + MACRO_2$	0.01	1195.0	0.000180
$C_5H_8 + O_3 \rightarrow MeOO + HCOOH + CO$	0.01	1195.0	0.000180
$C_{10}H_{16} + OH \rightarrow SOG$	12.0	-444.0	52.9
$C_{10}H_{16} + NO_3 \rightarrow SOG$	1.19	-925.0	6.12
$C_{10}H_{16} + O_3 \rightarrow SOG$	0.00101	732.0	0.0000862
Additional reactions			
$C_5H_8 + OH \rightarrow SOG + OH$	27.0	-390.0	99.3
$C_5H_8 + NO_3 \rightarrow SOG + NO_3$	3.15	450.0	0.692
$C_5H_8 + O_3 \rightarrow SOG + O_3$	0.01	1195.0	0.000180
$VOC_{ANT} + OH \rightarrow SOG + OH$	12.0	-444.0	52.9
$VOC_{BB} + OH \rightarrow SOG + OH$	12.0	-444.0	52.9

The aerosol component of UKCA is the 2-moment modal version of the Global Model of Aerosol Processes (GLOMAP-mode) (Mann et al., 2010). Aerosol components considered are sulphate (SO_4), sea salt (SS), black carbon (BC), primary organic aerosol (POA) and secondary organic aerosol (SOA). The reader is referred to Section 2.4 for a more detailed description of GLMAOP-mode.

The emissions used are all monthly-varying decadal-average emissions, centred on the year 2000. Anthropogenic and biomass burning gas-phase emissions are prescribed following Lamarque et al. (2010). Biogenic emissions of isoprene, monoterpene and methanol (CH_3OH) are also prescribed, taken from the Global Emissions Inventory Activity (GEIA),

based on Guenther et al. (1995). Note, although biogenic VOC emissions can be calculated on-line within JULES (Section 2.2), the objective here is to simulate both emissions and metrology as close to the period of observations. Hence, the well-established emissions of Guenther et al. (1995) are used instead of the interactive emissions.

A diurnal cycle in isoprene emissions is imposed based on the solar zenith angle. POA and BC emissions from fossil fuel combustion are prescribed following Lamarque et al. (2010). Year 2000 POA and BC emissions from savannah burning and forest fires are prescribed, taken from the Global Fire Emissions Database (GFEDv2 (van der Werf et al., 2010)). All carbonaceous emissions are emitted into the insoluble mode and are transferred to the soluble mode by condensation ageing. Ageing proceeds at a rate consistent with a 10-monolayer coating being required to make a particle soluble.

3.2.1 **Formation of SOA in the default version of the model**

In UKCA, VOCs undergo oxidation ([o] = OH, O_3 and NO_3). VOC oxidation products considered with a low enough volatility to condense are represented by a single surrogate compound, SOG. The reaction yield (α) describes the molar quantity (stoichiometric coefficient) of low volatility vapours formed. SOG condenses irreversibly onto the surface of pre-existing aerosol, calculated following Fuchs (1971).

$$VOC + [o] \rightarrow \alpha\, SOG \rightarrow SOA \qquad \text{(E3.1)}$$

In UKCA, monoterpenes ($C_{10}H_{16}$), are the only VOC considered in SOA formation. The reaction yield applied to monoterpenes is assumed to be 13 %, which is identical to other global modelling studies, (Mann et al.,

2010;Scott et al., 2014;Scott et al., 2015), and is taken from Tunved et al. (2006), who estimate the yield at 10 – 13 %. Global annual monoterpene emissions are 142 Tg (monoterpene) a^{-1} and their spatial distribution is shown in Figure 3.1. Figure 3.2 displays the seasonal cycle in global monthly-total monoterpene emissions.

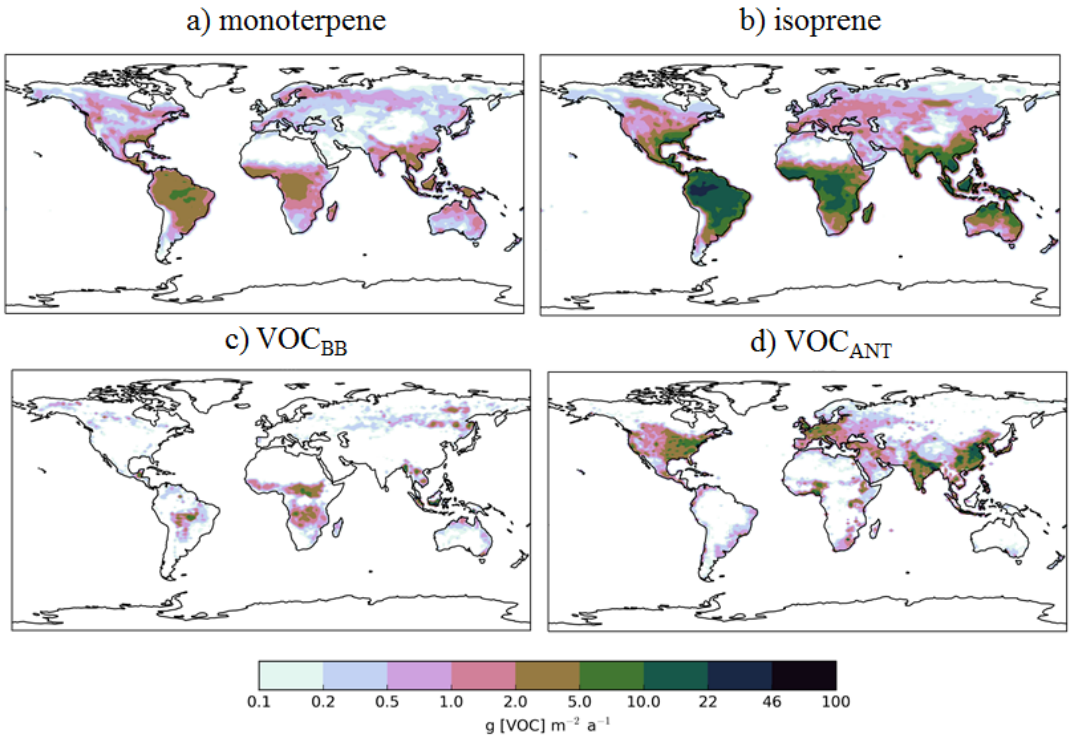

Figure 3.1 - Annual-total SOA precursor emissions from the different global VOC sources; monoterpene and isoprene taken from Guenther et al. (1995), VOC_{BB} taken from EDGAR, and VOC_{ANT} taken from Lamarque et al. (2010) Units are g (VOC) m^{-2} a^{-1}.

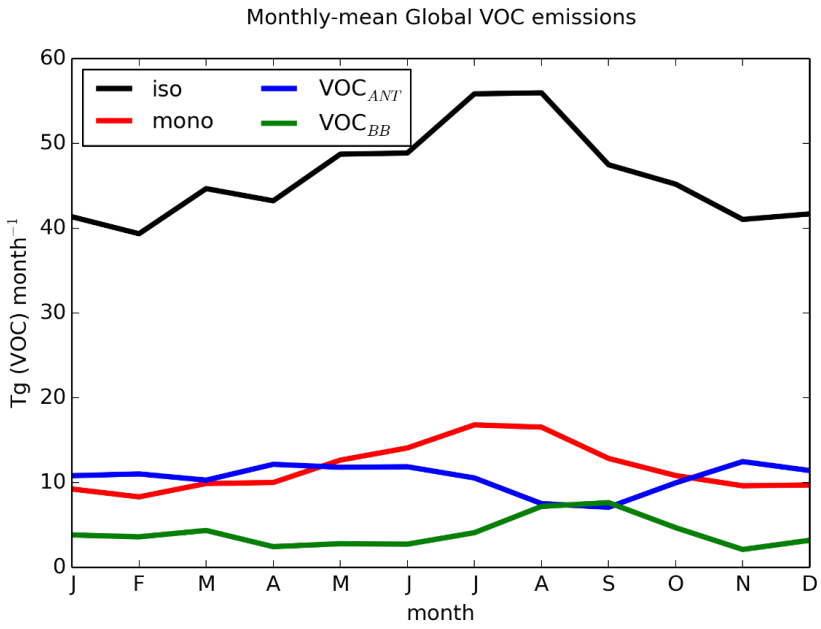

Figure 3.2 - Seasonality of global SOA precursor emissions from the different VOC sources: monoterpene (red), isoprene (black), VOC_{ANT} (blue) and VOC_{BB} (green) (Tg (VOC) $month^{-1}$).

3.2.2 **New VOC sources of SOA**

For this chapter, new SOA sources are added to the UKCA model. Specifically, isoprene and lumped anthropogenic and biomass burning VOCs are added as precursors of SOA. Biogenic isoprene emissions are taken from the GEIA database (Guenther et al., 1995) and are equal to 561 Tg (isoprene) a^{-1}. Isoprene reaction kinetics are taken from Atkinson et al. (1989). For the biomass burning source of SOA, CO emissions from biomass burning are used to define its spatial distribution (Lamarque et al., 2010) and scaled to reproduce the global annual VOC total emissions from biomass burning estimated from Emissions Database for Atmospheric Research (EDGAR) (49 Tg (VOC) a^{-1}). The biomass burning source of SOA is hereafter referred to as VOC_{BB}. Note, in contrast to biomass burning POA emissions, which are emitted from 0 – 3 km, VOCBB are emitted at the surface. Anthropogenic emissions of aromatic compounds, benzene,

dimethylbenzene and trimethylbenzene, are taken from Lamarque et al. (2010), and used together to define the spatial distribution for the anthropogenic source of SOA. These are then scaled to reproduce the global annual anthropogenic VOC total emissions estimated by EDGAR (127 Tg (VOC) a^{-1}). This represents the anthropogenic source of SOA and will be referred to as VOC_{ANT}.

The anthropogenic and biomass burning VOCs are lumped species, which results in difficulty in selecting reaction kinetics for these species. The VOCs released from anthropogenic and biomass burning having a range of carbon-carbon bonding types, with a range of carbon chain length, and a range of functional groups. The exact speciation of these mixtures is not resolved, especially for higher molecular weight species (Yokelson et al., 2013). However, more recent measurements of biomass burning (Stockwell et al., 2015;Hatch et al., 2017) and vehicle fuel (May et al., 2014;Zhao et al., 2015) emissions in laboratory conditions reveal substantial quantities of oxygenated aliphatic, aromatic (Section 1.4), polycyclic aromatic (Section 1.4), furans, as well as large fractions of unknown species.

Considering the range in chemical speciation, two compounds are used to represent the reactivity of the anthropogenic and biomass burning precursors in this study – naphthalene and monoterpene. For all simulations, VOC_{ANT} and VOC_{BB} are assumed to react solely with OH. Initially, VOC_{ANT} and VOC_{BB} are assumed to have identical reactivity to monoterpene. As monoterpene is a relatively reactive species, this provides an upper estimate for the rate for anthropogenic and biomass burning VOC oxidation. A lower estimate of SOA production from VOC_{BB} is provided by assuming reactivity of naphthalene. Naphthalene has been used as surrogate compound for IVOCs (Pye and Seinfeld, 2010) and is roughly 50 % less reactive than monoterpene. Both monoterpene and naphthalene species are used to represent the reactivity of VOC_{ANT}/VOC_{BB} as they provide relatively wide estimates of the reactivity of these surrogate compounds. For all the new

species added to SOA production: isoprene, VOC_{ANT} and VOC_{BB}, initially, a reaction yield of 13 % is applied. As discussed in Section 3.1, reaction yields vary from one study to another, as well as within individual studies. Furthermore, VOC_{ANT} and VOC_{BB} are surrogate compounds, representing a mixture of species. The initial assumption of identical reaction yields for all species does not negate the findings from laboratory studies, which suggest reaction yields are highly dependent on both molecular structure. However, the substantial uncertainties of reaction yields, coupled with these species representing lumped species, prevents accurate selection of laboratory-derived reaction yields for specific compounds. In addition, identical reaction yields allows differences in SOA concentrations to be solely attributed to differences in the spatial pattern, seasonality, and magnitude of VOC precursor emissions. However, the influence of reaction yields on the SOA lifecycle is explored in two additional simulations described below; the reaction yields for isoprene is assumed to be 3 %, which is suggested by (Kroll et al., 2005, 2006). Also, the reaction yield for VOC_{ANT} is increased from 13 to 40 %, which is motivated by the widespread model negative bias in urban environments among global modelling studies.

The spatial pattern of precursor emissions from these additional SOA sources is also shown in Figure 3.1. The seasonal cycle of the global precursor emissions from all of the VOC sources is also shown in Figure 3.2. Biogenic and biomass burning emissions peaking during NH summer, whereas anthropogenic emissions are highest during NH spring and winter. Rate coefficients are taken from Atkinson et al. (1989) and are summarised in Table 3.1.

3.2.3 **Model simulations**

Table 3.2 presents the simulations performed in this chapter. Eight model simulations are performed using the different VOC sources of SOA for two years 1999-2000. The first year is discarded as spin up and the analysis is based on the year 2000 (Table 2).

For all SOA components and across all simulations, SOA is solely removed by wet and dry deposition. The control simulation (Control) uses monoterpene as the only SOA precursor. Isoprene (its biogenic terrestrial source only), VOC_{BB} and VOC_{ANT} are introduced in additional simulations: Iso, BB and Ant respectively. All sources of SOA are combined in the AllSources simulation.

A number of sensitivity simulations were also carried out. The first sensitivity study tests a lower isoprene reaction yield of 3 % (Iso (3%)) which is suggested by laboratory data (Kroll et al., 2005, 2006). The second sensitivity study tests a higher VOC_{ANT} reaction yield of 40 % (Ant (40%)) which is suggested by (Spracklen et al., 2011). Another study has also investigated such a large anthropogenic SOA source, however, this was done by scaling simulated anthropogenic SOA concentrations (Heald et al., 2011). A final sensitivity study tests the influence of the assumed reactivity of VOC_{BB} on SOA. Here, with a reaction yield of 13 %, the reactivity is assumed to be identical to naphthalene. Naphthalene is chosen as it has been used as a surrogate compound to represent IVOCs in a global modelling study (Pye and Seinfeld, 2010) and it is roughly 50 % less reactive than monoterpene (Atkinson and Arey, 2003).

Table 3.2– Summary of simulations carried out in study. Reaction kinetics for each source are shown in Table 3.1. For the BB_Slow simulation, VOC_{BB} assumes the reactivity of naphthalene (Atkinson and Arey, 2003).

Simulation	SOA sources included	Reaction yield / %
Control	monoterpene	13
Iso	monoterpene	13
	isoprene	13
BB	monoterpene	13
	VOC_{BB}	13
Ant	monoterpene	13
	VOC_{ANT}	13
AllSources	monoterpene	13
	isoprene	13
	VOC_{BB}	13
	VOC_{ANT}	13
Iso (3%)	monoterpene	13
	isoprene	3
Ant (40%)	monoterpene	13
	VOC_{ANT}	40
BB_slow*	monoterpene	13
	VOC_{BB}	13

3.3 Impact of new VOC emissions sources types on the global SOA budget

In this section, the effects of individual sources of SOA on the global SOA budget are evaluated. Table 3.3 presents simulated annual SOA production rates for the simulations described in Table 3.2, as well as estimates taken from the literature. When monoterpene is the only source of SOA, the annual global SOA production rate is 19.9 Tg (SOA) a^{-1}. With reaction yields of 13 %, the inclusion of isoprene (Iso), VOC_{BB} (BB) and VOC_{ANT} (Ant) increases the annual global SOA production rate by 19.6, 9.5 and 24.6 Tg (SOA) a^{-1}, respectively. Note, the stoichiometric yield applied to VOC (isoprene, monoterpene, VOC_{ANT}, and VOC_{BB}), oxidation to estimate the amount of condensable products (SOG) is 13 %. However, due to differences in the relative molecular mass (M_r) among VOCs and SOG, this stoichiometric yield is not equivalent to the mass yield. For instance, a stoichiometric molar yield of 13 % applied to the oxidation of isoprene (M_r = 68 g mol^{-1}) is equivalent to a mass yield of 29 %. Hence, if all the emitted isoprene (561 Tg (C_5H_8) a^{-1}) were to react via the new reaction channels (Table 3.1), after applying the 13 % stoichiometric yield (or 29 % mass yield), the global-total annual-total SOA production rate from this source would be 162 Tg (SOA) a^{-1}. However, this is not the case. Instead, of the emitted isoprene, only 70 Tg (C_5H_8) a^{-1}) is oxidised via these new reaction pathways, which, after application of the 13 % molar yield (or 29 % mass yield), results in a global-total annual-total SOA production rate of 20 Tg (SOA) a^{-1}; the remaining isoprene (541 Tg (C_5H_8) a^{-1}) is oxidised via the pre-existing reactions of the MIM (Table 3.1; Section 3.2). Consequently, even though a 13 % molar yield is applied to isoprene oxidation (or 29 % mass yield), the resulting global-total annual-total SOA production rate is 20 Tg (SOA) a^{-1}, which corresponds to an overall SOA yield of 3.6 %.

Table 3.3 - Global annual SOA production from this study and the literature (Tg (SOA) a^{-1}). In this study, estimates derived from the isoprene (Iso(3%)) and anthropogenic (Ant(40%)) sensitivity simulations in this study are indicated. All remaining estimates from this study are based on simulations using identical reaction yields of 13 %. From the literature, estimates derived from top-down and observation methods are indicated. The remaining estimates form the literature are based on bottom-up approaches.

Component	SOA production / Tg (SOA) a^{-1}	
	This study	Literature
Biogenic	23.9[a] - 39.5 Monoterpene = 19.9 Isoprene = 4[a] – 19.6	46.4 (Khan et al., 2017) 26.8 (Henze et al., 2008) 27.6 (Farina et al., 2010) 18.6 (Tsigaridis and Kanakidou, 2007) 55 (Hoyle et al., 2007) 14.9 (Henze and Seinfeld, 2006) 97.5 (Hodzic et al., 2016) 13 (Spracklen et al., 2011)*
Biomass burning	9.5	15.5 (Hodzic et al., 2016) 3-26 (Spracklen et al., 2011) * 44-95 (Shrivastava et al., 2015) 1-15 (Cubison et al., 2011)+ 34 (Hallquist et al., 2009)*
Anthropogenic	24.6 – 70.0[b]	1.6 (Farina et al., 2010) 3.1 (Heald et al., 2011) 19.2 (Hodzic et al., 2016) 100 (Spracklen et al., 2011) *
Total	48.5[a] – 74.0 – 119.4[b]	132 (Hodzic et al., 2016) 19 (13 – 121) (Tsigaridis et al., 2014) 12-70 (Tsigaridis and Kanakidou, 2007) 140 (50-380) (Spracklen et al., 2011) * 250 (50 – 450) (Heald et al., 2010) * 26.5 (Heald et al., 2011) 280 – 1820 (Goldstein and Galbally, 2007) *

a - estimated using an isoprene yield of 3 %; b - estimated using an anthropogenic yield of 40 %; * - estimated using top-down methods; + - estimated using observations

With isoprene and monoterpene as sources of SOA, the global annual biogenic SOA production rate is 39.5 Tg (SOA) a^{-1} (Table 3.3). This is in reasonable agreement with estimates of biogenic SOA production from most other global modelling studies (14.9 – 55 Tg (SOA) a^{-1}; Table 3.3) despite possible differences in which biogenic VOCs are included in the SOA schemes. One global modelling study suggests an annual global biogenic SOA production rate of 97.5 Tg (SOA) a^{-1} ((Hodzic et al., 2016); Table 3.3) based on reaction yields that account for wall losses during chamber studies. In contrast, an observationally-constrained top-down estimate of biogenic SOA production (13 Tg (SOA) a^{-1}; Table 3.3) is much lower than our estimate. In our sensitivity simulation, when the reaction yield describing SOA formation from isoprene is reduced to 3 %, the annual global biogenic SOA production rate decreases to 23.9 Tg (SOA) a^{-1} (Table 3.3), which is still consistent with other global modelling studies.

With a reaction yield of 13 %, the annual global SOA production rate from anthropogenic sources is 24.6 Tg (SOA) a^{-1} (Table 3.3). This is higher than other global modelling studies (range of 1.6 – 19.2 Tg (SOA) a^{-1}) but substantially lower than the observationally-constrained top-down estimate (100 Tg (SOA) a^{-1}) from Spracklen et al. (2011) which is termed ‘anthropogenic allycontrolled’, representing both anthropogenic VOCs and the influence of anthropogenic oxidants on biogenic VOCs. In the sensitivity simulation when SOA formation from anthropogenic sources is increased from 13 to 40 %, the annual global SOA production rate increased to 70.0 Tg (SOA) a^{-1}.

Compared to other sources, biomass burning is the smallest source of SOA, yet still significant (9.5 Tg (SOA) a^{-1}; Table 3.3). The magnitude of SOA production from biomass burning is consistent with observations (1 - 15 Tg (SOA) a^{-1}; Table 3) and top-down studies (3 – 34 Tg (SOA) a^{-1}; Table 3.3). However, biomass burning SOA production rates vary substantially from different modelling studies. The reason for such large differences between

Hodzic et al. (2016) and Shrivastava et al. (2105), both of which simulate biomass burning SOA formation from S/IVOCs, could be due to the lack of knowledge of S/IVOCs emissions and chemistry, resulting in the need for assumptions when including SOA formation from these species in models (Shrivastava et al., 2017).

When all sources of SOA are included with identical reaction yields, the annual global SOA production rate is 74.0 Tg (SOA) a^{-1}. This lies within the range of other estimates based on bottom-up methods (13 – 132 Tg (SOA) a^{-1}; Table 3.3). However, top-down approaches, such as scaling of the sulphate budget (Goldstein and Galbally, 2007), or constraining the SOA budget by satellite (Heald et al., 2010) or in-situ observations (Spracklen et al., 2011), are substantially greater (50 – 1820 Tg (SOA) a^{-1}; Table 3.3).

With identical reaction yields, the annual-average global SOA burden, from monoterpene, isoprene, biomass burning and anthropogenic precursors is 0.19, 0.22, 0.13 and 0.38 Tg (SOA), respectively. With monoterpene only, the annual average global lifetime of SOA is 3.5 days. Inclusion of isoprene and biomass burning as sources of SOA has little effect on the SOA lifetime, with annual-average global lifetime of SOA ranging from 3.7 – 4.0 days in these simulations. However, inclusion of an anthropogenic source of SOA increases the SOA lifetime to 4.7 days, and to 5.1 days with an anthropogenic source with a 40 % yield. The effect of new sources of SOA on SOA lifetime suggest that SOA from monoterpene, isoprene and biomass burning has a similarly short lifetime, whereas SOA from anthropogenic sources has a relatively longer lifetime.

The variation in lifetime for the different SOA components is likely due to differences in the spatial distributions of SOA precursor emissions, as well as the extent of co-location of emissions and precipitation. Biogenic and biomass burning VOCs, primarily located in tropical forest regions of the southern hemisphere, experience different precipitation rates compared to

anthropogenic VOCs, which are primarily released in urban and industrial regions of the northern hemisphere. Vertical gradients in SOA production can also affect the SOA lifetime. However, in this study, all SOA precursors are emitted at the surface hence, the various SOA components in this study likely have very similar vertical gradients. Shrivastava et al. (2015) find that the SOA lifetime substantially increases when biomass burning precursors are emitted at higher altitudes. The range in SOA lifetimes over the different simulations in this study is in agreement with Tsigaridis et al. (2014), which ranged from 2.4 – 15 days. These SOA lifetimes are also in good agreement with Hodzic et al. (2016) who estimate the SOA lifetime from biogenic VOCs, anthropogenic and biomass burning VOCs combined, and anthropogenic and biomass burning S/IVOCs to be 2.2, 3.3 and 3.0 days, respectively.

The simulated global annual cycle of SOA production and SOA burden from varying sources of SOA is shown in Figure 3.3. Biogenic and biomass burning SOA production peaking during NH summer (Figure 3.4 a). This is due to both high emissions (Figure 3.2) and elevated photochemistry during this season. This results in both biogenic and biomass burning SOA burdens also peaking during this season (Figure 3.4 b). The seasonal cycle of the biomass burning SOA is consistent with Tsimpidi et al. (2016). The global SOA production rate and the SOA burden were also found to peak during NH summer in the multi-model study by Tsigaridis et al. (2014); however the seasonal cycle of SOA production and SOA burden for different SOA components could not be determined. The anthropogenic emissions peak during NH spring and winter (Figure 3.1), and are offset by the seasonal cycle of photochemistry (that influences oxidation), resulting in constant anthropogenic SOA production all year round (Figure 3.3 a). However, the anthropogenic SOA burden shows a pronounced seasonal cycle with a double peak during spring and autumn and a minimum during summer (Figure 3.3 b). Therefore, the seasonality of the anthropogenic SOA burden must be driven by the seasonality of the anthropogenic SOA lifetime, since it

differs from the seasonal cycle of SOA production. Indeed, anthropogenic SOA precursor emissions are highest over China and India (Figure 3.1). Over these regions, during summer, rainfall is greatest, which may result in a reduction in SOA lifetime due to greater wet deposition and a decrease in SOA burden. The seasonal profile of the global anthropogenic SOA burden is in agreement with that found by Tsimpidi et al. (2016); however, they suggest an alternative cause. In their model, SOA is treated as semi volatile and can partition between the aerosol and gas-phase (as opposed to in this study, where SOA is treated as non-reactive and non-volatile). In their study, partitioning is dependent on a number of parameters, including temperature. Tsimpidi et al. (2016) suggest that the summertime peak in photochemistry is compensated for by enhanced SOA evaporation. Further research is required to quantify the relative importance of each mechanism on the SOA burden.

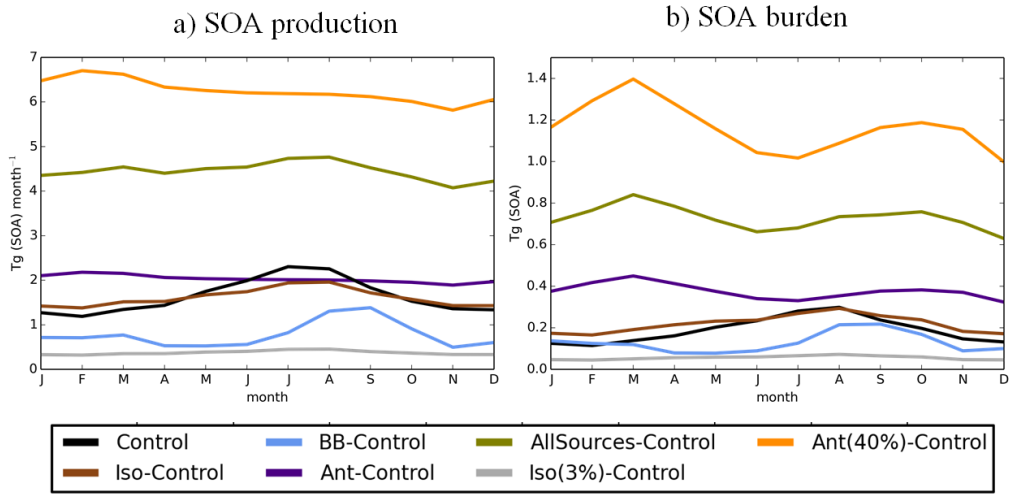

Figure 3.3 - Monthly average global SOA (a) production (Tg (SOA) month^{-1}) and (c) burden (Tg (SOA)), simulated by UKCA for the control simulation in black. For the other UKCA simulations described in Table 2, the monthly average global SOA production and burden are shown relative to the control simulation.

3.4 Impact of new VOC emissions source types on simulated SOA and POA distributions

In this section, the effects of new sources of SOA on both surface SOA and POA distributions are explored. Figure 3.4 shows the annual-average surface SOA concentrations simulated with a monoterpene source of SOA alone (Control) and with all sources of SOA (monoterpene, isoprene, VOC_{BB} and VOC_{ANT}) (AllSources) (Table 3.1). In the monoterpene only simulation, annual-average surface SOA concentrations range between 3 - 6 μg m^{-3} over tropical forest regions of South America and Africa, as well as lower SOA concentrations of up to 3 μg m^{-3} in the South East USA, and in parts of northern India, China and South East Asia (Figure 3.4 a). These patterns generally reflects the location of peak monoterpene emissions (Figure 3.1), which are emitted by vegetation only in the emissions inventory used here. Fast SOA production from monoterpene and a relatively short lifetime of SOA results in SOA concentrations peaking at the emissions source with a sharp decrease downwind.

The addition of new SOA sources (isoprene, VOC_{BB} and VOC_{ANT}) together alongside monoterpene roughly doubles annual-average surface SOA concentrations compared to simulations with monoterpene only. In particular, over the Amazon and the Congo region, annual average surface SOA concentrations peak between 5 and 10 μg m^{-3} (Figure 3.4 b). Over industrialised and urban regions of India and China, annual-average surface SOA concentrations exceed 10 μg m^{-3}. Over large parts of the USA, Europe and most of Asia, SOA concentrations exceed 0.6 μg m^{-3} (Figure 3.4 b).

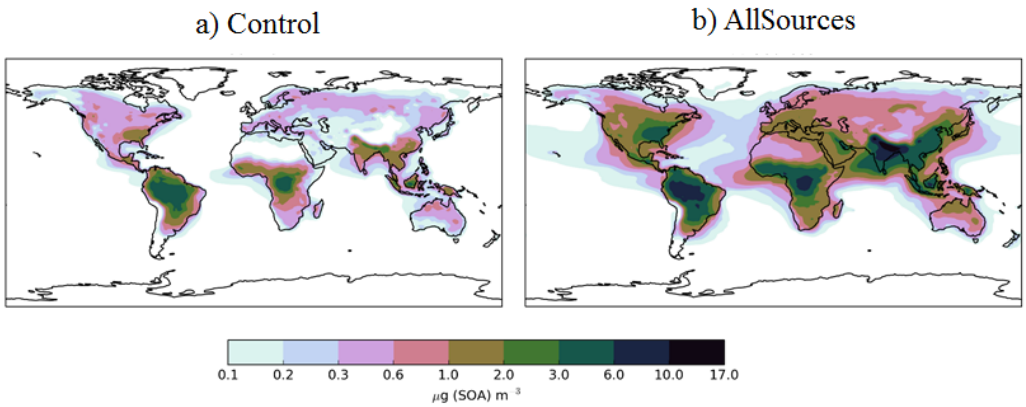

Figure 3.4 – Annual-average surface SOA concentrations (μg m^{-3}) for Control (monoterpene) and AllSources (monoterpene, isoprene, VOC_{BB}, VOC_{ANT}) simulations described in Table 3.2.

The spatial patterns of SOA concentrations associated with each individual SOA source and all three new sources combined are highlighted in Figure 3.5, which shows the difference in annual-average surface SOA concentrations for each separate SOA source relative to the monoterpene only case. The inclusion of all new sources of SOA increases annual-average surface SOA concentrations substantially (1-10 μg m^{-3}) in both the NH and southern hemisphere (SH), and over continental regions as well as to a lesser extent over downwind oceanic regions (up to 1 μg m^{-3}) (Figure 3.5 a). Isoprene is one of the most abundant VOC in the atmosphere globally, therefore, including this species in SOA production results in a substantial increase (3-10 μg m^{-3}) in SOA concentrations, especially in tropical regions (Figure 3.5 b). Both monoterpene and isoprene contribute comparably to SOA concentrations (Figure 3.5 b, Figure 3.4 a). Over the Amazon and Congo, the two biogenic sources of SOA (monoterpene and isoprene) produce SOA concentrations that typically range from 3 – 10 μg m^{-3} (Figures 3.5 b, 3.4 a), which is in agreement with other studies (Hodzic et al., 2016;Shrivastava et al., 2015;Farina et al., 2010). However, (Spracklen et al., 2011) suggests that biogenic sources yield a much lower amount of SOA

(global production = 13 Tg a^{-1}; Table 3.3) and, therefore, simulated SOA concentrations in this region in their study did not exceed 1 μg m^{-3} (Spracklen et al., 2011).

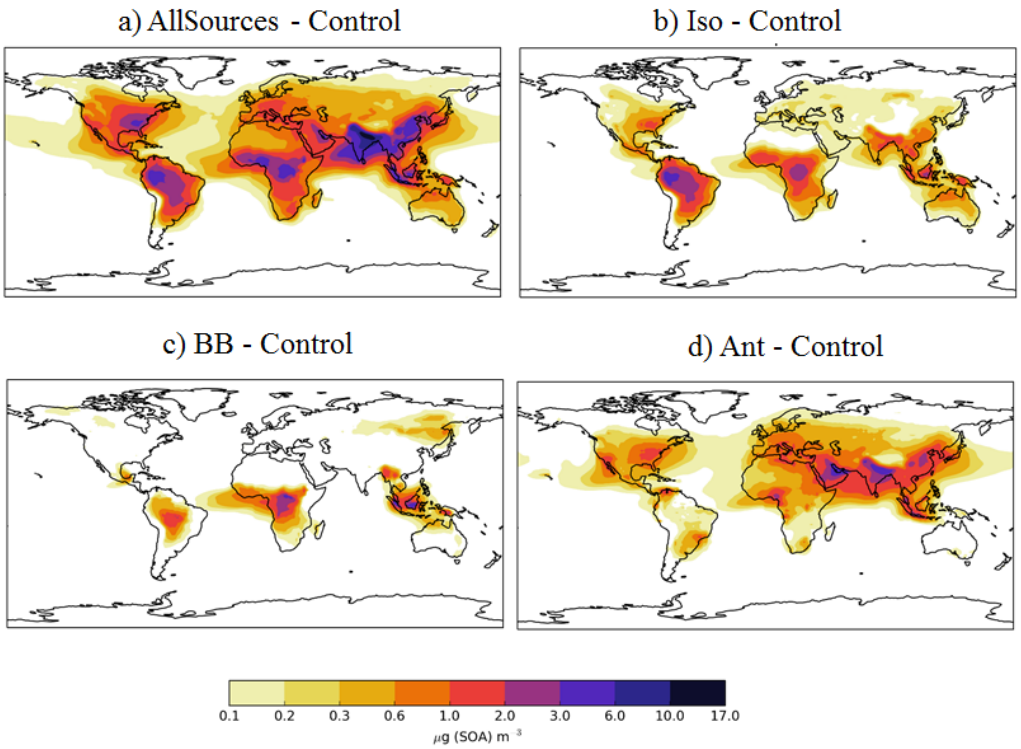

***Figure 3.5** – Differences in annual-average SOA concentrations (μgm^{-3}) relative to the control run for simulations (a) AllSources, (b) Iso, (c) BB and (d) Ant Simulations are described in Table 3.2.*

Biomass burning SOA also peaks in tropical forest regions of South America and the Congo region of Africa (Figure 3.5 c), corresponding to regions of intense forest and savannah fires (Figure 3.1). Over this region, annual average surface SOA concentrations from biomass burning typically range from 1-3 μg m^{-3} (Figure 3.5 c) and have lower values compared to SOA concentrations arising from the two biogenic sources. Biomass burning also contributes 0.2 – 1 μg m^{-3} to annual-average surface SOA concentrations over boreal forests of northern China and Eastern Siberia. The location and magnitude of these peak SOA concentrations is in

agreement with other global modelling and observationally-constrained studies (Spracklen et al., 2011;Tsimpidi et al., 2016) despite differences in biomass burning production rates (Table 3.3), highlighting the importance of SOA lifetimes in determining SOA concentrations.

The inclusion of an anthropogenic source of SOA increases SOA concentrations over much of the NH. Over industrialised and urban regions of China and India, annual-average surface anthropogenic SOA concentrations typically exceed 6 μg m^{-3} (Figure 3.5 d). The location of peak annual-average surface anthropogenic SOA concentrations, which is reflected by the location of anthropogenic combustion emissions (Figure 3.1), is in agreement with other global modelling studies (Spracklen et al., 2011;Tsimpidi et al., 2016;Hodzic et al., 2016). The magnitude of peak SOA concentrations are lower than Tsimpidi et al. (2016) but consistent with that of Spracklen et al. (2011). The inclusion of an anthropogenic source of SOA also results in increases in annual-average surface SOA concentrations in remote regions: between 0.1-0.6 μg m^{-3} over the North Atlantic and Pacific Oceans with larger values across the Indian Ocean (>1μg m^{-3}).

The difference in annual-average surface SOA concentrations for the isoprene and anthropogenic sensitivity simulations, relative to the monoterpene only simulation are shown in Figure 3.6. In the isoprene sensitivity simulation, reducing the reaction yield decreases the proportion of oxidation products which are condensable, therefore lowering SOA concentrations (c.f. Figure 3.6 a; Figure 3.5 b). Hence, SOA concentrations are only slightly elevated in this simulation compared to the monoterpene only simulation, leading to biogenic SOA concentrations over Amazon and Congo of ~10 μg m^{-3}. In addition, for a decrease in reaction yield from 13 to 3 % (factor of 4.3) the global annual-average surface SOA concentration from isoprene reduces by a factor of 4.25. This suggests that SOA concentrations, at least for the global mean, respond linearly to changes in reaction yields. In the anthropogenic sensitivity simulation, the reaction yield is increased such

that the annual average surface anthropogenic SOA concentrations increases by up to 17 μg m^{-3} across most industrialised regions relative to the monoterpene only simulation (Figure 3.6 b). The magnitude of these peak SOA concentrations are in broad agreement with Tsimpidi et al. (2016). Contrastingly, our peak simulated anthropogenic SOA concentrations exceed those from the Spracklen et al. (2011) study, despite our smaller production rate (Table 3.3), again, suggesting the importance of differences in SOA lifetime in determining SOA concentrations. For an increase in reaction yield of a factor of three, surface SOA concentrations increase by the same amount, further corroborating the linear dependence of surface concentrations on reaction yield, as observed in the isoprene sensitivity simulation.

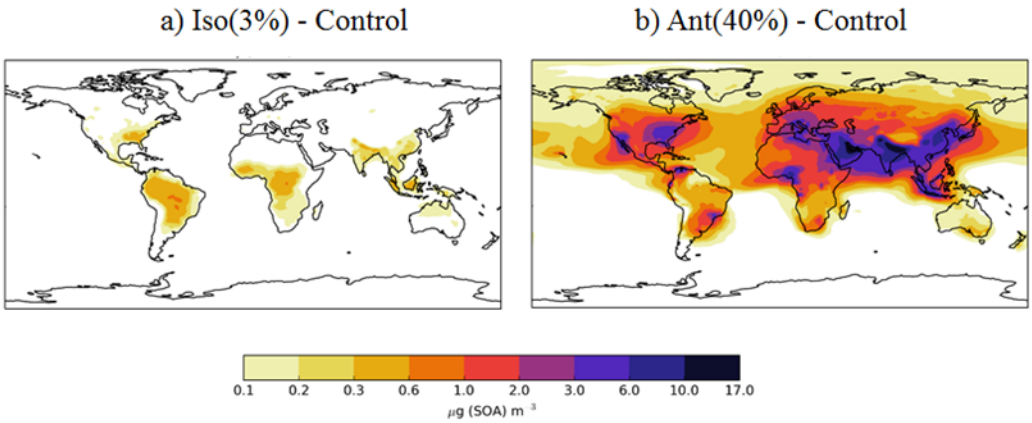

Figure 3.6 - Differences in annual-average SOA concentrations (μgm^{-3}) relative to the control run for further sensitivity simulations (a) Ant (40%), (b) Iso (3%). Simulations are described in Table 3.2.

The SOA spatial distributions simulated in this study may be sensitive to the assumption of fast reaction kinetics for anthropogenic and biomass burning SOA precursors. Here, we have assumed anthropogenic and biomass burning sources of SOA are oxidised on a timescale identical to that of monoterpene. This is due to limited information on the identity of dominant

SOA precursors from these sources. The influence of assumed reactivity on simulated SOA from biomass burning is investigated in an additional sensitivity simulation where VOC_{BB} adopts the reactivity of naphthalene (Table 3.2; section 3.2.3) , an aromatic species which has been used as a surrogate compound for IVOCs (Pye and Seinfeld, 2010). Compared to monoterpene, naphthalene is roughly 50 % less reactive (Atkinson and Arey, 2003). However, despite this substantial reduction in reactivity, the global annual-total SOA production rate from biomass burning VOCs is reduced by less than 1 %. Also, the simulated spatial distributions are almost identical for the two VOC_{BB} species. Like all other SOA precursors in this study, VOC_{BB} does not undergo dry or wet deposition. Therefore, a reduction in the reactivity of VOC_{BB} does not affect the fate of this compound.

Next, the effects of new sources of SOA on simulated POA concentrations are explored. Figure 3.7 shows the annual-average surface POA concentrations simulated with monoterpene as the only VOC source. The emissions inventory used here includes POA emissions from both biomass burning and anthropogenic sources. Within UKCA, all emitted POA is assumed to be hydrophobic. Soluble vapours, such as sulphate and organic compounds (represented as SOG), condensing onto the surface of POA particles, transfer hydrophobic POA particles into the hydrophilic mode (condensation ageing). UKCA assumes 10 monolayers of soluble material are required to redistribute hydrophobic particles into the hydrophilic mode. Over the Amazon, total POA lies in the range of 0.34 – 2.2 μgm^{-3} and is almost entirely hydrophilic (Figure 3.7 a and b). This is due to sufficiently high SOA concentrations in the monoterpene-only source simulation, which also peak in this same region (Figure 3.4 a). Over the Congo region, total POA concentrations lie between 1.2 – 4 μgm^{-3} (Figure 3.7 a) and hydrophobic POA concentrations range from 0.17 to 1.51 μgm^{-3} (Figure 3.7 b). In this region, SOA concentrations are high enough (Figure 3.4 a) to re-distribute the majority of POA into the hydrophilic mode, however, a small amount

remains in the hydrophobic mode. Over northern China and eastern Siberia, total POA concentrations are extremely high, ranging from 4 to 25 μgm^{-3} (Figure 3.7 a). In this region, SOA concentrations are low (Figure 3.4 a), therefore, a substantial fraction of POA remains in the hydrophobic mode (range 2.59 – 13.2 μgm^{-3} (Figure 3.7 b). Overall, 25 % of the global annual-average POA burden is hydrophobic.

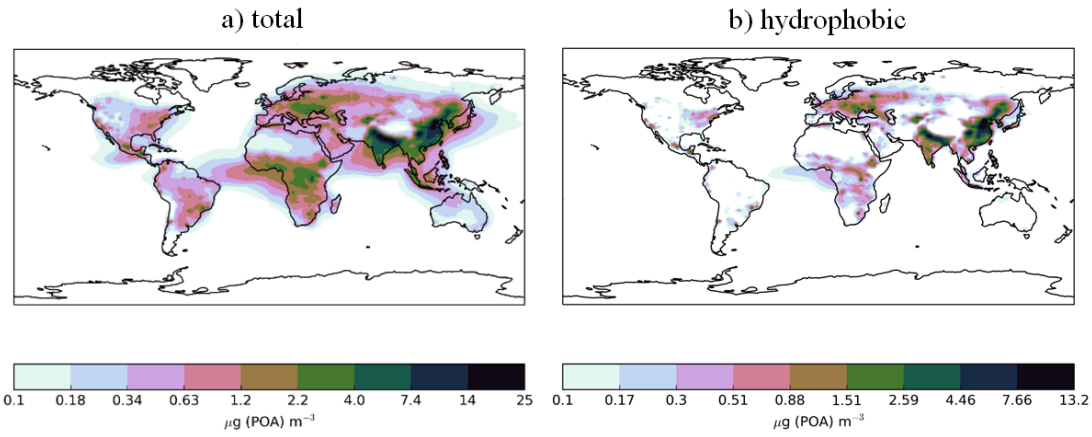

***Figure 3.7** – Annual-average surface (a) total (hydrophilic and hydrophobic), and (b) hydrophobic only, POA concentrations (μgm^{-3}) for the Control simulation. Within UKCA, all POA is emitted into the hydrophobic modes and re-distributed into the hydrophilic modes through condensation-ageing.*

When new sources of SOA are added to the model, condensation-ageing of POA increases and the proportion of hydrophilic POA increases. Critically, wet deposition removes hydrophilic particles but not hydrophobic particles. Therefore, inclusion of new sources of SOA decreases the POA lifetime and results in decreased POA concentrations. Figure 3.8 shows the difference in annual-average surface POA concentrations relative to the control simulation. Over the Congo region, inclusion of isoprene and biomass burning as sources of SOA results in a decrease in annual average surface POA concentrations of greater than 3 μgm^{-3} (Figure 3.8 a and b). In this region, the new sources of SOA enhances POA transfer from the

hydrophobic to hydrophilic modes, which are efficiently removed by deep tropical convection. Over Eastern Siberia, the inclusion of a biomass burning source of SOA also decreases POA concentrations.

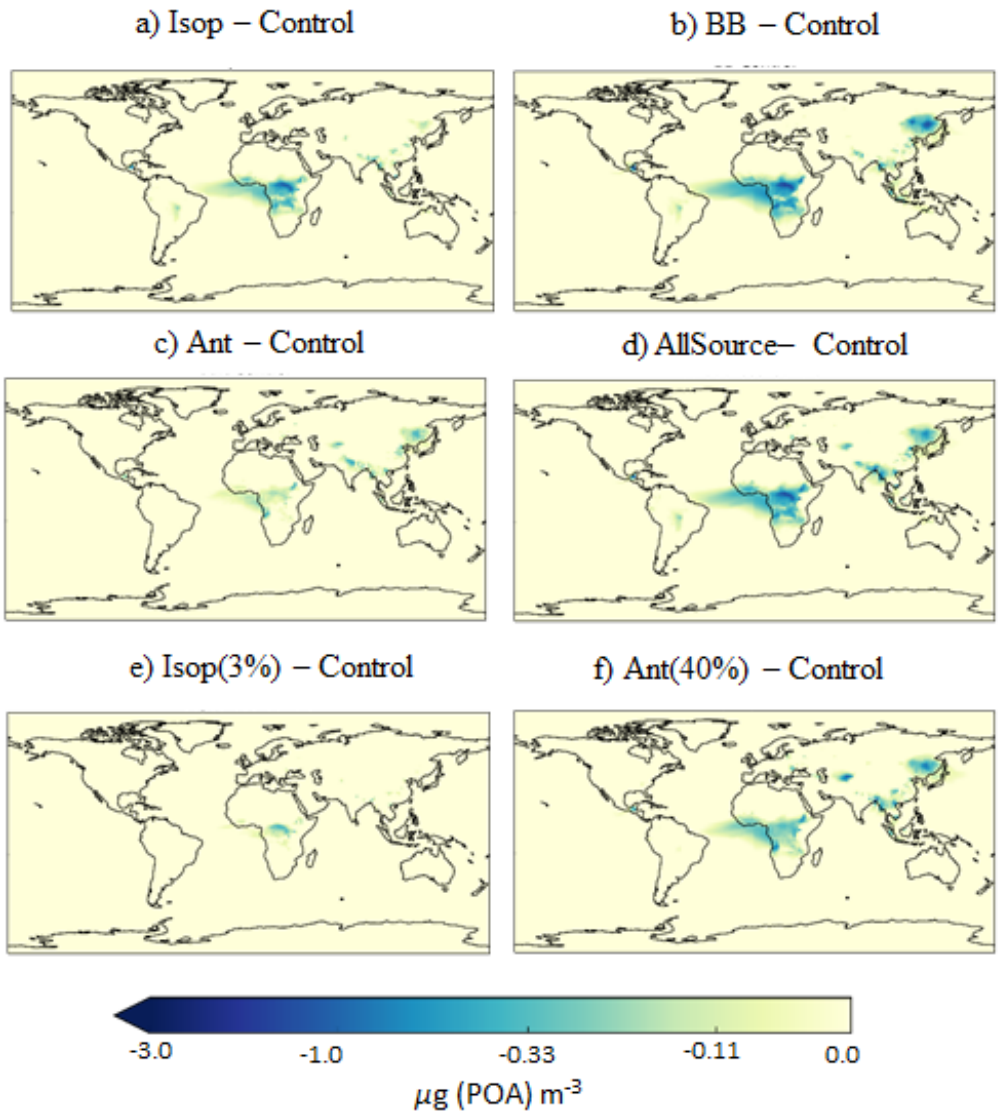

Figure 3.8 – Differences in annual average surface total POA concentrations (μgm^{-3}) relative to the control run for simulations (a) AllSources, (b) Iso, (c) BB and (d) Ant, which are described in Table 3.2. Regions of decreased POA correspond to regions of increased SOA concentrations, availability of hydrophobic POA and efficient wet removal.

Over the Amazon, although inclusion of isoprene and biomass burning results in substantial increases in SOA concentrations (Figure 3.5 b and c), there are negligible changes in POA concentrations (Figure 3.8). In this region of the world, in the monoterpene only simulation, the majority of POA is hydrophilic. For this reason, increased SOA concentrations in this region have no effect on the partitioning of POA between the hydrophobic and hydrophilic modes, hence, there is little change in POA lifetime. Over urban and industrialised regions of India and China, hydrophobic POA concentrations are much higher (Figure 3.7 b). In these regions, the inclusion of isoprene and anthropogenic sources of SOA results in substantial increases in SOA concentrations (Figure 3.5 6 b and d), therefore, hydrophilic POA concentrations in this region are increased. However, there are minimal changes in annual-average surface total POA concentrations (Figure 3.8) which is probably due to inefficient wet removal. Across all simulations, in various locations, inclusion of new sources of SOA reduces POA concentrations. However, the decrease in POA concentrations is always outweighed by the increase in SOA concentrations, thus, total OA increases.

To summarise, with monoterpene emissions only, SOA concentrations peak in the SH over tropical forest regions of South America and Africa. Including isoprene, biomass burning and anthropogenic sources of SOA results in substantial increases in SOA concentrations. Isoprene and biomass burning sources of SOA produce substantial increases in SOA concentrations over the Amazon and Congo compared to the monoterpene only source. The anthropogenic source of SOA increases SOA concentrations over industrialised and urban regions of China, India, USA and Europe. Sensitivity studies show that SOA concentrations respond linearly to changes in reaction yields. Upon inclusion of new SOA sources, increased SOA concentrations lead to decreased POA concentrations, however, in all regions of the globe, modelled total OA increases.

3.5 Impact of new VOC emissions source types on model agreement with observations

In this section, simulated SOA, POA and total OA concentrations previously presented (Section 3.3 – 3.4), are evaluated against observations (Chapter 2). First, simulated SOA and POA concentrations are compared to surface measurements. Next, to expand the spatial coverage of evaluation, simulated total OA concentrations are compared against surface observations. Finally, vertical profiles of simulated total OA concentration are compared against aircraft campaign observations.

3.5.1 Evaluation of surface SOA and POA concentrations

Surface observations used to evaluate the model are shown in Figure 2.3 of Chapter 2. Note that the overall number of sites is small and the measurement locations are primarily in NH mid-latitude regions where anthropogenic emissions are high (Figure 3.1). However, these sites sample urban, urban downwind, and remote environments over Europe, North America and Asia. The mean and normalised mean bias (NMB) are used to evaluate model agreement with observations. A summary of statistics evaluating simulated SOA, POA and OA are shown in Tables 3.4, 3.3, and 3.5, respectively.

Table 3.4 – Summary of statistics for simulated SOA against observed oxygenated OA for simulations described in Table 3.2. NMB represents the normalised mean bias. Measurements cover period 2000-2010, model results are for the year 2000.

	number of sites	Obs (AMS)	Model (UKCA)													
			Control		Iso		BB		Ant		AllSources		Ant(40%)		Iso(3%)	
		mean (µg m^{-3})	mean (µg m^{-3})	NMB (%)	mean (µg m^{-3})	NMB (%)	mean (µg m^{-3})	NMB (%)	mean (µg m^{-3})	NMB (%)	mean (µg m^{-3})	NMB (%)	mean (µg m^{-3})	NMB (%)	mean (µg m^{-3})	NMB (%)
all sites	37	3.68	0.33	-91	0.59	-84	0.38	-90	1.30	-65	1.83	-50	3.32	-10	0.39	-89
site type																
urban	14	4.76	0.36	-93	0.64	-86	0.42	-91	1.28	-53	1.92	-60	3.17	-34	0.42	-91
urban downwind	6	3.93	0.59	-85	1.07	-73	0.63	-84	1.85	-53	2.55	-35	4.50	14	0.70	-82
remote	17	2.70	0.22	-92	0.38	-86	0.26	-90	1.12	-58	1.50	-44	3.02	12	0.26	-90
Continent																
Europe	13	4.20	0.15	-93	0.24	-88	0.16	-92	0.84	-58	0.97	-52	2.25	12	0.18	-91
North America	12	2.02	0.70	-83	1.26	-70	0.79	-81	1.68	-60	2.64	-37	3.72	-12	0.83	-80
Asia	12	4.77	0.11	-98	0.22	-95	0.16	-97	1.35	-72	1.81	-62	3.94	-17	0.14	-97

Table 3.5– Summary of statistics for simulated POA against observed hydrocarbon-like OA for simulations described in Table 3.2. NMB indicated normalised mean bias. Measurements cover period 2000-2010, model results are for the year 2000.

	number of sites	Obs (AMS)	Model (UKCA)													
			Control		Iso		BB		Ant		AllSources		Ant(40%)		Iso(3%)	
		mean (µg m^{-3})	mean (µg m^{-3})	NMB (%)	mean (µg m^{-3})	NMB (%)	mean (µg m^{-3})	NMB (%)	mean (µg m^{-3})	NMB (%)	mean (µg m^{-3})	NMB (%)	mean (µg m^{-3})	NMB (%)	mean (µg m^{-3})	NMB (%)
all sites	37	3.68	0.33	-91	0.59	-84	0.38	-90	1.30	-65	1.83	-50	3.32	-10	0.39	-89
site type																
urban	14	4.76	0.36	-93	0.64	-86	0.42	-91	1.28	-53	1.92	-60	3.17	-34	0.42	-91
urban downwind	6	3.93	0.59	-85	1.07	-73	0.63	-84	1.85	-53	2.55	-35	4.50	14	0.70	-82
remote	17	2.70	0.22	-92	0.38	-86	0.26	-90	1.12	-58	1.50	-44	3.02	12	0.26	-90
Continent																
Europe	13	4.20	0.15	-93	0.24	-88	0.16	-92	0.84	-58	0.97	-52	2.25	12	0.18	-91
North America	12	2.02	0.70	-83	1.26	-70	0.79	-81	1.68	-60	2.64	-37	3.72	-12	0.83	-80
Asia	12	4.77	0.11	-98	0.22	-95	0.16	-97	1.35	-72	1.81	-62	3.94	-17	0.14	-97

Table 3.6– Summary of statistics for simulated OA against observed OA for simulations described in Table 3.2. NMB indicated normalised mean bias. Measurements cover period 2000-2010, model results are for the year 2000.

	number of sites	Obs (AMS)	Model (UKCA)													
			Control		Iso		BB		Ant		AllSources		Ant(40%)		Iso(3%)	
		mean (μg m^{-3})	mean (μg m^{-3})	NMB (%)	mean (μg m^{-3})	NMB (%)	mean (μg m^{-3})	NMB (%)	mean (μg m^{-3})	NMB (%)	mean (μg m^{-3})	NMB (%)	mean (μg m^{-3})	NMB (%)	mean (μg m^{-3})	NMB (%)
all sites	37	4.95	1.05	-79	1.30	-74	1.07	-78	1.99	-60	2.51	-49	4.00	-19	1.11	-78
site type																
urban	14	7.62	1.20	-84	1.47	-81	1.23	-84	2.10	-72	2.74	-64	3.98	-47	1.26	-83
urban downwind	6	4.72	1.05	-78	1.52	-69	1.08	-77	2.30	-51	3.01	-36	4.95	-5	1.65	-75
remote	17	2.83	0.92	-67	1.07	-62	0.93	-67	1.79	-37	2.15	-24	3.68	30	0.97	-66
Continent																
Europe	13	2.78	0.47	-83	0.55	-80	0.47	-83	1.15	-58	1.28	-54	2.56	-7	0.50	-82
North America	12	5.92	1.28	-78	1.82	-69	1.34	-78	2.24	-62	3.20	-46	4.27	-28	1.41	-76
Asia	12	6.05	1.38	-77	1.47	-76	1.37	-77	2.56	-58	3.00	-50	5.14	-15	1.41	-77

High SOA concentrations are observed in urban environments (mean = 4.76 μg m^{-3}) are maintained further downwind (mean = 3.93 μg m^{-3}) and in remote environments (mean = 2.70 μg m^{-3}) (Table 3.4). Contrastingly, observed POA concentrations peak in urban environments (mean = 2.79 μg m^{-3}) but decrease rapidly further downwind (mean = 0.78 μg m^{-3}) to almost negligible values in remote environments (mean = 0.14 μg m^{-3}) (Table 3.5). Zhang et al. (2007) suggest that cities act as sources of POA, whereas, both cities and remote environments are sources of SOA. Compared to other cities, observed SOA and POA are extremely high in densely populated cities. For example, observed SOA concentrations in Beijing and Mexico City are 17.3 and 14.55 μg m^{-3}, respectively, roughly 3 times greater than the mean observed SOA in urban environments (not shown). Observed POA concentrations in Beijing and Mexico City are 7.4 and 7.23 μg m^{-3}, respectively, roughly 2.5 times greater than the mean observed POA in urban environments (not shown).

Figure 3.9 compares simulated SOA and POA from the monoterpene only simulation against AMS measurements. When considering all observations, simulated SOA is substantially lower than observed (NMB = -

91 %) (Table 3.4, Figure 3.9 a) whereas simulated POA is in better but still relatively poor agreement with observed POA (mean = 0.71 μg m^{-3}, NMB = -43 %) (Table 3.5, Figure 3.9 b).

A model negative bias in SOA and POA is common among global models (Tsigaridis et al., 2014). It is suggested that this underestimate is partly due to the coarse grid resolution, which is unable to resolve both urban-scale pollution and heterogeneities in remote environments (Kaser et al., 2015), but for SOA, uncertainties in its sources and their reaction rates, as highlighted in section 3.1, will also be important.

The simulated negative bias in SOA occurs for all site type environments (NMB range -85 to -93 %) and all continental regions (NMB range -83 to -98 %) (Table 3.4). In the case of POA, the model has a negative bias that is larger in urban compared to urban downwind environments. This may indicate that the POA emissions inventory used by the UKCA model underestimates anthropogenic POA emissions. Known, missing sources of POA from the emissions inventory used here include cooking OA and S/IVOCs. Emissions of OA from residential and commercial cooking activities have been measured to contribute 17 – 19 % to total OA in urban environments (Ge et al., 2012;Mohr et al., 2012;Hayes et al., 2013). S/IVOCs can also contribute to POA (Robinson et al., 2007). The amount of S/IVOCs missing from traditional emissions inventories is estimated to be 0.25 – 2.8 times traditional POA emissions (Shrivastava et al., 2008;Robinson et al., 2010). Regionally, over Asia, simulated POA is in good agreement with observations (NMB= 2%; Table 3.5). However, the model underestimates POA over Europe (NMB = -59 %) and North America (NMB = -70 %) (Table 3.5). Underestimated POA concentrations over Europe have been reported in previous global modelling studies, and attributed to under estimated emissions from residential biofuel and biomass burning in residential areas (van der Gon et al., 2015).

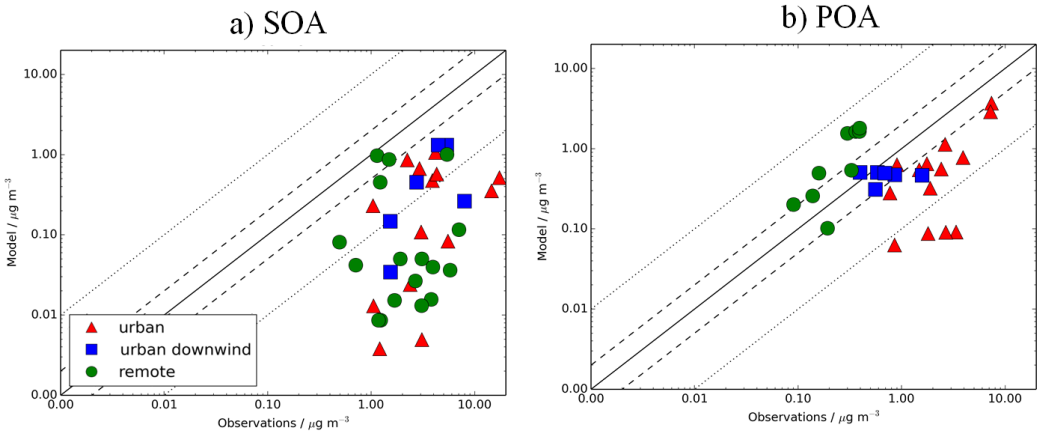

Figure 3.9 – Simulated versus observed (a) SOA and (b) POA concentrations (μg m^{-3}). Observed oxygenated-OA is assumed to be comparable to simulated SOA, whereas observed hydrocarbon-like OA is assumed to be comparable to simulated POA. Simulated concentrations are taken from the control run for the year 2000, described in Table 3.2. Observations for the time period 2000-2010 are classified as urban (red triangles), urban downwind (blue squares) or remote (green circles). The 1:1 (solid), 1:2 and 2:1 (dashed), and 1:10 and 10:1 (dotted) lines are indicated. Model-observation statistics for SOA, POA and OA are shown in Tables 3.4, 3.5 and 3.6, respectively.

In remote environments, simulated POA is overestimated compared to observations (mean = 0.70 μg m^{-3}, NMB = 410 %) (Table 3.5, Figure 3.9 b). This may be due to the assumption that POA is non-volatile and unreactive in UKCA (i.e. missing sinks). Similarly, Spracklen et al. (2011) also treats POA as non-volatile and unreactive and, consequently, overestimates POA compared to observations in remote environments. By considering heterogeneous POA oxidation to form SOA, the NMB against observed POA reduces from 274 to 45 % (Spracklen et al., 2011). Additionally, Tsimpidi et al. (2016) allows POA to oxidise to form SOA via the gas phase and finds relatively good agreement between simulated and observed POA concentrations in remote environments.

Next, the impact of new sources of SOA on model agreement with observations is explored. Figure 3.10 shows simulated SOA against

observations for the simulations that include all the SOA sources and the individual sources in addition to monoterpene (Iso, Ant, BB; Table 3.2). When considering all the measurement site data, the inclusion of all new sources of SOA reduces the model negative bias in surface SOA concentrations compared to observations from -91 to -50% (Figure 3.10 a, Table 3.4). This improvement in the model negative bias is primarily due to the inclusion of the anthropogenic source of SOA (NMB = -65 %) (Figure 3.9 d, Table 3.4). This is because the anthropogenic source of SOA generates high SOA concentrations (Figure 3.5 d) in areas with a high density of observations (Figure 2.3). When restricting observations classified by environments (urban, urban downwind and remote) or continent (i.e. Europe, North America and Asia), the reduction in the model negative bias when all sources of SOA are included is also mainly due to the anthropogenic source of SOA. The inclusion of isoprene and biomass burning as sources of SOA, reduces the NMB by only 7 and 1 %, respectively, compared to the monoterpene source only results (Figure 3.10 b and c, Table 3.4). Although simulated SOA concentrations from both isoprene and biomass burning are high (Figure 3.5 b and d), generally, peak concentrations associated with these sources do not occur in locations with measurements of SOA (Figure 2.3).

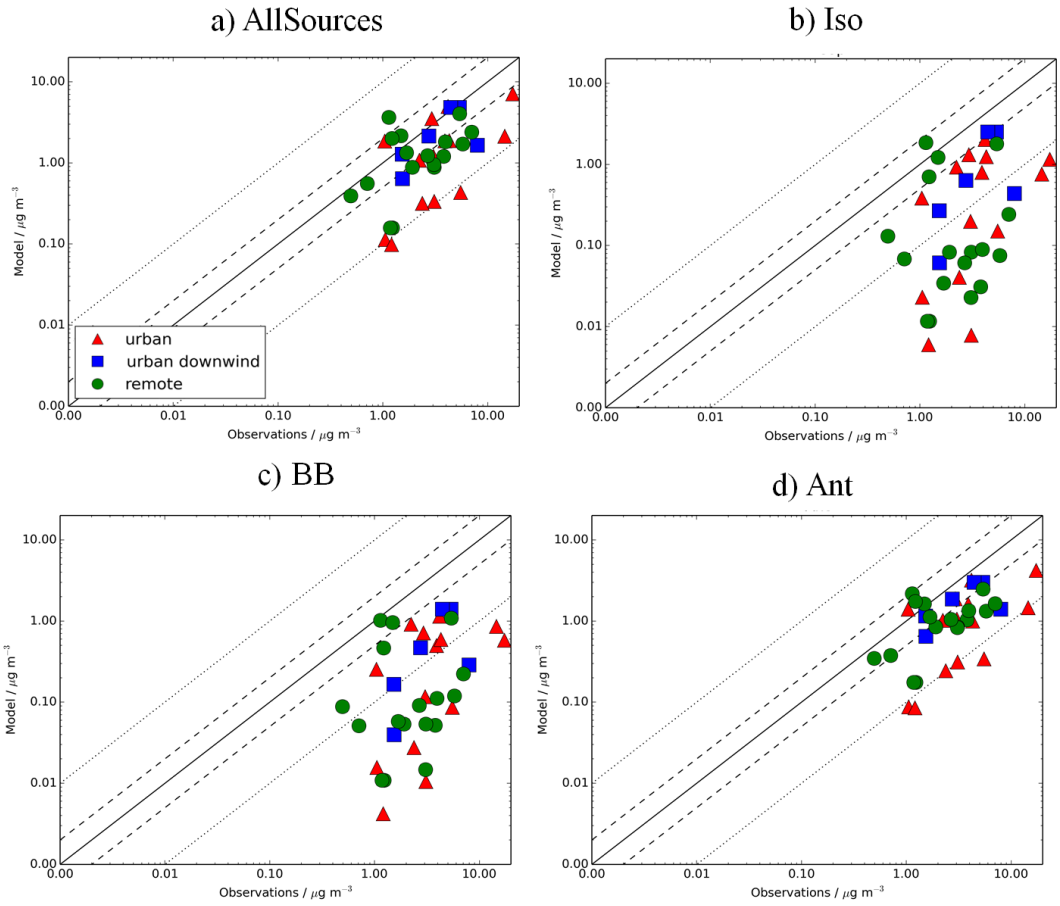

***Figure 3.10** – Simulated versus observed SOA (μg m^{-3}) for simulations (a) AllSources, (b) Iso, (c) BB, and (d) Ant, described in Table 3.2. Observations for the time period 2000-2010 are classified as urban (red triangles), urban downwind (blue squares) or remote (green circles). Observed oxygenated-OA is assumed to be comparable to simulated SOA. The 1:1 (solid), 1:2 and 2:1 (dashed), and 1:10 and 10:1 (dotted) lines are indicated. Model-observation statistics for SOA are shown in Table 3.4.*

Figure 3.11 shows simulated versus observed SOA concentrations for the isoprene and anthropogenic sensitivity simulations with reaction yields of 3 % and 40 %, respectively. When the reaction yield of anthropogenic SOA formation is increased from 13 to 40 %, model negative biases are reduced further. When all sites are considered, simulated SOA concentrations are in fairly good agreement with observations (NMB = -10 %), highlighting a large influence from anthropogenic sources of SOA at these measurement site locations, and the requirement of a higher reaction yield than 13% to match

observed levels of SOA. However, simulated SOA concentrations are still underestimated in urban environments (NMB = -34 %) and slightly overestimated further downwind (NMB = 14 %) and at remote site locations (NMB = 12 %). This positive bias downwind and in remote environments could be due to an overestimated SOA lifetime. Hodzic et al. (2016) suggests that global models typically overpredict SOA lifetime by low SOA wet deposition rates. When SOA scavenging efficiency was increased in their model simulations, the SOA lifetime decreased from 6 – 10 days to 2.2 – 3.3 days, and positive biases in simulated SOA concentrations downwind were reduced (Hodzic et al. (2016)). With a reaction yield of 40% for anthropogenic SOA formation, simulated SOA is slightly overestimated over Europe (NMB = 12 %) and underestimated over North America and Asia (NMB= -12 to -17 %). For the isoprene sensitivity simulation, there is almost no change in the model negative bias at these NH mid-latitude measurement locations in comparison to the monoterpene only source simulation. As highlighted above, there are no measurements of SOA concentrations in tropical isoprene-sensitive regions for suitable model evaluation.

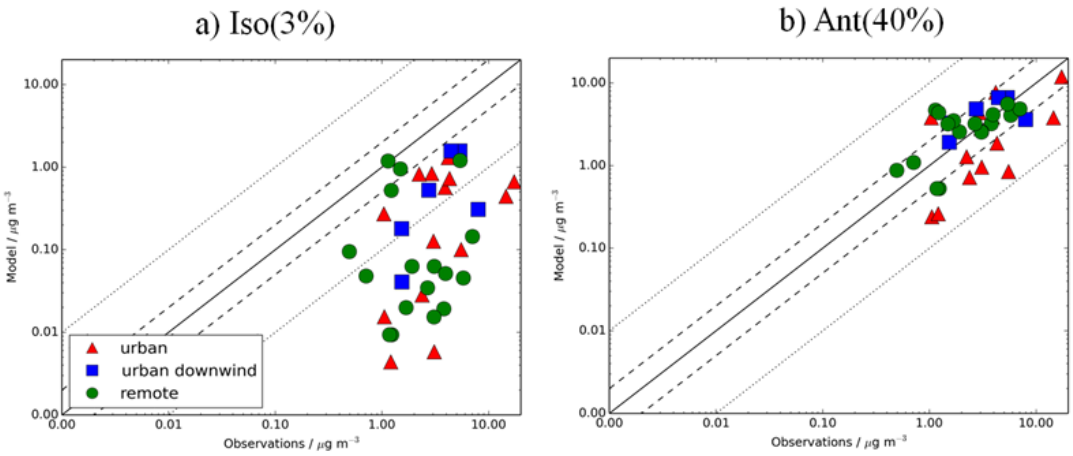

Figure 3.11 – Simulated versus observed SOA (μg m^{-3}) for sensitivity simulations (a) Iso (3%) and (b) Ant (40%), described in Table 2. Observations for the time period 2000-2010 are classified as urban (red triangles), urban downwind (blue squares) or remote (green circles). Observed oxygenated-OA is assumed to be comparable to simulated SOA. The 1:1 (solid), 1:2 and 2:1 (dashed), and 1:10 and 10:1 (dotted) lines are indicated. Model-observation statistics for SOA are shown in Table 3.4.

When considering POA concentrations, the agreement between simulated and observed POA is largely unchanged by the inclusion of new sources of SOA. With the new SOA sources, POA condensation-ageing increases, resulting in the newly soluble POA particles undergoing wet removal. This decreases POA lifetime and causes POA concentrations to decrease, as described above in relation to Figure 9. When considering all observations, the inclusion of new sources of SOA has a reduction in the model negative bias with the NMB changing by ~2 % (Table 3.5); this is also the case for individual site types and across the three continental regions.

The observations used to evaluate SOA and POA concentrations thus far have been primarily located in the NH mid-latitudes. The geographical coverage over which the model is evaluated is expanded by including observations of total OA over the urban environment of Santiago (Chile) and the rural environments of Manaus (Brazil) and Welgegund (South Africa) (Figure 2.3).

Figure 3.12 shows simulated OA for the different SOA sources against observed OA for the three additional non-speciated OA measurements. Observed OA concentrations over Manaus (Brazil) and Welgegund (South Africa) are 0.77 and 3.49 μg m^{-3}, respectively. These concentrations are typical of remote environments in the NH mid-latitudes (mean = 2.83 μg m^{-3}; Table 3.6). Over Manaus (Brazil), out of all the new sources of SOA added to the model, the addition of isoprene as an SOA source has the largest impact on increasing simulated OA concentrations at this location. However, in the case of Manaus (Brazil), OA concentrations are overestimated with the inclusion of isoprene as an SOA source (Figure 3.12 b). This suggests that a lower isoprene reaction yield (Iso (3%)) may be more accurate (OA concentrations ~1.5 μg m^{-3}). Conversely, over Welgegund (South Africa) with only a monoterpene source of SOA, simulated OA is substantially lower than observed OA concentrations. Therefore, inclusion of new sources of SOA reduces the model negative bias at this location. Additionally, the anthropogenic sensitivity simulation has a substantial improvement in the model negative bias over Welgegund (South Africa) suggesting that this downwind location is heavily influenced by anthropogenic emissions from the urban centre (Cape Town). This also appears to be the case for the urban downwind and remote sites in the NH mid-latitudes where the simulated OA concentrations for all sources and for anthropogenic sensitivity simulations yield the lowest model bias compared to observations (mean values for remote sites: 2.15 and 3.68 μg m^{-3} respectively; Table 3.6). Alternatively, Shrivastava et al. (2105) find that simulated OA at this site is primarily attributed to biomass burning.

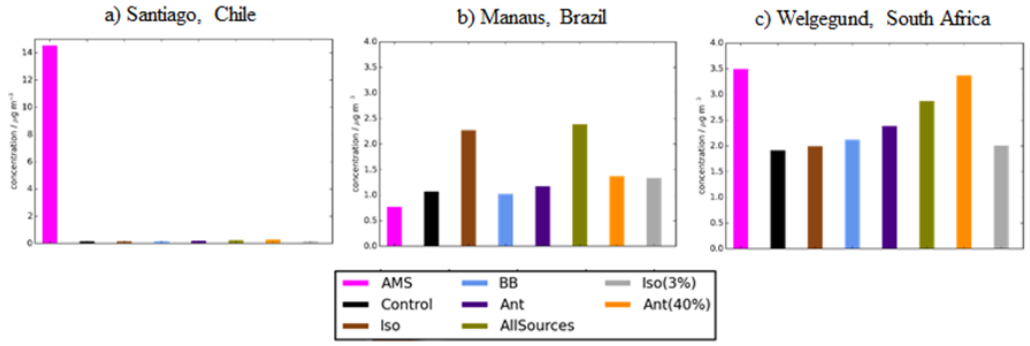

Figure 3.12 - Simulated and observed OA surface concentrations (μg m^{-3}) over an urban environment, (a) Santiago (Chile) and remote environments, (b) Manaus (Brazil) and (c) Welgegund (South Africa). Bars indicate observed (pink) and simulated OA surface concentrations from the control (black), Iso (brown), BB (light blue), Ant (dark blue), AllSources (green), Ant (40%) (yellow) and Iso (3%) (grey). Model simulations are described in Table 3.2.

Typical of densely populated cities, observed OA concentrations over Santiago are substantially higher than the modelled OA concentrations in all simulations. (Figure 3.11 a); which primarily reflects the difficulty of a coarse resolution global model to represent urban centres. Incorporation of these three observations expands the geographical coverage over which the model can be evaluated, especially over regions influenced by biogenic emissions. However, since these observations are not speciated, model biases in simulated OA concentrations cannot be attributed to SOA or POA concentrations. Biases in simulated SOA and POA concentrations can sometimes act in unison (i.e. urban environments) or in competition (i.e. remote) with one another (Tables 3.4 and 3.5), hence the underlying processes are harder to discern. Additionally, there is a very low density of observations in these key regions of the world, therefore, the representativity of these sites for the region as a whole is unknown.

In summary, when considering monoterpene as the only source of SOA, simulated SOA concnetrations are lower than observed in all site types environments, as well as over North North America, Europe and Asia. Model

performance is improved substantially when all new sources of SOA are included in the model, particularly due to the inclusion of an anthropogenic source of SOA. When the yield of anthropogenic SOA formation is increased, model agreement with observed SOA is further improved at all site types. However, there is now a very slight positive bias compared to observed SOA further downwind and in remote environments. When the spatial coverage of observations is expanded, to include measurements over South America and Africa, isoprene becomes an important source of SOA. However, as very few observations have been made in this region. the observations cannot be used to robustly evaluate the effects of all the different SOA sources. This highlights the need for more observations, particularly over regions of the world influenced by biogenic and biomass burning emissions.

3.5.2 **Evaluation of OA vertical profile**

In this section, simulated OA vertical profiles are compared to aircraft measurements from different campaigns that are described in Chapter 2. The measurement campaigns cover different chemical environments in the atmosphere, sampling remote regions, regions influenced by biomass burning in North America and polluted regions in Europe.

Figure 3.13 shows the simulated OA vertical profile against the AMS aircraft measurements. Generally, observed OA concentrations peak in the lowermost kilometre and decline with altitude (e.g. EUCAARI, AIDENT, OP3 and TROMPEX). Biomass burning (ARCTAS campaigns; Figure 3.12 – bottom left) perturbs the vertical profile and results in elevated OA concentrations up to ~ 8 km. Observed OA concentrations in the ARCTAS campaigns are extremely high and extremely variable. Low OA concentrations from these campaigns reflect the remote regions of North America which are being sampled from. High OA concentrations from this

campaign also reflect the plume-chasing approach, sampling directly from biomass burning plumes and resulting in extremely high OA concentrations.

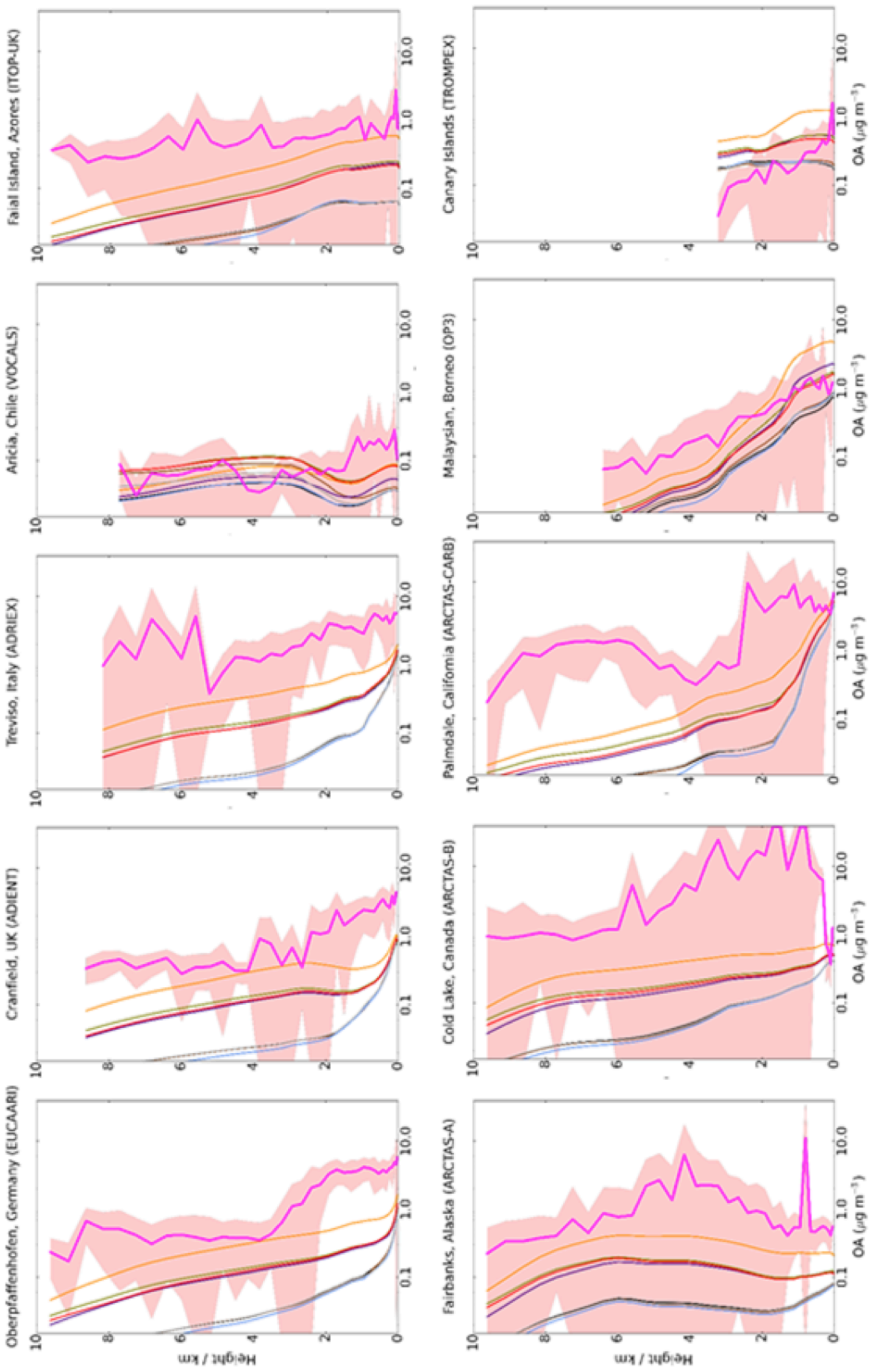

Figure 3.13 – Mean vertical profile of ambient OA (μg m^{-3}) for 10 field campaigns with the mean UKCA for the simulations described in Table 3.2. The standard deviation of the binned observations at each model layer are shown (peach envelope). Colours used are identical to Figure 3.12.

The monoterpene only simulation typically underestimates observed OA concentrations in all environments and at all altitudes (Figure 3.13). This is common among global models when evaluated against aircraft campaigns, in which simulated SOA is purely biogenic (Utembe et al., 2011;Khan et al., 2017). The simulated OA from the monoterpene only simulation compares relatively well in remote environments (Figure 3.13- right hand side), typically lying within one standard deviation of the observations.

When all SOA sources are included, OA concentrations increase, resulting in a smaller negative bias between simulated and observed OA concentrations at all altitudes. This is primarily due to the inclusion of the anthropogenic SOA source. However, simulated OA concentrations are larger than measured OA concentrations during the VOCALS and TROMPEX campaigns, especially at higher altitudes.

The anthropogenic sensitivity simulation generally improves model agreement with aircraft observations even further for the polluted and biomass burning influenced campaigns, such that the simulated OA concentrations now generally fall within one standard deviation of the measurements at most altitudes (Figure 3.13 left hand side). In contrast, OA concentrations simulated for the remote campaigns, OP3 and TROMPEX, are now substantially overestimated compared to measurements away from the surface. This is in agreement with Heald et al. (2011) who found that a large anthropogenic source for SOA results in positive biases in simulated OA concentrations in remote environments. Other reasons for disagreement between model results and observations relate to our comparison methodology, whereby observed OA concentrations span the time period 2000-2010 and simulated OA concentrations are from the year 2000 (section 3).

The inclusion of a biomass burning source of SOA has very little effect on model agreement with aircraft campaigns, even for campaigns influenced

by biomass burning activity (ARCTAS). However, simulated biomass burning emissions peak over South America and Central Africa (Figure 3.1 c), whereas the aircraft campaigns influenced by biomass burning emissions were conducted in North America (Figure 2.3). Furthermore, biomass burning emissions vary substantially from year to year. Therefore, the mismatch in time period and the use of decadal mean emissions is particularly relevant for regions influenced by biomass burning. Higher temporal resolution emissions in biomass burning influenced regions may help model agreement. Indeed, the use of daily-varying fire emissions inventories has been shown to help reproduce observed OA concentrations (Wang et al., 2011). In contrast, Shrivastava et al. (2105) find good agreement between simulated and observed OA when considering ARCTAS measurements, primarily due to their simulation of biomass burning SOA. These results highlight that biomass burning remains a highly uncertain source of SOA. Here, biomass burning SOA is considered from VOCs, with a global annual-total emission rate of 49 Tg (VOA) -1, and injected at the surface. Contrastingly, Shrivastava et al. (2015) treated biomass burning SOA from S/IVOCs, with global annual-total emissions of 450 Tg (VOC) a^{-1}, which are injected at the surface as well as at higher altitudes. Clearly, further research is required to identity the dominant sources of biomass burning SOA, as well emissions estimates and chemistry.

3.6 Conclusions

Studies on different SOA sources are usually cnoducted in isolation and compared against different sets of observations, resulting in difficulty in drawing robust conclusions on the role of each SOA source on the SOA global budget and on model agreement with observations. In this chapter, a global chemistry and aerosol model (UKCA) was used to simulate SOA using

all the known major sources of SOA comparing results to a consistent set of observations and examining their seasonal influence.

When monoterpene is the only source of SOA, the simulated annual global production rate is 19.9 Tg (SOA) a^{-1}. The inclusion of isoprene, biomass burning and anthropogenic sources of SOA increases the annual global SOA production rate by 19.6, 9.5 and 24.6 Tg (SOA) a^{-1} respectively. When all sources are included, the simulated annual global production rate is 74.0 Tg (SOA) a^{-1}, which lies within the range of estimates from other global modelling studies but is substantially lower than top-down estimates. In addition, it is found that SOA concentrations, at least for the global mean, respond linearly to changes in reaction yields.

During NH summer, high biogenic and biomass burning emissions combine with enhanced levels of photochemistry, resulting in the global SOA production rate and global SOA burden also peaking during this season. Contrastingly, the net effect of two seasonal cycles (a winter peak in anthropogenic emissions and a summer peak in photochemistry that influences oxidation) results in a global anthropogenic SOA production rate which is constant all year around. However, the global anthropogenic SOA burden shows a seasonal cycle, peaking during NH spring and winter. This is due to the seasonal cycle of the SOA lifetime, which is shortest during summer. As peak anthropogenic SOA concentrations occur over India and China, the summertime reduction in anthropogenic SOA lifetime is possibly due to enhanced wet removal. Simulated annual average SOA concentrations from both biogenic and biomass burning sources peak in the SH, in tropical forest regions of South America and Africa. Contrastingly, simulated annual average SOA concentrations from anthropogenic sources peak in the NH, over industrialised and urban regions of India, China, Europe and USA.

The addition of new SOA sources also affects the concentrations of primary organic aerosol (POA) due to enhanced condensation-ageing. This increases the proportion of hydrophilic POA and, therefore, reduces the POA lifetime. POA concentrations decrease over the Congo region and Siberia, which correspond to regions of increased SOA concentrations, available hydrophobic POA, and efficient wet removal.

Considering surface sites in the NH mid-latitudes, simulated SOA concentrations from the simulations with monoterpene as the only SOA source are substantially lower than observed (NMB = -91 %). Inclusion of all three new sources of SOA, isoprene, anthropogenic and biomass burning, improves model agreement with observations (NMB = -50 %). This is primarily due to the inclusion of an anthropogenic source of SOA whereas inclusion of isoprene and biomass burning as sources of SOA have little effect on model agreement with observations. However, a substantial underestimate remains in simulated SOA concentrations. When the reaction yield of SOA formation from anthropogenic sources was increased from 13 to 40 % (production = 73.6 Tg a^{-1}), model agreement with observations improves even further (NMB = -10 %). However, simulated SOA concentrations in urban environments are lower than observed (NMB = -34 %) whereas, further downwind (NMB = 14 %) and in remote environments (NMB = 12 %), simulated SOA concentrations are in relatively good agreement compared to observations albeit slightly overestimated. A large anthropogenic source of SOA may be plausible, however, the reaction yield required greatly exceeds that derived from most chamber studies to date, revealing a knowledge gap to be filled. Including POA oxidation may further improve the negative bias in modelled SOA and reduce POA lifetime, thus reducing the large positive bias in simulated POA in remote regions.

However, these results relate primarily to the NH mid-latitudes where anthropogenic emissions are highest. Extending the observational dataset to include measurements in the SH, Santiago (Chile), Manaus (Brazil), and

Welgegund (South Africa), shows that isoprene also has an effect on model agreement with observations, with simulated SOA concentrations closer to observed values at Welgegund (South Africa) but produce a greater overestimate at Manaus (Brazil) compared to observations. However, the lack of observations in regions influenced by biogenic and biomass burning results in very little constraint on these sources of SOA. When considering aircraft campaigns, with monoterpene as the only source of SOA, simulated SOA concentrations are substantially lower than observed in all environments and at all altitudes. Inclusion of new sources of SOA improves model agreement further, again, primarily due to the inclusion of an anthropogenic source of SOA.

There are several limitations in this study. Firstly, as highlighted, the scarcity of available observations result in difficulty in constraining simulated SOA. More observations of SOA are required in the SH, particularly over tropical forest regions of South America and Africa, where simulated SOA concentrations from biogenic and biomass burning sources are extremely high. The lumping of anthropogenic and biomass burning VOC species into single compounds also represents a significant uncertainty in this study. Emitted VOC species from each source are likely to have different emissions distributions, reaction kinetics and reaction yields which will likely result in differences in simulated SOA which will have not been captured in this study. However, explicitly simulating each VOC is hindered by a lack of knowledge of the dominant species and the required computational expense. Additionally, in this study, using the UKCA model VOC oxidation products of low enough volatility to condense are lumped into a single surrogate compound (SOG). Therefore, this assumption does not account for the volatility distribution of oxidation products. Chemical ageing in the atmosphere may be more efficiently represented using the volatility basis set (VBS) (Donahue et al., 2006). Additionally, dry and wet deposition of SOA precursors is not included in this model due to the lumping of species and

uncertainties in deposition parameters. Including dry and wet deposition of SOA precursors will likely reduce SOA concentrations. Another limitation to this study is the absence of aqueous SOA formation in aerosols (Ervens, 2015) and cloud water (McNeill et al., 2012). Further laboratory studies are required to provide detailed oxidation mechanisms of VOC species such that they can be implemented into chemistry-climate models. Future modelling work will evaluate dry deposition, wet deposition, and an evolving volatility distribution or SOA precursors, and their impacts on SOA formation.

Nevertheless, this chapter considers SOA formation from a number of different sources in a global composition-climate model, and compares against a consistent set of observations. Overall, the inclusion of new sources of SOA improves the ability of the UKCA model to simulate SOA distributions across many world regions. Additionally, the new estimate of the global SOA budget from UKCA lies within the range of estimates from other global modelling studies. Future modelling work should aim to improve confidence in SOA formation mechanisms, and to explicitly simulate multigenerational oxidation products (Chapter 4). Furthermore, observations of SOA are required in regions influenced by biogenic and biomass burning emissions, such as South America and Africa.

Chapter 4 The impact of VOC physical and chemical processing on the SOA lifecycle

This chapter is in the review process of publishing within an open-access journal called ‘Geoscientific Model Development‘ (GMD). The article is a collaboration with Professor Ruth Doherty, Dr Fiona O’Connor, Dr Graham Mann, Professor Hugh Coe, and Dr Dantong Liu. The article is available online (https://doi.org/10.5194/gmd-2018-142). Jamie Michael Kelly set-up, developed and performed all simulations, and wrote the first draft of the manuscript. Professor Ruth Doherty, Dr Fiona O’Connor provided advice on the modelling and analysis work, and also provided feedback on the manuscript. Dr Graham Man provided advice on the model development. Professor Hugh Coe and Dr Dantong Liu provided data from an aircraft campaign. The editor (Dr Jason Willians) provided additional feedback during the review process.

Jamie M. Kelly, Ruth M. Doherty, Fiona M. O’Connor, Graham W. Mann, Hugh Coe, and Dantong Liu, (2018), The roles of volatile organic compound deposition and oxidation mechanisms in determining secondary organic aerosol production: A global perspective using the UKCA chemistry-climate model (vn8.4)’, Geoscientific Model Development, (in review), https://doi.org/10.5194/gmd-2018-142.

4.1 Introduction

The emissions of Volatile Organic Compounds (VOCs) from various source types has a strong influence on the SOA lifecycle (Chapter 3). Once emitted, depending on the chemical and meteorological conditions, as well as the identity of the VOCs, physical and chemical processes further govern how much SOA is produced.

Organic gases can be physically removed from the atmosphere by undergoing dry or wet deposition. This processes can therefore prevents SOA formation (Section 1.9.5). Recent field and modelling studies suggest that several known SOA precursors are susceptible to deposition. A few global modelling studies include both dry and wet deposition of SOA precursors, but the deposition parameters used vary by several orders of magnitude (Section 1.9.5).

For an emitted organic gas, there is a plethora of potential oxidation pathways (Section 1.7.1-1.7.7). Crucially, the variability in oxidation pathways alters which products are formed. For instance, observed SOA yields from monoterpene (Section 1.7.2), isoprene (Section 1.7.1) and aromatic VOCs (Section 1.9.5) reduce with increasing levels of NO_X. As this sensitivity is observed even though NO_X is not involved in the first reaction step of these VOCs, the influence of NO_X must be on second or later generation products. However, these VOC multigenerational oxidation reactions are often reduced to less than two reaction steps when implemented in global models (Section 1.9.5).

The objectives of this chapter are two-fold. The first objective is further develop the SOA scheme within UKCA by extending deposition to include VOC precursors of SOA, and to enhance the complexity of VOC oxidation mechanisms. The second objective of this chapter is to quantify the influence

of these variations in VOC physical and chemical processing on the SOA lifecycle.

This chapter is organised as follows. The global chemistry-climate model used in this chapter is described in Section 4.2; this section also includes a description of the model developments applied to the SOA scheme. Next, the influence of precursor deposition on SOA is investigated (Section 4.3). In Section 4.4, the sensitivity of modelled SOA to oxidation mechanisms and VOC reactivity is explored. Concluding remarks and further work are discussed in Section 4.5.

4.2 Chemistry-climate model description

In this section, the chemistry-climate model used in this chapter is briefly described. The chemistry-climate model used in this chapter has been described before (Chapter 2), and is also developed in Chapter 3. Simulations are performed with the United Kingdom Chemistry and Aerosol (UKCA) model (Morgenstern et al., 2009; Mann et al., 2010; O'Connor et al. 2014) coupled to the Global Atmosphere 4.0 (GA4.0) configuration (Walters et al., 2014) of the Hadley Centre Global Environmental Model version 3 (HadGEM3; Hewitt et al. (2011)). Horizontal winds and temperature in the model are nudged towards ERA-Interim reanalyses (Dee et al., 2011) using a Newtonian relaxation technique with a relaxation time constant of 6 hours (Telford et al., 2008).

The United Kingdom Chemistry and Aerosol (UKCA) model used in this study combines the "TropIsop" tropospheric chemistry scheme from O'Connor et al. (2014) with the stratospheric chemistry scheme from Morgenstern et al. (2009). The aerosol component of UKCA is the 2-moment modal version of the Global Model of Aerosol Processes (GLOMAP-mode)

(Mann et al., 2010).Gas-phase and aerosol-phase chemistry of the model are described in greater detail in Section 2.3 and 2.4, respectively.

The emissions used are all decadal-average emissions, centred on the year 2000, and monthly varying. Anthropogenic and biomass burning gas-phase emissions are prescribed following Lamarque et al. (2010). Biogenic emissions of isoprene, monoterpene and methanol (CH_3OH) are also prescribed, taken from the Global Emissions Inventory Activity (GEIA), based on Guenther et al. (1995). A diurnal cycle in isoprene emissions is imposed based on the solar zenith angle. POA and BC emissions from fossil fuel combustion are prescribed following Lamarque et al. (2010). POA and BC emissions from savannah burning and forest fires are prescribed, taken from the Global Fire Emissions Database (GFEDv2 (van der Werf et al., 2010)). Emissions used for all simulations in this chapter are identical to those used in Chapter 3. All carbonaceous emissions are emitted into the insoluble mode and are transferred to the soluble mode by condensation ageing. Ageing proceeds at a rate consistent with a 10-monolayer coating being required to make a particle soluble.

4.2.1 **Initial treatment of SOA**

In this section, the current treatment of SOA in the UKCA model is first described, followed by descriptions of new treatments of precursor deposition and oxidation mechanisms. The SOA scheme used for the basis of this chapter corresponds to the ‘AllSources’ simulation in Chapter 3. Within the model, SOA is treated by a coupling between the UKCA gas-phase chemistry and GLOMAP-mode. Emitted parent hydrocarbon gases undergo a single-step oxidation, forming a secondary organic gas (SOG) which condenses, forming SOA. This is shown in E4.1, below. Note, this equation is analogous to E3.1.

$$VOC + [o] \xrightarrow{k_{VOC+[O]}} \alpha_{VOC+[O]} SOG \rightarrow SOA \quad \text{(E4.1)}$$

where VOC is the concentration of the emitted parent hydrocarbon, [o] is the oxidant concentration, $k_{VOC+[O]}$ is the temperature-dependent rate coefficient (E4.1), $\alpha_{VOC+[O]}$ is the stoichiometric coefficient, and SOG is the secondary organic gas. SOG condenses irreversibly to form SOA in UKCA. The yield is identical for all oxidation reactions (13 %), regardless of VOC or oxidant. Essentially, the volatility distribution is assumed to be identical for all reactions, irrespective of parent VOC and oxidant. In the model, no SOA precursor undergoes dry or wet deposition.

In this chapter, SOA production is considered from VOCs. These include monoterpene, isoprene, a lumped biomass burning VOC (VOC_{BB}) and a lumped anthropogenic (VOC_{ANT}) (Chapter 3). Monoterpene and isoprene contain both single and double carbon bonding and therefore react with ozone (O_3) and the hydroxyl (OH) and nitrate (NO_3) radicals, forming SOG and subsequently SOA (E4.1). Note, for isoprene, oxidation in the context of SOA production (E4.1) occurs independently to isoprene oxidation in the Mainz Isoprene Mechanism described in Section 2.1. Reaction kinetics for isoprene and monoterpene (α-pinene) oxidation are taken from Atkinson and Arey (2003), and are shown in Table 4.1.

As discussed in Chapter 3, VOC_{ANT} and VOC_{BB} are surrogate compounds, which do not retain molecular information, and therefore, do not have laboratory derived rate constants. Initially, the assumption is made that VOC_{ANT} and VOC_{BB} are reduced compounds, with only single carbon bonding and react predominantly with OH. VOC_{ANT} and VOC_{BB} are also assumed to have a similar reactivity to monoterpene towards OH oxidation, but do not react with O_3 or NO_3. These assumptions in the parent hydrocarbon reactivity are discussed further in Section 2.4.2. As stated above, none of the SOA precursors in this scheme are wet or dry deposited. In summary, the current SOA scheme suffers from a lack of mechanistic

detail in oxidation mechanisms, and neglects precursor deposition. In the following sub-sections, modifications to the model are described and the impacts of these processes quantified.

Table 4.1- Kinetic parameters used to calculate rate coefficient (E4.1) for both existing and new SOA precursors, taken from Atkinson and Arey (2003).

Reaction	k_0 / 10^{-12} x cm^3 $molecule^{-1}$ s^{-1}	B / K	k (298) / 10^{-12} x cm^3 $molecule^{-1}$ s^{-1}	Stoichiometric yield / %
existing reaction kinetics				
monoterpene+ OH	12.0	-444.0	52.9	13
monoterpene+ O_3	0.00101	732.0	0.0000862	13
monoterpene+ NO_3	1.19	-925.0	6.12	13
isoprene + OH	27.0	-390.0	99.3	13
isoprene + O_3	0.01	1195.0	0.000180	13
isoprene + NO_3	3.15	450.0	0.692	13
new reaction kinetics				
naphthalene + OH	15.7	-117.0	23.2	100
toluene + OH	1.82	-338.0	5.62	100
benzene + OH	2.34	193.0	1.22	100
RO_2 + HO_2	1.41	-700.0	14.7	See table 4.3
RO_2+ NO	2.62	-350.0	8.42	See table 4.3

4.2.2 **Addition of SOA precursor deposition**

Precursors of SOA include the emitted parent hydrocarbons (monoterpene, isoprene, VOC_{ANT}, VOC_{BB}) and the secondary organic product (SOG). Several modifications were made to UKCA to investigate the influence of precursor deposition on SOA. Firstly, wet deposition of the gas-phase species, as described in Section 2.1.1, is extended to include all SOA precursors. The effective Henry's Law coefficient, for all SOA precursors, was either set to 10^5 or 10^9 M atm^{-1}. These values of H_{eff} were taken from estimates by Hodzic et al. (2014). Secondly, the treatment of dry removal of gas-phase species (section 2.1.2) was extended to include all SOA

precursors and they were assumed to have identical surface resistances. Table 4.2 shows the surface resistances for the SOA precursors over the 9 surface types. The aerodynamic and quasi-laminar surface resistances were calculated online, based on relative molecular mass and meteorology. During field studies over forested regions, organic hydroperoxides (ROOH) were observed to undergo significant dry deposition (Hall et al., 1999;Valverde-Canossa et al., 2006;Nguyen et al., 2015). Surface resistances derived from these field studies range from 5 – 40 sm^{-1} (Hall et al., 1999;Nguyen et al., 2015). Hence, these field-derived surface resistances of ROOH ('Low'; Table 4.2) were used to provide a lower estimate of the surface resistances of SOA precursors. Surface resistances corresponding to the dry deposition of CO ('High'; Table 4.2) are used to provide an upper limit of the surface resistances of SOA precursors.

Table 4.2 - Surface resistances for SOA precursors over the 9 different surface types in the model. 'Low' represents surface resistances of ROOH, which were derived from field studies (Hall et al., 1999;Nguyen et al., 2015). 'High' represents surface resistances of CO.

surface type	Surface resistance (r_c) / sm^{-1}	
	Low	High
Broadleaf trees	30	3700
Needleleaf trees	10	7300
C3 grasses	10	4550
C4 grasses	10	1960
Shrubs	10	4550
Urban	10	-
Water	10	-
Bare soil	10	4550
Ice	20000	-

4.2.3 **New $VOC_{ANT/BB}$ oxidation mechanism**

Initially, $VOC_{ANT/BB}$ follows a single-step oxidation mechanism, with a single fixed SOA yield, and with a reactivity based on α-pinene (Table 4.1). However, of the anthropogenic and biomass burning VOCs related to SOA production, aromatic compounds are identified as important components in field studies (Von Schneidemesser et al., 2010;Ding et al., 2012;Guo et al., 2012;Peng et al., 2013). Furthermore, environmental chamber studies suggest aromatic hydrocarbons undergo multi-generational oxidation reactions, with SOA yields dependent on oxidant concentrations (Ng et al., 2007b;Chan et al., 2009;Kautzman et al., 2010;Li et al., 2016;Al-Naiema and Stone, 2017;Li et al., 2017b;Schwantes et al., 2017). Therefore, in order to examine how SOA is affected by variations in oxidation mechanisms, chamber-derived aromatic oxidation pathways are applied to $VOC_{ANT/BB}$. This section outlines how the chamber-derived aromatic oxidation pathway, postulated by Ng et al. (2007b), is applied to the mechanistic description of SOA production from $VOC_{ANT/BB}$ within UKCA.

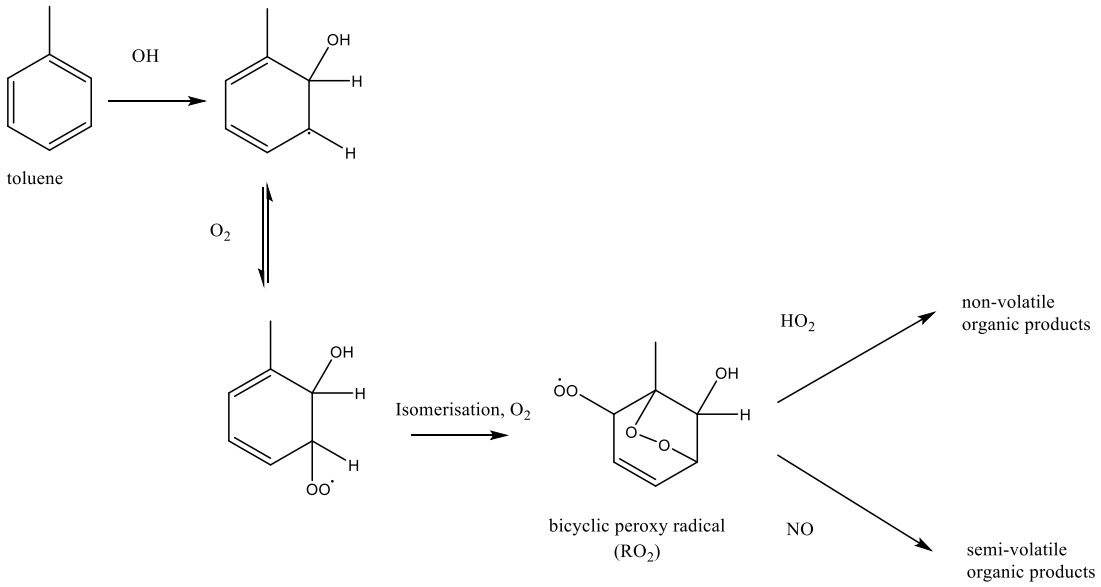

Figure 4.1 - Formation of lower volatility vapours from toluene photooxidation, as described in Ng et al. (2007b). Note, this figure is also presented in Chapter 1, but replicated here for clarity.

Figure 4.1 shows a mechanistic description of SOA production from toluene, accounting for the influence of NOx on SOA production, adapted from Ng et al. (2007b). Briefly, toluene undergoes oxidation by OH, followed by addition of oxygen and isomerisation, to form a bicyclic peroxy radical, RO_2. The bicyclic peroxy radical undergoes competitive reactions with hydroperoxyl radical (HO_2) and NO. The HO_2 pathway forms non-volatile products, whereas products of the NO pathway are semi-volatile. Although Figure 4.1 shows a mechanistic description of toluene oxidation, the oxidation of other methylated aromatic compounds will also follow a similar pathway. This mechanism for aromatic oxidation, as shown in Figure 4.1, was applied to $VOC_{ANT/BB}$ oxidation. The rate determining step in Figure 4.1 is the initial oxidation by OH and, therefore, the mechanism can be simplified as shown below:

$$VOC + [o] \xrightarrow{k_{VOC+OH}} RO_2 \xrightarrow{k_{RO_2+HO_2}} \alpha_{RO_2+HO_2} SOG \rightarrow SOA$$

$$\xrightarrow{k_{RO_2+NO}} \alpha_{RO_2+NO} SOG \rightarrow SOA \qquad \text{(E4.2)}$$

where VOC represents $VOC_{ANT/BB}$, k_{VOC+OH} represents the rate constant for aromatic oxidation by OH, RO_2 represents the bicyclic peroxy radical, $k_{RO2+HO2}$ and $\alpha_{RO2+HO2}$ represent the rate constant and the stoichiometric coefficient for the RO_2+HO_2 reaction, respectively, and k_{RO2+NO} and α_{RO2+NO} represent the rate constant and the stoichiometric coefficient for the RO_2+NO reaction, respectively. Within the model, the difference in volatility distribution between the products of the RO_2 reactions are controlled by the stoichiometric coefficients ($\alpha_{RO_2+HO_2}$ and α_{RO_2+NO}). Note, this reaction mechanism is analogous to E1.3.

Previous modelling studies use a similar method to treat SOA production via the RO_2+HO_2 pathway. Assuming that the products from oxidation of explicit aromatic compounds are non-volatile, Henze et al. (2008) uses a stoichiometric yield of around 18 %. Using IVOC emissions based on naphthalene, Pye and Seinfeld (2010) uses a stoichiometric coefficient of 73 %. However, both Henze et al. (2008) and Pye and Seinfeld (2010) treat products from the RO_2+NO pathway as semi-volatile, with stoichiometric yields ranging from 2 to 107 %, and equilibrium partitioning coefficients ranging from 0.0037 to 3.3150 m^3 μg^{-1}. The reaction kinetics for aromatic oxidation used here are shown in Table 4.1.

4.2.4 **Model simulations**

In this chapter, 10 simulations are performed to explore the influence of hydrocarbon deposition and oxidation mechanisms on SOA, and are described in Table 4.3. The duration of all simulations is two years, spanning

from 1999 to 2000. The first year is discarded as spin-up, and analysis was performed on the second year - 2000.

Firstly, a control simulation was conducted, where the oxidation of all parent hydrocarbons (isoprene, monoterpene, VOC_{ANT} and VOC_{BB}) followed E4.1 and no SOA precursors were lost by wet or dry deposition processes. Next, the influence of VOC deposition on SOA is explored. To begin with, precursors were assumed to have low surface resistances (Low; Table 4.2), thus, testing the upper limit for precursor dry deposition (Dry_High; Table 4.3). Next, the strength of precursor surface resistance is increased (High; Table 4.2), testing the lower limit for deposition rates (Dry_Low; Table 4.3). Next, SOA precursors were treated as soluble and were, therefore, included in the wet deposition scheme. As with dry removal, the upper and lower limits of precursor wet deposition are tested by carrying out two simulations, one with a higher solubility (Wet_High), and one with a lower solubility (Wet_Low). An additional simulation is conducted to test whether the effects of precursor dry and wet deposition on SOA are additive (DryH_WetL). Note, for this simulation, dry and wet deposition are included with low surface resistances (Low; Table 4.2) and low solubility. Alternative combinations of surface resistances and solubility could have been used to quantify the combined influence of precursor dry and wet deposition on SOA.

Next, the influence of VOC oxidation mechanisms on SOA is explored by modifying the mechanistic description of SOA production from anthropogenic and biomass burning VOCs. As discussed in Section 4.1, oxidation mechanisms within SOA schemes vary substantially. Therefore, in this section, where necessary, changes to $VOC_{ANT/BB}$ oxidation were made in a step-wise fashion, in order to isolate the effects of individual changes.

Firstly, the combined effects of the use of a reactive aromatic compound (naphthalene) and introducing a reaction intermediate (RO_2) are explored in the Multi_nap simulation, where $VOC_{ANT/BB}$ follows E4.2. In this

simulation, stoichiometric reaction yields of 13 % are applied to both RO_2 oxidative pathways, which is identical to the reaction yield applied to simulations following the single-step mechanism (E4.1). The effects of changes to parent $VOC_{ANT/BB}$ reactivity, the chemical fate of the new reaction intermediate, and SOA production from this intermediate are discussed separately, in Sections 4.4.1.1, 4.4.1.2, and 4.4.1.3, respectively.

Next, the influence of accounting for the difference in volatility distribution of products between the peroxy radical pathways is accounted for in a further model experiment (Multi_nap_yield), which is discussed in Section 4.4.1.4. This is achieved by increasing the SOA yield from 13 to 66 % for the HO_2 pathway, whilst leaving the reaction yield for the NO pathway unchanged at 13 %. A stoichiometric yield of 66 % is selected as this allows quantification of the theoretical upper limit of SOA production from this pathway. RO_2 and SOG have differing relative molecular masses. Consequently, a stoichiometric yield of 66 % corresponds to a mass yield of 100 %. Therefore, 66 % is the highest stoichiometric yield that ensures conservation of mass without the addition of other atoms, such as oxygen.

The influence of parent hydrocarbon reactivity is then explored, whilst maintaining identical reaction mechanisms and yields (Section 4.4.1.5). In this simulation, $VOC_{ANT/BB}$ adopts the reactivity of toluene (Multi_tol_yield) and benzene (Multi_benz_yield) (Table 4.3). Note, for the simulations investigating the influence of oxidation mechanisms on SOA, isoprene and monoterpene oxidation is unchanged. The emissions of all SOA precursors (isoprene, monoterpene, and $VOC_{ANT/BB}$) are identical in all the simulations.

Table 4.3 Simulations conducted in this study. Surface resistances, Low and High, are shown in Table 4.2. For both surface resistances and Heff, all SOA precursors are assumed to have identical parameters. The oxidation mechanism for isoprene and monoterpene follows Eq (8) in all simulations. Emissions for all SOA precursors are identical across all simulations.

	Surface resistance profile	H_{eff} / M atm^{-1}	$VOC_{ANT/BB}$ oxidation mechanism	$k_{VOC_{ANT/BB}+OH}$(298 K) / 10^{-12} x cm^3 $molecule^{-1}$ s^{-1}	$\alpha_{RO_2+HO_2}$ / %	α_{RO_2+NO} / %	Global annual-total SOA production / Tg (SOA) a^{-1}
Control	-	-	Eq (8)	52.87	-	-	75
Dry_High	Weak	-	Eq (8)	52.87	-	-	51
Dry_Low	Strong	-	Eq (8)	52.87	-	-	73
Wet_Low	-	10^5	Eq (8)	52.87	-	-	63
Wet_High	-	10^9	Eq (8)	52.87	-	-	62
DryH_WetL	Weak	10^5	Eq (8)	52.87	-	-	47
Multi_nap	Weak	10^5	Eq (9)	23.32	13	13	46
Multi_nap_yield	Weak	10^5	Eq (9)	23.32	66	13	71
Multi_tol_yield	Weak	10^5	Eq (9)	5.66	66	13	61
Multi_benz_yield	Weak	10^5	Eq (9)	1.22	66	13	46

4.3 Influence of precursor deposition on the SOA lifecycle

In this section, the influence of VOC deposition (Section 4.2.2) on simulated SOA is quantified. Next, the influence of VOC deposition on model agreement with observations is evaluated.

4.3.1 **Simulated SOA budget and concentrations**

When precursor deposition is neglected from the model, the simulated global annual-total SOA production rate is 75 Tg (SOA) a^{-1} (Control; Table 4.3). The inclusion of VOC dry deposition with high surface resistances (High; Table 4.2) reduces the global annual-total SOA production rate by only 2 Tg (SOA) a^{-1} (2 %) (Dry_Low; Table 4.3). However, the rate of VOC dry deposition is highly sensitive to the value of surface resistance. The inclusion of VOC dry deposition with lower surface resistances (Low; Table 4.2) reduces the global annual-total SOA production rate by 24 Tg (SOA) a^{-1} (32 %) (Dry_High; Table 4.3). Therefore, inclusion of precursor dry deposition reduces the global annual-total SOA production rate by 2-24 Tg (SOA) a^{-1}, or 2-32 %, with this range reflecting uncertainties in surface resistances (Table 4.3).

Wet removal also has a substantial impact on SOA. For example, under the assumption of an effective Henry's coefficient of 10^5 M atm^{-1}, wet deposition reduces the global annual-total SOA production rate by 12 Tg (SOA) a^{-1} (15 %) compared to when no precursors undergo deposition (Wet_Low; Table 43). However, as discussed in Section 4.1, H_{eff} has been calculated to range from 10^5 to 10^9 M atm^{-1} for VOC precursors of SOA from different sources (Hodzic et al., 2014). In this study, when H_{eff} of SOA precursors is increased to 10^9 M atm^{-1}, wet removal reduces the global annual-total SOA production rate by only 13 Tg (SOA) a^{-1} (17 %) (Wet_High; Table 4.3). Therefore, the influence of precursor wet deposition on SOA is rather insensitive to uncertainties in the range of effective Henry's coefficients.

Generally, global (Hodzic et al., 2016) and regional (Bessagnet et al., 2010;Knote et al., 2015) scale modelling studies suggest that dry deposition of precursor dominates over wet deposition. Therefore, for subsequent

simulations, where both dry and wet removal were included in the model (DryH_WetL), surface resistances corresponding to Dry_High, which had the largest impact on global SOA production, were used, along with H_{eff} of 10^5 M atm^{-1} (Wet_Low). The influence of dry and wet deposition of precursors on the global SOA budget are not additive. The combination of dry and wet deposition of VOCs reduces the global annual-total SOA production rate by 28 Tg (SOA) a^{-1} (37 %) (DryH_WetL; Table 4.3). Overall, deposition of SOA precursors has a substantial impact on the global SOA budget, with the global annual-total SOA production rate from all VOC source ranging from 47 to 74 Tg (SOA) a^{-1}, with the range reflecting uncertainties in precursor deposition (Table 4.3).

Figure 4.2 shows the sensitivity of annual-average surface SOA concentrations to precursor deposition. The spatial distribution of SOA closely reflects the location of biogenic, anthropogenic and biomass burning emissions, as noted previously (Kelly et al. 2018). Over India, extremely high anthropogenic emissions combine with moderate biogenic emissions to result in annual-average surface SOA concentrations reaching up to 17 µg (SOA) m^{-3} (Figure 4.2 a). Over tropical forest regions of South America and Africa, biogenic and biomass burning emissions are extremely high, resulting in annual-average surface SOA concentrations ranging from 2 to 10 µg (SOA) m^{-3} (Figure 4.3 a). Over Europe and North America, moderate emissions from anthropogenic and biogenic sources generate annual-average surface SOA concentrations in the range of 0.3 – 6 µg (SOA) m^{-3} (Figure 4.2 a).

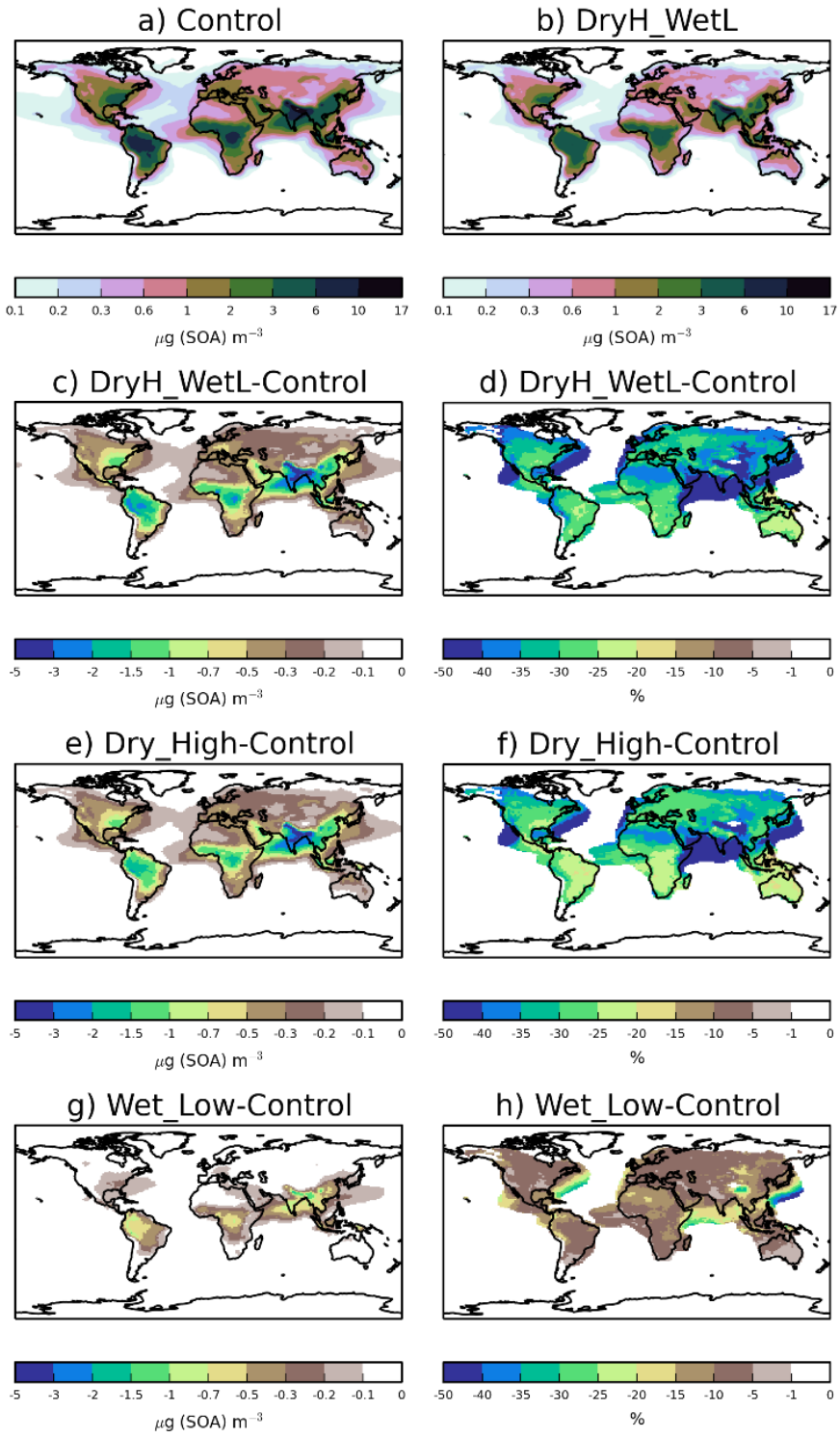

Figure 4.2 - Annual-average surface SOA concentrations for a) Control, and b) DryH_WetL simulations, and absolute and percentage differences in annual-average surface SOA concentrations for (c - d) DryH_WetL, (e - f) Wet_Low, and (h – i) Dry_High simulations relative to the Control.

Over India and tropical forest regions of South America and Africa, including VOC dry deposition reduces annual-average surface SOA concentrations by 1.5 to 5 μg (SOA) m^{-3} (Figure 4.2 e), corresponding to reductions of 15 to 50 % (Figure 4.2 f). Over these same regions, inclusion of precursor wet deposition reduces annual-average surface SOA concentrations by 0.5 to 1.5 μg (SOA) m^{-3} (Figure 4.2 g), corresponding to reductions of 5 – 10 % (Figure 4.2 h). Over North America, annual-average surface SOA concentrations are reduced by 0.3 – 1.5 μg (SOA) m^{-3} when precursor dry removal is included (Figure 4.2 e), corresponding to a reduction of around 20 to 35 % (Figure 4.2 f). Over Europe, dry deposition lowers annual-average surface SOA concentrations by around 0.2 μg (SOA) m^{-3} (25 – 40 %, Figures 4.2 e, f). Over both North America and Europe, the inclusion of wet deposition reduces annual average surface SOA concentrations by less than 0.2 μg (SOA) m^{-3} (Figure 3 g), but this corresponds to reductions of 20 to 35 % (Figure 4.2 h).

Until now, the impacts of precursor deposition on SOA concentrations have only been quantified over Europe (Bessagnet et al., 2010) and North America (Knote et al., 2015). The sensitivity of SOA to precursor dry removal is in broad agreement with Bessagnet et al. (2010), who estimates that precursor dry deposition reduces July-average surface SOA concentrations by 20 – 40 % over Europe, compared to 25 - 35 % for the same period in our study. Also, Knote et al. (2015) estimates that precursor dry deposition reduces annual-average surface SOA concentrations by 46 % over North America, compared to up to 20 - 35 % in our study. The modelled sensitivity of SOA concentrations to wet deposition in this study is in relatively good agreement with Knote et al. (2015), who estimates a 10 % reduction in annual-average surface SOA concentrations over North America when precursor wet deposition is included, which agrees with the 5 - 15 % reduction found here.

When dry and wet removal of VOC precursors are both included, SOA concentrations are substantially lower. However, as noted before, the effects of these removal processes do not add linearly. Inclusion of both dry and wet deposition of SOA precursors reduces annual-average surface SOA concentrations by 25 – 40 % over most continental regions (Figure 3 d), with maximum reductions of 5 μg (SOA) m^{-3} over India (Figure 4.2 c).

The lifetime of SOA precursors with respect to both oxidation and deposition is small. Hence, SOA precursors undergo very little transport before removal. Therefore, dry and wet deposition rates of VOCs are largest over terrestrial environments, where they are released.

4.3.2 Comparison of simulated and observed OA concentrations

In this section, the influence of SOA precursor deposition on model agreement with observations is quantified. First, simulated SOA and OA concentrations are evaluated against surface observations in the northern hemisphere (NH) and southern hemisphere (SH), respectively. Next, vertical profiles of simulated OA concentrations are compared against aircraft observations.

Figure 4.3 shows SOA concentrations for the simulations described in Table 4.2, compared to observed surface SOA concentrations across the NH mid-latitudes (Figure 2.3; Chapter 2). When deposition of SOA precursors is omitted from the model, simulated SOA concentrations are substantially lower than observed, with a normalised mean bias (NMB) of -50 % (Figure 4.3 a). The model negative bias is present for each site-environment type but most evident in urban environments. For several sites in urban environments, observed SOA concentrations exceed simulated SOA concentrations by

greater than a factor of 10 (Figure 4.3 a – red triangles). The model negative bias is also consistent regionally. Without SOA precursor deposition, the NMB for Europe, North America and Asia is -50, -37 and -62 %, restively.

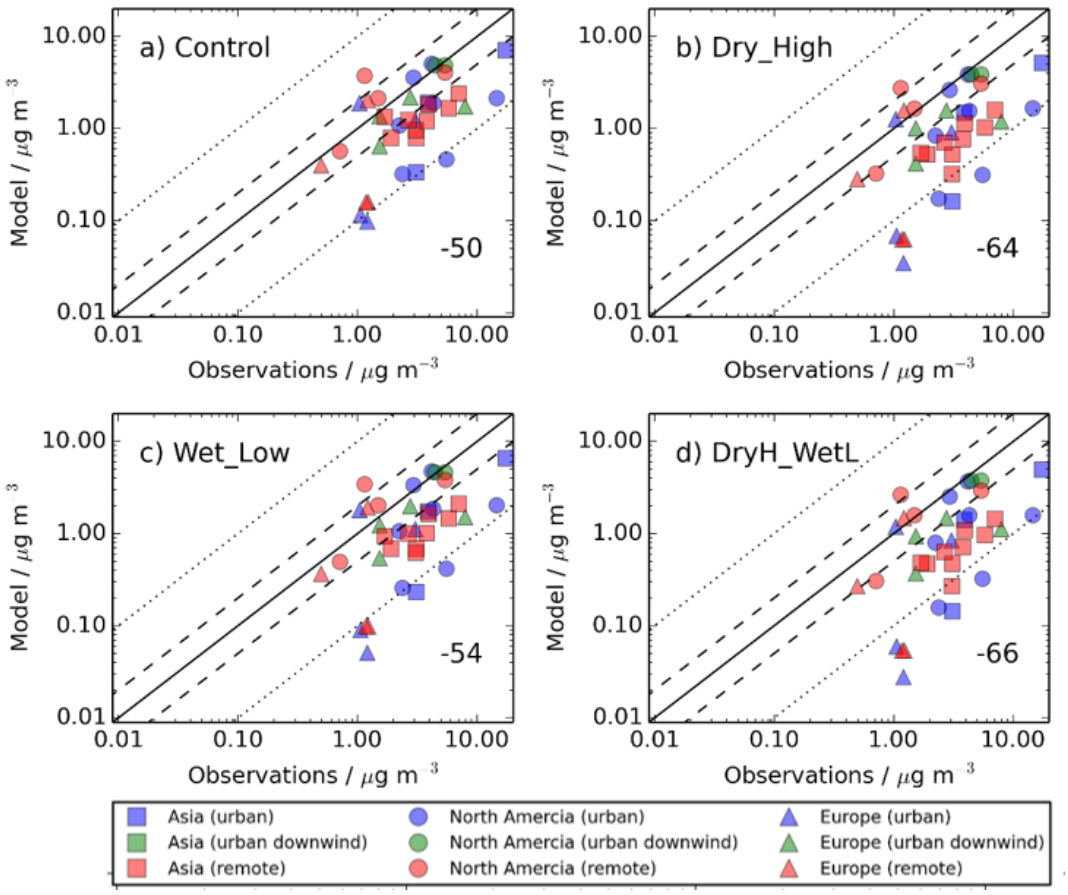

Figure 4.3 - Simulated versus observed surface SOA concentrations (μg m^{-3}) for a) Control, b) Dry_High, c) Wet_Low and d) DryH_WetL simulations, described in Table 4.3. Observations, originally compiled by Zhang et al. (2007), for the time period 2000-2010, are classified by site type - urban (blue), urban downwind (green) or remote (red), and continent – Asia (squares), North America (circles) and Europe (triangles). Observed oxygenated-OA is assumed to be comparable to simulated SOA. The 1:1 (solid), 1:2 and 2:1 (dashed), and 1:10 and 10:1 (dotted) lines are indicated. Numerical values in the bottom right of each panel indicate the normalised mean bias (%).

The model negative bias with respect to observed SOA concentrations is common among global models (Tsigaridis et al., 2014). For several

modelling studies, the negative bias is primarily attributed to either underestimated reaction yields, underestimated emissions, and/or missing emissions sources. Hodzic et al. (2016) partially attributes the model negative bias with respect to observations to laboratory-derived SOA yields which do not account for wall losses. Other studies highlight VOC emission uncertainties such as underestimates in inventories (Li et al. (2017a), or the absence of semi- and intermediate-volatility organic compounds (S/IVOCs) which can contribute to SOA (Pye and Seinfeld, 2010).

Inclusion of precursor deposition further reduces model agreement with observations. As discussed in Section 4.3.1, including VOC dry deposition reduces the global annual-total SOA production rate by 32 % (24 Tg (SOA) a^{-1}), whereas including VOC wet deposition reduces SOA production by 15 % (12 Tg (SOA) a^{-1}) (Table 4.3). Therefore, the model negative bias is larger when including dry deposition (NMB = -64 %; Figure 4.3 b) compared to that when including wet deposition (NMB = -54 %; Figure 4.3 c). However, as the effects of VOC precursor dry and wet removal on simulated SOA are not additive, model performance is not substantially worse when both wet and dry deposition are considered (NMB = -66 %; Figure 4.3 d). When the measurement sites are categorised by region, with both dry and wet removal included, the NMB across Europe, North America and Asia is -66, -53 and -77 %, respectively.

Observed and simulated OA are shown in Figure 4.4 for two sites in the tropics and SH, over Manaus (Brazil) and Welgegund (South Africa). Without precursor deposition, simulated SOA is overestimated compared to observed OA over Manaus (Brazil) (Figure 4.4 a), but underestimated over Welgegund (South Africa) (Figure 4.4 b). Therefore, inclusion of precursor deposition improves model performance over Manaus (Brazil) (Figure 4.4 a), but not over Welgegund (South Africa) (Figure 4.4 b). However, the scarcity of observations in the tropics and the SH result in difficulty in drawing robust

conclusions on the influence of precursor deposition on model agreement with observations in this region.

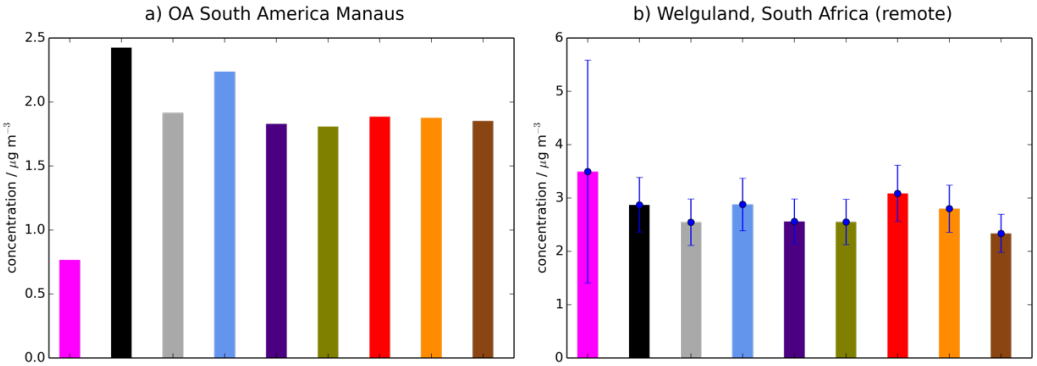

Figure 4.4 – Simulated and observed OA surface concentrations (μg m^{-3}) over remote sites in the SH, a) Manaus (Brazil), and b) Welgegund (South Africa). Bars indicate OA concentrations from observed (pink), and simulated from the Control (black), Dry_High (grey), Wet_Low (blue), DryH_WetL (purple), Multi_nap (green), Multi_nap_yield (red), Multi_tol_yield (yellow), and Multi_benz_yield (brown) simulations, described in Table 4.3. For Welgegund, both observed and simulated monthly mean OA concentrations span an entire year. The standard deviations across this year, based on the monthly-mean data, are indicated in blue. For Manaus however, the measurements of OA only span one month, hence, no standard deviation is shown for this site.

Figure 4.5 shows the simulated OA vertical profiles against the AMS aircraft measurements. Without precursor deposition, model negative biases are again evident and are largest in polluted and biomass burning influenced regions in the NH. For example, over Europe (AIDENT, ADRIEX and EUCAARI) and North America (ARCTAS-A, ARCTAS-B and ARCTAS-CARB), OA concentrations are underestimated by 71% (ARCTAS-CARB; Figure 4.5 j) to 97 % (ARCTAS-B; Figure 4.5 h) when considering all altitudes. When VOC precursors of SOA do not undergo deposition, over Western Afrcia, simulated OA concentrations are in good agreement between 0 and 3 km (Figure 4.5 k). However, above 3 km, model and simulated OA concentrations begin to deviate, with observed OA increasing

with altitude, but modelled OA decreasing with altitude (Figure 4.5 k). When considering all altitudes of the AMMA campaign, modelled and measured OA concentrations are in fairly good agreement, with a NMB of -53 % (Figure 4.5 k).

Over North America and Europe, including precursor deposition slightly worsens the model negative bias. When both precursor dry and wet deposition are included, the model underestimates observed OA concentrations by 75% (ARCTAS-CARB; Figure 4.5 j) to 98 % (ARCTAS-B; Figure 4.5 h). Over West Afrcia, when VOC precursors of SOA undergo deposition, the model underestimates observed OA concentrations by 61 % (Figure 4.5 k).

Compared to other environments, in remote regions, model agreement with observations is relatively good, and the inclusion of precursor deposition results in both improvements and degradations in model biases in simulated OA compared to observations. Without SOA precursor deposition, simulated OA levels in VOCALS and ITOP-UK, similar to the pollution and biomass burning influenced regions, are much lower compared to observed OA (NMB = -22 and -78 %; Figure 4.5 a and g, respectively). Therefore, inclusion of precursor deposition further reduces model agreement with observations (NMB = -49 and -91 %; Figure 4.5 a and g, respectively). In contrast, for the TROMPEX and OP3 campaigns, when precursor deposition is neglected, simulated OA is higher than observed (NMB = 25 and 5 %; Figure 4.5 b and c, respectively). Inclusion of precursor deposition at these locations changes the model positive bias into a negative bias (NMB = -23 and -22 %; Figure 4.5 b and c, respectively). For all aircraft campaigns conducted in remote environments, generally, simulated OA lies within one standard deviation of the observed concentration, irrespective of whether deposition of precursors is considered or not.

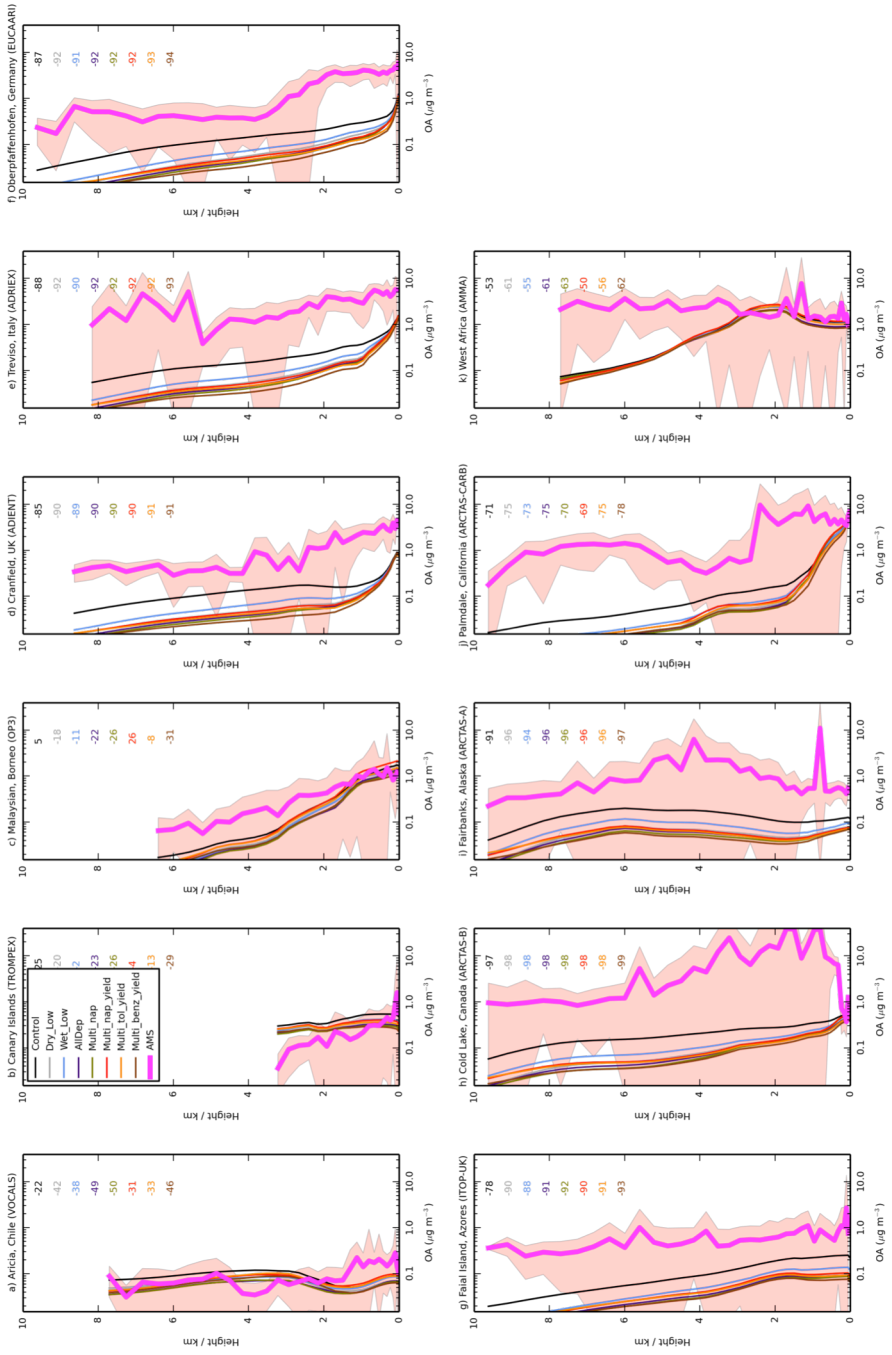

Figure 4.5 – Mean vertical profile of OA (μg m^{-3}) from 11 field campaigns (pink) with monthly mean modelled OA from UKCA for the simulations described in Table 4.3. The standard deviation of the binned observations at each model layer is shown (peach envelope). For each campaign, the normalised mean bias (%) for each simulation is also included in the top right of each panel.

Overall, the inclusion of precursor deposition influences model agreement with observations somewhat. In particular, inclusion of precursor deposition worsens model negative biases with respect to observations in the NH mid-latitudes. However, differences between simulated OA concentrations from these simulations is substantially less than the difference between simulated and observed OA. These results highlight that variations in VOC deposition contribute to considerable uncertainty in both the global SOA budget and have some impact on model agreement with observations.

4.4 The influence of aromatic oxidation mechanisms on SOA

In this section, the sensitivity of SOA to hydrocarbon oxidation mechanisms is quantified. Here, oxidation mechanisms for anthropogenic and biomass burning VOCs are modified as described in Section 4.2.3. To begin with, the influence of anthropogenic and biomass burning VOC oxidation mechanisms on simulated SOA is explored. Next, the impact on model agreement with observations is evaluated. In all simulations, deposition of SOA precursors is included (Table 4.3), emissions of all SOA precursors are held constant, and the mechanistic description describing the oxidation of biogenic SOA precursors (monoterpene and isoprene) is held fixed, following E4.1.

4.4.1 **Simulated SOA budget and concentrations**

Firstly, the single-step oxidation mechanism of $VOC_{ANT/BB}$ with reactivity based on α-pinene and a fixed reaction yield of 13 % is described (DryH_WetL). The global annual-total reaction fluxes and SOA production

rates from anthropogenic and biomass burning hydrocarbons are shown in Figure 4.6. As described in Section 4.2.4, the global annual-total $VOC_{ANT/BB}$ emission rate is 176 ($VOC_{ANT/BB}$) a^{-1}, which is held fixed across all simulations. In this case, the global annual-total $VOC_{ANT/BB}$ oxidation rate by OH is 94 Tg (VOC) a^{-1} (DryH_WetL; Figure 4.6). The remaining 82 Tg (VOC) a^{-1} undergoes deposition (not shown). For this single-step mechanism, oxidation of the emitted parent hydrocarbon directly forms the non-volatile product, SOG, which condenses almost immediately. A fixed reaction yield of 13 % is assumed, resulting in a global annual-total SOA production rate of 18.4 Tg (SOA) a^{-1} (Figure 4.6). Note, due to differences in relative molecular masses for $VOC_{ANT/BB}$ and SOG, the stoichiometric yield is not equivalent to the mass yield. Expressed as a fraction of emitted parent VOC (176 Tg (VOC) a^{-1}), the overall yield of SOA production from anthropogenic and biomass burning VOCs (18.4 Tg (SOA) a^{-1}) is around 10 %.

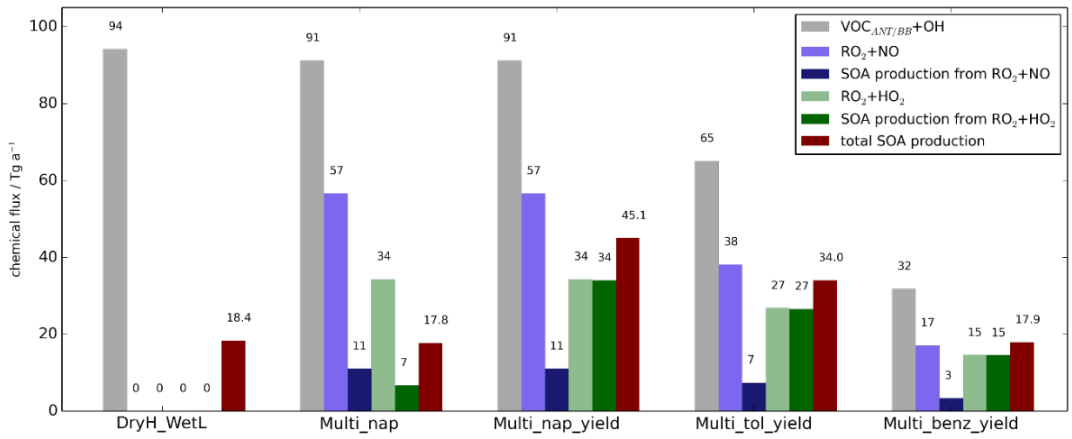

Figure 4.6 – Global annual-total reaction fluxes and total SOA production rate from anthropogenic and biomass burning hydrocarbons, for the simulations described in Table 4.3. The global annual-total $VOC_{ANT/BB}$ emission rate, of 176 ($VOC_{ANT/BB}$) a^{-1}, is identical across all simulations.

The combination of a single step oxidation mechanism and the assumption of a relatively reactive parent hydrocarbon results in rapid production of SOA. Figure 4.7 shows the spatial distributions of annual-total surface $VOC_{ANT/BB}$ emissions, annual-average surface OH concentrations, annual-total vertically integrated $VOC_{ANT/BB}$+OH oxidation rates, and the resulting SOA production rates. As expected, the spatial distributions of $VOC_{ANT/BB}$ emissions mainly reflects anthropogenic activity. Over high emissions regions, OH concentrations are also relatively high. Over India, China, Europe and North America, annual-average OH concentrations are in the range of 32 – 130 $x10^{-3}$ ppt(v) (Figure 4.7 b). Therefore, for most major $VOC_{ANT/BB}$ emissions source regions, OH availability is high, resulting in rapid oxidation; reaction fluxes of $VOC_{ANT/BB}$+OH peak very close to emissions sources (c.f. Figure 4.7 a, c). However, uncertainty in simulated OH concentrations will be translated into uncertainty in SOA production. OH is the principal oxidising agent of the atmosphere. Therefore, in order to successfully model OH, many other species (e.g. methane) also need to be modelled correctly (Lelieveld et al., 2016). Due to its very short lifetime (~seconds) and low concentrations, OH is difficult to measure (Stone et al., 2012). Therefore, the scarcity of observations results in difficulty in constraining simulated OH concentrations in a global model.

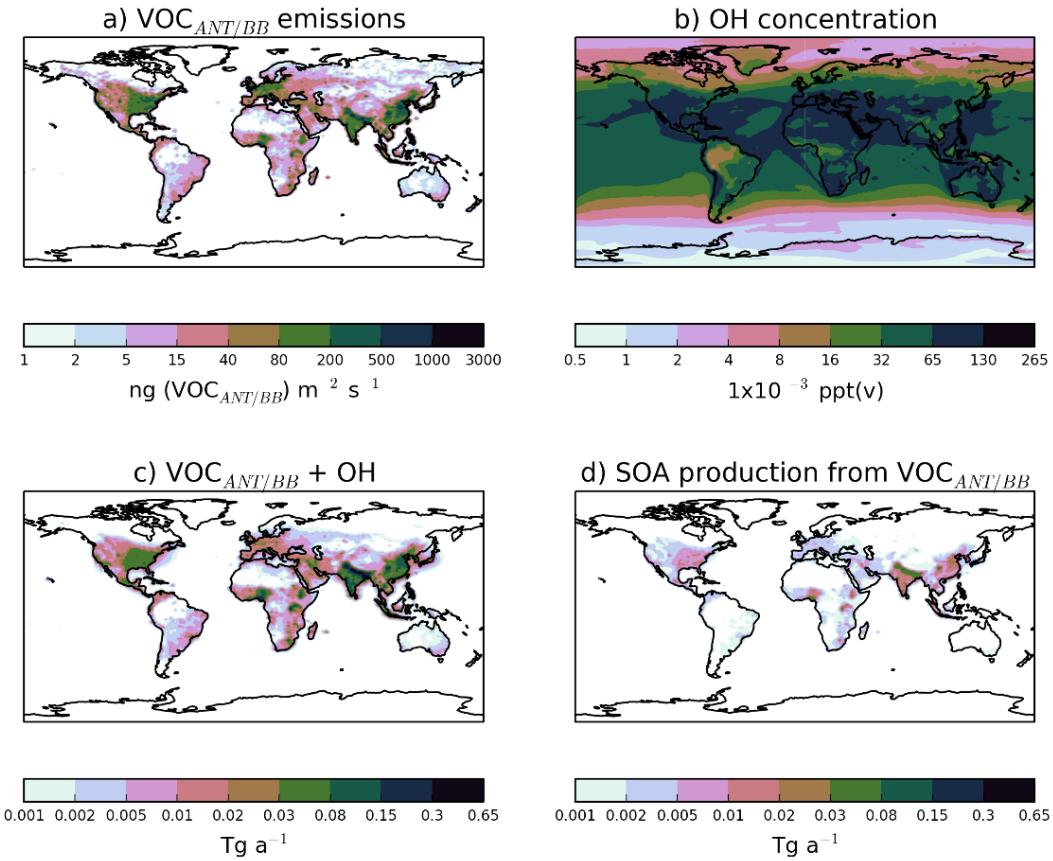

Figure 4.7 – Global distributions of a) the annual-total $VOC_{ANT/BB}$ emission rate (ng ($VOC_{ANT/BB}$) m^{-2} s^{-2}), b) the annual mean surface OH concentrations (ppq(v)), c) the annual-total vertically integrated $VOC_{ANT/BB}$ oxidation rate by OH (Tg a^{-1}), and d) the corresponding annual-total SOA production rate (Tg a^{-1}), when SOA precursor deposition and a single oxidation step with a yield of 13 % is applied (DryH_WetL; Table 4.3).

Also, as shown in E4.1, oxidation of the parent VOC results in immediate production of the condensing species, SOG. Hence, not only do parent VOCs undergo rapid oxidation, but the product of this reaction is in the form of condensable organic vapours. Therefore, this combination of high parent VOC reactivity with few reaction steps results in extremely localised SOA production from anthropogenic and biomass burning emissions. This is in contrast to other global modelling studies, which predict more regionally distributed SOA production (Pye and Seinfeld, 2010;Tsimpidi et al., 2016).

Differences in the geographical extent to which SOA production occurs may be attributed to precursor reactivity and the number of reaction intermediates. For example, here, the parent hydrocarbon is a VOC, with a rate constant of 52.9 $x10^{-12}$ cm^3 $molecule^{-1}$ s^{-1} at 298 K (Table 4.1), forming SOA in a single-step reaction mechanism. Hence, local SOA production is simulated (Figure 8 d). Conversely, SOA production is more regionally distributed when treated from S/IVOC multigenerational chemistry, where the parent hydrocarbon and oxidation products all react relatively slowly (Tsimpidi et al., 2016). High observed OA concentrations over remote regions (Boreddy et al., 2015;Boreddy et al., 2016) provide evidence for the slow and sustained mechanistic description of SOA production from S/IVOCs (Tsimpidi et al., 2016). High observed OA concentrations within industrialised emissions source regions (Zhang et al., 2007) support the fast mechanistic description of SOA production from VOCs simulated here.

To summarise, the combination of fast reactivity and a single step oxidation mechanism favours extremely localised SOA production, with parent VOCs undergoing rapid oxidation and subsequent condensation close to source.

In the following sub-sections, SOA formation mechanisms are altered, including increases to the number of reactions steps, accounting for the influence of oxidants on SOA yields, and reducing the chemical reactivity of the parent VOC (E4.2; Section 2.4.2). This begins with an evaluation of the multigenerational mechanism with reactivity based on naphthalene (Multi_nap), and how this mechanism compares to the single-step oxidation mechanism with reactivity based on α-pinene (DryH_WetL). For this comparison, the individual effects of reduced parent VOC reactivity, introduction of the reaction intermediate, and SOA production from the reaction intermediate, are evaluated separately in Sections 4.1.1.1 to 4.1.1.3. Next, the effects of accounting for the difference in volatility between RO_2 oxidation products is evaluated (Multi_nap_yield) in Section 4.1.1.4. Finally,

less reactive parent hydrocarbons are explored in Section 4.1.1.5 (Multi_tol_yield and Multi_benz_yield).

4.4.1.1 **Initial OH oxidation of parent hydrocarbon**

Production of SOA from anthropogenic and biomass burning hydrocarbons is modified in the following sub-sections to follow the multigenerational mechanism of E4.2. Naphthalene, the most reactive aromatic VOC considered in this study, is first selected (section 4.2.3), with identical reaction yields applied to both RO_2 pathways (Multi_nap simulation; Table 4.3).

The initial reaction of $VOC_{ANT/BB}$ with OH is compared to that of a single oxidation reaction step (DryH_WetL; Table 4.3). At 298 K, the rate constants for α-pinene and naphthalene oxidation by OH are 52.9 and 23.3 $x10^{-12}$ cm^3 $molecule^{-1}$ s^{-1}, respectively (Table 4.1). The global annual-total $VOC_{ANT/BB}$ oxidation rate reduces by 3 Tg (VOC) a^{-1} (or 3 %), from 94 Tg (VOC) a^{-1} using the reactivity of α-pinene, to 91 Tg (VOC) a^{-1} using the reactivity of naphthalene (Figure 4.6). Therefore, the global $VOC_{ANT/BB}$ oxidation rate is relatively insensitive to a ~50 % reduction in reactivity. When applying a 13 % stoichiometric yield to this reaction sequence (Table 3), this reduction in parent VOC oxidation rate contributes to a marginal change in the global annual-total SOA production rate (0.6 Tg (SOA) a^{-1}).

The response of regional VOC oxidation rates to a ~50 % reduction in the reactivity vary in both magnitude and sign. Figure 4.8 shows the difference in annual-total vertically integrated $VOC_{ANT/BB}$ oxidation rates for all the multigenerational oxidation mechanism simulations in Table 4.3, relative to the single oxidation pathway with reactivity based on α-pinene (DryH_WetL; Table 4.3). Reduced chemical reactivity lowers oxidation rates

within emission source regions. For example, over India and parts of Africa, annual-total $VOC_{ANT/BB}$ oxidation rates reduce by up to 0.05 Mg ($VOC_{ANT/BB}$) m^{-2} a^{-1} (Figure 4.8 a); these changes in annual-total $VOC_{ANT/BB}$ oxidation rates within emissions source regions correspond to reductions between 10 and 30 % (not shown). By contrast, downwind of many emissions source regions, the lower reactivity acts to enhance $VOC_{ANT/BB}$ oxidation rates. For example, over the Arabian Sea, over Southeast China, off the coast of Nigeria, and over the southeast USA, annual-total $VOC_{ANT/BB}$ oxidation rates increase by 0.01 - 1Mg ($VOC_{ANT/BB}$) m^{-2} a^{-1} in response to a ~50 % reduction in parent VOC reactivity (Figure 4.8 a). These changes in annual-total $VOC_{ANT/BB}$ oxidation rates downwind of emissions source regions correspond to reductions which exceed 60 % (not shown). As discussed in Section 4.4.1, adoption of the reactivity of α-pinene for the $VOC_{ANT/BB}$+OH reaction results in peak VOC oxidation rates at emission source, with VOCs undergoing very little transport (Figure 4.7 c). Therefore, by reducing the reactivity by ~50 %, fewer $VOC_{ANT/BB}$ are oxidised at source but transport of $VOC_{ANT/BB}$ away from source is promoted.

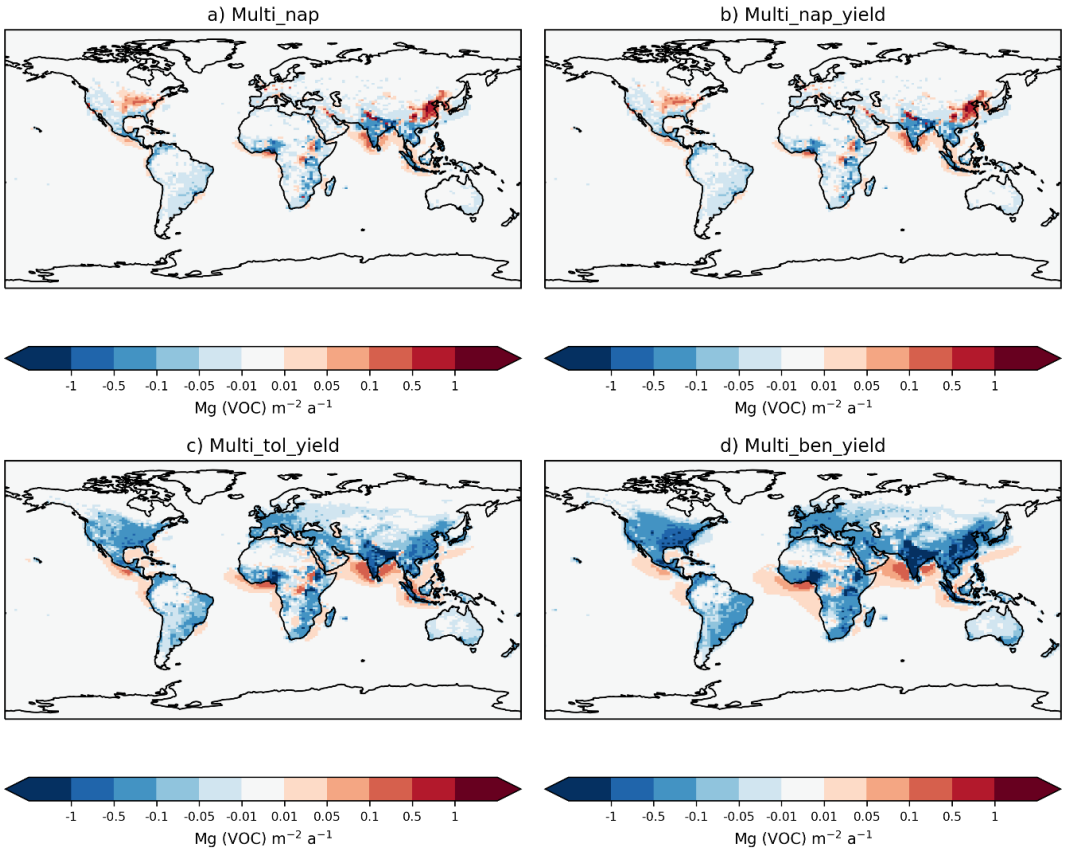

Figure 4.8 – Global distribution of the absolute differences in annual-total vertically integrated $VOC_{ANT/BB}$ oxidation rates (Tg (VOC) m^{-2} a^{-1}) in a) the Multi_nap, b) the Multi_nap_yield, c) the Multi_tol_yield, and d) the Multi_ben_yield simulations relative to the DryH_WetL simulation.

4.4.1.2 **Chemical fate of the new reaction intermediate, RO_2**

With a multi-generational pathway, oxidation of the parent VOC forms a new reaction intermediate, the peroxy radical RO_2. In this case, $VOC_{ANT/BB}$ oxidation results in a global annual-total peroxy radical production rate of 91 Tg (RO_2) a^{-1} (Multi_nap simulation; Figure 4.6). Introduction of this new

reaction intermediate has the potential to either reduce and/or delay SOA production, depending on assumptions regarding the strength of deposition and chemical reactivity of this intermediate. For example, SOA production would be reduced if the peroxy radical undergoes significant deposition, which is dependent on deposition parameters such as surface resistances and solubility (section 4.2.2). Additionally, SOA production could be reduced or delayed if the chemical removal of RO_2 is slow. The influence of introducing the peroxy radical as a reaction intermediate is therefore predetermined by assumptions in deposition parameters and reaction kinetics. In all simulations, RO_2 is assumed to have identical solubility and surface resistances to all other SOA precursors, $H_{eff} = 10^5$ M atm^{-1} and 'Low' surface resistances (Table 4.2). At 298 K, the rate constants for RO_2 oxidation by HO_2 and NO, taken from Atkinson and Arey (2003), are 14.8 and 8.5 $x10^{-12}$ cm^3 $molecule^{-1}$ s^{-1}, respectively (Table 4.1). Consequently, of the 91 Tg of RO_2 generated annually, oxidation by NO and HO_2 removes 57 and 34 Tg (RO_2) a^{-1}, respectively (Multi_nap_yield; Figure 4.6). Deposition of RO_2 is inconsequential at 0.1 Tg (RO_2) a^{-1} (not shown). This extremely low deposition rate is because the chemical removal of the peroxy radical is extremely fast. The global annual-average lifetime of RO_2 with respect to oxidation is ~1 day, which is relatively short in comparison to atmospheric transport timescales. Therefore, due to marginal deposition and fast oxidation, introduction of the peroxy radical reaction intermediate will probably have no effect on either the SOA production rate or the geographical distribution of SOA production, which are both quantified in the following section (4.4.1.3).

Chemical removal of the peroxy radical via the two oxidative pathways is an important factor in governing the strength of SOA production, as discussed later in (Sections 4.4.1.3 onwards). RO_2 is chiefly removed by NO, as opposed to HO_2 radicals. This is demonstrated in Figure 4.9, which shows the relative contributions of the HO_2 and NO peroxy radical oxidative

pathways to the total chemical removal of RO_2 (top row) and to SOA production (bottom row). On a global and annual mean basis, removal by NO accounts for 62 % of RO_2 chemical loss (Figure 4.9 a). Other global modelling studies which consider the peroxy radical as a reaction intermediate from aromatic compounds or IVOCs, also predict RO_2 removal to be dominated by NO. Henze et al. (2008) estimate that, for peroxy radicals generated from benzene, xylene and toluene, 61 % react via the NO pathway. Peroxy radicals generated from IVOCs, with parent hydrocarbon reactivity based on naphthalene, 66 % are consumed by NO (Pye and Seinfeld, 2010). These results suggest that the chemical fate of the peroxy radical is robust despite the likelihood of variations in precursor emissions and oxidant concentrations between this and the aforementioned studies.

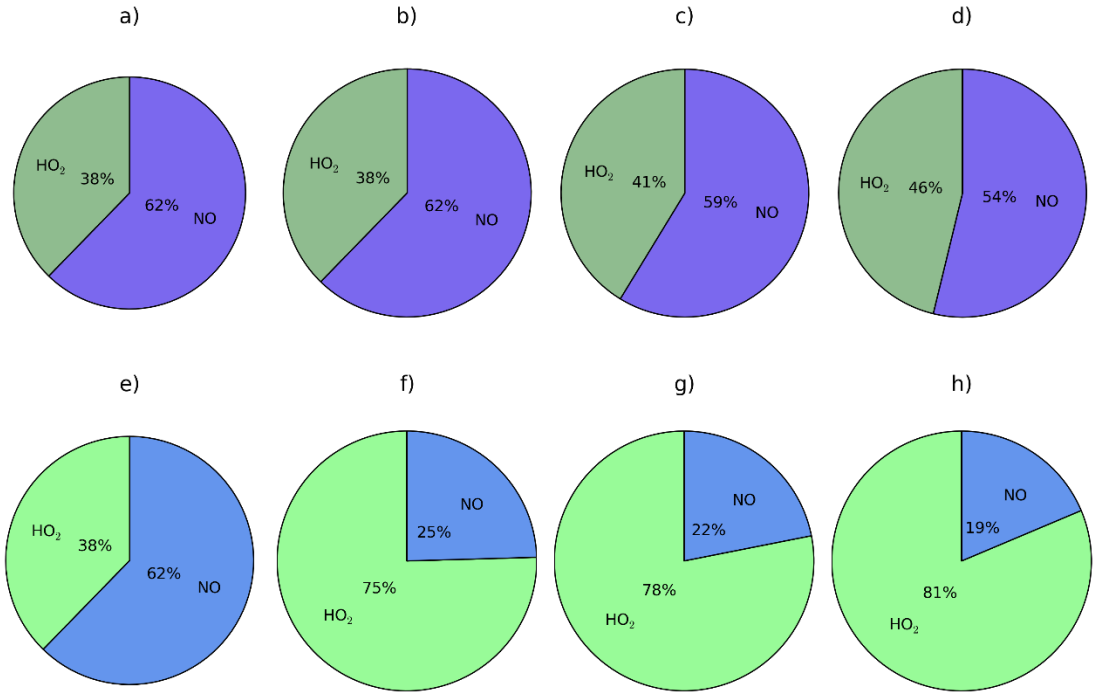

Figure 4.9 – For the peroxy radical, chemical removal (top row; a – d) and SOA production (bottom row; e – h) for the Multi_nap (first column; a and e), Multi_nap_yield (second column; b and f), Multi_tol_yield (third column; c and g), and Multi_benz_yield (fourth column; d and h) simulations, which are described in Table 4.3.

The substantial preference for RO_2 radicals to react via the NO pathway instead of the HO_2 pathway can be attributed to differences in oxidant availability (i.e. concentrations) and in reaction rates. Note, in the UKCA model, HO_2 is assumed to undergo wet removal. Firstly, consider the difference in oxidant levels. Figure 4.10 shows the spatial distribution of annual-average surface concentrations of NO and HO_2, as well as the ratios NO/HO_2 and (k_{RO2+NO} x NO) / ($k_{RO2+HO2}$ x HO_2). NO is extremely spatially heterogeneous (Figure 4.10). Within the model, sources of NOx include the prescribed anthropogenic, biomass burning and soil emissions, as well as lightning-NOx which is calculated interactively. At the surface, the highest annual-average surface NO concentrations (1-23 ppb(v)) are simulated over industrialised and urban regions of North America, China and Europe, as well

as, over the Amazon and Congo regions (Figure 4.10 a). Over remote marine environments, away from anthropogenic and biomass burning sources, concentrations of NO are low (Figure 4.10 a). In contrast, concentrations of HO_2 are much lower and more evenly distributed across the surface (Figure 4.10). Over the majority of both continental and marine regions, annual-average surface HO_2 concentrations range between 2 and 23 ppt(v) (Figure 4.10 b). Therefore, over most environments, NO concentrations are far greater, with annual-average surface NO concentrations ranging from 10 ($NO/HO_2 = 10^1$) to 10,000 ($NO/HO_2 = 10^4$) times more than HO_2 (Figure 4.10 c). Only in the remote marine environments are HO_2 levels higher in absolute magnitude compared to NO, with simulated annual-average surface HO_2 concentrations reaching 10 times that of NO ($NO/HO_2 = 10^{-1}$; Figure 4.10 c). At higher levels, NO/HO_2 reduces, suggesting an increasing importance of the HO_2 pathway at higher altitudes. However, due to the fast chemical reactivity, the majority of SOA production occurs at the surface. For the majority of the atmosphere, the difference in the magnitudes of the oxidant concentrations favours the RO_2+NO pathway over the RO_2+HO_2 pathway.

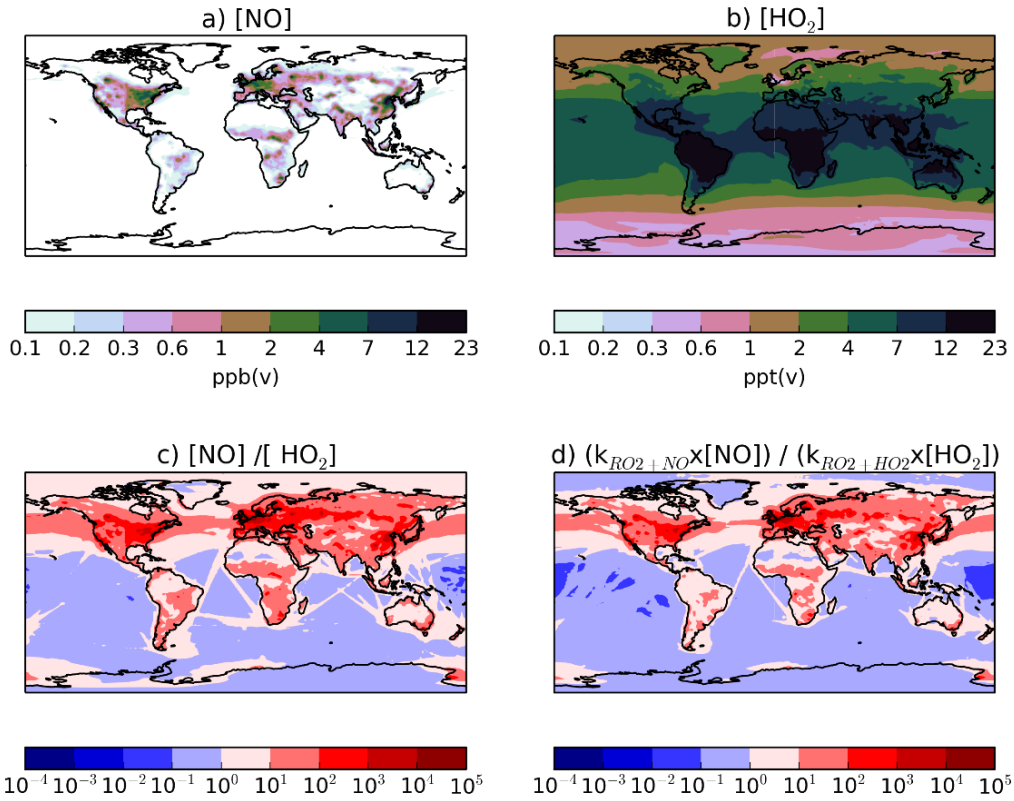

Figure 4.10 – Global distributions of annual-average (a) surface NO concentrations (ppb(v)), (b) surface HO_2 concentrations (ppt(v)), c) the ratio of surface NO/HO_2, and d) the ratio of surface (k_{RO2+NO} x NO)/($k_{RO2+HO2}$ x HO_2), where k represents the rate coefficient at 298 K. Note that the concentrations of the HO_2 radical are in units of ppt(v), whereas NO is in units of ppb(v).

Differences in reactivity of RO_2 with respect to the oxidants also affects the fate of this radical. At 298 K, the rate constant for RO_2+NO is 8.42 x 10^{-12} cm^3 $molecule^{-1}$ s^{-1}, almost half that of RO_2+HO_2 (k(298 K) = 14.7 x10^{-12} cm^3 $molecule^{-1}$ s^{-1}; Table 4.1). Therefore, the higher rate constant for oxidation by HO_2 in comparison to NO favours the RO_2+HO_2 pathway.

The ratio, (k_{RO2+NO} x NO) / ($k_{RO2+HO2}$ x HO_2), combines the difference in rate constants together with differences in the ratio of oxidant concentrations, and ranges from 10^0 to 10^4 over most continental regions, but is as low as 10^{-2} over remote marine environments, such as the Pacific

Ocean and South Atlantic Ocean (Figure 4.10 d). Hence, the net effect of differences in oxidant concentrations and rate constants is to favour peroxy radical removal via the NO oxidative pathway (Figure 4.9 a; Figure 4.10 d). This preference for the NO radical pathway is enhanced even further by considering the likelihood of RO_2 being co-located with NO. RO_2 is a second generation oxidation product of $VOC_{ANT/BB}$, which is released by anthropogenic and biomass burning sources. NO emissions are predominantly emitted from anthropogenic and biomass burning sources. Therefore, peroxy radicals are very likely to be formed in NO-rich environments, further favouring the probability of entering the RO_2+NO pathway. Furthermore, adoption of naphthalene reactivity for $VOC_{ANT/BB}$, which is still relatively high, prevents transport away from high-NO regions. Overall, peroxy radicals preferentially react via the NO pathway due to relatively higher NO concentrations than HO_2, despite the HO_2 pathway having a higher rate constant.

4.4.1.3 **Production of SOA from new reaction intermediate, RO_2**

For this multi-step reaction scheme with parent VOC reactivity based on naphthalene (Multi_nap), the initial oxidation and subsequent reaction of the intermediate were discussed in Sections 4.4.1.1 and 4.4.1.2, respectively. In this section, the production of SOA from this mechanism is examined. In this oxidation scheme, identical reaction yields of 13 % are applied for both the HO_2 and NO pathways. For the RO_2+NO reaction, a global annual-total reaction flux of 57 Tg (RO_2) a^{-1} results in an SOA production rate of 11 Tg (SOA) a^{-1} (Multi-nap; Figure 4.6). Similarly, for the RO_2+HO_2 pathway, a global annual-total reaction flux of 34 Tg (RO_2) a^{-1} results in an SOA production rate of 7 Tg (SOA) a^{-1} (Figure 4.6). Hence, the relative

contribution of the RO_2 oxidative pathways to SOA production is simply a reflection of the relative contribution of each pathway to RO_2 consumption. Therefore, the RO_2+NO pathway accounts for 62 % of the global annual-total RO_2 oxidation rate (Figure 4.9 a), and also accounts for 62 % of the annual-total SOA production rate from anthropogenic and biomass burning hydrocarbons (Figure 10 e). The sum of global annual-total SOA production from anthropogenic and biomass burning sources, from both oxidative pathways, is 17.8 Tg (SOA) a^{-1} (Figure 7). This is just 0.6 Tg (SOA) a^{-1} (or 3 %) less than the global annual-total SOA production rate when using a single-step oxidation mechanisms with reactivity based on α-pinene (DryH_WetL; Figure 4.6). Note, this 0.6 Tg (SOA) a^{-1} reduction in SOA production is solely due to the 3 % reduction in the $VOC_{ANT/BB}$ oxidation rate (Section 4.4.1.1). This therefore confirms that, due to the marginal deposition rate of RO_2, the introduction of the reaction intermediate has no effect on global SOA production.

The difference in annual-average surface SOA concentrations for the multigenerational oxidation mechanisms relative to the single step reaction with reactivity based on α-pinene are shown in Figure 4.11. The effects of a ~50 % reduction in parent VOC reactivity in combination with the introduction of the reaction intermediate on regional annual-average surface SOA concentrations vary in both magnitude and sign but, generally, are small. These differences in SOA concentrations (Figure 4.11 a and b) closely resemble differences in parent VOC oxidation rates in response to the change in chemical reactivity (Figure 4.8 a). Over regions where reduced reactivity has lowered $VOC_{ANT/BB}$ oxidation rates, such as India and and industrialised parts of Africa (Figure 4.8 a), annual-average surface SOA concentrations have reduced by around 0.1 to 0.5 µg (SOA) m^{-3} (Figure 4.11 a), corresponding to reductions of 5 – 20 % (Figure 4.11 b). On the other hand, for some downwind regions, such as Northern India, Southeast China and Southeast USA, annual-average surface SOA concentrations increase

by 0.1 – 4 μg (SOA) m^{-3} (Figure 4.11 a), corresponding to increases of 5 – 30 % (Figure 4.11 b). Overall, annual-average surface SOA concentrations change by less than 3 % (not shown) and the global annual-average SOA burden changes by less than 1 % (not shown). The strong similarity between the difference in SOA concentrations (Figure 4.11 a) and VOC oxidation rates (Figure 4.8 a) also confirms how introduction of the reaction intermediate did not affect the geographical distribution of SOA production.

To summarise, moving from a single-step oxidation mechanism with the reactivity of α-pinene and with a single SOA yield, to a multi-step oxidation mechanism with a slower reactivity based on naphthalene with a single SOA yield has very little effect on SOA production and surface concentrations. The slower reactivity of naphthalene reduces the global $VOC_{ANT/BB}$ oxidation by 3%, contributing to a reduction in the global annual-total SOA production rate of 0.6 Tg (SOA) a^{-1} (3 %). Introduction of the reaction intermediate, but with no change to reaction yields, has no effect on global SOA.

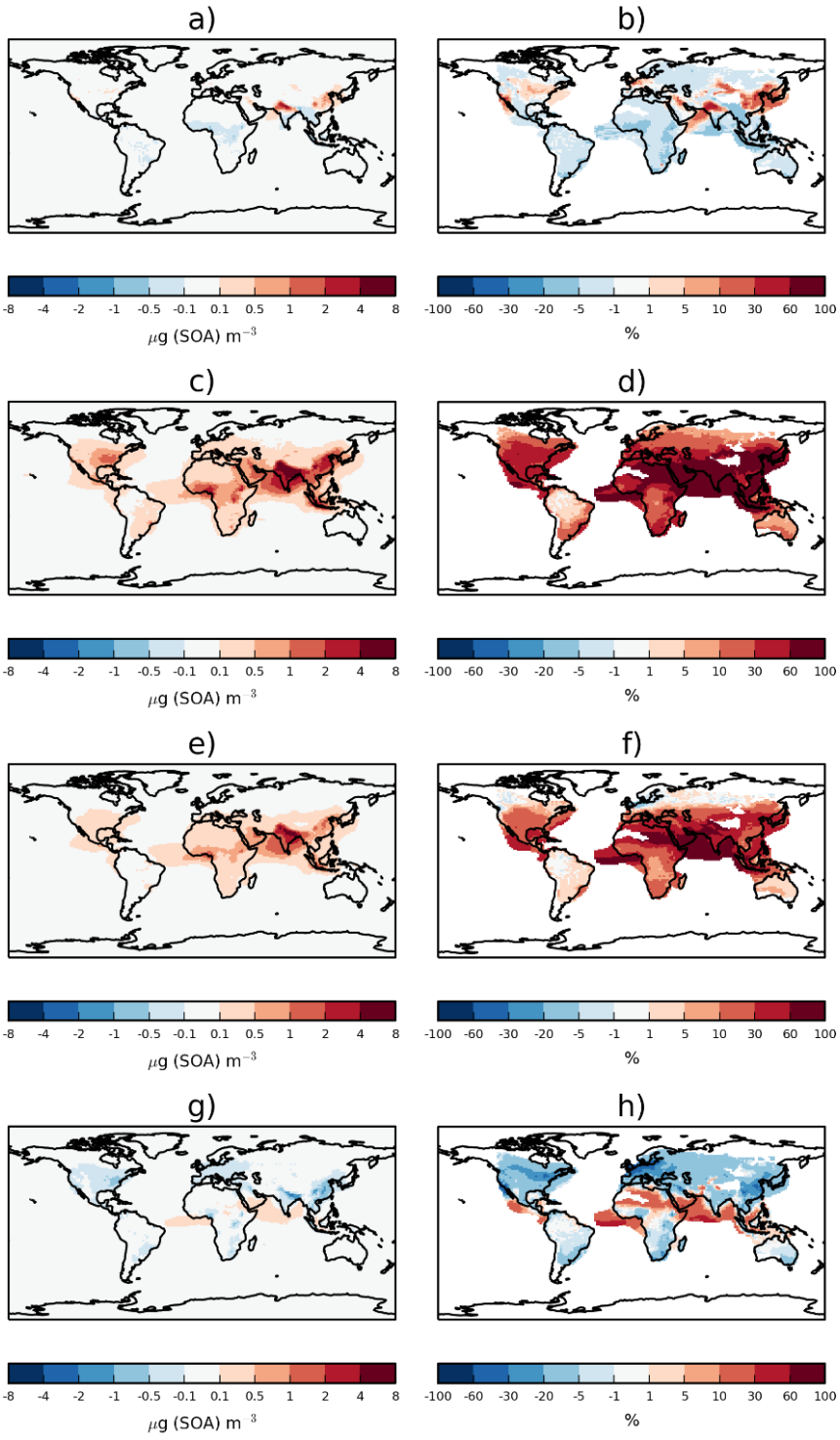

Figure 4.11 – Difference in annual-average surface SOA concentrations, expressed as absolute concentrations (μg m^{-3}) (left column) and as a percentage (right column) between Multi_nap (top row; a - b), Multi_nap_yield (second row; c - d), Multi_tol_yield (third row; e - f), and Multi_benz_yield (fourth row; g - h) and the DryH_WetL simulation, which are all described in Table 3.

4.4.1.4 Accounting for the difference in volatility between HO_2 and NO oxidation products

In this section, the effects of accounting for the difference in volatility between RO_2 oxidation products is examined. This is done by altering the reaction yields for RO_2 reactions, whilst maintaining the same chemical mechanism (E4.2) and precursor emission rate.

For aromatic compounds, , the volatility and, therefore, the amount of SOA produced, depends on the concentrations of NOx (Section 4.1). One explanation for this relationship is that the HO_2 pathway forms non-volatile products, whereas the NO pathway forms semi-volatile products. As semi-volatile compounds have a greater propensity to be in the gas phase, this explains why observed SOA yields are higher in low-NOx conditions. Hence in a further simulation, the difference in volatility between products of different peroxy radical oxidation pathways are accounted for, whereby the yield for the RO_2+HO_2 reaction is increased from 13 to 66 %, whilst the yield for the RO_2+NO reaction is left at 13 % (Multi_nap_yield; Table 4.3). Increasing the molar yield of SOG production from the RO_2+HO_2 reaction can be considered as equivalent to assuming a greater fraction of products are non-volatile. As discussed in Section 2.5, the assumption of a 66 % stoichiometric reaction yield was selected as it corresponds to a 100 % mass yield and therefore allowing the theoretical upper limit of SOA production via the HO_2 pathway to be quantified whilst conserving mass.

With a higher molar yield of 66 %, global SOA production from the RO_2+HO_2 reaction increases to 34 Tg (SOA) a^{-1} as compared to 7 Tg (SOA) a^{-1} using a 13 % yield for this reaction (Figure 4.6). As a consequence of this increase to the hydroperoxyl reaction yield, the HO_2 pathway now accounts for 75 % of SOA production from anthropogenic and biomass burning sources (Figure 4.11 f), despite only 38 % of the RO_2 radicals reacting via

this pathway (Figure 4.9 b). This is in remarkably good agreement with previous studies. Pye and Seinfeld (2010) also estimate that the HO_2 pathway accounts for 75 % of SOA production from I-VOCs. In addition, Henze et al. (2008) estimates that, for SOA production from benzene, toluene and xylene, 72 % is produced via the HO_2 pathway.

Accounting for differences in volatility between RO_2 oxidation products increases the global SOA production rate by 27.3 Tg (SOA) a^{-1} (or 153 %), from 17.8 Tg (SOA) a^{-1} when a molar yield of 13 % is applied to both pathways (Multi_nap), to 45.1 Tg (SOA) a^{-1} when a molar yield of 66 % is applied (Multi_nap_yield). Under these conditions, the overall aerosol yield from anthropogenic and biomass burning VOC emissions is 25 %, which lies within the range from other modelling studies, either based on explicit aromatic compounds or IVOCs, which range from 22 – 30 % (Henze et al., 2008;Pye and Seinfeld, 2010).

The relative spatial homogeneity of HO_2 radicals over land and ocean, as shown in Figure 4.10 b, suggests that increasing the yield for this pathway could lead to enhanced SOA production globally. However, as discussed in Section 4.4.1.1, the naphthalene+OH rate constant results in relatively fast oxidation rates. Therefore, RO_2 radicals are still being generated close to the emissions source. For these reasons, increasing the reaction yield for the HO_2 reaction pathway increases SOA concentrations mainly over major anthropogenic emission source regions (Figure 4.11 c, d). In response to this increased yield, over India, China, Africa and Europe, annual-average surface SOA concentrations have increased by 0.5 – 8 µg (SOA) m^{-3} (Figure 4.11 c), corresponding to increases of 10 – 100 % (Figure 4.11 d). Note, differences in SOA concentrations are positive everywhere, whereas both positive and negative changes were found when comparing differences in SOA concentrations between multi-generational and single oxidative pathways results without accounting for volatility changes (c.f. Figure 4.11 b and d). In summary, both globally (Figure 4.6) and regionally (Figure 4.11 d),

when accounting for the different SOA yields for the RO_2 oxidative pathways, despite a reduction in $VOC_{ANT/BB}$ global SOA production rates, surface SOA concentrations increase everywhere. Therefore, the lower reactivity in $VOC_{ANT/BB}$ is compensated for by lower volatility products from the HO_2 oxidation pathway leading to net increases in modelled SOA.

4.4.1.5 **Production of SOA from less reactive hydrocarbons**

The anthropogenic and biomass burning VOC precursor of SOA in the UKCA model, $VOC_{ANT/BB}$, is a lumped species (Section 4.2.3). This specie therefore, represents a mixture of species with a range of physicochemical properties. In this section, the uncertainty related to its chemical reactivity and the effects on SOA production are explored.

At 298 K, the rate constant for aromatic compounds with respect to OH oxidation ranges from 1.22 to 23.2 $x10^{-12}$ cm^3 $molecule^{-1}$ s^{-1}, respectively (Table 4.1 and 4.3). Therefore, adoption of the naphthalene reactivity in the multi-generational pathway simulations described above represents an upper limit for the $VOC_{ANT/BB}$ oxidation rate when considering SOA relevant aromatic compounds. In this section, the VOC reactivity is varied across a series of different aromatic compounds: naphthalene, toluene and benzene (Multi_nap_yield, Multi_tol_yield and Mult_benz_yield; Table 4.3). However, the mechanistic description and stoichiometric yields describing SOA formation from $VOC_{ANT/BB}$ are identical and follow E4.2.

Firstly, consider how reactivity affects SOA production among the multigenerational oxidation mechanisms (Multi_nap_yield, Multi_tol_yield and Multi_benze_yield). Reducing the chemical reactivity of $VOC_{ANT/BB}$ reduces oxidation, whilst at the same time, favours the likelihood of RO_2 radicals entering the high-yield HO_2 pathway. The global annual-total $VOC_{ANT/BB}$

oxidation rates are 91, 65 and 32 Tg ($VOC_{ANT/BB}$) a^{-1} using the reactivity of naphthalene, toluene and benzene, respectively (Figure 4.6). Hence, as reactivity is reduced, oxidation is lowered at the expense of deposition. In response to this reduced oxidation rate, fewer RO_2 radicals are being generated, which therefore, drives reductions in SOA production. The global annual-total SOA production rates are 45.1, 34.0, 17.9 Tg (SOA) a^{-1} using the reactivity of naphthalene, toluene and benzene, respectively (Figure 4.6). However, as the reactivity is reduced, the chances of RO_2 radicals entering the high-yield HO_2 pathway is increased, therefore, slightly offsetting the effects of the reduced RO_2 production rate. The fraction of peroxy radicals entering the HO_2 pathway is 38, 41 and 46 % using the reactivity of naphthalene, toluene and benzene, respectively (Figure 4.9 d, e and h, respectively). As shown in Figure 4.10 d, the HO_2 pathway dominates only in remote marine environments. Hence, as the reactivity of the parent hydrocarbon is reduced, $VOC_{ANT/BB}$ oxidation rates close to emissions sources reduce, but increase further downwind (Figure 4.8 c and d). Therefore, lower reactivity enhances the likelihood of peroxy radicals being generated downwind of emissions sources, where the HO_2 pathway is favoured. These findings are consistent with Henze et al. (2008), who predicted increased fluxes through the HO_2 pathway for peroxy radicals derived from less reactive parent aromatic hydrocarbons. Overall, reduced parent hydrocarbon reactivity reduces the sources of peroxy radicals but favours lower volatility RO_2 + HO_2 oxidation products.

Secondly, consider the net effects of using aromatic oxidation to describe SOA production from $VOC_{ANT/BB}$ (Multi_nap_yield, Multi_tol_yield and Multi_benze_yield), versus using the single-step mechanism with reactivity based on α-pinene (DryH_WetL). Compared to α-pinene, the aromatic compounds, naphthalene, toluene and benzene are 50, 75 and 95 % less reactive, respectively (Table 2). As discussed in Section 4.4.1.1, using the chemical reactivity of naphthalene compared to monoterpene leads

to a 3 % reduction in $VOC_{ANT/BB}$ oxidation, which drives a 0.6 Tg (SOA) a^{-1} (1 %) reduction in global annual-total SOA production (c.f. DryH_WetL and Multi_nap; Figure 7). However, as shown in Section 4.4.1.4, this reduction in VOC oxidation is entirely offset by accounting for the high-yield pathway of the RO_2+HO_2 reaction, leading to a 27.3 Tg (SOA) a^{-1} (153 %) increase in global annual-total SOA production (c.f. DryH_WetL and Multi_nap_yield; Figure 4.6). Using the chemical reactivity of toluene compared to α-pinene also reduces the $VOC_{ANT/BB}$ oxidation, but this time by 31 % (c.f. DryH_WetL and Mutli_tol_yield; Figure 4.6). However, similar to the case of naphthalene, this reduction in $VOC_{ANT/BB}$ oxidation is still outweighed by accounting for the high-yield HO_2 pathway, such that global annual-total SOA production increases by 15.6 Tg (SOA) a^{-1} (or 85 %), from 18.4 Tg (SOA) a^{-1} in the single step oxidation mechanism based on α-pinene, to 34.0 Tg (SOA) a^{-1} in the multi-step oxidation mechanisms based on toluene (c.f. DryH_WetL and Mutli_tol_yield; Figure 4.6). On the other hand, benzene is considerably less reactive than α-pinene, leading to 66 % reduction in the global annual-total $VOC_{ANT/BB}$ oxidation rate (c.f. DryH_WetL and Mutli_benz_yield; Figure 4.6). In this case, the reduction in $VOC_{ANT/BB}$ oxidation is so large, that it is not compensated for by accounting for the difference in volatility between RO_2 oxidation products. Hence, using the reactivity of benzene, the global annual-total SOA production rate reduces by 0.5 Tg (SOA) a^{-1} (or 3 %), from 18.4 Tg (SOA) a^{-1} in the single step oxidation mechanism based on α-pinene, to 17.9 Tg (SOA) a^{-1} in the multi-step oxidation mechanisms based on benzene (c.f. DryH_WetL and Mutli_benz_yield; Figure 4.6). These results demonstrate how, from a global perspective, the combined effects of introduction of the peroxy radical intermediate which also accounts for the difference in SOA yields between HO_2 and NO pathways can either lead to an increase (Multi_nap_yield and Multi_tol_yield) or reduction (Multi_benze_yield) in SOA production that, critically, depends on the assumed chemical reactivity of the parent VOC.

The spatial distribution of SOA is also influenced by these changes in $VOC_{ANT/BB}$ oxidation mechanisms. For cases where reactivity is based on either naphthalene (Figure 4.11 c and d) or toluene (Figure 4.11 e and f), accounting for the high yield HO_2 pathway compensates for reduced reactivity, such that annual-average surface SOA concentrations increase globally in comparison to the single step oxidation mechanism with reactivity based on α-pinene (DryH_WetL). The spatial pattern for the multigenerational oxidation mechanism based on benzene (Multi_benz_yield) and the single-step oxidation mechanism based on α-pinene (DryH_WetL) are also very different (Figure 4.11 g and h), despite only a small difference in the global annual-total SOA production rate (Figure 4.6); in the multigenerational oxidation mechanism with reactivity based on benzene, $VOC_{ANT/BB}$ has slowed down substantially, and newly introduced RO_2 radicals are being formed in downwind environments, leading to reduced SOA concentrations in emissions sources regions, but increased SOA concentrations downwind. Over emissions source regions, such as China, India and North America, annual-average surface SOA concentrations are lower by up to 4 μg (SOA) m^{-3} (Figure 4.11 g). Over continental outflow regions, such as the Arabian Sea and the Bay of Bengal, annual-average surface SOA concentrations have increased by 0.1 – 0.5 μg (SOA) m^{-3} (Figure 4.11 h). Although the global annual-total SOA production rates are identical, the global annual-average SOA burden is 10 % greater when using benzene as the parent VOC undergoing multi-generational oxidation, highlighting the strong spatial gradients in SOA lifetime. The spatial pattern simulated in the multigenerational oxidation pathway with reactivity based on benzene, is in greater agreement with the more regionally distributed SOA concentrations simulated in models based on S/IVOC sources (Pye and Seinfeld, 2010;Tsimpidi et al., 2016).

4.4.2 Comparison of simulated and observed OA concentrations

In this section, the influence of anthropogenic and biomass burning hydrocarbon oxidation mechanisms on model agreement with observations is quantified. Reduced parent hydrocarbon reactivity combined with accounting for the different SOA yield pathways of the peroxy radical affects model agreement with observations. Figure 4.12 shows simulated versus observed surface SOA concentrations for the NH from the simulations described in Table 4.3. In the multi-step oxidation pathway simulations, using naphthalene and toluene, the annual-total SOA production rate increased relative to the single step fast oxidation pathway. This increase was due to the difference in volatility between products of the peroxy radical oxidation pathways, despite the reduction in parent hydrocarbon reactivity. Therefore, simulated SOA concentrations are in closer agreement to observations (Multi_nap_yield; NMB = -46 %; Figure 4.12 b and Multi_tol_yield; NMB = -56 %; Figure 4.12 c) compared to the values using the single oxidation pathway (NMB = -66 %; Figure 4.3 d). However, simulated SOA concentrations have the largest negative bias for the multi-step simulation with benzene as the parent hydrocarbon (NMB = -71 %; Figure 4.12 d). Global annual-total emissions of benzne and toluene are 5.6 and and 6.9 Tg (C) a^{-1}, resptively (Henze et al., 2008), whereas emissions of naphthalene are 0.22 Tg (C) a^{-1} (Pye and Seinfeld, 2010). This suggests benzene and toluene could be more realistic surrogate compounds to represent $VOC_{ANT/BB}$ chemistry, as opposed to naphthalene. This is due to the slow reactivity of benzene resulting in a small $VOC_{ANT/BB}$ oxidation rate, which is higher downwind of emissions compared to the point of emissions (Figure 4.11 h). Figure 4.12 demonstrates that mechanisms of oxidation have a strong influence on model agreement with observations. However, the model negative bias is persistent in all

simulations, despite the oxidation pathways spanning a wide range of both chemical reactivity and reaction yields.

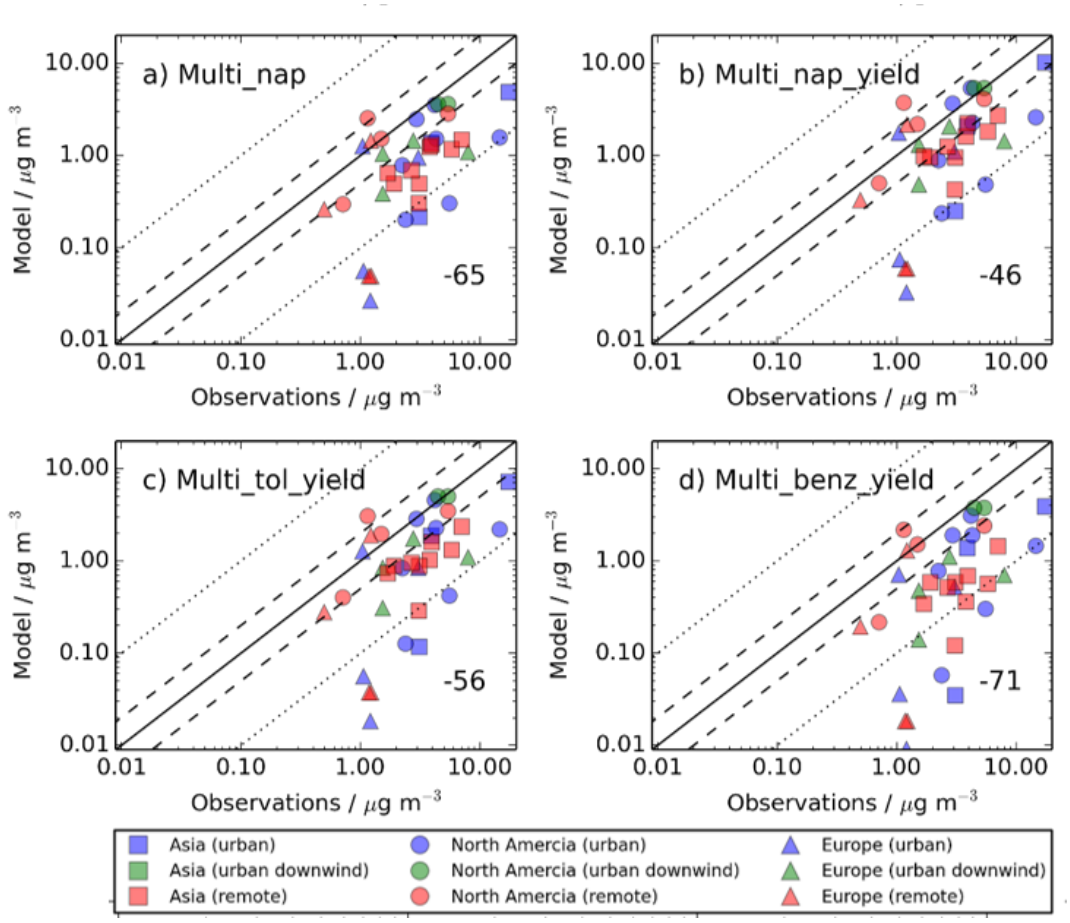

Figure 4.12 – Simulated versus observed SOA concentrations (μg m^{-3}) for a) Multi_nap, b) Multi_nap_yield c) Multi_tol_yield and d) Multi_benz_yield simulations, described in Table 4.3. Observations for the time period 2000-, are classified by site type - urban (blue), urban downwind (green) or remote (red), and continent – Asia (squares), North America (circles) and Europe (triangles). Observed oxygenated-OA is assumed to be comparable to simulated SOA. The 1:1 (solid), 1:2 and 2:1 (dashed), and 1:10 and 10:1 (dotted) lines are indicated. Numerical values in the bottom right of each panel indicate the normalised mean bias (%).

For the aircraft campaigns, mechanisms of anthropogenic and biomass burning oxidation have a limited influence on model agreement with observations. For the campaigns in remote regions, VOCALS (Figure 4.5 a),

TROMPEX (Figure 4.5 b) and OP3 (Figure 4.5 c), and over Western Africa (AMMA; Figure 4.5 k), introduction of the reaction intermediate combined with a reduction in reactivity (c.f. DryH_WetL and Multi_nap) has no effect on the NMB. However, the multi-step reaction mechanisms which do account for the high yield pathways have a substantial impact on the NMB; with reactivity based on naphthalene or toluene, the NMB reduces (Multi_nap_yield and Multi_tol_yield), but the NMB increases when the reactivity is based on benzene (Multi_benz_yield). Contrastingly, model performance in Europe and North Amercia = (Figure 4.5 h - j) remains similar as $VOC_{ANT/BB}$ oxidation is modified. This warrants further discussion. As explained in previous sections, the global SOA production rate is extremely sensitive to the mechanisms of $VOC_{ANT/BB}$ oxidation. However, model performance over the pollution and biomass burning influenced regions is relatively insensitive to VOC oxidation mechanisms. This is likely to be a reflection of the location of aircraft campaigns and how they are categorised. For example, the aircraft campaigns categorised as influenced by biomass burning are in North America, but peak biomass burning emissions are located over tropical forest regions of South America and Africa. Furthermore, the aircraft campaigns categorised as influenced by pollution are all in Europe. Again, this does not correspond to the location of peak anthropogenic emissions over Asia. Therefore, mechanisms of anthropogenic and biomass burning oxidation have substantial impacts on simulated SOA production rates, but almost no effect on model agreement with aircraft observations in ‘pollution and biomass burning influenced’ regions, due to a lack of aircraft coverage.

4.5 Conclusions

In this chapter, the description of both deposition and oxidation for SOA precursors was developed in a global chemistry-climate model. Several

model integrations were conducted and the treatments of deposition and oxidation mechanisms of SOA precursors were varied. Subsequent effects on the global SOA budget were quantified and simulated OA was evaluated against a suite of surface and aircraft campaigns spanning both the southern and northern hemispheres.

Within UKCA, SOA formation is considered from VOCs – monoterpene, isoprene, a lumped anthropogenic VOC (VOC_{ANT}) and a lumped biomass burning VOC (VOC_{BB}). Under the assumption that no precursors undergo deposition, the global annual-total SOA production rate is 75 Tg (SOA) a^{-1} and simulated OA concentrations are generally lower than observed (NMB = -50 %). Extending deposition to include SOA precursors has substantial impacts on both the global SOA budget and model agreement with observations. Including SOA precursor dry deposition reduces the global annual-total SOA production rate by 2 – 24 Tg (SOA) a^{-1} (2 - 32 %), with the range reflecting uncertainties in surface resistances. Including SOA precursor wet deposition reduces the global annual-total SOA production rate by 12 Tg (SOA) a^{-1} (15 %) and is relatively insensitive to changes in effective Henry's Law coefficient. The effects of dry and wet deposition on the global SOA budget are not additive; the inclusion of both these processes reduces the global annual-total SOA production rate by 28 Tg (SOA) a^{-1} (37 %). Inclusion of VOC deposition generally increases model negative biases with respect to observations. For SOA, across northern hemisphere mid-latitude sites, inclusion of both dry and wet deposition of VOCs increases the NMB from -50 to -66 %. However, for OA, over Manaus (Brazil), when precursor deposition is neglected from the model, simulated OA concentrations exceed observed OA concentrations.

Production of SOA from aromatic compounds, which are typically emitted from anthropogenic and biomass burning activities, has been partially elucidated by environmental chamber studies. Briefly, parent aromatic hydrocarbons are oxidised by the hydroxyl radical (OH) to form a

reaction intermediate, the peroxy radical (RO_2). RO_2 undergoes competitive reactions; with HO_2 the products are non-volatile, whereas with NO the products are semi-volatile. Hence, higher HO_2 concentrations favour higher yields of SOA.

The influence of VOC oxidation mechanisms on the global SOA budget was also examined. For the anthropogenic and biomass burning sources of SOA ($VOC_{ANT/BB}$), a series of simulations were performed with varying a) parent hydrocarbon reactivity, b) number of reaction intermediates, and c) accounting for differences in volatility between oxidation products from various pathways. The global annual-total SOA production rate from anthropogenic and biomass burning sources is 18.4 Tg (SOA) a^{-1} when the parent hydrocarbon, $VOC_{ANT/BB}$, undergoes a single-step oxidation, with a fixed reaction yield of 13 %, and a reactivity based on α-pinene. Using the reactivity of naphthalene, toluene or benzene, the global annual-total $VOC_{ANT/BB}$ oxidation rate changes by -3, -31 or -66 %, respectively, when compared to using the reactivity of α-pinene. Increasing the number of reaction intermediates, by including RO_2 as a product of $VOC_{ANT/BB}$ oxidation, slightly delays SOA production but has no effect on the global SOA production rate. Hence, when the reactivity of $VOC_{ANT/BB}$ is reduced from α-pinene to naphthalene, in combination with the introduction of the reaction intermediate, the global annual-total SOA production rates changes by just -0.6 Tg (SOA) a^{-1} (or -3 %), from 18.4 Tg (SOA) a^{-1} to is 17.8 Tg (SOA) a^{-1}. However, the subsequent competitive chemical reactions of RO_2 control the volatility distribution of products. To account for this, the reaction yield for the RO_2+HO_2 pathway was increased from 13 to 66 %. The reaction yield for the RO_2+NO pathway was left unchanged, at 13 %. Accounting for the difference in volatility between RO_2 products increases the global annual-total SOA production rate from anthropogenic and biomass burning by 153 %, from 17.8 Tg (SOA) a^{-1} in the simulation with yields of 13 % for both RO_2

reactions, to 45.1 Tg (SOA) a^{-1} when the yield for the RO_2+HO_2 is increased 66 %.

Overall, the effects of using aromatic oxidation to describe SOA formation from anthropogenic and biomass burning compounds versus using a single-step mechanism with reactivity based on α-pinene, can be explained in terms of reductions in parent VOC reactivity and accounting for the high-yield HO_2 pathway, as opposed to the introduction of the reaction intermediate. For both naphthalene and toluene, reduced reactivity in comparison to α-pinene is small, and is entirely offset by accounting for the difference in volatility between RO_2 oxidation products. By contrast, benzene is significantly less reactive than α-pinene, and accounting for the different in volatility between RO_2 oxidation products cannot outweigh this. For example, for naphthalene, changes in oxidation rate (-3 %) are outweighed by accounting for the difference in volatility between RO_2 reactions, such that the global annual-total SOA production rate changes by 27.3 Tg (SOA) a^{-1} (or 145 %), from 18.4 Tg (SOA) a^{-1} in the single step oxidation mechanism based on α-pinene to 45.1 Tg (SOA) a^{-1} in the multi-step oxidation mechanisms based on naphthalene. Similarly, for toluene, changes in the oxidation rate (-33 %) are still outweighed by accounting for the high-yield HO_2 pathway, such that the global annual-total SOA production rate changes by 15.5 Tg (SOA) a^{-1} (or 85 %), from 18.4 Tg (SOA) a^{-1} in the single step oxidation mechanism based on α-pinene, to 34.0 Tg (SOA) a^{-1} in the multi-step oxidation mechanisms based on toluene. However, for the case of benzene, the substantial change in oxidation rate (-66 %) is not outweighed by accounting for the difference in volatility between RO_2 reactions, such that the global annual-total SOA production rate changes by -0.5 Tg (SOA) a^{-1} (or -3 %), from 18.4 Tg (SOA) a^{-1} in the single step oxidation mechanism based on α-pinene, to 17.9 Tg (SOA) a^{-1} in the multi-step oxidation mechanisms based on benzene. Therefore, from a global perspective, the net effects of increased reaction steps and accounting for the influence of NOx on reaction

yields, can either increase (85 – 150 %) of reduce (-3 %) SOA production depending on the assumed chemical reactivity of the parent VOC.

These variations in oxidation mechanisms can either improve or worsen model agreement with observations, depending on the chemical reactivity of the parent VOC. For the single-step oxidation mechanism with a fixed reaction yield of 13 % and reactivity based on α-pinene, the model underestimated SOA across northern hemisphere mid-latitudes, with an NMB of -66 %. However, for multi-generation oxidation mechanisms with varying reaction yields, and reactivity based on either naphthalene, toluene or benzene, the NMB across northern hemisphere mid-latitudes is either -46, -56 or -71 %, respectively. These results highlight how, increases to reaction intermediates and accounting for the influence of NOx, has the ability to both improve and worsen model agreement with observations which, crucially, depends on the assumed chemical reactivity of the parent VOC. Global annual-total emissions of benzne and toluene are 5.6 and and 6.9 Tg (C) a^{-1}, resptively (Henze et al., 2008), whereas emissions of naphthalene are 0.22 Tg (C) a^{-1} (Pye and Seinfeld, 2010). This suggests benzene and tolune could be more relasitc surrogate compounds to represent $VOC_{ANT/BB}$ mchemistry, as opposed to naphthalene.

These results highlight that the global SOA budget is highly sensitive to hydrocarbon physicochemical processes. For example, the global annual-total SOA production rate has varied from 47 to 75 Tg (SOA) a^{-1} due to variations in VOC deposition. The global annual-total SOA production rate from anthropogenic and biomass burning emissions has varied from 17.9 to 45.1 Tg (SOA) a^{-1} due to variations in VOC oxidation mechanisms. The lowest estimate of the global annual-total SOA production rate from this study would result from the combination of including precursor deposition with the multi-step oxidation pathway with reactivity of benzene. The highest estimate of the global annual-total SOA production rate from this study would comprise of assuming no precursor deposition, but with anthropogenic and

biomass burning hydrocarbons undergoing a multi-step oxidation with reactivity based on naphthalene.

Despite the limitations of this study, such as the lack of chemical complexity and geographical coverage of observations, it is apparent that SOA precursor deposition and oxidation contribute considerably towards uncertainties in both the global SOA budget and model agreement with observations. These results highlight the need for greater insight into the physicochemical processes of gas-phase hydrocarbons related to SOA production, together with a greater density of observations.

Chapter 5 Impact of future change in climate and emissions on SOA lifecycle

At the time of writing, this chapter is in preparation for submission to a journal. Jamie Michael Kelly set-up and performed all model simulations and analysis in this chapter. This includes generation of both present-day and future emissions, and incorporating the interactive biogenic volatile organic compound emissions algorithm into the model. Jamie Michael Kelly wrote the first draft of this chapter. Dr Fiona O'Connor and Professor Ruth Doherty both advised on model set-up and simulations, and provided feedback for chapter revisions. Dr Gerd Folberth advised on implementing the interactive biogenic volatile organic compound emissions scheme into the model.

5.1 Introduction

Having developed the SOA within the UKCA model by including new VOC sources of SOA (Chapter 3), and then testing the sensitivity of the SOA lifecycle to variations in VOC physical and chemical processing (Chapter 4), the next objective of this thesis is to quantify how future changes in climate and emissions will affect the SOA lifecycle.

Climate change has the potential to affect the distribution of secondary pollutants, such as SOA, via changes in production, removal and transport (Section 1.9.6). For instance, climate change may alter the production of SOA via changes in biogenic VOC emissions, or by changes in oxidants such as ozone (O_3) and the hydroxyl radical (OH) (Doherty et al., 2013;Voulgarakis et al., 2013). For semi-volatile SOA, organic compounds are in thermodynamic equilibrium between the aerosol phase and the vapour phase (Section 1.8.2). Therefore, the warming associated with climate change implies a decrease in the SOA burden since higher temperatures favour evaporation and disfavours condensation (Tsigaridis and Kanakidou, 2007). The changes in precipitation patterns associated with climate change may affect the removal of SOA by altering the SOA lifetime (Allen et al. 2016; Hou et al., 2018). The transport of both SOA and precursor gases and oxidants may be affected by future changes in dynamical processes, such as wind speed, mixing depth, and cyclone frequency (Jacob and Winner, 2009).

Biogenic VOC emissions are affected by changes in climate, anthropogenic land-use and, for some compounds, atmospheric carbon dioxide (CO_2) concentrations (Section 1.9.6). Isoprene and monoterpene account for ~65 % of the present-day global annual-total biogenic VOC emission rate (Guenther et al., 2012). These species are side products of leaf photosynthesis. Consequently, changes in light (Monson et al., 2007), temperature (Guenther et al., 1995) and water (Niinemets et al., 2010) can

affect the emissions of these species by directly altering basal emission rates and by altering vegetation distributions (Schurgers et al., 2011). Above ambient CO_2 concentrations, the synthesis of isoprene and monoterpene may be inhibited ('CO_2 inhibition'). For several isoprene-emitting species, strong evidence of CO_2 inhibition is observed (Rosenstiel et al., 2003;Possell et al., 2005). In the case of monoterpene, CO_2 inhibition is only been observed in a limited number of monoterpene-emitting species (Llorens et al., 2009;Loreto and Schnitzler, 2010). Anthropogenic land-use can also affect biogenic VOC emissions (Unger, 2014). However, the plant species that emit isoprene and monoterpene are usually different. Generally, crops have low biogenic VOC emissions whereas woody vegetation has higher biogenic VOC emission rate. Therefore, agricultural expansion in forested regions may result in reduced biogenic VOC emissions (Rosenkranz et al., 2015).

Global chemistry-climate models and dynamic vegetation models can be used to estimate the response of biogenic VOC emissions to projected changes in climate, atmospheric CO_2 concentrations, and anthropogenic land-use. The results from these studies, however, are uncertain. Heald et al. (2008) suggest future increases in global annual-total biogenic isoprene emissions of +22 % by the 2100s under the Intergovernmental Panel on Climate Change (IPCC) Special Report on Emissions Scenario (SRES) A1B. This projected increase in biogenic isoprene emissions is driven by rising temperature, but does not account for CO_2 inhibition or changes in anthropogenic land use. Under climate change whilst also accounting for CO_2 inhibition, comparing isoprene emissions for the 2100s relative to the 2000s, most studies suggest a decrease in global isoprene emissions of: 1% under the IPCC Representative Concentration Pathway (RCP) 8.5 (Pacifico et al., 2012); 8% under SRES A1B (Heald et al., 2009); 13 % under the SRES A2 (Young et al., 2009). In contrast, for the same period, Lin et al. (2016) project an increase of 21 % in global isoprene emissions under

RCP8.5. The increase in isoprene emissions found by Lin et al. (2016) is postulated as due to a high climate model sensitivity (which stimulates isoprene emissions), combined with a strong sensitivity of their isoprene emission parametrisation to temperature as well as a reduced lower sensitivity of isoprene emissions to atmospheric CO_2 concentrations. When combined, the impact of changes in climate and anthropogenic land-use, whilst accounting for CO_2 inhibition, Squire et al. (2014) report a 55 % reduction in global annual-total isoprene emission by 2100 compared to the 2000s under the SRES A1B. Individually, changes in climate, CO_2 concentrations and anthropogenic land-use change the global annual-total isoprene emission rate by +17, -42, and -31 % respectively (Squire et al., 2014).

Very few studies to date examine how monoterpene emissions evolve over the 21st century. Under climate change alone, by the 2100s compared the 2000s, global annual-total monoterpene emissions changes by +23 % under the SRES A1B (Heald et al., 2008) and by +87 % under RCP8.5 (Lin et al., 2016). Similarly, under climate change alone, by the 2100s under the SRES A1B, Wu et al. (2012) find a change in global annual-total monoterpene emissions of +10 %, and a change of +12 % when changes in both climate and anthropogenic land-use are both accounted for. Under changes in climate and anthropogenic land-use, whilst accounting for CO_2 inhibition Hantson et al. (2017) suggest a ~30% reduction in global annual-total monoterpene emissions by the 2100s under RCP8.5 compared to the 2000s. Overall, the sensitivity of SOA to future changes in biogenic VOC emissions is unknown since estimates of future changes in biogenic VOC emissions vary in both magnitude and sign.

Anthropogenic and biomass burning emissions may change in the future which, in turn, may affect SOA. Anthropogenic and biomass burning activities can affect SOA production through three separate mechanisms. Firstly, these emissions sources can release direct precursors of SOA.

Examples of these include VOCs (Section 1.7.4) and S/IVOCs (Section 1.7.5). Secondly, these emissions sources can either directly emit, or contribute towards, the formation of other aerosol components, which can affect gas-to-particle partitioning of organic compounds. For instance, these emissions sources emit POA, which provide a surface for condensation of semi-volatile organic gases to condense onto. Thirdly, these emissions sources emit aerosol precursors which affect aqueous phase SOA production; after emission of SO_2, sulphate aerosol can be formed. The liquid water associated with sulphate provides a media for VOCs to oxidise into SOA precursors within the aqueous phase. Under all IPCC RCP emission scenarios, anthropogenic and biomass burning emissions of VOCs, POA and SO_2, are projected to decrease by the end of the 21st century. This suggests that, under the RCPs, projected changes in anthropogenic and biomass burning emissions by the 2090s will contribute to reduced SOA levels.

Table 5.1 highlights previous studies quantifying the sensitivity of the SOA production rate and burden to future changes in climate and emissions. These studies use chemistry-climate models and account for future changes in both climate and emissions. The exception to this is Tsigaridis and Kanakidou (2007), where a chemistry-transport model is used, hence, projected changes in emissions are explicitly accounted for, but future climate change is represented by imposing a 2 K increase in the tropospheric air temperature. Hence, all these studies account for both future changes in climate and emissions by varying degrees.

Across these studies, a relative consensus has been reached, estimating an increase in the SOA burden under future changes in climate and emissions. However, the magnitude of this increase, and the driving factors which cause this increase, are relatively diverse across these studies. For instance, Liao et al. (2006b) suggest a 54 % increase in the global SOA burden by 2100 under IPCC SRES A1B (Table 5.1) and attribute this to increased biogenic VOC emissions and increased anthropogenic and

biomass burning POA emissions (which increase the surface area for condensing organic vapours). However, this study assumes SOA is purely biogenic. Under the IS92a scenario, Tsigaridis and Kanakidou (2007) find an increase in the global SOA burden of 146 % by the year 2100 compared to 2000 (Table 5.1). This is due to increased emissions of biogenic VOCs, anthropogenic and biomass burning POA, and anthropogenic and biomass burning aromatic VOCs. Heald et al. (2008) suggests a 36 % increase in the global SOA burden under SRES A1B by 2100 due to increased emissions of biogenic VOCs, anthropogenic and biomass burning POA, and anthropogenic and biomass burning aromatic VOCs (Table 5.1). All the aforementioned studies do not account for CO_2 inhibition of biogenic VOC emissions in their SOA projections, although later studies do. Lin et al. (2016), who do consider CO_2 inhibition on isoprene, suggest a 2 % increase in the global SOA burden by 2100 compared to 2000 under RCP8.5 (Table 5.1). This increase is driven by a lengthening of the SOA lifetime by 15 %, which is tempered somewhat by global SOA production reducing by 13 % in response to reductions in anthropogenic SO_2 emissions (and the associated effects on sulphate aerosol concentrations and aerosol liquid water) as well as changes in anthropogenic land-use; the latter is not considered in other studies in Table 5.1.

From the aforementioned studies of how SOA will change in the future, different assumptions are made regarding the VOC sources of SOA. One study assumes SOA is purely biogenic (Liao et al., 2006b), whereas others include the anthropogenic and biomass burning sources of SOA, but only consider the aromatic fraction of these emissions sources (Tsigaridis and Kanakidou, 2007;Heald et al., 2008;Lin et al., 2016). These assumptions are important because studies of present-day SOA distributions identify substantial model negative biases with respect to observed SOA, that are most evident in urban regions (Tsigaridis et al., 2014). These model underpredictions in urban sites can be reconciled somewhat by assuming all

anthropogenic VOC species contribute to SOA formation (Spracklen et al., 2011), as opposed to only the aromatic component of anthropogenic and biomass burning VOCs. In addition, CO_2 inhibition of isoprene emissions is observed across many isoprene-emitting species, yet this process is only included in one study of future SOA (Lin et al., 2016).

In this study, the SOA lifecycle is defined to include (i) the global SOA budget, (ii) the relative contribution of each VOC source to SOA production, and (iii) the spatial distributions of SOA concentrations. The objective of this study is to quantify how the SOA lifecycle is influenced by future changes in climate, emissions, and their combined effects under RCP8.5 for the 2100s relative to the 2000s. The novelty of this study is that all anthropogenic and biomass burning VOCs are included in SOA formation and that CO_2 inhibition on isoprene emissions is accounted for. This paper is organised as follows. Firstly, the chemistry-climate model is described (Section 5.2), The SOA lifecycle under present-day conditions is then described (Section 5.3). Next, the sensitivity of the SOA lifecycle to future changes in climate alone (Section 5.4) and anthropogenic and biomass burning alone (Section 5.5) is quantified. Following this, the combined effects of changes in climate and emissions on the SOA lifecycle are evaluated (Section 5.6). Finally, concluding remarks are made (Section 5.7).

Table 5.1 Previous studies evaluating how the global annual-average SOA burden and global annual-total SOA production rate will change in the future. All studies are based around 2000s and 2100s. Burden and production indicated the difference in 2090s relative to 2000s. All studies account for future changes in both climate and emissions. All studies use chemistry-climate models, except Tsigaridis and Kanakidou (2007)*, where a chemistry-transport model used, and therefore imposes a uniform +2K warming throughout the troposphere to represent global warming. +ORVOC refers to Other Reactive Volatile Organic Compounds.

Study	ΔBurden / %	ΔProduction / %	Scenario/ Pathway	Key drivers	Are anthropogenic and biomass burning considered as sources of SOA?	Is CO_2 inhibition of isoprene emissions accounted for?	Are future changes in anthropogenic land-use accounted for?
Liao et al. (2006b)	+54	-	SRES A2	58 % increase in monoterpene emissions 58 % increase in ORVOC^{+} emissions 130 % increase in POA emissions	No	No	No
Tsigaridis and Kanakidou (2007)	+146	+215	IS92a*	120 % increase in monoterpene emissions 84 % increase in POA emissions 191 % increase in aromatic emissions	Aromatics only	No	No
Heald et al. (2008)	+36	+24	SRES A1B	19 % increase in monoterpene emissions 22 % increase in isoprene emissions 60 % increase in POA emissions 27 % increase in aromatic emissions	Aromatics only	No	No
Lin et al. (2016)	+2	-13	RCP8.5	21 % increase in isoprene emissions 15 % increase in SOA lifetime 46 % decrease in sulphate burden Change in anthropogenic land-use	Aromatics only	Yes	Yes

5.2 Methods

For this study, the HadGEM3-UKCA model is used (Chapter 2). The SOA scheme used is identical to that used in chapter 3. Here, simulations with the HadGEM3-UKCA model are performed in free-running mode in order to perform present-day and future simulations. Biogenic VOC emissions are interactive and hence sensitive to changes in climate (Section 2.3). The model schemes are briefly described and the experimental set-up is outlined. A more detailed model description is presented in Chapter 2.

5.2.1 **HadGEM3-UKCA model**

In this section, the chemistry-climate model used in this chapter is briefly described. Simulations are performed with the United Kingdom Chemistry and Aerosol (UKCA) model (Morgenstern et al., 2009; Mann et al., 2010; O'Connor et al. 2014) coupled to the Global Atmosphere 4.0 (GA4.0) configuration (Walters et al., 2014) of the Hadley Centre Global Environmental Model version 3 (HadGEM3; Hewitt et al. (2011)). The United Kingdom Chemistry and Aerosol (UKCA) model used in this study combines the tropospheric chemistry scheme from O'Connor et al. (2014) with the stratospheric chemistry scheme from Morgenstern et al. (2009). There are 75 species with 285 reactions. The aerosol component of UKCA is the 2-moment modal version of the Global Model of Aerosol Processes (GLOMAP-mode) (Mann et al., 2010). Aerosol components considered are sulphate (SO_4), sea salt (SS), black carbon (BC), primary organic aerosol (POA) and secondary organic aerosol (SOA). For a more detailed description of the representation of atmospheric composition within UKCA, the reader is referred to Section 2.3 and 2.4.

Within the model, SOA is treated by a coupling between the UKCA gas-phase chemistry and GLOMAP-mode (see Chapter 2). As described in Section 2.5 emitted VOCs undergo a single-step oxidation, forming a secondary organic gas (SOG) which condenses, forming SOA. This is shown in E5.1. Note, this is identical to E4.1, but reproduced here for clarity.

$$VOC + [o] \xrightarrow{k_{VOC+[O]}} \alpha_{VOC+[O]} SOG \rightarrow SOA \quad \text{(E5.1)}$$

where VOC is the emitted parent hydrocarbon, [o] is the oxidant concentration, $k_{VOC+[O]}$ is the temperature-dependent rate coefficient, $\alpha_{VOC+[O]}$ is the stoichiometric coefficient, and SOG is the secondary organic gas. Similarly to SOA schemes applied in other global models (Tsigaridis et al., 2014), SOG and SOA are considered non-volatile i.e. SOG condenses irreversibly into the aerosol phase (Section 1.8.2).

The VOC sources of SOA (Section 1.6.2) considered in this study are monoterpene, isoprene, VOC_{ANT}, and VOC_{BB}. Biogenic emissions of sesquiterpenes are not included. Sesquiterpenes are highly reactive (Atkinson and Arey, 2003) and have observed SOA yields ranging from 6 to 125 % (Hoffmann et al., 1997;Griffin et al., 1999;Ng et al., 2007a;Winterhalter et al., 2009;Alfarra et al., 2012;Chen et al., 2012;Jaoui et al., 2013). However, the present-day emission rate of sesquiterpenes is small in comparison to isoprene and monoterpene (Guenther et al., 2012) and very few studies have investigated how sesquiterpene emissions will change in the future. Another SOA source not included in this study is S/IVOCs. For some sites, this emission source is the dominant fraction of ambient SOA (Robinson et al., 2007;Robinson et al., 2010). However, the emission rate of S/IVOCs is extremely uncertain, with estimates of present-day global annual-total S/IVOC emissions ranging from 54 (Hodzic et al., 2016) to 450 Tg a^{-1} (Shrivastava et al., 2015).

Monoterpene and isoprene react with the oxidants: ozone (O_3), the hydroxyl (OH) and nitrate (NO_3) radicals, forming SOG and subsequently SOA (Eq 1). Reaction kinetics for isoprene and monoterpene oxidation are taken from Atkinson and Arey (2003), and are shown in Table 2. VOC_{ANT} and VOC_{BB} are assumed to be reduced compounds, with only single carbon bonding and react solely with OH. VOC_{ANT} and VOC_{BB} are assigned a chemical reactivity identical to monoterpene. Under this SOA scheme where no SOA precursors undergo deposition (Chapter 3), the impact of variations in parent VOC reactivity have very little effect on the global oxidation rate of these species (Kelly et al., 2018). Identical reaction yields of 13 % are assumed for all VOCs and all oxidation pathways based on our previous studies (Kelly et al. 2018).

Table 5.2 – Reaction kinetics for VOC precursors of SOA considered in this study, taken from Atkinson and Arey (2003). Note, this table is identical to Table 2.1, but reproduced here for clarity.

Reaction	k_0 / 10^{-12} x cm^3 $molecule^{-1}$ s^{-1}	B / K	k (298) / 10^{-12} x cm^3 $molecule^{-1}$ s^{-1}
monoterpene+ OH	12.0	-444.0	52.9
monoterpene+ O_3	0.00101	732.0	0.0000862
monoterpene+ NO_3	1.19	-925.0	6.12
isoprene + OH	27.0	-390.0	99.3
isoprene + O_3	0.01	1195.0	0.000180
isoprene + NO_3	3.15	450.0	0.692

5.2.2 **The JULES land-surface model**

Here, the land surface component of the model used to derive biogenic VOC emissions described in chapter 2. The land surface component of the GA4.0 configuration of HadGEM3 is the Global Land 4.0 (GL4.0) configuration of the Joint UK Land Environment Simulator (JULES; Best et al. (2011); Clark

et al. (2011); Walters et al. (2014)). This component of the model includes five plant functional types (PFTs) (broadleaf trees, needleleaf trees, C_3 grass, C_4 grass, and shrubs) and four non-vegetated surface types (urban, inland water, bare soil, and ice). The fractional cover of each surface type is prescribed from the International Geosphere-Biosphere Programme (IGBP) dataset (Loveland et al., 2000). Photosynthesis for C_3 and C_4 plants is calculated following Collatz et al. (1991) and Collatz et al. (1992), respectively.

In order to capture the sensitivity of biogenic VOC emission to factors such as climate change and atmospheric CO_2 concentrations, interactive biogenic VOC emissions are used. The method for calculating these emissions is described in detail in Chapter 2 (Section 2.2). Briefly, photosynthetic-based isoprene emission following Arneth et al. (2007b) are included in JULES following Pacifico et al. (2011). Monoterpene emissions from vegetation are based on Guenther et al. (1995) which is also described in Section 2.2. Essentially, PFT-specific emission factors are modified according to environmental conditions.

Table 5.3 shows the PFT-specific emission factors, as well as global annual-total emission rates for both isoprene and monoterpene for the present-day and the future (2090s). These emissions are generated from model simulations, which are discussed in more detail in Section 5.2.3. Global annual-total monoterpene emissions increase by 79 % in the 2090s under RCP8.5. In contrast, isoprene emissions are effectively constant as a result of the competing effects of higher temperatures and higher CO_2 concentrations.

Table 5.3 – PFT- -specific emission factors for isoprene and monoterpene, taken from (Pacifico et al., 2011). gdw is gram dry weight and h is hour. Also, included are global annual total emissions for the present day (1995-2005) and for the future (2090-2100) under RCP8.5.

PFT	Emission factor (μgC gdw^{-1} h^{-1})	
	Isoprene	Monoterpene
Broadleaf trees	35	1
Needleleaf trees	12	2.4
C_3 grass	16	0.8
C_4 grass	8	1.2
Shrubs	20	1.25
Time period	Global annual total emission rates (Tg (VOC) a^{-1})	
	Isoprene	Monoterpene
1995-2005	505	63
2090-2100	500 (-1 %)	113 (+79 %)

5.2.3 **Experimental set-up, emissions and model simulations**

The model simulations are set-up to be representative of the climatological time periods of 1995-2005 (2000s) and 2090-2100 (2090s). These simulations use prescribed decadal-mean monthly-varying sea surface temperature (SST) and sea ice extent (SIE) fields, taken from the HadGEM2 Coupled Model Intercomparison Project Phase 5 (CMIP5) transient centennial simulations (Jones et al., 2011) under RCP8.5. The 2000s period is based on the CMIP5 “historical” period which is the starting period for all RCPs. The 2090s simulations follow RCP8.5 (Riahi et al., 2011). This pathway is characterised by large increases in long-lived greenhouse gases,

which in HadGEM3 produces an increase in the global mean temperature of 4.6°C in 2100 (Andrews et al., 2012). This model has a high climate sensitivity, since across the 15 CMIP5 models, this pathway results in an increase in the global-mean surface temperature for the same time period ranging from 2.6 to 4.8°C (Collins et al., 2014).These HadGEM2 transient simulations also prescribe surface concentrations of long-lived green-house gases (GHG), such as methane (CH_4), CO_2, nitrous oxide (N_2O), chlorofluorocarbons (CFCs) and hydrofluorocarbons (HFCs), taken from Jones et al. (2011). Hence, GHGs are prescribed in these simulations, not emitted. GHG concentrations are defined separately for the chemistry scheme and radiation schemes. With the exception of long-lived greenhouse gases in the radiation scheme, there is no feedback from the chemistry or aerosols to the climate.

Table 5.4 shows a summary of global annual-total emissions used by the model. With the exception of isoprene, monoterpene and lightning-NOx, all natural emissions are held fixed at present-day levels for both time periods. Anthropogenic and biomass burning emissions represent the climatological time periods of 1995-2005 (2000s) hereafter referred to as present-day and 2090-2100 (2090s) under RCP8.5.

Table 5.4 - Annual Annual-total emissions for the 2000s and 2090s. For anthropogenic and biomass burning emissions, estimates for the present-day are taken from Lamarque et al. (2011), and future emissions follow IPCC RCP8.5 (Riahi et al., 2011). Isoprene and monoterpene emissions are calculated interactively (Table 5.3; Section 5.2). All emissions are in the units of Tg (species) a^{-1}, with the exception of NO_X, which in the form of Tg (NO_2) a^{-1}. VOC_{ANT} and VOC_{BB} are calculated to be representative of RCP8.5, as described in 2.3. CH_4 concentrations are 1750 ppb in the 2000s and 3752 ppb in the 2090s.

Species	Present-day (1995-2005)				Future (2090-2100)			
	Total	Anthropogenic	Biomass burning	Other	Total	Anthropogenic	Biomass burning	Other
NO_X	148.6	104.8	17.8	soil - 18.4 aircraft - 2.9 Lightning- 13.6	108.0			Soil – 18.4 aircraft – 12.3 Lightning-19.8
CO	1150	608.7	460.2	ocean - 45.0	732.0	373.6	313.8	ocean - 45.0
HCHO	9.0	3.2	5.9	-	5.0	1.2	3.8	-
C2 hydrocarbons	27.1	15.4	11.7	-	17.5	9.8	7.6	-
C3 hydrocarbons	13.6	7.5	6.1	-	7.8	4.5	3.3	-
Me_2CO	45.7	0.7	5.0	land - 40.0	43.9	0.3	3.6	land – 40.0
MeCHO	8.7	-	8.7	-	6.4	-	6.4	-
SO_2	103.7	103.7	-	natural -	23.2	23.2	-	natural -
BC	7.9	5.3	2.6	-	4.3	2.4	1.9	-
OC	29.8	6.5	23.3	-	19.1	2.9	16.2	-
Isoprene	505	-	-	biogenic – 505	500	-	-	biogenic – 500
Monoterpene	63	-	-	biogenic – 63	113	-	-	biogenic - 113
VOC_{ANT}	127	127	-	-	123	123	-	-
VOC_{BB}	49	-	49	-	33	-	33	-
$VOC_{ANT/BB}$	176	127	49	-	156	123	33	-

Emissions of the anthropogenic and biomass burning precursors of SOA, VOC_{ANT} and VOC_{BB}, receptively, are also constructed to follow future changes under RCP8.5. In the case of VOC_{ANT}, aromatic VOC emissions from anthropogenic activity are used to define a spatial and seasonal pattern (Lamarque et al., 2011), that are then scaled to equal the anthropogenic total VOC emission rate (Lamarque et al., 2011). This method is used for VOC_{ANT} emission estimates for both the 2000s and the 2090s. Under this pathway, global annual-total VOC_{ANT} emissions reduce by 4 Tg (VOC_{ANT}) a^{-1} (-3 %), from 127 Tg (VOC_{ANT}) a^{-1} in the present-day, to 123 Tg (VOC_{ANT}) a^{-1} in the 2090s under RCP8.5 (Table 5.4).

In the case of VOC_{BB}, for the present-day, biomass burning emissions of CO (Lamarque et al., 2011) are first used to define a spatial and seasonal pattern; these are then scaled to equal the biomass burning total VOC emission total estimated from the Emissions Database for Global Atmospheric Research (EDGAR). Hence, this provides an emission factor which can be applied to biomass burning CO emissions to calculate biomass burning VOC emissions. EDGAR only provide a present-day estimate of emissions. Therefore, the present-day emission factor is then applied to the biomass burning CO emissions for the 2090s from RCP8.5 to provide an estimate for VOC_{BB} emissions for that same period. Under RCP8.5, global annual-total VOC_{BB} emissions decrease by 16 Tg (VOC_{ANT}) a^{-1} (-33 %), from 49 Tg (VOC_{BB}) a^{-1} in the present-day, to 33 Tg (VOC_{BB}) a^{-1} in the future (Table 5.4).

When combined, VOC_{ANT} and VOC_{BB} are referred to as $VOC_{ANT/BB}$. Present-day global annual-total emissions of VOC_{ANT} and VOC_{BB} are 127 Tg (VOC_{ANT}) a^{-1} and 49 Tg (VOC_{BB}) a^{-1}, respectively (Table 5.4). Hence, the present-day emission rate of $VOC_{ANT/BB}$ is 176 Tg ($VOC_{ANT/BB}$) (Table 5.4). In the 2090s under RCP8.5, global annual-total emissions of VOC_{ANT} and VOC_{BB} are 123 Tg (VOC_{ANT}) a^{-1} and 33 Tg (VOC_{BB}) a^{-1}, respectively and when combined $VOC_{ANT/BB}$ is 156 Tg (Table 5.4). Overall, global annual-total $VOC_{ANT/BB}$ emissions reduce by 11 % under RCP8.5 in the 2090s compared to the 2000s, which is primarily a result of decreases in VOC_{BB}.

Simulated present-day global annual-total isoprene emissions are 505 Tg (C_5H_8) a^{-1} (Table 5.4). This is consistent with estimates from other global modelling studies, which range from 412 to 600 Tg (C_5H_8) a^{-1} (Sanderson et al., 2003;Tao and Jain, 2005;Lathiere et al., 2005;Arneth et al., 2007a;Heald et al., 2008;Heald et al., 2009;Pacifico et al., 2012;Lin et al., 2016). Present-day simulated global annual-total monoterpene emissions are 63 Tg ($C_{10}H_{16}$) a^{-1} (Table 5.4), which is at the low end of estimates from the literature, which range from 33 to 131 Tg ($C_{10}H_{16}$) a^{-1} (Levis et al., 1999;Guenther et al.,

1995;Lathiere et al., 2005;Kaplan et al., 2006;Arneth et al., 2007a;Heald et al., 2008;Lin et al., 2016). However, compared to isoprene, estimates of monoterpene emissions are considerably more variable (Arneth et al., 2008). Future changes in biogenic VOC emissions under climate change are discussed in more detail in Section 5.5.1.

Four 10-year model integrations are conducted in this study, which are summarised in Table 5.5. Firstly, a present-day simulation ('PD') is performed for the 2000s, from which changes in the SOA lifecycle are analysed. Next, the SOA lifecycle under future climate conditions is simulated ('Clim'; Table 5.5). For this simulation, SSTs, SIE and GHG concentrations within the radiation scheme adopt values for the 2090s decade. Anthropogenic and biomass burning emissions, and GHG concentrations within the chemistry scheme are held fixed at present-day values for this simulation. This simulation includes interactive effects of climate on biogenic VOC emissions, including the impact of atmospheric CO_2 concentration changes on isoprene emissions (Table 5.3). Following this, the SOA lifecycle under future anthropogenic and biomass burning emissions is simulated ('Em'; Table 5.5). For this simulation, anthropogenic and biomass burning emissions, and GHG concentrations for the chemistry scheme adopt values for the 2090s following RCP8.5, whilst the climate (SSTs and SIE) is fixed at present-day (2000s) conditions. Finally, the SOA lifecycle under both future climate and emissions is simulated ('Clim+Em'; Table 5.5) whereby SSTs, SIE, anthropogenic and biomass burning emissions, and greenhouse-gas concentrations for both the chemistry and radiation schemes all adopt 2090s values for RCP8.5. For all integrations, the first year is discarded as spin-up and analysis is based on the remaining 10 years. The fractional cover of each surface type is held fixed across all simulations. Hence, vegetation distributions are not affected by changes in climate or anthropogenic land-use. All analysis is based on the decadal-means, unless otherwise stated.

Table 5.5 - Summary of simulations conducted in this study

Simulation	anthropogenic and biomass burning emissions + GHG (within chemistry scheme)	Biogenic emissions of isoprene and monoterpene	SSTs and SIE + GHG (within radiation scheme)
PD	2000s	2000s	2000s
Clim	2000s	2090s	2090s
Em	2090s	2000s	2000s
Clim+Em	2090s	2090s	2090s

5.3 The SOA lifecycle in the present-day

In this section, the SOA lifecycle under present-day conditions is evaluated (PD; Table 5.5). Figure 5.1 shows the decadal-mean annual-mean surface SOA concentrations for the present-day, as well as differences between the future and the present-day for the simulations described in Table 5.5. Annual-mean surface SOA concentrations typically range 3 – 12 μg m^{-3} over India, East and South-East Asia, parts of South America, and sub-Saharan Africa (Figure 5.1 a). Lower annual-mean SOA levels (not exceeding 3 μg m^{-3}) are simulated over North America, Europe, Siberia and Australia (Figure 5.1 a). Moderately high SOA concentrations (0.3 to 2 μg m^{-3}) are also predicted downwind of high emissions source regions in India, South East Asia and the Congo, notably the Arabian Sea, the Bay of Bengal and the tropical Atlantic Ocean (Figure 5.1 a). Over the remaining oceanic regions,

annual-mean surface SOA concentrations negligible (less than 0.1 μg m^{-3}; Figure 5.1 a).

The chemical mechanism used in this chapter is identical to that used in Chapters 3 ('AllSources') and 4 ('Control'). However, here, biogenic VOC emissions are calculated online (Section 5.2.2) and simulations span a decade. Whereas in the previous chapters, biogenic VOC emissions are prescribed (Guenther et al., 1995) and simulations span one year. The biogenic VOC emissions used here are slightly lower than in Chapters 3 and 4. Under this chemical mechanisms, simulated SOA is in relatively good agreement with observed SOA across the NH mid-latitudes (-50 %; Section 3.5.1). This model negative bias is common among global models (Tsigaridis et al., 2014) and may stems from missing SOA sources (Chapter 3).

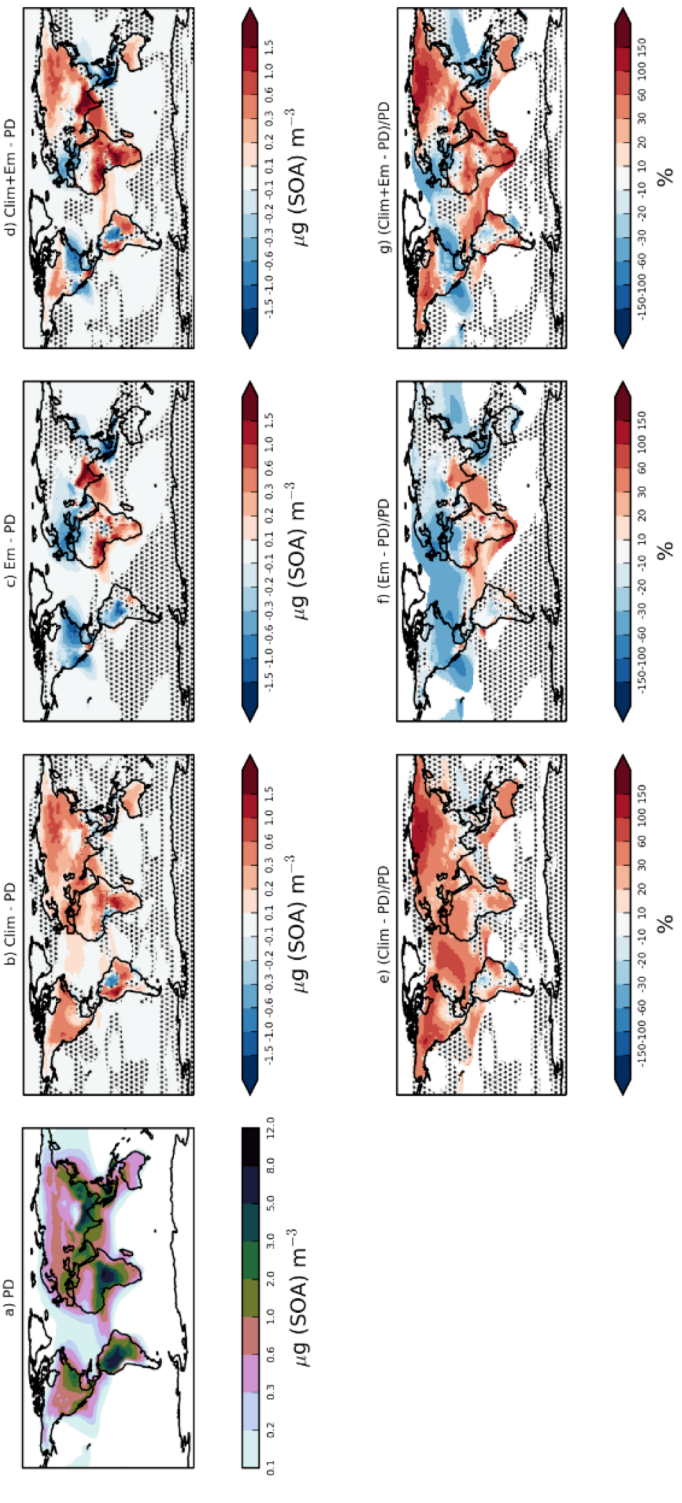

Figure 5.1- Decadal-mean annual-mean surface SOA concentrations (μg m^{-3}) for a) the present-day simulation (PD) (1996-2005). Difference in annual-mean surface SOA concentrations for future (2091-2100) SOA concentrations under RCP8.5 relative to the present-day simulations, for; b) and e) - future climate (Clim), c) and f) - future emissions (Em), and d) and g) - future climate and emissions combined (Clim+Em). Hatched areas indicate where absolute differences are not significant at the 0.05 level, as evaluated with the Student t-test using the 10 years of annual-mean data.

Table 5.6 provides the decadal-mean global SOA budget for the simulations presented in Table 5.5. Considering all VOC sources, the simulated annual-total SOA production rate is 60.6 Tg (SOA) a^{-1} and the global annual-mean SOA burden is 0.71 Tg (SOA) (PD; Table 5.6). Here, SOA is treated as non-volatile, inert and soluble, hence, the sole removal process is deposition. Considering both dry and wet removal, the global annual-mean SOA lifetime is 4.4 days (Table 5.6). Simulated present-day global SOA budget terms for this study are consistent with the range of estimates from the AERCOM multi-model study, also provided in Table 5.6.

Table 5.6 - Decadal-mean mean global SOA budgets for simulations in this study. For the present-day (2000s), italics indicate the multi-model range from Tsigaridis et al. (2014). The difference in budget terms for future (2090s) relative to the present-day (2000s) expressed as a percentage are shown within parentheses.

	PD	Clim	Em	Clim+Em
Production / Tg (SOA) a^{-1}	60.6, *13-121*	66.7 (+10 %)	56.9 (-6 %)	63.1 (+4 %)
Burden / Tg (SOA)	0.71, *0.3-2.2*	0.87 (+23 %)	0.69 (-3 %)	0.85 (+20 %)
Lifetime / days	4.4, *2.4-15*	4.9 (+12 %)	4.5 (+4 %)	5.0 (+15 %)

Figure 5.2 shows the decadal-mean annual-total SOA production rates from the various VOC species and their respective oxidation channels for the simulations in Table 5.5. This provides a breakdown of the SOA production pathways and quantifies the relative importance of each VOC source and oxidant species. Global annual-total SOA production rates for

monoterpene, isoprene and $VOC_{ANT/BB}$ are 8.1, 17.4 and 35.1 Tg (SOA) a^{-1}, respectively (Figure 5.2 a). The global annual-total biogenic SOA production rate is 25.5 Tg (SOA) a^{-1}, and is calculated as the sum of SOA production from both monoterpene and isoprene across all three oxidation pathways (25.5 = 8.1 + 17.4) (Figure 5.2 a). Overall, biogenic VOCs account for 42 % (25.5 Tg (SOA) a^{-1}) of the global annual-total SOA production rate (60.6 Tg (SOA) a^{-1}), with $VOC_{ANT/BB}$ accounting for 58 % (35.1 Tg (SOA) a^{-1}). Hence, in the present-day, SOA production is strongly influenced by $VOC_{ANT/BB}$ non-natural sources which predominately react with OH. Hence, considering all VOCs, 83 % (50.2 Tg (SOA) a^{-1}; Figure 5.2 a) react via the OH pathway.

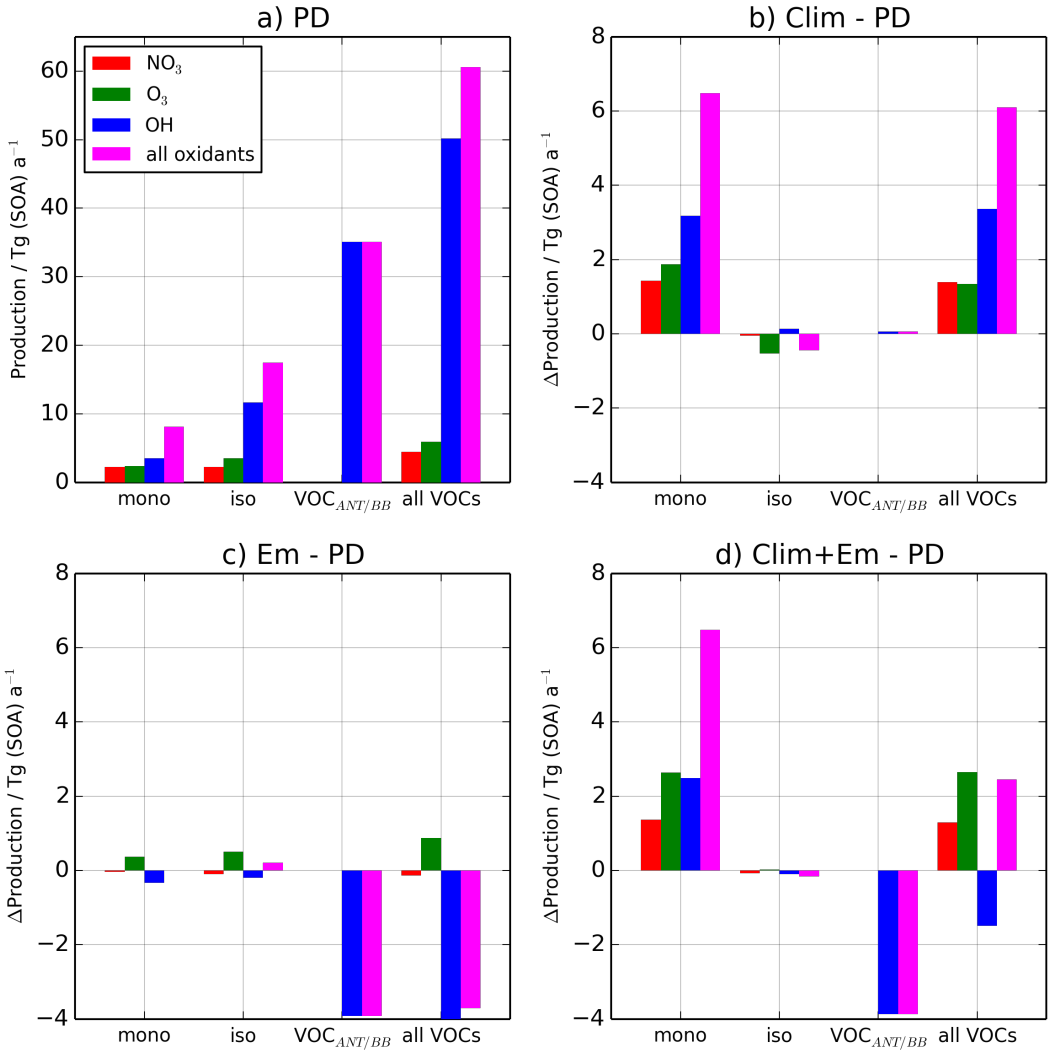

Figure 5.2 – Global decadal-mean annual-total SOA production rates (Tg (SOA) a^{-1}) for the different VOC species through the various oxidation channels for the present day (PD) simulation (1996-2005), and the difference in production rates for the future simulations (2091-2100) relative to the present-day simulation (Clim-PD, Em-PD, Clim+Em - PD).

The global annual-total SOA production rate from biogenic VOCs estimated here (25.1 Tg (SOA) a^{-1}) is consistent with estimates from the literature, which range from 13 to 55 Tg (SOA) a^{-1} (Henze and Seinfeld, 2006;Tsigaridis and Kanakidou, 2007;Hoyle et al., 2007;Henze et al., 2008;Farina et al., 2010;Spracklen et al., 2011;Khan et al., 2017). However,

the SOA yields used in global modelling studies are typically derived from chamber studies. Wall-loses during these chamber studies may lead to substantial underestimates in the SOA yields (Zhang et al., 2014). One global modelling study that does account for chamber-wall loses, suggests a global annual-total biogenic SOA production rate of 98 Tg (SOA) a^{-1} (Hodzic et al., 2016). Overall, variability in biogenic SOA production estimates can be attributed to which biogenic VOCs are included (e.g. isoprene, monoterpenes, sesquiterpenes) and the SOA yields used for these species.

The global annual-total SOA production rate from anthropogenic and biomass burning emissions estimated here (35.1 Tg (SOA) a^{-1}) is higher than some other bottom-up global modelling studies, which range from 1.4 to 6 Tg (SOA) a^{-1} (Tsigaridis and Kanakidou, 2007;Heald et al., 2008;Lin et al., 2016). However, these studies only include the aromatic component of these emissions sources types, with global annual-total aromatic emissions of 16 – 32 Tg (VOC) a^{-1}. By contrast, in this study, all VOC emissions from these emissions source types are assumed to form SOA (emission rate = 176 Tg ($VOC_{ANT/BB}$) a^{-1}). In addition to VOCs, anthropogenic and biomass burning activities also release S/IVOCs, which can contribute to SOA formation (Donahue et al., 2006;Donahue et al., 2012). However, S/IVOC emission estimates, and their potential to form SOA are highly uncertain (e.g. Shrivastava et al. (2015). As a result, S/IVOC emissions are not considered here.

An additional potentially important source of SOA that is also not considered here is aqueous phase production (Ervens, 2015). Estimates of the global annual-total SOA source strength within cloud and aerosol liquid are 13 – 47 and 0 – 13 Tg (SOA) a^{-1}, respectively (Lin et al., 2012;Lin et al., 2014).

The seasonality in SOA precursor emissions and SOA production is displayed in Figure 5.3. Emissions of both monoterpene and $VOC_{ANT/BB}$ are

higher in the Northern Hemisphere (NH) compared to the Southern Hemisphere (SH). The NH accounts for 61 and 77 % of the global annual-total monoterpene and $VOC_{ANT/BB}$ emission rates respectively (not shown). In contrast, annual-total isoprene emissions rates are approximately equal in both hemispheres, except in June-August, when they peak in the NH. Emissions of both monoterpene and isoprene are calculated interactively based on meteorological factors such as temperature and sunlight (Section 5.2.2). Consequently, emissions of both these species peak during local summertime (Figure 5.3 b and c). In the NH, where $VOC_{ANT/BB}$ is primarily anthropogenic, emission rates do not show a clear seasonal cycle (Figure 3 b). In contrast, in the SH, where $VOC_{ANT/BB}$ is mostly of biomass burning origin, emission rates peak between July and November (Figure 5.3 c).

The seasonal cycle in SOA production (Figure 5.3 d, e and f) follows the seasonal cycle in precursor emissions (Figure 5.3 a, b and c). The NH peak in SOA production during local summer (Figure 5.3 e) is attributed to biogenic emissions also peaking during this season (Figure 5.3 b). The SH peak in SOA production between July and November (Figure 5.3 f) appears to be driven by biomass burning VOC emissions also peaking during this season (Figure 5.3 c). However, also in the SH, although isoprene emissions are very high between January and April (Figure 5.3 c), there is little or no peak in SOA production at the same time (Figure 5.3 f). This could be due to limited oxidant availability during this season. On an annual basis, the NH accounts for 66 % of the global annual-total SOA production rate. Overall, global SOA production peaks during NH local summer (Figure 3 d), which is consistent with (Tsigaridis et al., 2014).

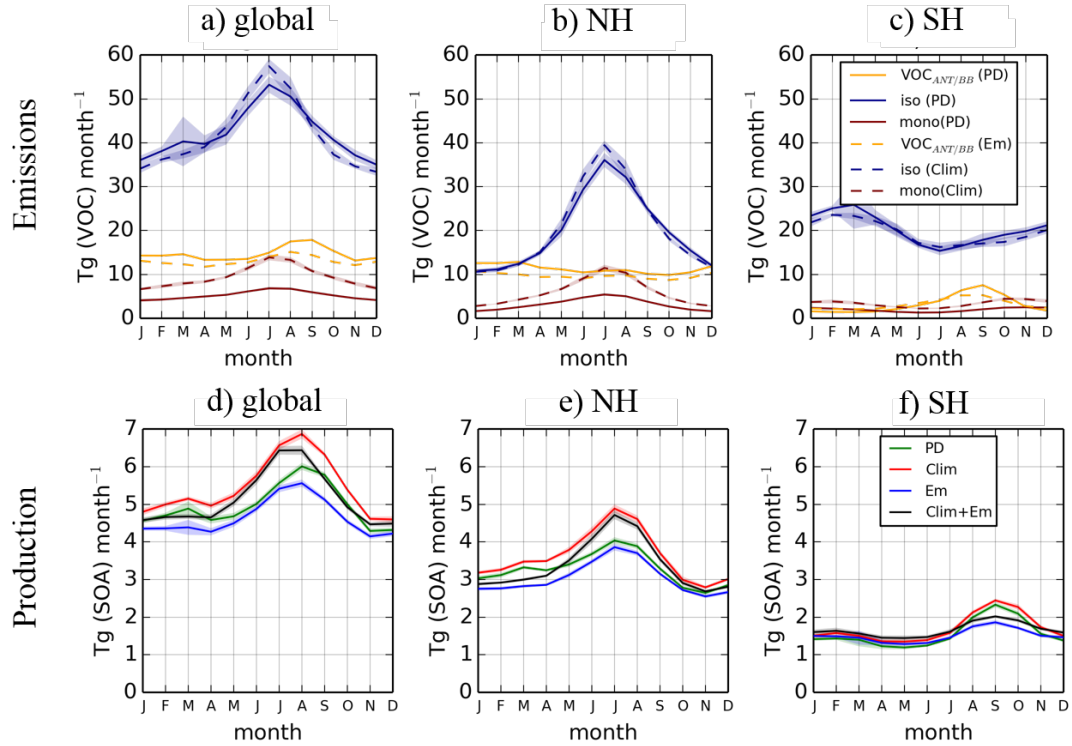

Figure 5.3 – Decadal-mean monthly-total VOC emission rates (top row) and SOA production rates (bottom row) for the simulations presented in Table 5. Envelopes indicate ±1σ, which is constructed from the 10 years of monthly data.

5.4 Climate change impacts on the SOA lifecycle

Here, the influence of climate change alone on the SOA lifecycle is examined (Clim – PD). Under fixed anthropogenic and biomass burning emissions, climate change alters both the global SOA budget and spatial pattern of SOA concentrations. Over most land environments, climate change leads to increased SOA concentrations (Figure 5.1 b). Over Peru and the Congo region, climate change causes decadal-mean annual-mean surface SOA concentrations to increase by more than 1.5 μg m^{-3} (Figure 5.1 b), corresponding to increases of 10 to 30 % (Figure 5.1 e). Over North Amercia, Siberia and South Asia, annual-mean surface SOA concentrations increase by 0.3 – 1 μg m^{-3} (Figure 5.1 b), or 60 – 150 % (Figure 1 e). However, over the Southeast USA, Southeast China, and Southern Brazil,

climate change has little effect on SOA concentrations (Figure 5.1 b). For Northern Brazil, the coast of Western Africa, and parts of South East Asia, annual-mean surface SOA concentrations reduce by up to 1 μg m^{-3} (Figure 5.1 b), (-30 %; Figure 5.1 e) in response to climate change.

Compared to the present-day, climate change increases the global annual-mean SOA burden by 23 %, from 0.71 Tg (SOA) in the present-day to 0.87 Tg (SOA) in the 2090s under future climate change (Clim; Table 5.6). This projected increase in the SOA load is a result of a 10 % (6.1 Tg (SOA) a^{-1}) increase in the global annual-total SOA production rate, combined with a 12 % increase in the lifetime (Table 5.6). This climate-induced increase in SOA production is a result of increased production from monoterpene. Climate change increases the global annual-total SOA production rate from monoterpene by 6.5 Tg (SOA) a^{-1}, whereas production of SOA from isoprene reduces by 0.4 Tg (SOA) a^{-1} (Figure 5.2 b). The climate interactions leading to these changes in the global SOA budget and SOA sptial distriobutions are examined in the following sub-sections. This begins with the emissions of the VOC precursors of SOA (Section 5.5.1), followed by oxidant availability (Section 5.5.2), temperature-dependent reaction rates (Section 5.5.3), and SOA deposition (Section 5.5.4). These reuslts are then summarised and compared to the literature (Section 5.5.5).

5.4.1 **Climate change impacts on biogenic VOC emissions**

Natural emissions are sensitive to climate change. Figure 5.4 shows the decadal-mean annual-mean surface air temperature for the present-day and the difference between the 2090s following RCP8.5 and the present-day. The global-mean surface air temperature increases by 4.6 °C under future climate, with the greatest warming occurring in the high latitudes of the NH (Figure 5.4 b). As discussed in section 5.2.3, HadGEM3 has a high climate sensitivity.

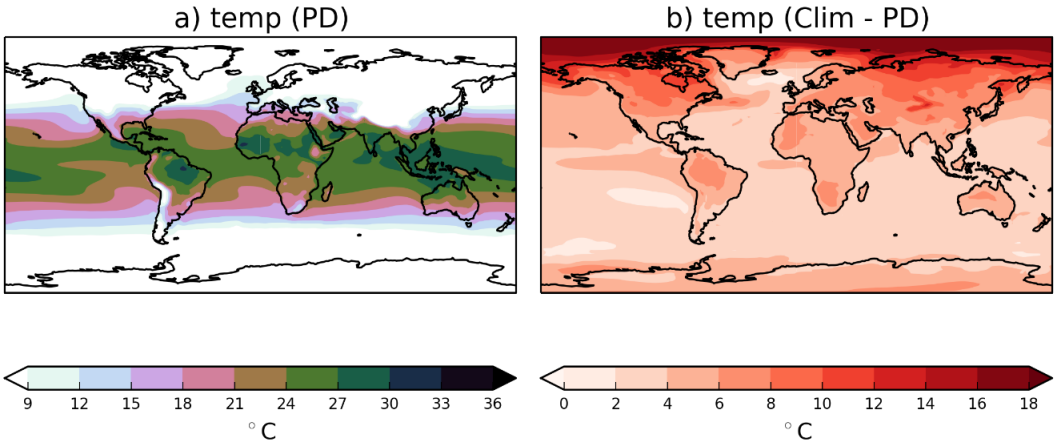

Figure 5.4 - Decadal-mean annual-mean surface air temperature for the present-day (PD) (1996-2005) and the difference between the future climate following RCP8.5 (Clim; 2091-2100) and the present-day (PD).

Climate change increases the global annual-total gross primary productivity by 44 %, from 110 Pg (C) a^{-1} in the present-day to 158 Pg (C) a^{-1} under future climate conditions (not shown). Also, the prescribed atmospheric CO2 concentration rises from 369 ppm in the present-day, to 939 ppm in the future climate simulation (not shown). Globally, climate change has little impact on annual-total isoprene emissions which decrease by 1% from 505 Tg (C_5H_8) a^{-1} in the present-day to 499 Tg (C_5H_8) a^{-1} in the future (Table 5.3; section 5.2.3). Under RCP8.5, warming (Figure 5.4 b) and an increase in CO_2 concentrations have opposing effects on isoprene emissions (Section 5.2.2), with the net effect being a negligible change in global isoprene emission rates. Contrastingly, monoterpene emissions, which do not include CO_2 inhibition (Section 5.2.2), increase by 50 Tg a^{-1} (79 %) from 63 Tg ($C_{10}H_{16}$) a^{-1} in the present-day to 113 Tg ($C_{10}H_{16}$) a^{-1} in the 2090s under climate change (Table 5.3; section5. 2.3). These changes in global biogenic VOC emission rates dictate the climate-induced changes in the global SOA budget; global annual-total SOA production from monoterpene

increases by 6.5 Tg (SOA) a^{-1} (79 %) but reduces by 0.4 Tg (SOA) a^{-1} from isoprene SOA (Figure 5.2 b).

Figure 5.5 summarises projected future changes in biogenic VOC emissions from this study and the literature. Here, global isoprene emissions reduce by just 1 % in the future due to climate change and CO_2 inhibition, which is in agreement with most previous studies including these effects (Heald et al., 2009;Young et al., 2009;Pacifico et al., 2012;Squire et al., 2015). However, under RCP8.5 (same scenario used for these simulations), Lin et al. (2016) suggest the high climate sensitivity of the GCM employed (with a global average temperature increase of 4.1°C in the 2100s compared to the 2000s), and hence the stimulation by warming has a stronger effect on isoprene emissions compared to CO_2 inhibition, which is lessened at high CO_2 concentrations (943 ppm) in their study. These competing effects result in a 94 Tg (C) a^{-1} increase in isoprene emissions under climate change (Lin et al. 2016). However, the climate sensitivity, as noted above- a 4.6°C increase in the global average temperature between the 2000s and 2090s - is larger in this study. Resolving the sensitives of isoprene emissions toward temperature and CO_2 concentrations is of central importance for determining how isoprene emissions will evolve over the 21st century. In addition to CO_2 inhibition, projected changes in anthropogenic land use may contribute to changes in isoprene emissions in the future; these are not included in this study. By 2100 under A1B compared to the 2000s, Squire et al. (2014) find that future climate change, CO_2 inhibition, and anthropogenic land use change cause the global annual-total isoprene emission rate to reduce by 55 % (259 Tg (C_5H_8) a^{-1}) decrease.

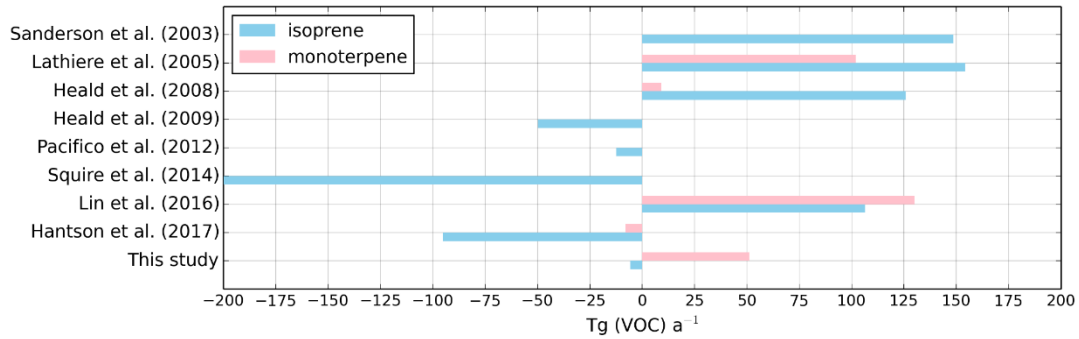

Figure 5.5 – Changes in annual-total biogenic VOC emission rates (Tg (VOC) a^{-1}) from this study, combined with estimates from the literature. For all studies shown here, the 2090s represents the future and the 2000s represents the present-day. Model simulations vary considerably in terms of which scenarios are used and what factors are included (e.g. CO_2 inhibition, anthropogenic land use, and dynamic vegetation), with studies before 2008 not incorporating CO_2 inhibition effects on isoprene.

As discussed in Section 5.1, projected changes in monoterpenes emissions are also uncertain. In relation to monoterpene emissions, the impact of climate change alone whilst assuming fixed land cover results in increases to global annual-total emission rates ranging from 4.6 Tg ($C_{10}H_{16}$) a^{-1} (23 %) (Heald et al., 2008) to 115 Tg ($C_{10}H_{16}$) a^{-1} (87 %) (Lin et al., 2016). Wu et al. (2012), also accounting for land-use change, suggest a more conservative increase of 12% in 2100 under the SRES A1B climate scenario. Considering changes in both climate and anthropogenic lands-use, whilst accounting for CO_2 inhibition, Hantson et al. (2017) suggest a ~30 % (9 Tg ($C_{10}H_{16}$) a^{-1}) reduction in in global annual-total monoterpene emissions by the 2100s under RCP8.5 relative to the 2000s.

Figure 5.6 shows the spatial pattern of simulated biogenic VOC emissions for the 2000s and the 2090s under RCP 8.5. For isoprene emissions, it is evident that the balance between the opposing effects of higher temperatures and higher CO_2 concentrations on emissions (Table 5.3; Figure 5.5) is not globally widespread (Figure 5.6 d). This is likely due to regional variability in (i) the temperature increases (Figure 4 b) and, (ii) the

leaf internal CO_2 concentrations (section 5.2.2). Over parts of Alaska, Siberia, Peru, and Central Africa, annual-total isoprene emissions increase by more than 5 g (C_5H_8) m^{-2} s^{-2} (Figure 5.5 d). Contrastingly, over parts of the southeast USA, Northern Brazil, Western Africa, and Southeast Asia, annual-total isoprene emissions decrease by more than 5 g (C_5H_8) m^{-2} s^{-2} (Figure 5.6 d). However, for monoterpene emissions, across all continental regions, climate change results in increases of decadal-mean annual-total monoterpene emissions of 0.2 - 1 g ($C_{10}H_{16}$) m^{-2} s^{-1} (Figure 5.6 e).

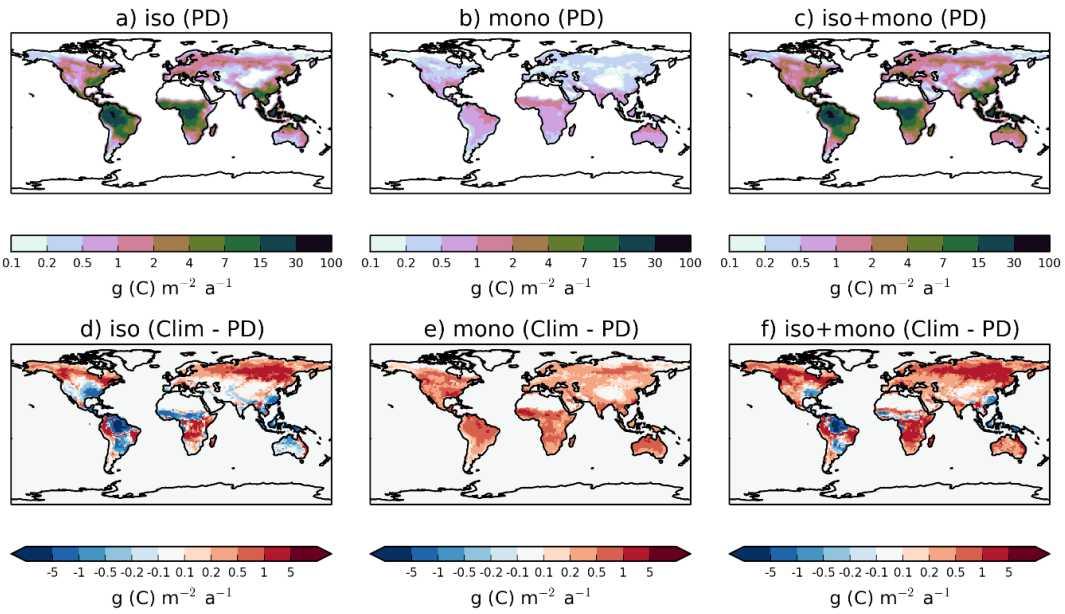

Figure 5.6 – Simulated decadal-mean annual-total climate-sensitive biogenic VOC emissions (g (C) m^{-2} s^{-1}) for isoprene and monoterpene for the present-day (PD; 1996-2005) and future climate simulations (Clim; 2091-2100).

Across all continents, the magnitude of climate-induced changes in isoprene emissions (Figure 5.6 d) exceeds that of climate-induced changes in monoterpene emissions (Figure 5.6 e). For example, climate change causes isoprene emission changes of more than +/- 5 g (C_5H_8) a^{-1} (Figure

5.6 d), whereas monoterpene emission increases do not exceed 1 g ($C_{10}H_{16}$) a^{-1} (Figure 5.6 d). With the exception of Australia and parts of India, the combined changes in total biogenic VOC emissions (Figure 5.6 f) are a reflection of changes in isoprene, as opposed to monoterpene. These changes in isoprene emissions (Figure 5.6 d) and monoterpene (Figure 5.6 e) emissions, when combined (Figure 5.6 f), explain the climate-induced changes in SOA distributions (Figure 5.1 b). However, in the Southeast USA, Southeast China, and Southern Brazil, despite simulated reductions in biogenic VOC emissions (Figure 5.5 d), SOA concentrations do not change significantly (Figure 5.1 b).

5.4.2 **Climate change impacts on oxidants**

Oxidant availability is a critical factor in determining how quickly freshly emitted VOCs are oxidised to low-volatility SOA precursors (E5.1; Section 5.2.1). In response to climate change, the global-mean annual-mean surface concentrations of OH, NO_3 and O_3 change by +12, +11, and -10 %, respectively (not shown). Surface and zonal-mean decadal-mean annual-mean concentrations of the hydroxyl (OH) and nitrate (NO_3) radicals, and ozone (O_3) for the simulations in Table 5 are shown in Figures 5.7 and 5.8, respectively. Future increases in OH (Figure 5.7 b and Figure 5.8 b) are likely due to an increase in surface water vapour (+29 %), which drives a 30 % increase in the reaction between water vapour and excited singlet oxygen, $O(^1D)$, to produce OH (R1.1-1.3, Chapter 1), as well as increases in NO_2 (discussed below). Future increases in NO_3 (Figure 5.7 f and Figure 5.8 f) may be explained in terms of increased lightning-NO_x emissions (+46 %) but also by enhanced peroxyacetylnitrate decomposition (e.g. Doherty et al. 2013). Note, the formation of OH from HO_2 is often NO_X-limited, hence, these climate-induced increases in NO_x can reinforce the aforementioned

increases in OH due to enhanced H_2O+ $O(^1D)$ (R1.1-1.3). The response of O_3 to climate change is a combination of enhanced H_2O+ $O(^1D)$, which is a sink for O_3, and the aforementioned increases in NO_x. Considering the coarse resolution of the model used here, NO_X can be regarded as a source of O_3. Furthermore, the Brewer-Dobson circulation, which is responsible for the poleward transport of tropical stratospheric ozone, weakens under climate change; therefore, under climate change at higher altitudes (6 – 10 km), ozone concentrations increase in the tropics but decrease at the poles (Figure 5.8 j). Note, whereas tropospheric ozone is modelled, stratospheric ozone is prescribed, and held fixed for all model integrations in this study. Hence, future stratospheric ozone recovery is not accounted for in this study.

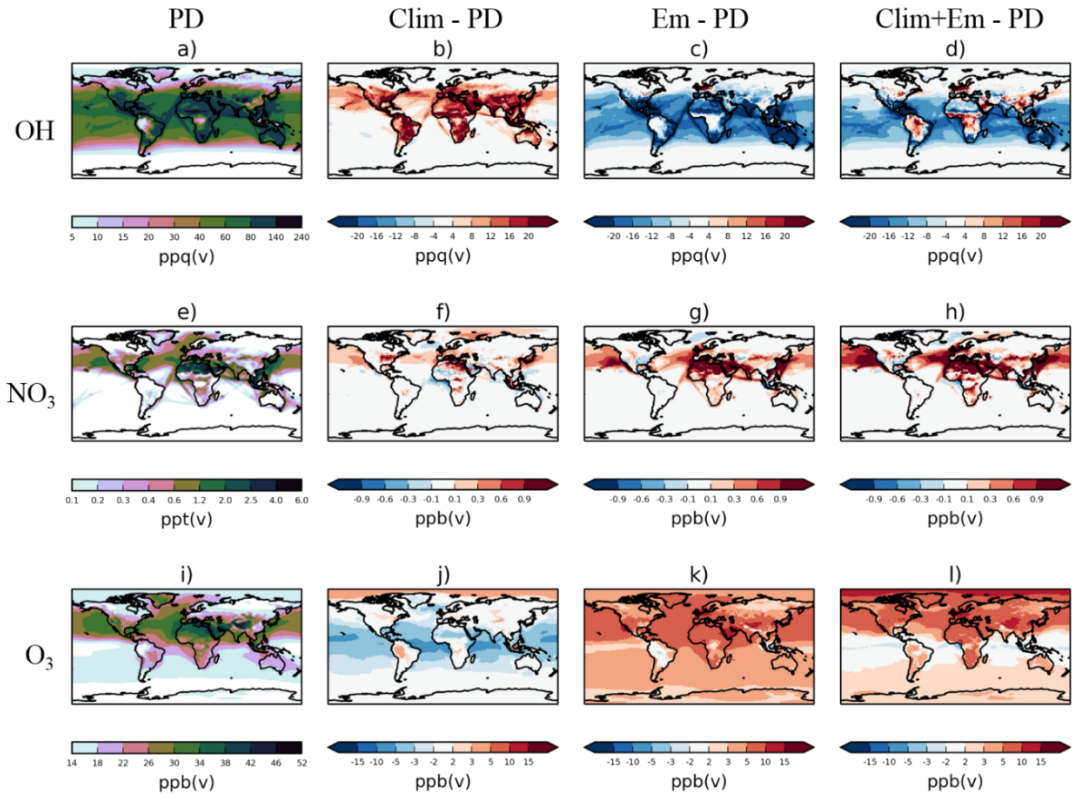

Figure 5.7 – Present-day (1996-2005) and future (2091-2100) decadal mean annual-mean surface concentrations of OH (top row; a – d), NO_3 (middle row; e – h), and O_3 (bottom row; i - l). Oxidants for the present-day (PD) are displayed in first column (a, e and i). Oxidants for the future climate simulation (Clim) are shown in the second column (b, f and j), for the future anthropogenic and biomass burning emissions simulation (Em) are shown in the third column (c, g and k), and for the future climate and emissions combined simulation (Clim+Em) are shown in the fourth column (d, h and l), all relative to the present-day (PD).

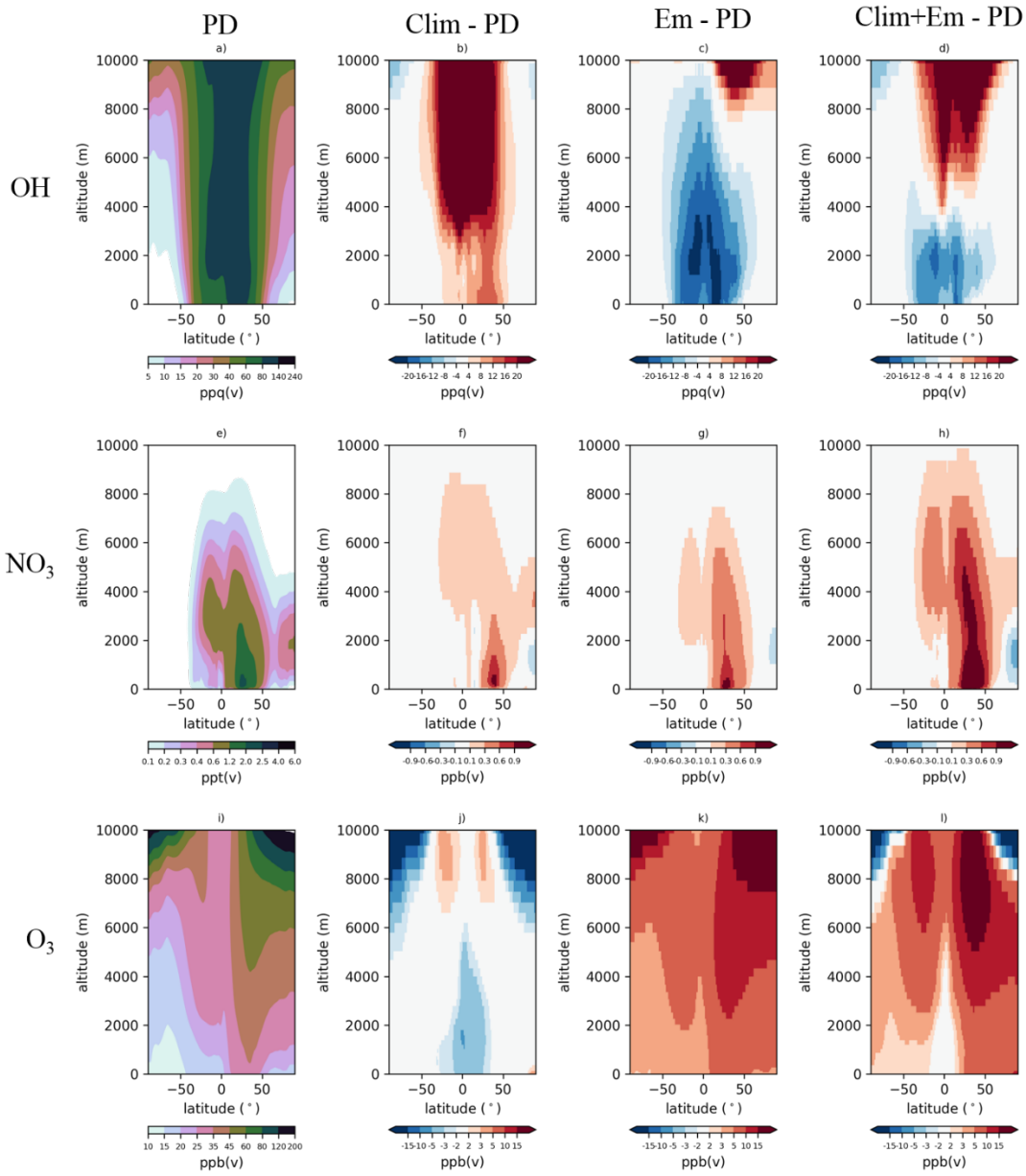

Figure 5.8 - Present-day (1996-2005) and future (2091-2100) decadal mean annual-mean zonal concentrations of OH (top row; a – d), NO_3 (middle row; e – h), and O_3 (bottom row; i - l). Oxidants for the present-day (PD) are displayed in first column (a, e and i). Oxidants for the future climate simulation (Clim) are shown in the second column (b, f and j), for the future anthropogenic and biomass burning emissions simulation (Em) are shown in the third column (c, g and k), and for the future climate and emissions combined simulation (Clim+Em) are shown in the fourth column (d, h and l), all relative to the present-day (PD).

All VOC precursors of SOA are assumed to be emitted at the surface (even biomass burning sources). These surface emissions combine with a high oxidant availability, leading to the majority (88 %) of emitted VOCs being oxidised within the lowermost 2 km of the atmosphere. Therefore, future changes in oxidants at the surface (Figure 5.7) are more relevant for understanding how climate change influences SOA production, as opposed to changes in oxidants at higher altitudes (Figure 5.8). In addition, only terrestrial VOC emissions are considered in this study. Hence, future changes in oxidants over land are more relevant than over the ocean for understanding how climate change influences the efficiency of VOC oxidation (and SOA production). Over land, oxidants generally increase under climate change (Figure 5.7), and therefore contribute to more efficient VOC oxidation within the emission source regions.This effect is most evident for SOA production from $VOC_{ANT/BB}$. The climate-induced increases in OH concentrations over land results in in more efficient $VOC_{ANT/BB}$ oxidation over North America, Europe, India and China, but less efficient oxidation downwind of these regions (e.g. over the oceans) (not shown). Globally, however, there is no change in the SOA production rate from $VOC_{ANT/BB}$ (Figure 5.2 b), which implies that SOA production from $VOC_{ANT/BB}$ is VOC limited, as opposed to oxidant limited (i.e. SOA production is controlled by changes in VOCs, not oxidants). Also, these climate-increases in oxidant concentrations (Figure 5.7 b, f and j) will contribute to increases in SOA production from biogenic VOCs (Figure 5.2 b). Overall, climate change increases oxidant concentrations, leading to more efficient SOA production within emissions source regions.

5.4.3 Climate change impacts on temperature-dependent reaction rates of SOA precursors and oxidants

The reaction rate of VOCs and oxidants is temperature dependent. Hence, global warming can affect the speed at which SOA is formed. Within the UKCA model, reaction rates are solved following the Arrhenius equation. Molecular collisions are favoured by elevated temperatures. Changes in temperature also affect the chance of reaction upon collision, with elevated temperatures favouring exothermic reactions. In response to an increase in temperature of 5 K (close to the global-mean temperature change; section 5.4.1), the reaction rates for the SOA precursors considered in this study (Table 1) vary by -1 % (monoterpene+NO_3) to 9 % (isoprene+ O_3). These changes in reaction rates are relatively small and will therefore have very little effect on SOA formation.

5.4.4 Climate change impacts on the efficiency of SOA deposition

Climate change affects the efficiency of SOA removal (i.e. the SOA lifetime). In the UKCA model, as SOA is assumed to be hydrophilic and non-volatile, it is removed by both dry and we deposition. The SOA lifetime is therefore a reflection of SOA deposition efficiency. In the present-day, the global annual-average SOA lifetime is 4.4 days (Table 5.6). This value increases by 12 % under future climate change, to 4.9 days (Table 5.6). Hence, climate change reduces the efficiency of SOA deposition. This future increases in the SOA lifetime could be due to either (i) changes in regional (including altitudinal) SOA production, (ii) changes in regional precipitation, or (iii) both of these effects.

Figure 5.9 shows vertically integrated precipitation rates from HadGEM3 for the present-day and differences in the future climate relative to the present-day. Precipitation varies both horizontally (Figure 5.9 a) and vertically (not shown). This creates spatial gradients in the SOA lifetime with respect to wet removal. For instance, the SOA lifetime is longest in regions of low precipitation, such as the poles (Figure 5.9 a) and at higher altitudes. Short SOA lifetimes are expected in regions with high precipitation, such as the tropics (Figure 5.9 a) and at the surface. Isoprene emission rates are so high that this species is not fully oxidised at the surface (Henze and Seinfeld, 2006). Consequently, the lifetime of SOA from isoprene (9 days) is longer than the lifetime of SOA from monoterpene (7 days), as monoterpene produces SOA mainly at lower altitudes where it undergoes wet removal more efficiently (Heald et al., 2008). The significance of this horizontal and vertical variability in SOA lifetime is that any changes in where SOA is being produced can alter the SOA lifetime. In the future, regional changes in biogenic VOC emissions (Section 5.5.1) and oxidants (Section 5.5.2) have the potential to alter regional SOA production rates, which, in turn, can affect the SOA lifetime.

In addition to regional changes in SOA production, regional changes in precipitation itself can also affect the SOA lifetime. Whilst, the global-mean annual-mean precipitation rate increases by 7 % in the future, regionally, changes in precipitation vary in both magnitude and sign (Figure 5.9 b). Projections of precipitation under climate change are somewhat uncertain. Nevertheless, the simulated regional changes in precipitation here (Figure 5.9 b) are in reasonable agreement with the multi-model mean of Collins et al. (2014) and HadGEM2 results in Allen et al (2016). Under climate change, precipitation rates decrease over Peru, Northern Brazil, Southeast USA, Europe and the outflow region of sub-Saharan Africa (Figure 5.9 b), contributing to a lengthening of the global-mean annual-mean SOA lifetime through reduced wet deposition efficiency. However, over central Africa,

India, China, the Bay of Bengal and the Arabian Sea, precipitation increases under climate change (Figure 5.9 b), contributing to a shorter SOA lifetime in the future due to greater wet deposition efficiency.

Here, the exact cause for the lengthening of the SOA lifetime is unknown, yet this feature is identified in other global modelling studies. For example, Lin et al. (2016) find a 6 % increase in the global SOA lifetime in response to climate change under RCP8.5. Similarly, finding a lengthening of the lifetime for several different aerosol components, Allen et al. (2016) attribute this to a reduced wet deposition efficiency of aerosol associated with large scale precipitation over the NH mid-latitudes. Therefore, an increase in the aerosol lifetime appears to be a consistent feature of RCP8.5.

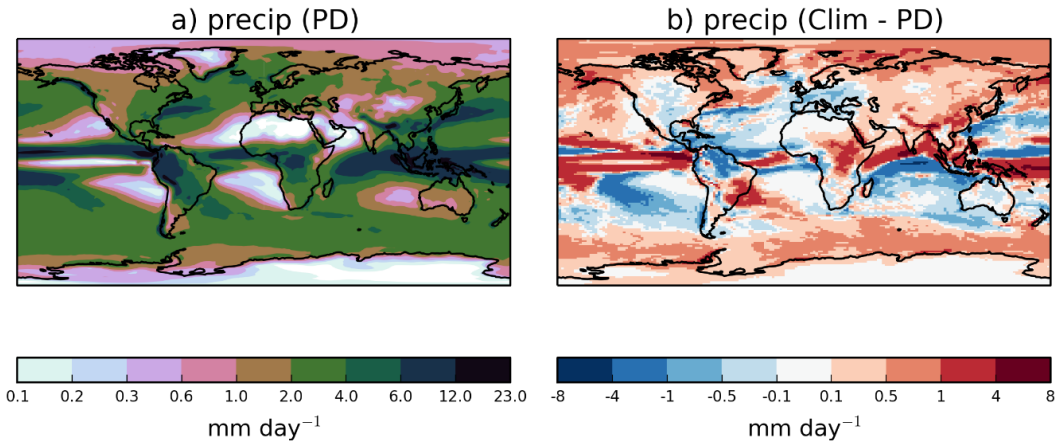

Figure 5.9 – Precipitation for the present-day (PD; 1996-2005) and future climate (Clim; 2091-2100) simulations.

5.4.5 **Discussion of climate change impacts on SOA lifecycle**

Overall, climate change alone results in a 23 % increase in the global SOA burden under RCP8.5 by the 2090s relative to the 2000s. This increase in

the SOA burden is due to the combined effects of a 10 % increase in the global annual-total SOA production rate and a 12 % increase in the SOA lifetime. The increase in the SOA production rate appears to be driven by a 79 % increase in global annual-total monoterpene emissions. This climate-induced increase in the SOA burden and its attribution to biogenic VOC emissions change is in reasonable agreement with all previous studies. Under SRES A2, Liao et al. (2006a) find a 9 % increase in the global SOA burden by 2100 due to a 38 % increase in biogenic emissions of monoterpene and Other Reactive Volatile Organic Compounds (ORVOCs). Heald et al. (2008) isolate the sensitivity of SOA to climate-sensitive biogenic emissions alone under SRES A2, finding a 22 % increase in the global SOA burden in response to increases in global annual-total emissions of monoterpene and isoprene of 19 and 22 %, respectively. In addition, previous studies also suggest future changes in wet deposition to impact the SOA or other aerosols components lifetime (Lin et al. 2012; Allen et al. 2016)

5.5 Future anthropogenic and biomass burning emissions impacts on SOA lifecycle

In this section, the sensitivity of the SOA lifecycle to future changes in anthropogenic and biomass burning emissions (fixed climate) is quantified (Em – PD). With future emission changes, over many continental emission source regions, notably North America, Central Brazil, Europe, Japan, East and Southeast Asia, annual-mean surface SOA concentrations reduce by 0.3 to 1.0 μg m^3 compared to the present-day (Figure 5.1 c) – this corresponds to reductions ranging between 10 and 100 % (Figure 1 f). In contrast, annual-mean surface SOA concentrations increase by more than 1.5 μg m^{-3} (or 30 – 60 %) over large parts of Africa, India, and Central America (Figure 5.1 c and f).

Under RCP8.5, the global annual-average SOA burden reduces by 3 % by the 2090s compared to the present-day (Table 5.6). This is due a decrease in the global annual-total SOA production rate (6 %) and an increase in the SOA lifetime (4 %) (Table 5.6). The reduced SOA production rate is attributable to lower SOA production from $VOC_{ANT/BB}$+OH (3.9 Tg (SOA) a^{-1}; 11 %) under future emissions (Figure 5.2 c). Note that SOA production from biogenic VOCs is also slightly influenced by future changes in anthropogenic and biomass burning emissions despite the biogenic emissions remaining constant (Figure 5.2 c). The mechanisms by which future changes in anthropogenic and biomass burning emissions control the SOA lifecycle are examined in the following sub-sections. These include projected changes in aerosol and precursor emissions (Section 5.5.1), the impact of these emissions on oxidants (Section 5.5.2), and future changes in the SOA lifetime (Section 5.5.3). These results are then summarised and compared to the literature (Section 5.5.4).

5.5.1 **Projected changes in aerosol and aerosol precursor emissions**

As mentioned previously (Section 5.1), anthropogenic and biomass burning activities releases direct SOA precursors (VOCs and S/IVOCs), and other aerosol/aerosol precursors which affect SOA gas-to-particle partitioning and aqueous phase reactions. In the UKCA model, $VOC_{ANT/BB}$ is the SOA precursor released from anthropogenic and biomass burning activities. Emissions of $VOC_{ANT/BB}$ are projected to reduce by 11 %, from 176 Tg (VOC) a^{-1} in the present-day to 126 Tg (VOC) a^{-1} in the 2090s under RCP 8.5 (Table 5.4). This explains the 3.9 Tg (SOA) a^{-1} (11 %) reduction in SOA production from this source (Figure 5.2 c). Figure 5.10 shows the spatial pattern of annual-total $VOC_{ANT/BB}$ emissions for the present-day and the change in the

future relative to the present-day. Annual-total $VOC_{ANT/BB}$ emissions reduce by more than 5 g (VOC) m^{-2} a^{-1} over the major industrialised source regions of North America, Europe and East/Southeast Asia in the future (Figure 5.10 b). In contrast, over India and parts of Africa, $VOC_{ANT/BB}$ emissions are projected to increase by more than 5 g (VOC) m^{-2} a^{-1} (Figure 5.10 b). These projected regional changes in $VOC_{ANT/BB}$ emissions (Figure 5.10 b) also dictate regional changes in SOA concentrations (Figure 5.1 f). Hence, both globally and regionally, changes in $VOC_{ANT/BB}$ emissions appear to control the response of SOA to future emissions changes.

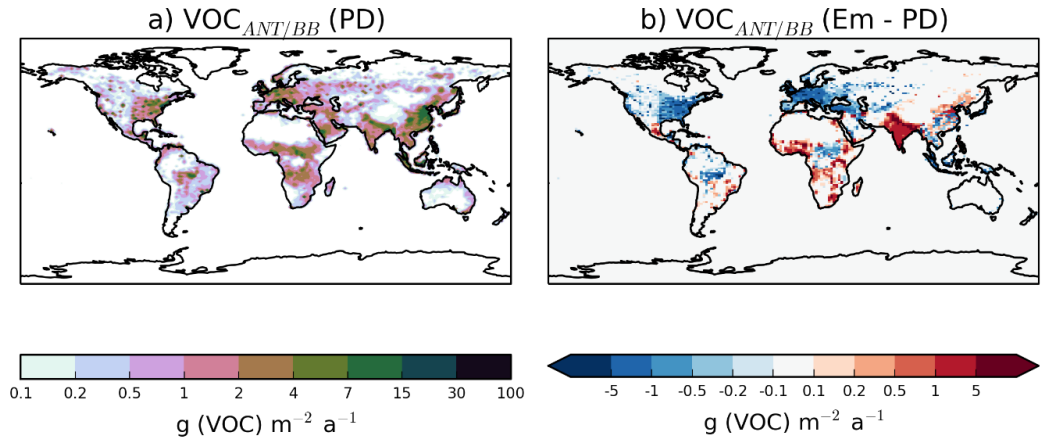

Figure 5.10 – Prescribed $VOC_{ANT/BB}$ emissions (g (VOC) m^{-2} s^{-1}) for the present-day (1996-2005) and future emissions (2091-2100). For VOC_{ANT}, aromatic emissions are used to first define a spatial and seasonal pattern, which are then scaled to equal total VOC emission estimates (Section 2.3). For VOC_{BB}, an emission factor is applied to biomass burning CO emissions (Section 2.3).

In addition to VOCs, other aerosol precursors (e.g. SO_2) and aerosol (e.g. POA and BC) are also projected to change under RPC8.5. Global annual-total SO_2, POA and BC emissions from anthropogenic and biomass burning activities are all projected to reduce in the 2090s under RCP8.5, by 76, 33 and 46 %, respectively. However, these emission changes have little or no impact on SOA production here since in this study, non-volatile

hydrocarbon oxidation products (SOG; Section 5.2.1) condense irrespective of pre-existing aerosol surface area. However, in other studies where SOA is treated as semi-volatile, hydrocarbons are in dynamic equilibrium between the gas and aerosol phases, with partitioning rates dependent on a number of factors, including pre-existing aerosol surface area and temperature. This creates a dependency of SOA production on SO_2 and POA concentrations (Liao et al., 2006b). In addition, the reduction in sulphate emissions implies a reduction in aqueous phase SOA production (Lin et al., 2016); however, this SOA formation pathway is not treated in this study.

5.5.2 **Future anthropogenic and biomass burning emissions impacts on oxidants**

The oxidising capacity of the atmosphere is also affected by changes in anthropogenic and biomass burning emissions (Figure 5.7 and Figure 5.8). Projected changes in anthropogenic and biomass burning emissions cause the global-mean annual-mean surface concentrations of OH, O_3, and NO_3 to change by -21, +27, and+23 %, respectively (not shown). The CH_4 concentration is projected to double by the 2090s under RCP8.5 (Table 5.4), which drives a 114 % increase in the reaction flux between CH_4 and OH. Figure 11 shows the spatial distributions of CO and NO_X for the 2000s and for the 2090s under RCP8.5. Similar to CH_4, CO is a sink for OH and a source of O_3. Global CO emissions reduce by 35 % by the 2090s under RCP8.5 (Table 5.4). Over North America, Europe and Southeast Asia, CO emissions decrease (Figure 5.11 c). These reductions in CO emissions therefore buffer the effect of the worldwide increase in CH_4 concentrations on OH levels. This is particularly evident for parts of Europe. In this region, the effects of increased CH_4 on OH concentrations are entirely offset by reductions in CO, leading to increased OH concentrations (Figure 5.7 c). In

contrast, anthropogenic and biomass burning CO emissions are projected to rise over India (Figure 5.11 c). Therefore, in this region, increased CH_4 concentrations, augmented by increased CO emissions, result in large reductions in surface OH concentrations under future emissions in 2100 (Figure 5.7 c). Overall, projected changes in anthropogenic and biomass burning emissions under RCP8.5 result in a 21 % reduction in surface OH concentrations. NO_X emissions are also projected to change in the future, with largely similar distribution changes to that of CO emissions i.e. reductions over North America, Europe and South East China, but increases over India and parts of Africa (Figure 5.11 d). Hence, in terms of their impact on O_3, these changes in NO_X exacerbate the changes in CO. Overall, O_3 increases by 23 % in the future emissions simulations (Figure 5.7 k) – this is primarily driven by the CH_4 increase as noted in previous studies (e.g. Wild et al., 2012; Fiore et al., 2012). NO_X plays a crucial role in the production of OH from HO_2, therefore, these changes in NO_X (Figure 5.11 e) may also affect the production of OH.

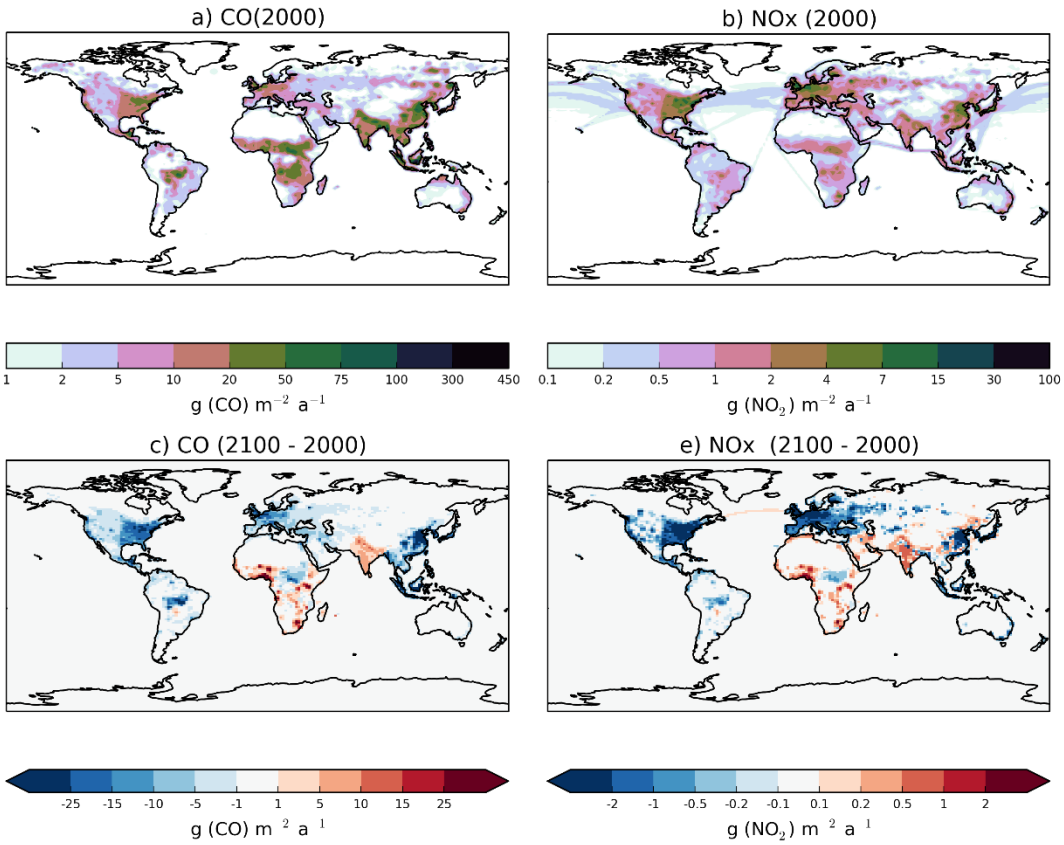

Figure 5.11 – Spatial distribution of multi-annual annual-total emissions of CO (a and c) and NO_X (b and e) for the present-day (a and b) and differences in emissions in the future relative to the present-day (c and e). For anthropogenic and biomass burning emissions of both these species, present day (1999-2005) emissions are taken from Lamarque et al. (2010) and future emissions (2091-2100) follow Riahi et al. (2011). Natural sources of CO and NO_X, from oceans and soil, respectively, are held constant at present-day values. Note, lightning-NO_X emissions are not included in this figure.

The NO_3 radical is also strongly influenced by projected changes in anthropogenic and biomass burning emissions; however, the mechanism for this change is less clear. Global annual-total NO_X emissions reduce by 27 % in the future, yet global-mean annual-mean surface NO_3 concentrations increase by 41 % under the future emissions scenario. The NO_3 radical is a night-time species, with formation being controlled through complex oxidant chemistry.

These changes in oxidant concentrations partially explain the changes in SOA production and distributions. For instance, over North America and Europe, lower $VOC_{ANT/BB}$ (Figure 5.10 b) emissions are compounded by lower OH concentrations (Figure 5.7 c), leading to substantial reductions in SOA concentrations (Figure 5.2 c). Furthermore, these changes in oxidant concentrations also explain why biogenic SOA production is affected by changes in anthropogenic and biomass burning emissions. As a consequence of reduced OH concentrations (11 %) and increased O_3 concentrations (23%), biogenic SOA production decreases via the OH pathway, but increases via the O_3 pathway (Figure 5.2 c). However, in terms of overall biogenic SOA production, these changes across the various oxidation channels have cancelling and, hence, small effects both on a global scale (Figure 5.2 c) and a regional scale (not shown). Therefore, the relative insensitivity of global SOA production from biogenic VOCs to changes in oxidants implies that SOA production from this source is VOC limited, as opposed to oxidant limited.

5.5.3 **Future anthropogenic and biomass burning emissions impacts on the efficiency of SOA deposition**

With future anthropogenic and biomass burning emissions, the global-mean annual-mean SOA lifetime is 4 % higher compared to the present-day (Table 5.6). As the climate in these two simulations is identical, this change in SOA lifetime must be due to regional changes in SOA production. Precipitation varies horizontally (Figure 5.9 a) and vertically (not shown), therefore creating gradients in wet deposition efficiency (i.e. the SOA lifetime). Reductions of $VOC_{ANT/BB}$ emissions (Figure 5.10 b) in high precipitation regions, such as Southeast Asia and the Amazon (Figure 5.9 a) may contribute to the longer global-mean SOA lifetime. In addition, if change in

$VOC_{ANT/BB}$ emissions or oxidants alter the vertical profile of SOA, the lifetime can also be affected. Overall, future changes in anthropogenic and biomass burning emissions reduce the efficiency of SOA deposition (i.e. lengthening the SOA lifetime), therefore contributing towards an increase in the SOA burden.

5.5.4 Discussion of future anthropogenic and biomass burning emissions impacts on SOA lifecycle

Under future anthropogenic and biomass burning emissions for the 2090s for RCP8.5, the global annual-mean SOA burden is 3 % lower than in the present-day (Table 5.6). This projected reduction in the SOA load is due to a reduced global annual-total SOA production rate (-6 %) and tempered somewhat by an increase in the global annual-mean SOA lifetime (4 %) compared to the present-day (Table 5.6). The reduced global SOA production is driven by an 11 % reduction in $VOC_{ANT/BB}$ emissions (Table 5.4).

The changes in SOA spatial distributions in response to projected changes in anthropogenic and biomass burning emissions here are in broad agreement with other studies; SOA decreases over Europe and North America but increases over India and Africa (Tsigaridis and Kanakidou, 2007;Heald et al., 2008;Lin et al., 2016). For these regions, future changes in SOA appear to be dictated by projected change in anthropogenic and biomass burning precursor emissions, similar to this study. However, in contrast to this study, where SOA is assumed to be non-volatile, previous studies of the impacts of emissions changes on SOA treat SOA as semi-volatile. Under the semi-volatile treatment of SOA, condensation and evaporation of hydrocarbons between the gas and aerosol phases also depends on pre-existing aerosol surface. Hence, projected changes in

primary emissions also affect SOA condensation. For example, Liao et al. (2006b) do not consider any anthropogenic or biomass VOCs in SOA formation, yet projected increases in POA emissions of 84 % drive an increase in the global SOA burden of 31 % (which is entirely biogenic). Some studies also project increases in both aromatic and POA emissions under future IPCC emissions scenarios. Consequently, these studies project an increase in SOA production of 10 (Heald et al., 2008) to 50 % (Tsigaridis and Kanakidou, 2007), similar to and larger than in our study, respectively. Under RCP8.5, anthropogenic and biomass burning emissions of sulphate are projected to reduce by more than a factor of 4 by the year 2100, leading to 24 % reduction in aqueous phase SOA production (Lin et al., 2016). These effects are not considered in this study.

5.6 Combined effects of future changes in climate and emissions on SOA lifecycle

In this section, the combined effects of changes in climate and emissions on the SOA lifecycle are quantified (Clim+Em - PD). Regionally, the effects of changes in climate and emissions on SOA concentrations are primarily dictated by changes in climate sensitive biogenic emissions as well as anthropogenic and biomass burning VOC emissions. In the USA, Europe, Japan, and South East Asia, annual-mean surface SOA concentrations reduce by 0.3 – 1 μg m^{-3} (Figure 5.1 d), or 10 – 60 % (Figure 5.1 g). In these regions, the impact of $VOC_{ANT/BB}$ emissions reductions (Figure 5.1 c) outweigh the effects of increased biogenic VOC emissions (Figure 5.1 b) such that SOA concentrations decrease (Figure 5.1 d). In contrast, over Siberia, northern Canada, Australia and Peru, the impacts of future reductions in anthropogenic and biomass burning emissions (Figure 5.1 c) are outweighed by increases in biogenic emissions (Figure 5.1 b) leading to

increases in SOA concentrations (Figure 5.1 d). In India and South Africa, future changes in both emissions and climate contribute to elevated SOA levels (Figure 5.1 b - d). Hence, in these regions, projected increases in anthropogenic and biomass burning VOC emissions together with elevated biogenic VOC emissions, lead to decadal-mean annual-mean SOA concentration increases which exceed 1.5 μg m^{-3} (Figure 5.1 d), corresponding to increases of up to 100 % (Figure 5.1 g).

The global SOA budget and the relative importance of various VOC emissions sources to SOA production are both projected to change in the future. The global annual-mean SOA burden is 20 % higher under future climate and emissions following RCP8.5 compared to present-day (Table 5.6). This is due to increases in both the global annual-total SOA production rate (4 %) and the global annual-mean SOA lifetime (15 %) (Table 5.6). The projected 4 % increase in the production rate is due to the effects of projected changes in climate and emissions, which independently change the global annual-total SOA production rate by 10 and -6 %, respectively (Table 5.6), as described in Sections 5.5 and 5.6. In the present-day, the global annual-total SOA production rate is 60.6 Tg (SOA) a^{-1}, with biogenic VOCs accounting for 42 % (25.5 Tg (SOA) a^{-1}) and $VOC_{ANT/BB}$ accounting for the remaining 58 % (35.1 Tg (SOA) a^{-1}) (Section 5.3). This split between natural and anthropogenic sources is altered by future changes in climate and emissions, which increase the monoterpene SOA production rate by 6.5 Tg (SOA) a^{-1} and reduce the anthropogenic and biomass burning SOA production rate by 3.9 Tg (SOA) a^{-1} (Figure 5.2 d) compared to present-day. Therefore, under future climate and emissions, the global annual-total SOA production rate from all sources is higher (63.1 Tg (SOA) a^{-1}) and biogenic VOCs accounting for 50.5 % (31.9 Tg (SOA) a^{-1}), and $VOC_{ANT/BB}$ account for 49.5 % (31.2 Tg (SOA) a^{-1}). These results therefore suggest a growing importance of natural sources of SOA in the future. In addition, from a global air quality perspective of the SOA burden, even stronger anthropogenic

emissions reductions are required in order to counter the effects of projected increases in monoterpene emissions and attain the same air quality standards as at the present-day.

Despite these significant changes to the global SOA burden, the seasonal cycle in precursor emissions and SOA production is fairly similar for both the present-day and under future emissions and climate (Figure 5.3). Also, the NH accounts for ~65 % of global annual-total SOA production in both the present-day and future. This suggests that the seasonal cycle, and the split between hemispheres is relatively stable between the present-day and the future under future changes in emissions and climate.

The combined effects of changes in climate and emissions on oxidant concentrations depends on the species being considered. For NO_3, global-mean annual-mean surface concentrations increase (Figure 5.7 h) by 60 % due to the combined effects of projected changes in climate and emissions which independently increase NO_3 concentrations (Figure 5.7 f, g) by 11 % and 41 % respectively. Future changes in OH and O_3 concentrations appear to be driven by projected changes in emissions, but tempered somewhat by the effects of climate change. For example, for O_3, compared to present-day, global-mean annual-mean surface concentrations increase (Figure 5.7 l) by 15 %, which is primarily driven by projected changes in emissions (Figure 5.7 k). For the OH radical, global-mean annual-mean surface concentrations reduce (Figure 5.7 d) by 14 % under future climate and emissions compared to the present-day. In summary, future changes in climate and emissions lead to enhanced NO_3 and O_3 surface concentrations, but reduced OH surface concentrations.

In the present-day, 83 % (50.2 Tg(SOA) a^{-1}; Figure 5.2 a) of SOA is formed via the OH channel. This preferences for the OH channel is a reflection of the OH reactivity and the assumption that $VOC_{ANT/BB}$ reacts solely with this oxidant (whereas monoterpene and isoprene react with all

three oxidants). Figure 5.2 d demonstrates how the relative importance of each oxidant is affected by future changes in climate and emissions. Under future changes in climate and emissions, OH accounts for 77 % (48.7 Tg (SOA) a^{-1}) of the global annual-total SOA production from all sources, compared to 83% for present-day. Therefore, the importance of OH as an oxidant for SOA precursors reduces slightly in the future, but remains the principal oxidant. The reduced importance of OH in the future stems from (i) reduced $VOC_{ANT/BB}$ emissions (Figure 9 b), (ii) reduced OH concentrations (Figure 5.7 d), and (iii) increased concentrations of O_3 and NO_3 (Figure 5.7 h and l). However, as noted in section 5.5.2 and 5.6.2, changes in oxidant concentrations affect the regional distribution of SOA, but have only a minor impact on the global SOA production rate.

Compared to the 2000s, by the 2090s under both changes in climate and emissions, the global annual-average SOA burden increases (+20 %) due to increases in both the production rate (+4 %) and the lifetime (+15 %). Here, climate impacts lead to enhanced SOA burden via increased biogenic monoterpene emissions (+79 %) and a lengthening of the SOA lifetime (+23 %). Projected changes in anthropogenic and biomass burning emissions under RCP8.5 generally counter these climate impacts on SOA, but are not large enough to outweigh them. Global annual-total $VOC_{ANT/BB}$ emissions reduce by 11 %, with strong reductions over North America, Europe, and Eat/Southeast Asia but increases over parts of India and Africa.

Earlier studies suggest substantially larger increases in the SOA burden in the future, ranging from +36 to +146 % (Liao et al., 2006b;Tsigaridis and Kanakidou, 2007;Heald et al., 2008). However, these studies use older IPCC emissions projections, where anthropogenic and biomass burning emissions are projected to increase in the future. Furthermore, these earlier studies do not account for CO_2 inhibition on biogenic emissions. Under the same scenario used in this study (RCP8.5), Lin et al. (2016) project a much smaller increase (+ 2 %) in the SOA burden

in the future – crucially, anthropogenic and biomass burning emissions of SOA precursors (aromatics) and SO_2 reduce, and changes in anthropogenic land use are also accounted. Consequently, Lin et al. (2016) find a 12 % decrease in the global SOA production, but this is countered by a lengthening of the SOA lifetime (15 %), thus, explaining the projected rise in the SOA burden. Therefore, the projected increase in the global SOA burden found in this study (+20 %) is larger than that of Lin et al. (2106) but generally smaller than that of earlier studies (+36 to +146 %).

5.7 Conclusions

The SOA lifecycle is initiated by the emissions of VOCs from biogenic, anthropogenic and biomass burning sources. VOCs oxidise to form non-volatile products, which condense, forming SOA. SOA is removed from the atmosphere by both dry and wet deposition. As SOA can perturb the Earth's radiation balance through aerosol-radiation and aerosol-cloud interactions, projected changes in SOA may alter future aerosol forcings as well as air quality. Under the Representative Concentration Pathway (RCP) 8.5, this study quantifies how the SOA lifecycle is influenced by future changes in climate and emissions alone, and their combined effects, from all major VOC source types and with fixed vegetation. In the present-day, anthropogenic and biomass burning VOCs contribute 58 % (35 Tg (SOA) a^{-1}) to the SOA production rate from all sources (60.6 Tg (SOA) a^{-1}), with biogenic VOCs accounting for 42 % (25.1 Tg (SOA) a^{-1}).

Under climate change alone, the global annual-mean SOA burden is 23 % higher in the future compared to the present-day. This projected increase in the global SOA burden is a result of increases in both the global annual-total SOA production rate (10 %) and the global-mean annual-mean

SOA lifetime (12 %). The climate-driven increase in SOA production is primarily due to changes in biogenic monoterpene VOC emissions. Under climate change, global annual-total biogenic emissions of monoterpene and isoprene change by +79 and -1 %, respectively. Emissions of both monoterpene and isoprene are stimulated by future warming of the atmosphere but the latter are also suppressed by the projected rise in CO_2 concentrations. Therefore, the climate-driven increase in global SOA production is attributable to the global increase in monoterpene emissions as opposed to isoprene emissions. Regionally, both biogenic VOCs are responsible for regional changes in SOA concentrations under climate change. However, climate-induced changes in monoterpene emissions are relatively small in magnitude and spatially homogenous – increases in annual-total monoterpene emission range 0.2 – 1 g (C) m^{-2} s^{-1}. In contrast, the response of regional isoprene emissions to changes in climate are large and vary in both magnitude and sign (-5 to +5 g (C) m^{-2} s^{-1}). Together, these regional changes in biogenic VOC emissions drive the regional changes in SOA distributions under climate change.

The sensitivity of SOA to projected changes in anthropogenic and biomass burning emissions under RCP8.5 is independently quantified. Compared to the present-day, the global annual-mean SOA burden is 3 % lower in the future due to projected changes in anthropogenic and biomass burning emissions under this pathway. This reduction in the global SOA load is driven by a 6 % reduction in the global annual-total SOA production rate and modulated slightly by a 4 % increase in the global-mean annual-mean SOA lifetime. The decrease (6 %) in SOA production is a result of an 11 % reduction in anthropogenic and biomass burning VOC ($VOC_{ANT/BB}$) emissions by 2100 under RCP8.5. The projected changes in $VOC_{ANT/BB}$ emissions drive changes in regional SOA concentrations. Reductions in anthropogenic and biomass burning VOC emissions over North America, Europe and South East Asia lead to reductions in SOA concentrations in these same regions.

Increased anthropogenic and biomass burning VOC emissions over India and parts of Africa lead to increases in SOA concentrations in these same regions. Biogenic VOC emissions are also modified which impact SOA production rates slightly as a result of the changes in oxidant levels with reduced anthropogenic and biomass burning emissions.

Finally, the combined effects of future changes in climate and emissions on the SOA lifecycle is quantified. Compared to the present-day, the global annual-mean SOA load rises by 20 % in the 2090s under RCP8.5. This increase in the global SOA burden is in response to a 4 % increase in the global annual-total SOA production rate, combined with a lengthening of the global-mean annual-mean SOA lifetime (15 %). The simultaneous increase in monoterpene emissions (79 %) and reduction in anthropogenic and biomass burning VOC emissions (11 %) implies an increasing role for natural aerosol sources to influence SOA production in the future; biogenic VOCs account for 50.5 % (31.9 Tg (SOA) a^{-1}) and $VOC_{ANT/BB}$ accounts for 49.5 % (31.2 Tg (SOA) a^{-1}) of the global annual-total SOA production rate in the future (63.1 Tg (SOA) a^{-1}). From a global perspective of the SOA burden, anthropogenic and biomass burning emissions reductions under RCP8.5 are not large enough to counter the impacts of (i) the projected rise in biogenic emissions, and (ii) the increase in the SOA lifetime. Under future emissions and climate in the 2090s, the largest increases in SOA concentrations are projected over India and parts of southern Africa. In these regions, future changes in climate (via increases in biogenic emissions) and emissions (via increases in $VOC_{ANT/BB}$ emissions), lead to increases in annual-mean SOA concentrations which exceed 1.5 μg m^{-3}. For most regions, where anthropogenic and biomass burning VOC emissions decrease under RCP 8.5, these reductions are slightly compensated for by increased biogenic VOC emissions. For example, over North America, Europe and Southeast Asia, the overall effect of changes in climate and emissions is a reduction in annual-mean SOA concentrations of around 1 μg m^{-3}.

There are a number of uncertainties in this study. Monoterpene emissions are impacted by meteorological variables (e.g. temperature, light, etc.) but not CO_2 inhibition as this relationship is not well quantified. Hence, further research in this area is needed to understand how increasing atmospheric CO_2 concentrations influence monoterpene emissions across the globe. Other studies have included future vegetation changes due to land cover and anthropogenic land use change but these are uncertain and are not included here. In addition, the yields for all the VOC sources considered are assumed to be identical (13 %) and are fixed, irrespective of NO_X concentrations, humidity, acidity (Chapter 4). Other sources of SOA, such as S/IVOC emissions, and aqueous phase production of SOA are not included in this study.

Several previous studies quantify how the SOA lifecycle will change in the future. However, these studies either assume SOA is purely biogenic, or only include the aromatic component of anthropogenic and biomass burning VOCs. For the first time, this study quantifies how future changes in climate and emissions affect the SOA lifecycle, whilst accounting for all major VOC source types and including the effects of CO_2 inhibition on isoprene emissions. This study demonstrates how climate impacts on natural biogenic VOC emissions and the efficiency of SOA deposition drive a 20 % increase in the global annual-average SOA burden and highlights an increasing role of natural sources of aerosols in the future.

Chapter 6 **Conclusions**

6.1 Introduction

In this section, the concluding remarks, limitations and future work of this thesis are discussed. Before doing so, a brief summary of the research questions and motivation of this thesis is made.

Secondary organic aerosol (SOA) is formed within the atmosphere after gaseous organic compounds have undergone a range of complex physical and chemical processing. Gaseous organic compounds are emitted from a variety of different source types, including both natural and anthropogenic. These emissions span a wide range of volatilities, from non-volatile (i.e. species remain exclusively in the aerosol phase) to volatile (i.e. species remain exclusively in the gas phase). Here, the SOA lifecycle refers to emissions of organic compound, chemical and physical gas-phase processing, SOA formation, particle-phase SOA processing, and eventual SOA deposition. In this thesis, particular attention is paid to the

Hence, the SOA lifecycle includes the global SOA budget, the relative contributions of each emissions source type to the global SOA production rate, and spatial distributions of SOA.

Several aspects of the SOA lifecycle remain highly uncertain. Firstly, global models generally simulate lower SOA concentrations than observed. Secondly, estimates of the global SOA production rate from top-down methods are higher than estimates from bottom-up modelling studies.

Thirdly, the relative contribution of various emissions source types (biogenic, anthropogenic, biomass burning) to the global SOA budget is unconstrained. These uncertainties imply the need for an improved representation of the

SOA lifecycle within global models. The motivation of this thesis is to reduce and/or understand the source of uncertainties in the SOA lifecycle.

The research questions and objectives of this thesis are presented in Figure 6.1, together with a definition of the SOA lifecycle. The objectives of this study are to quantify the sensitivity of the SOA lifecycle to (i) VOC emissions source type, (ii) VOC physical and chemical processing, and (iii) future changes in climate and emissions.

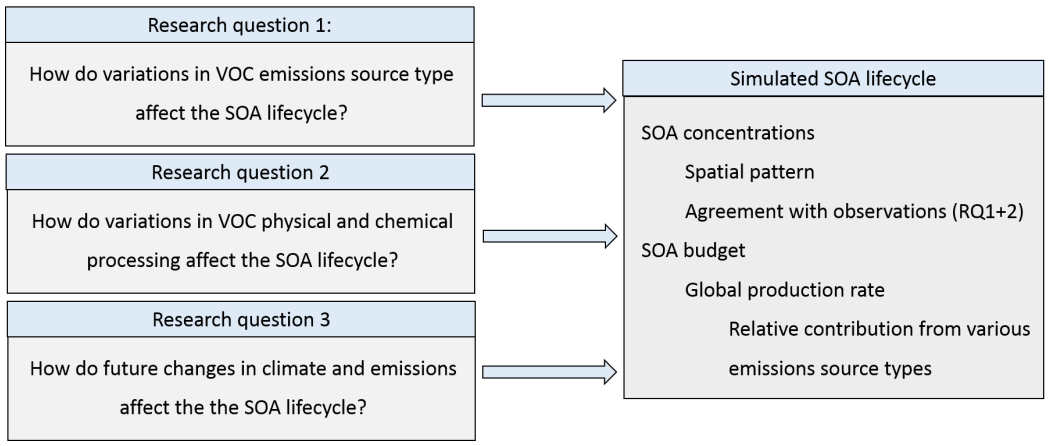

Figure 6.1 – Schematic representation of research questions and definition of SOA lifecycle.

In this section is organised as follows. To begin with, the main model developments and key results of the thesis are summarised (6.2). Next, the impacts of variations in VOC emissions source type on the global SOA budget and model agreement with observations is outlined (6.3). Following this, the sensitivity of the global SOA lifecycle to variations in the physical and chemical processing of VOCs discussed (6.4). Next, the impact of future changes in climate and emissions on the SOA lifecycle is summarised (6.5). Following this, limitations relevant for this thesis (6.6) and future work (6.7) are outlined.

6.2 Summary

This thesis contributes to i) improvements in the representation of the SOA lifecycle in a global chemistry-climate model, and ii) the understanding of the SOA lifecycle in the present-day and future. The representation of the SOA lifecycle has evolved throughout this thesis. New VOC emission source types of SOA are added to the UKCA chemistry-climate model. These are isoprene emissions from vegetation, VOC emissions from anthropogenic activities, and VOC emissions from biomass burning (Chapter 3). Deposition is extended to include all SOA precursors (Chapter 4). Finally, the oxidation mechanism describing SOA formation from anthropogenic and biomass burning sources ($VOC_{ANT/BB}$) is modified by a) adopting the reactivity of aromatic compounds, b) introducing the peroxy radical intermediate, and c) accounting for the influence of NO_X on peroxy radical reactions (Chapter 4).

These modifications provide new insights into the SOA lifecycle in the present-day and future. When monoterpene is the only source of SOA, the global annual-total SOA production rate is 20 Tg (SOA) a^{-1} and modelled SOA concentrations are lower than observed (e.g. NMB = -91 %) (Section 3). The inclusion of all new VOC emissions sources types increases the global annual-total SOA production rate by 275 % (to 75 Tg (SOA) a^{-1}) and markedly improves model agreement with observations (e.g. NMB = -50 %) (Section 3). The inclusion of SOA precursors in both dry and wet deposition reduces the global SOA production rate by 37 % (to 47 % (SOA) a^{-1}) and worsens model negative biases when comparing simulated and measured SOA concentrations at the same measurement sites (e.g. NMB = -66 %) (Section 4). Increasing the complexity of $VOC_{ANT/BB}$ oxidation by a) using naphthalene as a surrogate compound (with its reactivity) to represent $VOC_{ANT/BB}$, b) introducing the peroxy radical as an intermediate product of VOC oxidation, and c) accounting for the influence of NO_X on peroxy radical reactions, the global annual-total SOA production rate from $VOC_{ANT/BB}$

increases by 145 % and simulated SOA concentrations are brought closer to measured values (NMB = -46 %). Whilst inclusion of the peroxy radical intermediate does not impact global SOA production (<3 %), accounting for the NOX-dependent yield of proxy radical oxidation has a substantial impact on global SOA production (+145 %).

Finally, in chapter 4 the impact of future changes in climate and emissions on the SOA lifecycle is quantified. The global SOA burden increases by 20 % by the 2100s under the Relative Concentration Pathway (RCP) 8.5 compared to the present-day (Section 4). This future rise in the global SOA burden is primarily due to climate change. For instance, climate change increases monoterpene emissions by 79 % and increases the global SOA lifetime by 12 %.

In the following sub-sections, the research questions posed and the results of the thesis investigations are discussed in more detail.

6.3 The impact of VOC emissions source types on the SOA lifecycle

SOA is a major component of particulate matter. In order to develop legislation to improve PM air quality, the major sources of SOA must be understood. Whilst a number of studies examine different SOA sources, individual SOA precursor source types are often studied in isolation and are evaluated against differing observational datasets. Hence, it is difficult to draw robust conclusions on the relative importance of various SOA source types. The objectives of chapter 3 are to develop the SOA scheme within the UKCA chemistry–climate model and then perform simulations to assess how different VOC emissions source types influence the global SOA budget and model agreement with observations.

Model simulations are performed by including four different VOC emissions source types. For all simulations and for all VOC sources of SOA, SOA is formed in an identical manner. SOA formation is initiated by oxidation of the parent VOC. A stoichiometric yield is then applied to calculate the fraction of VOC oxidation products that are non-volatile. Non-volatile organics condense into the aerosol phase irreversibly, forming non-volatile SOA. With the exception of sensitivity simulations, a stoichiometric yield of 13 % is applied to all VOC sources of SOA when calculating the fraction of non-volatile oxidation products. This yield of 13 % lies within the range of estimates from chamber studies.

The pre-existing UKCA model considers SOA formation from monoterpene. Therefore, the model is developed to also consider SOA formation from isoprene, an anthropogenic VOC (VOC_{ANT}), and a biomass burning VOC (VOC_{BB}). All anthropogenic VOC emissions are included in VOC_{ANT}, and all biomass burning VOC emissions are included in VOC_{BB}. This is in contrast to many other global modelling studies where only the aromatic fraction of these emissions types are considered. Hence, the anthropogenic and biomass burning emission sources of SOA used in this thesis are higher than other most previous studies. VOC_{ANT} and VOC_{BB} are surrogate compounds representing a complex mixture of both straight and branched, alkanes, alkenes and aromatics, and with a range of functional groups. VOC_{ANT} and VOC_{BB} are assumed to have a chemical reactivity identical to α-pinene (the most abundant monoterpene species) and react solely with OH.

The chemical degradation of monoterpene in relation to SOA formation is well established in comparison to other SOA sources. Consequently, monoterpene is commonly used in SOA schemes of global models and, in some cases, is the only source of SOA (e.g. in UKCA). In this study, when emissions of monoterpene from vegetation (142 Tg (VOC) a^{-1}) are the only source of SOA, the simulated global annual-total SOA

production rate is 20 Tg (SOA) a^{-1}. Under this scheme, the NMB for simulated SOA with respect to observed SOA for surface sites across the northern-hemisphere (NH) mid-latitudes is -91%. The model negative bias is similar when sites are classified by environment (urban NMB = -93 %; urban downwind NMB = -85 %; remote sites NMB -92 %) or by continent (Europe NMB = -93 %; North America NMB = -83 %; Asia = -98 %). In the southern hemisphere (SH), simulated OA concentrations are underpredicted at an urban site in Santiago (Chile) and at Welgegund (South Africa), which is a site influenced by both urban and biomass burning activities. By contrast, over Manaus (Brail), a tropical remote site, simulated OA concentrations are slightly higher than observed. When compared to aircraft campaigns, simulated OA concentrations are much lower than observed at all altitudes and in all environments. Therefore, when monoterpene is the only source of SOA, with a relatively low global SOA production rate (20 Tg (SOA) a^{-1}), a model negative bias is present for almost all measurement sites.

The addition of biogenic as well as anthropogenic and biomass burning VOC sources of SOA to the UKCA model has a significant impact on the SOA lifecycle (Section 3.X). When emissions of isoprene from vegetation (561 Tg (C_5H_8) a^{-1}), VOCs from anthropogenic activities (127 (VOC_{ANT}) a^{-1}), and VOCs from biomass burning activities (49 Tg (VOC_{BB}) a^{-1}) are added to the SOA scheme in UKCA, the global annual-total SOA production rate increases by 275 % (to 75 Tg (SOA) a^{-1}). With this global annual-total SOA production rate biogenic VOCs account for 53 % (40 Tg (SOA) a^{-1}), whereas the anthropogenic and biomass burning VOCs account for 47 % (35 Tg (SOA) a^{-1}). With all these sources of SOA, the NMB when comparing simulated and observed SOA concentrations across the same NH mid-latitudes locations is -50 % - which is a marked improvement compared to when monoterpene is the only source of SOA (NMB = -91 %). In the SH, simulated OA is still underpredicted in Santiago (Chile) and Welgegund (South Africa) when all sources of SOA are included; however, the model

negative bias is smaller in comparison to when monoterpene is the only source of SOA. By contrast, over Manaus (Brazil), the model positive bias is exacerbated by the inclusion of all sources of SOA in the model. When compared to aircraft campaign data, even with all VOC sources of SOA included, simulated OA is still underpredicted at all altitudes for most sites. Therefore, with the exception of Manaus (Brazil), the inclusion of all VOC sources of SOA with identical reaction yields of 13 % improves model agreement with observations, but a significant model negative bias still remains.

Of all the new sources of SOA added to the UKCA model, VOC_{ANT} is responsible for largest improvement in model agreement with observations, as opposed to the inclusion of isoprene or VOC_{BB}. Previous studies also indicate an underestimated anthropogenic source of SOA in urban regions. In light of this, a sensitivity simulation is performed where SOA is assumed to be dominated by anthropogenic sources. Under an SOA scheme where only monoterpene and VOC_{ANT} are present, the yield for VOC_{ANT} is increased from 13 % to 40%, whilst the yield for monoterpene is held fixed at 13 %. Under these conditions, the global annual-total SOA production rate increases to 85 Tg (SOA) a^{-1}. Biogenic VOC emissions from monoterpene accounts for 24 % (20 Tg (SOA) a^{-1}) of the global SOA production rate, whilst anthropogenic VOCs account for 76 % (65 Tg (SOA) a^{-1}). Under this anthropogenically-dominated SOA scheme, the NMB for simulated SOA concentrations with respect to observed SOA concentrations across all NH mid-latitudes sites is -10 %. However, whilst simulated SOA concentrations are still underpredicted over urban environments (NMB = -10 %), simulated SOA concentrations are now slightly overpredicted over urban downwind (NMB = +14 %) and remote sites (NMB = 12 %). These results suggest that a missing anthropogenic source of SOA is plausible in the NH mid-latitudes. Under this single-step oxidation mechanism with a fixed SOA yield, simply increasing the SOA yield from the anthropogenic source may improve the

overall model negative bias, but may lead to overestimates downwind. This also suggests that the fixed yield approach to calculating SOA formation is too limited to represent the complexity of different SOA sources with their respective spatial distributions.

The inclusion of isoprene and VOC_{BB} have only a limited impact on model negative biases. However, this may reflect the lack of observations in regions influenced by these emissions source types. For instance, Manaus (Brazil) is the only measurement site that is significantly impacted by the addition of biogenic and biomass burning sources of SOA. For this site, the inclusion of new sources of SOA worsens the model positive bias. In light of this, together with literature estimates of the SOA yield from isoprene, a sensitivity simulation is performed. Here, the isoprene SOA yield is reduced from 13 to 3 %. However care must be taken in drawing conclusions from this. Using only one site to constrain a global emissions source is far from sufficient. A lack of measurements in tropical regions influenced by biogenic and biomass burning emissions remains a significant hindrance in understanding global SOA.

As noted, VOC_{ANT} and VOC_{BB} assume the reactivity of α-pinene, which is an alkene and therefore reacts relatively quickly. Yet anthropogenic and biomass burning VOC emissions mostly consist of aromatics and alkanes, and are therefore slow-reacting species. In light of this, an additional simulation is performed to test the sensitivity of SOA to the assumed reactivity of the parent VOC; the reactivity of VOC_{BB} is changed from α-pinene to naphthalene, a polycyclic aromatic compound typically associated with biomass burning and anthropogenic IVOCs and is ~50 % less reactive than α-pinene (Section 1.X). For this ~50 % reduction in reactivity, the global annual-total SOA production rate from biomass burning VOCs decreases by less than 1 %. This insensitivity between SOA production and assumed reactivity of parent VOC appears to be a result of (i) the fixed SOA yield approach – any reduction in VOC_{BB} reactivity will alter where VOC_{BB} is being

oxidised, but the location of VOC_{BB} oxidation does not affect the amount of SOA being produced as the yield is the same throughout the atmosphere, and (ii) deposition not being included – the sole sink for VOC_{BB} is oxidation followed condensation, hence, slowing oxidation by reducing the reactivity does not alter the fate of the species. For instance, if deposition is considered, reduced reactivity would favour deposition, therefore, reducing the global oxidation rate.

In summary, the simulations with the UKCA model performed in chapter 3 and thereafter now include all major VOC emissions source types of SOA precursors: monoterpene, isoprene, VOC_{ANT} and VOC_{BB}. Under the single-step oxidation mechanism, these sources explain around half of observed SOA mass. Of all the new sources added to the model, the anthropogenic VOC is responsible for the largest improvement in simulated and observed SOA. However, the majority of available measurements used in this thesis are located in NH mid-latitude regions, where there is high anthropogenic activity and emissions. Hence, the sensitivity simulation with increased anthropogenic SOA production improves model agreement even further, but leads to positive model biases downwind of urban centres and in remote regions.

6.4 The impact of VOC physical and chemical processing on the SOA lifecycle

In chapter 4, the SOA scheme within the UKCA model includes all major VOC sources (monoterpenes, isoprene, VOC_{ANT} and VOC_{BB}). The objectives of this chapter are to develop the SOA scheme further by extending deposition to include SOA precursors, and provide a more detailed description of VOC oxidation. The sensitivity of the SOA lifecycle to these variations in VOC deposition and oxidation is quantified.

Precursors of SOA are likely highly oxygenated (i.e. low volatility), which also implies high solubility (i.e. susceptible to wet removal). Furthermore, box modelling studies reveal highly soluble oxidation products from several important SOA parent hydrocarbons (including monoterpene and isoprene). In addition, field studies over forested regions of the USA identify significant removal of SOA precursors by dry deposition. These studies imply that dry and wet deposition of SOA precursors should be considered in models, yet this is not always the case. Deposition of SOA precursors is not included in many global modelling studies (e.g. UKCA), and for studies which do treat SOA precursor deposition, the parameters used to define deposition fluxes vary considerably from one study to another. The extent to which these variations in SOA precursor deposition affect the SOA budget and model agreement with observations on a global scale is yet to be quantified.

Simulations are performed with UKCA varying VOC deposition fluxes whilst maintaining fixed VOC emissions (monoterpene, isoprene, VOC_{ANT} and VOC_{BB}.). These simulations with varying SOA precursor deposition fluxes are compared to the scheme where no SOA precursors undergo deposition. Under the assumption that no precursors undergo deposition, the global annual-total SOA production rate is 75 Tg (SOA) a^{-1}, with biogenics accounting for 53 %, and $VOC_{ANT/BB}$ ($VOC_{ANT/BB}$ = VOC_{ANT} + VOC_{BB}) accounting for 47 % of the SOA production rate. Extending deposition to include SOA precursors lessens the amount of SOA being produced, resulting in substantial changes the SOA lifecycle. By including dry deposition of SOA precursors, the global annual-total SOA production rate reduces by 2 – 24 Tg (SOA) a^{-1} (2 - 32 %), with the range reflecting uncertainties in surface resistances. Including SOA precursor wet deposition reduces the global annual-total SOA production rate by 12 Tg (SOA) a^{-1} (15 %) and is relatively insensitive to changes in effective Henry's Law coefficient. The effects of dry and wet deposition on the global SOA budget

are not additive; the inclusion of both these processes reduces the global annual-total SOA production rate by 28 Tg (SOA) a^{-1} (37 %) to 47 Tg (SOA) a^{-1}. With deposition included, of the global annual-total SOA production rate (47 Tg (SOA) a^{-1}), biogenic VOCs account for 62 % (29 Tg (SOA) a^{-1}) and anthropogenic and biomass burning VOCs account for 38 % (18 Tg (SOA) a^{-1}). This implies anthropogenic and biomass burning VOCs are more susceptible to deposition as opposed to biogenic VOCs.

Prior to considering SOA precursors in deposition, generally, simulated SOA and OA concentrations are lower than observed (chapter 3). Hence, by considering both dry and wet deposition of SOA precursors, the model negatives bias is augmented. For instance, across the NH mid-latitude surface sites, the NMB with respect to observed SOA is larger from -50 to -66% when both dry and wet deposition of SOA precursors is considered. Similarly, the model negative biases for observed OA over Welgegund (South Africa) are greater when SOA precursor deposition is included. By contrast, over Manaus (Brazil) where simulated OA concentrations exceed observed, the inclusion of SOA precursor deposition slightly improves model performance. For most aircraft campaigns, inclusion of SOA precursor deposition exacerbates model negative biases.

Laboratory studies suggest that VOCs undergo several generations of oxidation before low-volatility organics are formed. In addition, due to the influence on oxidation channels, these studies also suggest that the yield of SOA is sensitive to the relative oxidant concentrations. SOA yields form aromatics, isoprene and monoterpenes are all sensitive to the NO_X concentration, decreasing with increasing levels of NO_X. Typically released from anthropogenic and biomass burning activities, aromatic compounds are phototooxidised, leading to the formation of a reaction intermediate, the peroxy radical (RO_2). This reaction intermediate is then oxidized by HO_2 with a high yield of SOA, or by NO with low yield of SOA. Hence, the influence of NO_X on SOA yields from aromatics is due to the competitive reactions of the

peroxy radical intermediate. These laboratory insights into VOC oxidation mechanisms are not always captured in the simpler SOA schemes of models. On the contrary, global models frequently assume VOCs forms SOA in a single-step oxidation reaction (hence, do not include the reaction intermediate) and with a fixed yield that is independent of NO_X – as is the case for SOA formation in the UKCA model as discussed above.

Simulations are performed varying VOC oxidation mechanisms, whilst maintaining fixed VOC emissions and deposition. When $VOC_{ANT/BB}$ undergoes a single-step oxidation with a fixed reaction yield of 13 % and a reactivity based on α-pinene, the global annual-total SOA production rate from anthropogenic and biomass burning sources is 18.4 Tg (SOA) a^{-1}. A series of simulations are then performed varying a) parent hydrocarbon reactivity, b) number of reaction intermediates, and c) the yield associated with the various reaction intermediate oxidative pathways. Using the reactivity of naphthalene, the global annual-total $VOC_{ANT/BB}$ oxidation rate increases by -3 % when compared to using the reactivity of α-pinene. In this case, where deposition is included, reducing the reactivity of the parent hydrocarbon does have an effect on SOA production as slower reactivity leads to greater deposition of the VOCs. Note, this is in contrast to the sensitivity simulation discussed in Section 6.2, where SOA production is insensitive to parent VOC oxidation due to deposition not being considered. Increasing the number of reaction intermediates, by including RO_2 as a product of $VOC_{ANT/BB}$ oxidation, slightly delays SOA production but has no effect on the global SOA production rate. Hence, when the reactivity of $VOC_{ANT/BB}$ is reduced from α-pinene to naphthalene, in combination with introducing the reaction intermediate, the global annual-total SOA production rates changes by just -0.6 Tg (SOA) a^{-1} (or -3 %), from 18.4 Tg (SOA) a^{-1} to 17.8 Tg (SOA) a^{-1}. However, the subsequent competitive chemical reactions of RO_2 control the product volatility distribution. To account for this in the UKCA model, the reaction yield for the RO_2+HO_2 pathway is increased from

13 to 66 %. The reaction yield for the RO_2+NO pathway is left unchanged at 13 %. Accounting for the difference in volatility between RO_2 products increases the global annual-total SOA production rate from anthropogenic and biomass burning by 153 %, from 17.8 Tg (SOA) a^{-1} in the simulation with yields of 13 % for both RO_2 reactions, to 45.1 Tg (SOA) a^{-1} when the yield for the RO_2+HO_2 is increased 66 %. In this case, biogenic VOCs are a more minor component of the global annual-total SOA production rate (37 %), with $VOC_{ANT/BB}$ accounting for 63 % of the global production rate from all sources. This substantial increase in SOA production is also accompanied by an improvement in model agreement with observations, particularly in the NH mid-latitudes (NMB = -46 %). Therefore, the net effects of increased reaction steps, accounting for the difference in volatility between RO_2 oxidation products, and using the reactivity of naphthalene, leads to an increase in the global annual-total SOA production rate and improved model agreement with observations. However, global annual-total emissions of naphthalene are 0.22 Tg (C) a^{-1}, which equates to less than 1 % of the global annual-total $VOC_{ANT/BB}$ emission rate. Hence, using naphthalene (and its reactivity) to represent the entire VOC mixture of anthropogenic and biomass burning emissions may not be suitable.

Under this new multigenerational oxidation mechanism with NO_X-dependent yields, additional simulations are conducted with $VOC_{ANT/BB}$ adopting the reactivity of more abundant aromatics, toluene (6.9 Tg (C) a^{-1}) and benzene (5.6 Tg (C) a^{-1}). The higher emission rates of these aromatics in comparison to naphthalene suggest they could be more representative of the anthropogenic and biomass burning VOC emission mixture. These aromatics are less reactive than naphthalene. As the reactivity of $VOC_{ANT/BB}$ is reduced from naphthalene to toluene to benzene, the global $VOC_{ANT/BB}$ oxidation rate also reduces, leading to less RO_2 radicals being generated. However, reduced reactivity also favours RO_2 radicals being generated further downwind of emissions source regions, where the probability of the radical

entering the RO_2+HO_2 high SOA yield pathway is higher. Under the multigenerational NO_X-dependent yield pathway, using either toluene or naphthalene, the global annual-total SOA production rate from $VOC_{ANT/BB}$ is 34.0 or 17.9 Tg (SOA) a^{-1}, respectively – these rates are +85 and -3 %, respectively, compared to the SOA production rate under the single-step oxidation mechanism with reactivity based on α-pinene and fixed SOA yields (18.4 Tg (SOA) a^{-1})(section 4.x).

These results highlight how variations in the physical and chemical processing of VOCs alters the amount the SOA produced, leading to variations in the global SOA budget and model agreement with observations. Greater observational constraints on VOC deposition parameters and oxidation mechanisms are required in order to reduce uncertainty in the SOA lifecycle.

6.5 The impact of future changes in climate and emissions on the SOA lifecycle

Climate change has the potential to alter the SOA lifecycle through several different mechanisms. The production of SOA (e.g. natural VOC emissions) and the removal of SOA (e.g. rainfall / wet deposition) can both be impacted. Furthermore, a substantial amount of SOA originates from anthropogenic and biomass burning activities. Hence, projected changes in these emissions source types may alter the SOA lifecycle and therefore lead to changes in aerosol forcing and in PM, especially of fine particles. Therefore quantifying how SOA will change in the future is important for assessing future climate and air quality.

From examinations of how SOA will change in the future, some studies do not include anthropogenic and biomass burning sources of SOA

or only include the aromatic fraction of these emission source types. Of the four previous studies that quantify how SOA will change in the future, only one accounts for the effects of CO_2 inhibition on isoprene emissions. The objective here is to quantify how the SOA lifecycle is influenced by future changes in climate, emissions, and their combined effects under RCP8.5 for the 2100s relative to the 2000s. The novelty here is that , within the SOA scheme, all VOC emissions source types are include, and that CO_2 inhibition of isoprene emissions is accounted for.

Under the Representative Concentration Pathway (RCP) 8.5, the response of the SOA lifecycle to future changes in climate and emissions alone, and their combined effects, from all major VOC source types and with fixed vegetation is quantified. For these simulations, all VOC precursors of SOA (monoterpene, isoprene, VOC_{ANT} and VOC_{BB}) undergo a single-step oxidation with a SOA yield of 13 %. Deposition of SOA precursors is not considered here. Anthropogenic and biomass burning emissions (including $VOC_{ANT/BB}$) are prescribed following RCP8.5. All natural emissions (with the exception of isoprene, monoterpene and lightning-NO_X) are held fixed at present-day values for all simulations. Biogenic emissions of monoterpene and isoprene are calculated interactively. Biogenic monoterpene emissions are calculated using a semi-empirical approach; relationships between leaf-level monoterpene emissions and factors such as temperature and light are scaled up to the canopy level. In contrast, biogenic isoprene emissions are linked directly to photosynthesis, the supply of isoprene building blocks is calculated (isoprene metabolism) and, increases is CO_2 concentrations inhibit the synthesis of isoprene ('CO_2 inhibition').

Under present-day climate and emissions, the global annual-total SOA production rate is 60.6 Tg (SOA) a^{-1}. Of this, biogenic VOCs (monoterpene and isoprene) account for 42 % (25.5 Tg (SOA) a^{-1}) and $VOC_{ANT/BB}$ accounts for the remaining 58 % (35.1 Tg (SOA) a^{-1})

Under climate change alone, the global annual-average SOA burden is 23 % higher in the future compared to the present-day. This projected increase in the global SOA burden is a result of increases in both the global annual-total SOA production rate (10 %) and a longer global-average annual-average SOA lifetime (12 %). Under climate change, global annual-total biogenic emissions of monoterpene and isoprene change by +79 and -1 %, respectively. Emissions of both monoterpene and isoprene are enhanced by the warming, but the latter is also suppressed by the projected rise in CO_2 concentrations. Therefore, the climate-driven increase in global SOA production is attributable to the global increase in monoterpene emissions as opposed to isoprene emissions. Regionally, both biogenic VOC types are responsible for regional changes in SOA concentrations under climate change. However, climate-induced changes in regional monoterpene emissions are relatively small in magnitude and spatially homogenous – increases in annual-total monoterpene emission range 0.2 – 1 g (C) m^{-2} s^{-1}. In contrast, the response of regional isoprene emissions to changes in climate are large and vary in both magnitude and sign (-5 to +5 g (C) m^{-2} s^{-1}). Together, these regional changes in biogenic VOC emissions drive the regional changes in SOA distributions under climate change.

The sensitivity of SOA to projected changes in anthropogenic and biomass burning emissions under RCP8.5 is also independently quantified. Compared to the present-day, the global annual-average SOA burden is 3 % lower in the future due to projected changes in anthropogenic and biomass burning emissions under this pathway. This reduction in the global SOA load is driven by a 6 % reduction in the global annual-total SOA production rate and modulated slightly by a 4 % increase in the global-average annual-average SOA lifetime. The decrease (6 %) in SOA production is a result of a projected 11 % reduction in anthropogenic and biomass burning VOC ($VOC_{ANT/BB}$) emissions by 2100 under RCP8.5. The projected changes in $VOC_{ANT/BB}$ emissions drive changes in regional SOA concentrations. Future

reductions in anthropogenic and biomass burning VOC emissions over North America, Europe and South East Asia lead to reductions in SOA concentrations in these same regions. Future increases in anthropogenic and biomass burning VOC emissions over India and parts of Africa lead to increases in SOA concentrations in these same regions.

Finally, the combined effects of future changes in climate and emissions on the SOA lifecycle is quantified. Compared to the present-day, the global annual-average SOA load is projected to rise by 20 % by the 2090s under RCP8.5. This increase in the global SOA burden is in response to a 4 % increase in the global annual-total SOA production rate, combined with lengthening of the global-average annual-average SOA lifetime (15 %). The simultaneous increase in monoterpene emissions (82 %) and reduction in anthropogenic and biomass burning VOC emissions (11 %) implies an increasing role for natural aerosol sources in the future. In the future, the global annual-total SOA production rate is 63.1 Tg (SOA) a^{-1}, with biogenic VOCs accounting for a larger proportion of 50.5 % (31.9 Tg (SOA) a^{-1}), and $VOC_{ANT/BB}$ accounting for 49.5 % (31.2 Tg (SOA) a^{-1}) of the SOA production rate. This compares to 42% and 58% for present-day, as outlined above. From a global perspective of the global SOA burden, anthropogenic and biomass burning emissions reductions under RCP8.5 are not large enough to counter the impacts of (i) the projected rise in biogenic emissions, and (ii) the increase in the SOA lifetime. Under future emissions and climate in the 2090s, the largest increases in SOA concentrations are projected over India and parts of southern Africa. In these regions, future changes in climate (via increases in biogenic emissions) and emissions (via increases in $VOC_{ANT/BB}$ emissions), lead to increases in annual-average SOA concentrations which exceed 1.5 μg m^{-3}. For most regions, where anthropogenic and biomass burning VOC emissions are projected to decrease under RCP8.5, these reductions are slightly compensated for by increased biogenic VOC emissions. For example, over North America, Europe and Southeast Asia,

the overall effect of changes in climate and emissions is a reduction in annual-average SOA concentrations of around 1 μg m^{-3}. Future changes in climate and emissions alter the relative VOC oxidation pathway, but OH remains the dominant oxidant in both the present-day (83 %) and future (77 %).

For the first time, this thesis quantifies how future changes in climate and emissions affect the SOA lifecycle, whilst accounting for all major VOC source types and including the effects of CO_2 inhibition on isoprene emissions. The results here imply a growth in the global SOA burden due to rising biogenic VOC emissions and a longer SOA lifetime under future climate and emissions, despite reductions in anthropogenic and biomass burning emissions. Finally, the effects of higher temperatures on climate-sensitive natural biogenic VOC emissions lead to an increasing role for natural aerosols in the future.

6.6 Limitations of thesis

Here, the limitations of this thesis are discussed. The objectives of this thesis are to quantify the sensitivity of the SOA lifecycle to variations in precursor emissions source types and gas-phase oxidation in the present-day, and to future changes in climate and emissions. Both laboratory and field studies suggest that SOA is semi-volatile, as opposed to non-volatile. However, in the UKCA model, SOA is treated as non-volatile. Under the assumption of non-volatile SOA, organic gases can condense, but aerosol-phase organics cannot evaporate. Assuming SOA is non-volatile may contribute to an overestimate in the SOA burden in the present-day. If a semi-volatile SOA approach is adopted, SOA is influenced by other aerosol components (e.g. POA and sulphate) as they provide a surface for SOA. Also, under a semi-

volatile approach of SOA, temperature affects gas-to-particle partitioning rates. Therefore, with regard to quantifying how SOA will change in the future, simulations in this thesis do not include the effect of projected changes in POA and sulphate on SOA, via available surface area, and they do not capture the effects of global warming on organic gas-to-particle partitioning.

Within the UKCA model, SOA is considered from VOCs. Hence, this thesis analyses the SOA lifecycle from VOCs only. SOA can also be produced from S/IVOC emissions (Section 1.7.5) and within the aqueous phase (Section 1.7.7). Considering these additional sources of SOA in the UKCA model could affect some of these results. In some cases, aqueous phase SOA production, and the production of SOA from S/IVOCs are identified as the dominant sources of SOA. However, key uncertainties in the physical and chemical processing of these formation pathways remain. For example, S/IVOC emissions are not included in traditional emissions inventories. Hence, S/IVOC emissions are usually estimated by applying an emission factor to POA, under the assumption that both these species are co-emitted. Another practical challenge to including S/IVOC source of SOA would be a reformulation of the SOA volatility, S/IVOCs lead to semi-volatile SOA, whereas SOA is treated as non-volatile in UKCA (discussed above).

In relation to the aqueous phase formation of SOA, key uncertainties remain, including (i) the amount of soluble VOCs formed in the atmosphere, (ii) how the soluble VOCs interact and dissolute into droplets, and (iii) the aqueous phase reactions of soluble VOCs leading to the production of SOA. Despite these uncertainties in SOA formation within the aqueous phase and from S/IVOCs, these sources of SOA are included in a few recent modelling studies.

A lack of observations of SOA is a major limitation in attempting to constrain the SOA lifecycle in models. The geographical and temporal

densities of SOA measurements are very limited. The majority of SOA observations are in the NH mid-latitudes, where anthropogenic emissions are high. Yet most models simulate peak SOA concentrations in the tropical forest of South America and Africa. The observations used in this thesis are able to constrain the anthropogenic sources of SOA much better than biogenic and biomass burning, which could potentially be skewing some conclusions drawn. Furthermore, out of all the observations for SOA, only one measurement spans an entire year. Long-term observations across multiple seasons and years would allow constraint of both the seasonal and interannual variability of SOA.

Other limitations to this thesis include the complexity of the VOCs represented in UKCA. For example, monoterpenes are a class of molecules that consist of two isoprene units (Section 1.6.2). Monoterpene isomers include but are not limited to, α-pinene, limonene, carvone, menthol, and myrecene. Across monoterpene isomers, the reactivity, oxidation pathways and SOA yields all vary. In this thesis, monoterpenes are all lumped into a single compound. Hence, the variability in monoterpene behaviour is not captured here. Resolving each monoterpene in a global model is prevented by the number of monoterpene species (which add computational expense), and compounded by the fact that only a faction have laboratory-derived data.

In addition, sesquiterpenes are not included as a biogenic VOC species in this thesis. This species is extremely reactive and recent laboratory studies have revealed extremely high SOA yields (Section 1.7.3). However, for the present-day, sesquiterpene emission rates are roughly 20 times less than isoprene emissions. Moreover, very few biogenic VOC emissions algorithms in chemistry-climate models include sesquiterpenes. Hence, when considering future projections of biogenic VOCs, sesquiterpenes are rarely included.

Finally, as demonstrated in chapter 5, the SOA lifecycle is sensitive to future changes in climate and emissions. However, this sensitivity is extremely sensitive to the specific details of the parameterisations employed for monoterpene and biogenic emissions. In particular, monoterpene emissions exhibit a large increase of 79% under climate change following RCP8.5. The current parameterisation used in UKCA does not include any CO_2 inhibitions effects due to a lack of literature documenting such an effect. In contrast, the temperature effect on isoprene emissions is balanced by the CO_2 effect in our study. Hence further work to understand the role of atmospheric CO_2 concentrations on monoterpene and other biogenic VOCs is needed. Also, this chapter assumes no changes in vegetation composition in the future. However, vegetation is sensitive to future changes in climate and anthropogenic land use. Global models which do account for changes in vegetation composition due to both climate change and anthropogenic land use find substantial decreases in biogenic VOC emissions in the future (Squire et al., 2015). Hence, by not accounting for these additional processes which influence biogenic VOC emissions, the projected increases in biogenic VOC emissions found in this study may be overestimated. Also, this chapter only studies one RCP, hence, does not explore a range of future pathways for climate and emissions.

6.7 Future work

This thesis quantifies how variations in VOC emissions source type and VOC physicochemical processing influences the SOA lifecycle in the present-day, and how future changes in climate and emissions influence the SOA lifecycle. In this section, examples of future work related to these research objectives are explored. The first three examples relate to further model developments in the SOA scheme, such as enhanced complexity in existing

VOC oxidation (6.7.1), additional SOA sources (6.7.2), and implementing a new description of SOA formation (6.7.3). The fourth example includes understanding the impacts of these model developments in the SOA scheme on human health and climate (6.7.4). The last two examples relate to assumptions in future changes in SOA, such as the climate-sensitive biogenic VOC emissions (6.7.5) and understanding why the SOA lifetime increase in the future (6.7.6).

6.7.1 Implementing the multigenerational NO_X-dependent oxidation mechanism to biogenic VOC sources of SOA

Observations indicate that VOCs form SOA after several generations of oxidation and with yields which are sensitive to NOx. Models however, typically represent SOA formation by a single-step oxidation and apply a fixed SOA yield. Overall, these simplifications to VOC oxidation have significant impacts on the global SOA budget and model agreement with observations, as demonstrated in Chapter 4 with $VOC_{ANT/BB}$. Building on this, in future work multigenerational NO_X-dependent oxidation schemes should also be applied for the biogenic precursors of SOA in the UKCA model, isoprene and monoterpene. In particular, accounting for the high-yield RO_2+HO_2 pathway may have a substantial impact on biogenic precursors of SOA considering these VOCs are usually emitted in remote, low-NO_X regions. Hence, the probability of biogenic peroxy radicals entering the high-yield RO_2+HO_2 pathways is even higher compared to the peroxy radicals generated from $VOC_{ANT/BB}$. This critical sensitivity of SOA formation towards NO_x, for all VOC sources of SOA, is interesting when considering the evolution of NO_x emissions from the pre-industrial era, to the present-day, and into the future. For example, low-NO_X emissions associated with the preindustrial era imply high SOA yield due to the probably dominance of the

RO_2+HO2 pathway over the RO2+No pathway. In the future, projected changes in anthropogenic NOx-emissions under the various RCPs may also exert changes in the strength of SOA production. Exploring how past, present and future climate and emissions affect SOA under multi-generational VOC oxidation mechanisms is yet to be explored.

6.7.2 **Additional sources of SOA**

The UKCA model could also benefit from the inclusion of SOA formation within the aqueous phase and form S/IVOCs. These formation pathways are highly uncertain (Section 1.5) and are susceptible to future changes in climate and emissions. To include S/IVOC emissions, an emissions factor could be applied to POA emissions. In contrast to this thesis where SOA precursor condense irreversibly, S/IVOCs require reversible partitioning. Hence, a semi-volatile approach to SOA is also required in order to include S/IVOC sources of SOA, as discussed in Section 1.6.

6.7.3 **Implement the volatility basis set**

Due to the high number of unique organic compounds in the atmosphere, attempting to resolve the multigenerational oxidation chemistry of SOA precursors could be futile. In light of this, the volatility basis set (VBS) accounts for the atmospheric aging of SOA precursors. Instead of explicitly modelling organic compound oxidation, the VBS applies an aging approach to organic compounds, which are grouped together either according to volatility, or volatility and O:C ratio. This approach is beginning to be used in box models and chemical transport models but is rarely included in global

chemistry-climate models. However, the VBS captures the entire volatility spectrum, hence, semi-volatile SOA is required.

6.7.4 Impacts of new VOC sources on human health and climate

The changes in the SOA budget and SOA spatial distributions in response to model developments suggests a re-evaluation of the role of SOA in human health and climate impacts. For example, in the present-day, under the default version of the model, the global SOA production rate is 20 Tg (SOA) a^{-1} and SOA production is limited to remote regions. Inclusion of new VOC sources of SOA increased the global SOA production rate by 275 % and leads to substantial SOA production in urban regions of NH mid-latitudes where population densities are high. Hence, the estimated health burden associated with PM is likely to increase as a direct result of these model developments. Future work would benefit from quantifying the impact of SOA on health burdens and climate.

6.7.5 The sensitivity of biogenic emissions to climate

Climate change enhances the production of SOA due to warming which stimulates monoterpene emissions (Chapter 5). In this study, CO_2 inhibition of monoterpene is not included. Whereas CO_2 inhibition of isoprene emissions is observed for several isoprene emitting plant species, CO_2 inhibition of monoterpene is only observed for a few monoterpene emitting plant species. If monoterpene synthesis is inhibited by CO_2, with a similar strength to CO_2 inhibition of isoprene, accounting for this could remove the future climate-driven increase in SOA production. Further work is required to

constrain the relationship between CO_2 and monoterpene emissions. If a relationship is found, incorporating this into a chemistry-climate model may weaken the sensitivity of the SOA production rate to future climate change.

6.7.6 **Climate impacts on processes affecting SOA**

In Chapter 5, a strong climate feedback on SOA deposition is identified. In the future, due to climate change alone, the global-average annual-average SOA lifetime increases by 23 %. This increase in the SOA lifetime plays a crucial role in countering the effects of projected reductions in anthropogenic and biomass burning emissions. However, the causes for this future increase in the SOA lifetime are challenging to isolate from the simulations performed to date in this thesis. There are several possible causes for a future increase in the SOA lifetime. Firstly, via regional changes in natural emissions and/or oxidants, climate change may alter regional SOA production rates. For example, increased SOA production in regions of low precipitation, and decreased SOA production in regions of high precipitation would both act to increase the global-average annual-average SOA lifetime. Also, regional changes in precipitation may also explain the future increases in the SOA lifetime. These mechanisms could be explored further using sensitivity experiments. Examples include (i) imposing future precipitation rates whilst holding all remaining climate variables, and emissions fixed at present-day values, and (ii) imposing future changes in biogenic VOC emissions whilst holding everything else at present-day values.

6.7.7 **Concluding remarks**

This thesis explores the SOA lifecycle in the present-day and future. Investigations into the formation mechanisms of SOA reveals that both emissions source type and environmental conditions are important for governing how much SOA is formed in the atmosphere. For instance, this thesis demonstrates how sources of SOA include both natural and anthropogenic emissions. This thesis highlights the sensitivity of SOA production to chemical (e.g. NO_X) and meteorological (e.g. precipitation) conditions. Results from this thesis also imply that, despite projected reductions in anthropogenic emissions, the SOA burden will increase in the future due to increased biogenic emissions and a lengthening of the SOA lifecycle. However, until studies exploring the SOA lifecycle are able to account for a greater fraction of the 37 million unique organic compounds present in the atmosphere, we cannot fully quantify the role of SOA in the Earth system with any certainty.

References

Ainsworth, E. A., Yendrek, C. R., Sitch, S., Collins, W. J., and Emberson, L. D.: The Effects of Tropospheric Ozone on Net Primary Productivity and Implications for Climate Change, in: Annual Review of Plant Biology, Vol 63, edited by: Merchant, S. S., Annual Review of Plant Biology, 637-661, 2012.

Ainsworth, E. A.: Understanding and improving global crop response to ozone pollution, Plant Journal, 90, 886-897, 10.1111/tpj.13298, 2017.

Al-Naiema, I. M., and Stone, E. A.: Evaluation of anthropogenic secondary organic aerosol tracers from aromatic hydrocarbons, Atmos. Chem. Phys., 17, 2053-2065, 10.5194/acp-17-2053-2017, 2017.

Alfarra, M. R., Hamilton, J. F., Wyche, K. P., Good, N., Ward, M. W., Carr, T., Barley, M. H., Monks, P. S., Jenkin, M. E., Lewis, A. C., and McFiggans, G. B.: The effect of photochemical ageing and initial precursor concentration on the composition and hygroscopic properties of beta-caryophyllene secondary organic aerosol, Atmos. Chem. Phys., 12, 6417-6436, 10.5194/acp-12-6417-2012, 2012.

Allen, R. J., Landuyt, W., and Rumbold, S. T.: An increase in aerosol burden and radiative effects in a warmer world, Nature Climate Change, 6, 269-274, 10.1038/nclimate2827, 2016.

Andreae, M. O., and Gelencser, A.: Black carbon or brown carbon? The nature of light-absorbing carbonaceous aerosols, Atmos. Chem. Phys., 6, 3131-3148, 10.5194/acp-6-3131-2006, 2006.

Anenberg, S. C., West, J. J., Horowitz, L. W., and Tong, D. Q.: The Global Burden of Air Pollution on Mortality: Anenberg et al. Respond, Environmental Health Perspectives, 119, A158-+, 10.1289/ehp.1003276R, 2011.

Anttila, P., Hyotylainen, T., Heikkila, A., Jussila, M., Finell, J., Kulmala, M., and Riekkola, M. L.: Determination of organic acids in aerosol particles from a coniferous forest by liquid chromatography-mass spectrometry, Journal of Separation Science, 28, 337-346, 10.1002/jssc.200401931, 2005.

Arey, J., Atkinson, R., and Aschmann, S. M.: PRODUCT STUDY OF THE GAS-PHASE REACTIONS OF MONOTERPENES WITH THE OH RADICAL IN THE PRESENCE OF NOX, J. Geophys. Res.-Atmos., 95, 18539-18546, 10.1029/JD095iD11p18539, 1990.

Arneth, A., Miller, P. A., Scholze, M., Hickler, T., Schurgers, G., Smith, B., and Prentice, I. C.: CO2 inhibition of global terrestrial isoprene emissions: Potential implications for atmospheric chemistry, Geophysical Research Letters, 34, 10.1029/2007gl030615, 2007a.

Arneth, A., Niinemets, U., Pressley, S., Back, J., Hari, P., Karl, T., Noe, S., Prentice, I. C., Serca, D., Hickler, T., Wolf, A., and Smith, B.: Process-based estimates of terrestrial ecosystem isoprene emissions: incorporating the effects of a direct CO2-isoprene interaction, Atmos. Chem. Phys., 7, 31-53, 2007b.

Arneth, A., Monson, R. K., Schurgers, G., Niinemets, U., and Palmer, P. I.: Why are estimates of global terrestrial isoprene emissions so similar (and why is this not so for monoterpenes)?, Atmos. Chem. Phys., 8, 4605-4620, 10.5194/acp-8-4605-2008, 2008.

Aschmann, S. M., Atkinson, R., and Arey, J.: Products of reaction of OH radicals with alpha-pinene, J. Geophys. Res.-Atmos., 107, 7, 10.1029/2001jd001098, 2002.

Atkinson, R., Baulch, D. L., Cox, R. A., Hampson, R. F., Kerr, J. A., and Troe, J.: EVALUATED KINETIC AND PHOTOCHEMICAL DATA FOR ATMOSPHERIC CHEMISTRY - SUPPLEMENT-III, International Journal of Chemical Kinetics, 21, 115-150, 10.1002/kin.550210205, 1989.

Atkinson, R., and Arey, J.: Atmospheric degradation of volatile organic compounds, Chem. Rev., 103, 4605-4638, 10.1021/cr0206420, 2003.

Bahreini, R., Ervens, B., Middlebrook, A. M., Warneke, C., de Gouw, J. A., DeCarlo, P. F., Jimenez, J. L., Brock, C. A., Neuman, J. A., Ryerson, T. B., Stark, H., Atlas, E., Brioude, J., Fried, A., Holloway, J. S., Peischl, J., Richter, D., Walega, J., Weibring, P., Wollny, A. G., and Fehsenfeld, F. C.: Organic aerosol formation in urban and industrial plumes near Houston and Dallas, Texas, J. Geophys. Res.-Atmos., 114, 10.1029/2008jd011493, 2009.

Bell, D. M., Imre, D., Martin, S. T., and Zelenyuk, A.: The properties and behavior of alpha-pinene secondary organic aerosol particles exposed to ammonia under dry conditions, Phys. Chem. Chem. Phys., 19, 6497-6507, 10.1039/c6cp08839b, 2017.

Bessagnet, B., Seigneur, C., and Menut, L.: Impact of dry deposition of semi-volatile organic compounds on secondary organic aerosols, Atmos. Environ., 44, 1781-1787, 10.1016/j.atmosenv.2010.01.027, 2010.

Best, M. J., Pryor, M., Clark, D. B., Rooney, G. G., Essery, R. L. H., Menard, C. B., Edwards, J. M., Hendry, M. A., Porson, A., Gedney, N., Mercado, L. M., Sitch, S., Blyth, E., Boucher, O., Cox, P. M., Grimmond, C. S. B., and Harding, R. J.: The Joint UK Land Environment Simulator (JULES), model description - Part 1: Energy and water fluxes, Geoscientific Model Development, 4, 677-699, 10.5194/gmd-4-677-2011, 2011.

Bonsang, B., Polle, C., and Lambert, G.: EVIDENCE FOR MARINE PRODUCTION OF ISOPRENE, Geophysical Research Letters, 19, 1129-1132, 10.1029/92gl00083, 1992.

Boreddy, S. K. R., Kawamura, K., and Haque, M. M.: Long-term (2001-2012) observation of the modeled hygroscopic growth factor of remote marine TSP aerosols over the western North Pacific: impact of long-range transport of pollutants and their mixing states, Phys. Chem. Chem. Phys., 17, 29344-29353, 10.1039/c5cp05315c, 2015.

Boreddy, S. K. R., Kawamura, K., Bikkina, S., and Sarin, M. M.: Hygroscopic growth of particles nebulized from water-soluble extracts of PM2.5 aerosols over the Bay of Bengal: Influence of heterogeneity in air

masses and formation pathways, Sci. Total Environ., 544, 661-669, 10.1016/j.scitotenv.2015.11.164, 2016.

Bourtsoukidis, E., Behrendt, T., Yanez-Serrano, A. M., Hellen, H., Diamantopoulos, E., Catao, E., Ashworth, K., Pozzer, A., Quesada, C. A., Martins, D. L., Sa, M., Araujo, A., Brito, J., Artaxo, P., Kesselmeier, J., Lelieveld, J., and Williams, J.: Strong sesquiterpene emissions from Amazonian soils, Nat. Commun., 9, 10.1038/s41467-018-04658-y, 2018.

Cabrera-Perez, D., Taraborrelli, D., Sander, R., and Pozzer, A.: Global atmospheric budget of simple monocyclic aromatic compounds, Atmos. Chem. Phys., 16, 6931-6947, 10.5194/acp-16-6931-2016, 2016.

Canagaratna, M. R., Jayne, J. T., Jimenez, J. L., Allan, J. D., Alfarra, M. R., Zhang, Q., Onasch, T. B., Drewnick, F., Coe, H., Middlebrook, A., Delia, A., Williams, L. R., Trimborn, A. M., Northway, M. J., DeCarlo, P. F., Kolb, C. E., Davidovits, P., and Worsnop, D. R.: Chemical and microphysical characterization of ambient aerosols with the aerodyne aerosol mass spectrometer, Mass Spectrometry Reviews, 26, 185-222, 10.1002/mas.20115, 2007.

Capes, G., Johnson, B., McFiggans, G., Williams, P. I., Haywood, J., and Coe, H.: Aging of biomass burning aerosols over West Africa: Aircraft measurements of chemical composition, microphysical properties, and emission ratios, J. Geophys. Res.-Atmos., 113, 10.1029/2008jd009845, 2008.

Capes, G., Murphy, J. G., Reeves, C. E., McQuaid, J. B., Hamilton, J. F., Hopkins, J. R., Crosier, J., Williams, P. I., and Coe, H.: Secondary organic aerosol from biogenic VOCs over West Africa during AMMA, Atmos. Chem. Phys., 9, 3841-3850, 10.5194/acp-9-3841-2009, 2009.

Cappa, C. D., and Jimenez, J. L.: Quantitative estimates of the volatility of ambient organic aerosol, Atmos. Chem. Phys., 10, 5409-5424, 10.5194/acp-10-5409-2010, 2010.

Cappa, C. D., and Wilson, K. R.: Evolution of organic aerosol mass spectra upon heating: implications for OA phase and partitioning behavior, Atmos. Chem. Phys., 11, 1895-1911, 10.5194/acp-11-1895-2011, 2011.

Carlton, A. G., Wiedinmyer, C., and Kroll, J. H.: A review of Secondary Organic Aerosol (SOA) formation from isoprene, Atmos. Chem. Phys., 9, 4987-5005, 2009.

Carslaw, K. S., Boucher, O., Spracklen, D. V., Mann, G. W., Rae, J. G. L., Woodward, S., and Kulmala, M.: A review of natural aerosol interactions and feedbacks within the Earth system, Atmos. Chem. Phys., 10, 1701-1737, 10.5194/acp-10-1701-2010, 2010.

Carslaw, K. S., Lee, L. A., Reddington, C. L., Pringle, K. J., Rap, A., Forster, P. M., Mann, G. W., Spracklen, D. V., Woodhouse, M. T., Regayre, L. A., and Pierce, J. R.: Large contribution of natural aerosols to uncertainty in indirect forcing, Nature, 503, 67-+, 10.1038/nature12674, 2013.

Cerully, K. M., Bougiatioti, A., Hite, J. R., Guo, H., Xu, L., Ng, N. L., Weber, R., and Nenes, A.: On the link between hygroscopicity, volatility, and oxidation state of ambient and water-soluble aerosols in the southeastern United States, Atmos. Chem. Phys., 15, 8679-8694, 10.5194/acp-15-8679-2015, 2015.

Chan, A. W. H., Kautzman, K. E., Chhabra, P. S., Surratt, J. D., Chan, M. N., Crounse, J. D., Kurten, A., Wennberg, P. O., Flagan, R. C., and Seinfeld, J. H.: Secondary organic aerosol formation from photooxidation of naphthalene and alkylnaphthalenes: implications for oxidation of intermediate volatility organic compounds (IVOCs), Atmos. Chem. Phys., 9, 3049-3060, 10.5194/acp-9-3049-2009, 2009.

Chan, M. N., Surratt, J. D., Chan, A. W. H., Schilling, K., Offenberg, J. H., Lewandowski, M., Edney, E. O., Kleindienst, T. E., Jaoui, M., Edgerton, E. S., Tanner, R. L., Shaw, S. L., Zheng, M., Knipping, E. M., and Seinfeld, J. H.: Influence of aerosol acidity on the chemical composition of secondary organic aerosol from beta-caryophyllene, Atmos. Chem. Phys., 11, 1735-1751, 10.5194/acp-11-1735-2011, 2011.

Chen, Q., Li, Y. L., McKinney, K. A., Kuwata, M., and Martin, S. T.: Particle mass yield from beta-caryophyllene ozonolysis, Atmos. Chem. Phys., 12, 3165-3179, 10.5194/acp-12-3165-2012, 2012.

Chung, S. H., and Seinfeld, J. H.: Global distribution and climate forcing of carbonaceous aerosols, J. Geophys. Res.-Atmos., 107, 33, 10.1029/2001jd001397, 2002.

Claeys, M., Graham, B., Vas, G., Wang, W., Vermeylen, R., Pashynska, V., Cafmeyer, J., Guyon, P., Andreae, M. O., Artaxo, P., and Maenhaut, W.: Formation of secondary organic aerosols through photooxidation of isoprene, Science, 303, 1173-1176, 10.1126/science.1092805, 2004.

Clark, D. B., Mercado, L. M., Sitch, S., Jones, C. D., Gedney, N., Best, M. J., Pryor, M., Rooney, G. G., Essery, R. L. H., Blyth, E., Boucher, O., Harding, R. J., Huntingford, C., and Cox, P. M.: The Joint UK Land Environment Simulator (JULES), model description - Part 2: Carbon fluxes and vegetation dynamics, Geoscientific Model Development, 4, 701-722, 10.5194/gmd-4-701-2011, 2011.

Cocker, D. R., Mader, B. T., Kalberer, M., Flagan, R. C., and Seinfeld, J. H.: The effect of water on gas-particle partitioning of secondary organic aerosol: II. m-xylene and 1,3,5-trimethylbenzene photooxidation systems, Atmos. Environ., 35, 6073-6085, 10.1016/s1352-2310(01)00405-8, 2001.

Collatz, G. J., Ball, J. T., Grivet, C., and Berry, J. A.: PHYSIOLOGICAL AND ENVIRONMENTAL-REGULATION OF STOMATAL CONDUCTANCE, PHOTOSYNTHESIS AND TRANSPIRATION - A MODEL THAT INCLUDES A LAMINAR BOUNDARY-LAYER, Agricultural and Forest Meteorology, 54, 107-136, 10.1016/0168-1923(91)90002-8, 1991.

Collatz, G. J., Ribas-Carbo, M., and Berry, J. A.: COUPLED PHOTOSYNTHESIS-STOMATAL CONDUCTANCE MODEL FOR LEAVES OF C4 PLANTS, Australian Journal of Plant Physiology, 19, 519-538, 10.1071/pp9920519, 1992.

Collins, M., Knutti, R., Arblaster, J., Dufresne, J. L., Fichefet, T., Friedlingstein, P., Gao, X. J., Gutowski, W. J., Johns, T., Krinner, G., Shongwe, M., Tebaldi, C., Weaver, A. J., Wehner, M., Allen, M. R., Andrews, T., Beyerle, U., Bitz, C. M., Bony, S., Booth, B. B., Brooks, H. E., Brovkin, V., Browne, O., Brutel-Vuilmet, C., Cane, M., Chadwick, R., Cook, E., Cook, K. H., Eby, M., Fasullo, J., Fischer, E. M., Forest, C. E., Forster, P., Good, P., Goosse, H., Gregory, J. M., Hegerl, G. C., Hezel, P. J., Hodges, K. I., Holland, M. M., Huber, M., Huybrechts, P., Joshi, M., Kharin, V., Kushnir, Y., Lawrence, D. M., Lee, R. W., Liddicoat, S., Lucas, C., Lucht, W., Marotzke, J., Massonnet, F., Matthews, H. D., Meinshausen, M., Morice, C., Otto, A., Patricola, C. M., Philippon-Berthier, G., Prabhat, Rahmstorf, S., Riley, W. J., Rogelj, J., Saenko, O., Seager, R., Sedlacek, J., Shaffrey, L. C., Shindell, D., Sillmann, J., Slater, A., Stevens, B., Stott, P. A., Webb, R., Zappa, G., and Zickfeld, K.: Long-term Climate Change: Projections, Commitments and Irreversibility, Climate Change 2013: The Physical Science Basis, edited by: Stocker, T. F., Qin, D., Plattner, G. K., Tignor, M. M. B., Allen, S. K., Boschung, J., Nauels, A., Xia, Y., Bex, V., and Midgley, P. M., Cambridge Univ Press, Cambridge, 1029-1136 pp., 2014.

Cox, P. M., Huntingford, C., and Harding, R. J.: A canopy conductance and photosynthesis model for use in a GCM land surface scheme, Journal of Hydrology, 212, 79-94, 10.1016/s0022-1694(98)00203-0, 1998.

Crounse, J. D., Paulot, F., Kjaergaard, H. G., and Wennberg, P. O.: Peroxy radical isomerization in the oxidation of isoprene, Phys. Chem. Chem. Phys., 13, 13607-13613, 10.1039/c1cp21330j, 2011.

Crounse, J. D., Nielsen, L. B., Jorgensen, S., Kjaergaard, H. G., and Wennberg, P. O.: Autoxidation of Organic Compounds in the Atmosphere, Journal of Physical Chemistry Letters, 4, 3513-3520, 10.1021/jz4019207, 2013.

Cubison, M. J., Ortega, A. M., Hayes, P. L., Farmer, D. K., Day, D., Lechner, M. J., Brune, W. H., Apel, E., Diskin, G. S., Fisher, J. A., Fuelberg,

H. E., Hecobian, A., Knapp, D. J., Mikoviny, T., Riemer, D., Sachse, G. W., Sessions, W., Weber, R. J., Weinheimer, A. J., Wisthaler, A., and Jimenez, J. L.: Effects of aging on organic aerosol from open biomass burning smoke in aircraft and laboratory studies, Atmos. Chem. Phys., 11, 12049-12064, 10.5194/acp-11-12049-2011, 2011.

Davidson, C. I., Phalen, R. F., and Solomon, P. A.: Airborne particulate matter and human health: A review, Aerosol Sci. Technol., 39, 737-749, 10.1080/02786820500191348, 2005.

Dee, D. P., Uppala, S. M., Simmons, A. J., Berrisford, P., Poli, P., Kobayashi, S., Andrae, U., Balmaseda, M. A., Balsamo, G., Bauer, P., Bechtold, P., Beljaars, A. C. M., van de Berg, L., Bidlot, J., Bormann, N., Delsol, C., Dragani, R., Fuentes, M., Geer, A. J., Haimberger, L., Healy, S. B., Hersbach, H., Holm, E. V., Isaksen, L., Kallberg, P., Kohler, M., Matricardi, M., McNally, A. P., Monge-Sanz, B. M., Morcrette, J. J., Park, B. K., Peubey, C., de Rosnay, P., Tavolato, C., Thepaut, J. N., and Vitart, F.: The ERA-Interim reanalysis: configuration and performance of the data assimilation system, Q. J. R. Meteorol. Soc., 137, 553-597, 10.1002/qj.828, 2011.

Ding, X., Wang, X. M., Gao, B., Fu, X. X., He, Q. F., Zhao, X. Y., Yu, J. Z., and Zheng, M.: Tracer-based estimation of secondary organic carbon in the Pearl River Delta, south China, J. Geophys. Res.-Atmos., 117, 10.1029/2011jd016596, 2012.

Doherty, R. M., Wild, O., Shindell, D. T., Zeng, G., MacKenzie, I. A., Collins, W. J., Fiore, A. M., Stevenson, D. S., Dentener, F. J., Schultz, M. G., Hess, P., Derwent, R. G., and Keating, T. J.: Impacts of climate change on surface ozone and intercontinental ozone pollution: A multi-model study, J. Geophys. Res.-Atmos., 118, 3744-3763, 10.1002/jgrd.50266, 2013.

Dommen, J., Metzger, A., Duplissy, J., Kalberer, M., Alfarra, M. R., Gascho, A., Weingartner, E., Prevot, A. S. H., Verheggen, B., and Baltensperger, U.: Laboratory observation of oligomers in the aerosol from

isoprene/NOx photooxidation, Geophysical Research Letters, 33, 10.1029/2006gl026523, 2006.

Donahue, N. M., Robinson, A. L., Stanier, C. O., and Pandis, S. N.: Coupled partitioning, dilution, and chemical aging of semivolatile organics, Environ. Sci. Technol., 40, 2635-2643, 10.1021/es052297c, 2006.

Donahue, N. M., Epstein, S. A., Pandis, S. N., and Robinson, A. L.: A two-dimensional volatility basis set: 1. organic-aerosol mixing thermodynamics, Atmos. Chem. Phys., 11, 3303-3318, 10.5194/acp-11-3303-2011, 2011.

Donahue, N. M., Kroll, J. H., Pandis, S. N., and Robinson, A. L.: A two-dimensional volatility basis set - Part 2: Diagnostics of organic-aerosol evolution, Atmos. Chem. Phys., 12, 615-634, 10.5194/acp-12-615-2012, 2012.

Eddingsaas, N. C., VanderVelde, D. G., and Wennberg, P. O.: Kinetics and Products of the Acid-Catalyzed Ring-Opening of Atmospherically Relevant Butyl Epoxy Alcohols, Journal of Physical Chemistry A, 114, 8106-8113, 10.1021/jp103907c, 2010.

Eddingsaas, N. C., Loza, C. L., Yee, L. D., Chan, M., Schilling, K. A., Chhabra, P. S., Seinfeld, J. H., and Wennberg, P. O.: alpha-pinene photooxidation under controlled chemical conditions - Part 2: SOA yield and composition in low- and high-NOx environments, Atmos. Chem. Phys., 12, 7413-7427, 10.5194/acp-12-7413-2012, 2012a.

Eddingsaas, N. C., Loza, C. L., Yee, L. D., Seinfeld, J. H., and Wennberg, P. O.: alpha-pinene photooxidation under controlled chemical conditions - Part 1: Gas-phase composition in low- and high-NOx environments, Atmos. Chem. Phys., 12, 6489-6504, 10.5194/acp-12-6489-2012, 2012b.

Edney, E. O., Kleindienst, T. E., Jaoui, M., Lewandowski, M., Offenberg, J. H., Wang, W., and Claeys, M.: Formation of 2-methyl tetrols and 2-methylglyceric acid in secondary organic aerosol from laboratory irradiated isoprene/NO(X)/SO(2)/air mixtures and their detection in ambient

PM(2.5) samples collected in the eastern United States, Atmos. Environ., 39, 5281-5289, 10.1016/j.atmosenv.2005.05.031, 2005.

Ehn, M., Thornton, J. A., Kleist, E., Sipila, M., Junninen, H., Pullinen, I., Springer, M., Rubach, F., Tillmann, R., Lee, B., Lopez-Hilfiker, F., Andres, S., Acir, I. H., Rissanen, M., Jokinen, T., Schobesberger, S., Kangasluoma, J., Kontkanen, J., Nieminen, T., Kurten, T., Nielsen, L. B., Jorgensen, S., Kjaergaard, H. G., Canagaratna, M., Dal Maso, M., Berndt, T., Petaja, T., Wahner, A., Kerminen, V. M., Kulmala, M., Worsnop, D. R., Wildt, J., and Mentel, T. F.: A large source of low-volatility secondary organic aerosol, Nature, 506, 476-+, 10.1038/nature13032, 2014.

El-Sayed, M. M. H., Wang, Y. Q., and Hennigan, C. J.: Direct atmospheric evidence for the irreversible formation of aqueous secondary organic aerosol, Geophysical Research Letters, 42, 5577-5586, 10.1002/2015gl064556, 2015.

Ervens, B.: Modeling the Processing of Aerosol and Trace Gases in Clouds and Fogs, Chem. Rev., 115, 4157-4198, 10.1021/cr5005887, 2015.

Farina, S. C., Adams, P. J., and Pandis, S. N.: Modeling global secondary organic aerosol formation and processing with the volatility basis set: Implications for anthropogenic secondary organic aerosol, J. Geophys. Res.-Atmos., 115, 17, 10.1029/2009jd013046, 2010.

Fenske, J. D., and Paulson, S. E.: Human breath emissions of VOCs, Journal of the Air & Waste Management Association, 49, 594-598, 10.1080/10473289.1999.10463831, 1999.

Forster, P., and Ramaswamy, V.: Changes in Atmospheric Constituents and in Radiative Forcing, Climate Change 2007: The Physical Science Basis, edited by: Solomon, S., Qin, D., Manning, M., Marquis, M., Averyt, K., Tignor, M. M. B., Miller, H. L., and Chen, Z. L., Cambridge Univ Press, New York, 129-234 pp., 2007.

Fuchs, N. A. a. S., A. G: Highly dispersed aerosols, Chapter: Topics in current aerosol research, Pergamon, New York, 1971.

Gao, S., Ng, N. L., Keywood, M., Varutbangkul, V., Bahreini, R., Nenes, A., He, J. W., Yoo, K. Y., Beauchamp, J. L., Hodyss, R. P., Flagan, R. C., and Seinfeld, J. H.: Particle phase acidity and oligomer formation in secondary organic aerosol, Environ. Sci. Technol., 38, 6582-6589, 10.1021/es049125k, 2004.

Ge, X. L., Setyan, A., Sun, Y. L., and Zhang, Q.: Primary and secondary organic aerosols in Fresno, California during wintertime: Results from high resolution aerosol mass spectrometry, J. Geophys. Res.-Atmos., 117, 15, 10.1029/2012jd018026, 2012.

Geng, F., Tie, X., Guenther, A., Li, G., Cao, J., and Harley, P.: Effect of isoprene emissions from major forests on ozone formation in the city of Shanghai, China, Atmos. Chem. Phys., 11, 10449-10459, 10.5194/acp-11-10449-2011, 2011.

Gentner, D. R., Isaacman, G., Worton, D. R., Chan, A. W. H., Dallmann, T. R., Davis, L., Liu, S., Day, D. A., Russell, L. M., Wilson, K. R., Weber, R., Guha, A., Harley, R. A., and Goldstein, A. H.: Elucidating secondary organic aerosol from diesel and gasoline vehicles through detailed characterization of organic carbon emissions, Proceedings of the National Academy of Sciences of the United States of America, 109, 18318-18323, 10.1073/pnas.1212272109, 2012.

Goldstein, A. H., and Galbally, I. E.: Known and unexplored organic constituents in the earth's atmosphere, Environ. Sci. Technol., 41, 1514-1521, 10.1021/es072476p, 2007.

Grieshop, A. P., Logue, J. M., Donahue, N. M., and Robinson, A. L.: Laboratory investigation of photochemical oxidation of organic aerosol from wood fires 1: measurement and simulation of organic aerosol evolution, Atmos. Chem. Phys., 9, 1263-1277, 2009.

Griffin, R. J., Cocker, D. R., Flagan, R. C., and Seinfeld, J. H.: Organic aerosol formation from the oxidation of biogenic hydrocarbons, J. Geophys. Res.-Atmos., 104, 3555-3567, 10.1029/1998jd100049, 1999.

Guenther, A., Hewitt, C. N., Erickson, D., Fall, R., Geron, C., Graedel, T., Harley, P., Klinger, L., Lerdau, M., McKay, W. A., Pierce, T., Scholes, B., Steinbrecher, R., Tallamraju, R., Taylor, J., and Zimmerman, P.: A GLOBAL-MODEL OF NATURAL VOLATILE ORGANIC-COMPOUND EMISSIONS, J. Geophys. Res.-Atmos., 100, 8873-8892, 10.1029/94jd02950, 1995.

Guenther, A. B., Jiang, X., Heald, C. L., Sakulyanontvittaya, T., Duhl, T., Emmons, L. K., and Wang, X.: The Model of Emissions of Gases and Aerosols from Nature version 2.1 (MEGAN2.1): an extended and updated framework for modeling biogenic emissions, Geoscientific Model Development, 5, 1471-1492, 10.5194/gmd-5-1471-2012, 2012.

Guo, S., Hu, M., Guo, Q. F., Zhang, X., Zheng, M., Zheng, J., Chang, C. C., Schauer, J. J., and Zhang, R. Y.: Primary Sources and Secondary Formation of Organic Aerosols in Beijing, China, Environ. Sci. Technol., 46, 9846-9853, 10.1021/es20425641, 2012.

Hall, B., Claiborn, C., and Baldocchi, D.: Measurement and modeling of the dry deposition of peroxides, Atmos. Environ., 33, 577-589, 10.1016/s1352-2310(98)00271-4, 1999.

Hallquist, M., Wenger, J. C., Baltensperger, U., Rudich, Y., Simpson, D., Claeys, M., Dommen, J., Donahue, N. M., George, C., Goldstein, A. H., Hamilton, J. F., Herrmann, H., Hoffmann, T., Iinuma, Y., Jang, M., Jenkin, M. E., Jimenez, J. L., Kiendler-Scharr, A., Maenhaut, W., McFiggans, G., Mentel, T. F., Monod, A., Prevot, A. S. H., Seinfeld, J. H., Surratt, J. D., Szmigielski, R., and Wildt, J.: The formation, properties and impact of secondary organic aerosol: current and emerging issues, Atmos. Chem. Phys., 9, 5155-5236, 2009.

Hantson, S., Knorr, W., Schurgers, G., Pugh, T. A. M., and Arneth, A.: Global isoprene and monoterpene emissions under changing climate, vegetation, CO2 and land use, Atmos. Environ., 155, 35-45, 10.1016/j.atmosenv.2017.02.010, 2017.

Hatch, L. E., Yokelson, R. J., Stockwell, C. E., Veres, P. R., Simpson, I. J., Blake, D. R., Orlando, J. J., and Barsanti, K. C.: Multi-instrument

comparison and compilation of non-methane organic gas emissions from biomass burning and implications for smoke-derived secondary organic aerosol precursors, Atmos. Chem. Phys., 17, 1471-1489, 10.5194/acp-17-1471-2017, 2017.

Hayes, P. L., Ortega, A. M., Cubison, M. J., Froyd, K. D., Zhao, Y., Cliff, S. S., Hu, W. W., Toohey, D. W., Flynn, J. H., Lefer, B. L., Grossberg, N., Alvarez, S., Rappenglueck, B., Taylor, J. W., Allan, J. D., Holloway, J. S., Gilman, J. B., Kuster, W. C., De Gouw, J. A., Massoli, P., Zhang, X., Liu, J., Weber, R. J., Corrigan, A. L., Russell, L. M., Isaacman, G., Worton, D. R., Kreisberg, N. M., Goldstein, A. H., Thalman, R., Waxman, E. M., Volkamer, R., Lin, Y. H., Surratt, J. D., Kleindienst, T. E., Offenberg, J. H., Dusanter, S., Griffith, S., Stevens, P. S., Brioude, J., Angevine, W. M., and Jimenez, J. L.: Organic aerosol composition and sources in Pasadena, California, during the 2010 CalNex campaign, J. Geophys. Res.-Atmos., 118, 9233-9257, 10.1002/jgrd.50530, 2013.

Heald, C. L., Henze, D. K., Horowitz, L. W., Feddema, J., Lamarque, J. F., Guenther, A., Hess, P. G., Vitt, F., Seinfeld, J. H., Goldstein, A. H., and Fung, I.: Predicted change in global secondary organic aerosol concentrations in response to future climate, emissions, and land use change, J. Geophys. Res.-Atmos., 113, 10.1029/2007jd009092, 2008.

Heald, C. L., Wilkinson, M. J., Monson, R. K., Alo, C. A., Wang, G. L., and Guenther, A.: Response of isoprene emission to ambient CO2 changes and implications for global budgets, Global Change Biology, 15, 1127-1140, 10.1111/j.1365-2486.2008.01802.x, 2009.

Heald, C. L., Ridley, D. A., Kreidenweis, S. M., and Drury, E. E.: Satellite observations cap the atmospheric organic aerosol budget, Geophysical Research Letters, 37, 5, 10.1029/2010gl045095, 2010.

Heald, C. L., Coe, H., Jimenez, J. L., Weber, R. J., Bahreini, R., Middlebrook, A. M., Russell, L. M., Jolleys, M., Fu, T. M., Allan, J. D., Bower, K. N., Capes, G., Crosier, J., Morgan, W. T., Robinson, N. H., Williams, P. I., Cubison, M. J., DeCarlo, P. F., and Dunlea, E. J.: Exploring the vertical

profile of atmospheric organic aerosol: comparing 17 aircraft field campaigns with a global model, Atmos. Chem. Phys., 11, 12673-12696, 10.5194/acp-11-12673-2011, 2011.

Henze, D. K., and Seinfeld, J. H.: Global secondary organic aerosol from isoprene oxidation, Geophysical Research Letters, 33, 10.1029/2006gl025976, 2006.

Henze, D. K., Seinfeld, J. H., Ng, N. L., Kroll, J. H., Fu, T. M., Jacob, D. J., and Heald, C. L.: Global modeling of secondary organic aerosol formation from aromatic hydrocarbons: high- vs. low-yield pathways, Atmos. Chem. Phys., 8, 2405-2420, 2008.

Hewitt, H. T., Copsey, D., Culverwell, I. D., Harris, C. M., Hill, R. S. R., Keen, A. B., McLaren, A. J., and Hunke, E. C.: Design and implementation of the infrastructure of HadGEM3: the next-generation Met Office climate modelling system, Geoscientific Model Development, 4, 223-253, 10.5194/gmd-4-223-2011, 2011.

Hinks, M. L., Brady, M. V., Lignell, H., Song, M. J., Grayson, J. W., Bertram, A. K., Lin, P., Laskin, A., Laskin, J., and Nizkorodov, S. A.: Effect of viscosity on photodegradation rates in complex secondary organic aerosol materials, Phys. Chem. Chem. Phys., 18, 8785-8793, 10.1039/c5cp05226b, 2016.

Hinks, M. L., Montoya-Aguilera, J., Ellison, L., Lin, P., Laskin, A., Laskin, J., Shiraiwa, M., Dabdub, D., and Nizkorodov, S. A.: Effect of relative humidity on the composition of secondary organic aerosol from the oxidation of toluene, Atmos. Chem. Phys., 18, 1643-1652, 10.5194/acp-18-1643-2018, 2018.

Hodzic, A., Aumont, B., Knote, C., Lee-Taylor, J., Madronich, S., and Tyndall, G.: Volatility dependence of Henry's law constants of condensable organics: Application to estimate depositional loss of secondary organic aerosols, Geophysical Research Letters, 41, 4795-4804, 10.1002/2014gl060649, 2014.

Hodzic, A., Kasibhatla, P. S., Jo, D. S., Cappa, C. D., Jimenez, J. L., Madronich, S., and Park, R. J.: Rethinking the global secondary organic aerosol (SOA) budget: stronger production, faster removal, shorter lifetime, Atmos. Chem. Phys., 16, 7917-7941, 10.5194/acp-16-7917-2016, 2016.

Hoffmann, T., Odum, J. R., Bowman, F., Collins, D., Klockow, D., Flagan, R. C., and Seinfeld, J. H.: Formation of organic aerosols from the oxidation of biogenic hydrocarbons, J. Atmos. Chem., 26, 189-222, 10.1023/a:1005734301837, 1997.

Hoyle, C. R., Berntsen, T., Myhre, G., and Isaksen, I. S. A.: Secondary organic aerosol in the global aerosol - chemical transport model Oslo CTM2, Atmos. Chem. Phys., 7, 5675-5694, 2007.

Hu, S. H., Herner, J. D., Robertson, W., Kobayashi, R., Chang, M. C. O., Huang, S. M., Zielinska, B., Kado, N., Collins, J. F., Rieger, P., Huai, T., and Ayala, A.: Emissions of polycyclic aromatic hydrocarbons (PAHs) and nitro-PAHs from heavy-duty diesel vehicles with DPF and SCR, Journal of the Air & Waste Management Association, 63, 984-996, 10.1080/10962247.2013.795202, 2013.

Huneeus, N., Schulz, M., Balkanski, Y., Griesfeller, J., Prospero, J., Kinne, S., Bauer, S., Boucher, O., Chin, M., Dentener, F., Diehl, T., Easter, R., Fillmore, D., Ghan, S., Ginoux, P., Grini, A., Horowitz, L., Koch, D., Krol, M. C., Landing, W., Liu, X., Mahowald, N., Miller, R., Morcrette, J. J., Myhre, G., Penner, J., Perlwitz, J., Stier, P., Takemura, T., and Zender, C. S.: Global dust model intercomparison in AeroCom phase I, Atmos. Chem. Phys., 11, 7781-7816, 10.5194/acp-11-7781-2011, 2011.

Hurley, M. D., Sokolov, O., Wallington, T. J., Takekawa, H., Karasawa, M., Klotz, B., Barnes, I., and Becker, K. H.: Organic aerosol formation during the atmospheric degradation of toluene, Environ. Sci. Technol., 35, 1358-1366, 10.1021/es0013733, 2001.

Jaoui, M., Kleindienst, T. E., Docherty, K. S., Lewandowski, M., and Offenberg, J. H.: Secondary organic aerosol formation from the oxidation of a series of sesquiterpenes: alpha-cedrene, beta-caryophyllene, alpha-

humulene and alpha-farnesene with O-3, OH and NO3 radicals, Environ. Chem., 10, 178-193, 10.1071/en13025, 2013.

Jayne, J. T., Leard, D. C., Zhang, X. F., Davidovits, P., Smith, K. A., Kolb, C. E., and Worsnop, D. R.: Development of an aerosol mass spectrometer for size and composition analysis of submicron particles, Aerosol Sci. Technol., 33, 49-70, 10.1080/027868200410840, 2000.

Jimenez, J. L., Canagaratna, M. R., Donahue, N. M., Prevot, A. S. H., Zhang, Q., Kroll, J. H., DeCarlo, P. F., Allan, J. D., Coe, H., Ng, N. L., Aiken, A. C., Docherty, K. S., Ulbrich, I. M., Grieshop, A. P., Robinson, A. L., Duplissy, J., Smith, J. D., Wilson, K. R., Lanz, V. A., Hueglin, C., Sun, Y. L., Tian, J., Laaksonen, A., Raatikainen, T., Rautiainen, J., Vaattovaara, P., Ehn, M., Kulmala, M., Tomlinson, J. M., Collins, D. R., Cubison, M. J., Dunlea, E. J., Huffman, J. A., Onasch, T. B., Alfarra, M. R., Williams, P. I., Bower, K., Kondo, Y., Schneider, J., Drewnick, F., Borrmann, S., Weimer, S., Demerjian, K., Salcedo, D., Cottrell, L., Griffin, R., Takami, A., Miyoshi, T., Hatakeyama, S., Shimono, A., Sun, J. Y., Zhang, Y. M., Dzepina, K., Kimmel, J. R., Sueper, D., Jayne, J. T., Herndon, S. C., Trimborn, A. M., Williams, L. R., Wood, E. C., Middlebrook, A. M., Kolb, C. E., Baltensperger, U., and Worsnop, D. R.: Evolution of Organic Aerosols in the Atmosphere, Science, 326, 1525-1529, 10.1126/science.1180353, 2009.

Jo, D. S., Park, R. J., Kim, M. J., and Spracklen, D. V.: Effects of chemical aging on global secondary organic aerosol using the volatility basis set approach, Atmos. Environ., 81, 230-244, 10.1016/j.atmosenv.2013.08.055, 2013.

Johnson, D., Cassanelli, P., and Cox, R. A.: Isomerization of simple alkoxyl radicals: New temperature-dependent rate data and structure activity relationship, Journal of Physical Chemistry A, 108, 519-523, 10.1021/jp037196k, 2004.

Jones, C. D., Hughes, J. K., Bellouin, N., Hardiman, S. C., Jones, G. S., Knight, J., Liddicoat, S., O'Connor, F. M., Andres, R. J., Bell, C., Boo, K. O., Bozzo, A., Butchart, N., Cadule, P., Corbin, K. D., Doutriaux-Boucher, M.,

Friedlingstein, P., Gornall, J., Gray, L., Halloran, P. R., Hurtt, G., Ingram, W. J., Lamarque, J. F., Law, R. M., Meinshausen, M., Osprey, S., Palin, E. J., Chini, L. P., Raddatz, T., Sanderson, M. G., Sellar, A. A., Schurer, A., Valdes, P., Wood, N., Woodward, S., Yoshioka, M., and Zerroukat, M.: The HadGEM2-ES implementation of CMIP5 centennial simulations, Geoscientific Model Development, 4, 543-570, 10.5194/gmd-4-543-2011, 2011.

Kanakidou, M., Seinfeld, J. H., Pandis, S. N., Barnes, I., Dentener, F. J., Facchini, M. C., Van Dingenen, R., Ervens, B., Nenes, A., Nielsen, C. J., Swietlicki, E., Putaud, J. P., Balkanski, Y., Fuzzi, S., Horth, J., Moortgat, G. K., Winterhalter, R., Myhre, C. E. L., Tsigaridis, K., Vignati, E., Stephanou, E. G., and Wilson, J.: Organic aerosol and global climate modelling: a review, Atmos. Chem. Phys., 5, 1053-1123, 2005.

Kaplan, J. O., Folberth, G., and Hauglustaine, D. A.: Role of methane and biogenic volatile organic compound sources in late glacial and Holocene fluctuations of atmospheric methane concentrations, Global Biogeochemical Cycles, 20, 10.1029/2005gb002590, 2006.

Kaser, L., Karl, T., Yuan, B., Mauldin, R. L., III, Cantrell, C. A., Guenther, A. B., Patton, E. G., Weinheimer, A. J., Knote, C., Orlando, J., Emmons, L., Apel, E., Hornbrook, R., Shertz, S., Ullmann, K., Hall, S., Graus, M., de Gouw, J., Zhou, X., and Ye, C.: Chemistry-turbulence interactions and mesoscale variability influence the cleansing efficiency of the atmosphere, Geophysical Research Letters, 42, 10894-10903, 10.1002/2015gl066641, 2015.

Kautzman, K. E., Surratt, J. D., Chan, M. N., Chan, A. W. H., Hersey, S. P., Chhabra, P. S., Dalleska, N. F., Wennberg, P. O., Flagan, R. C., and Seinfeld, J. H.: Chemical Composition of Gas- and Aerosol-Phase Products from the Photooxidation of Naphthalene, Journal of Physical Chemistry A, 114, 913-934, 10.1021/jp908530s, 2010.

Kavouras, I. G., Mihalopoulos, N., and Stephanou, E. G.: Formation of atmospheric particles from organic acids produced by forests, Nature, 395, 683-686, 10.1038/27179, 1998.

Kavouras, I. G., Mihalopoulos, N., and Stephanou, E. G.: Formation and gas/particle partitioning of monoterpenes photo-oxidation products over forests, Geophysical Research Letters, 26, 55-58, 10.1029/1998gl900251, 1999.

Khan, M. A. H., Jenkin, M. E., Foulds, A., Derwent, R. G., Percival, C. J., and Shallcross, D. E.: A modeling study of secondary organic aerosol formation from sesquiterpenes using the STOCHEM global chemistry and transport model, J. Geophys. Res.-Atmos., 122, 4426-4439, 10.1002/2016jd026415, 2017.

Kipling, Z., Stier, P., Schwarz, J. P., Perring, A. E., Spackman, J. R., Mann, G. W., Johnson, C. E., and Telford, P. J.: Constraints on aerosol processes in climate models from vertically-resolved aircraft observations of black carbon, Atmos. Chem. Phys., 13, 5969-5986, 10.5194/acp-13-5969-2013, 2013.

Kirschke, S., Bousquet, P., Ciais, P., Saunois, M., Canadell, J. G., Dlugokencky, E. J., Bergamaschi, P., Bergmann, D., Blake, D. R., Bruhwiler, L., Cameron-Smith, P., Castaldi, S., Chevallier, F., Feng, L., Fraser, A., Heimann, M., Hodson, E. L., Houweling, S., Josse, B., Fraser, P. J., Krummel, P. B., Lamarque, J. F., Langenfelds, R. L., Le Quere, C., Naik, V., O'Doherty, S., Palmer, P. I., Pison, I., Plummer, D., Poulter, B., Prinn, R. G., Rigby, M., Ringeval, B., Santini, M., Schmidt, M., Shindell, D. T., Simpson, I. J., Spahni, R., Steele, L. P., Strode, S. A., Sudo, K., Szopa, S., van der Werf, G. R., Voulgarakis, A., van Weele, M., Weiss, R. F., Williams, J. E., and Zeng, G.: Three decades of global methane sources and sinks, Nature Geoscience, 6, 813-823, 10.1038/ngeo1955, 2013.

Kleindienst, T. E., Lewandowski, M., Offenberg, J. H., Jaoui, M., and Edney, E. O.: Ozone-isoprene reaction: Re-examination of the formation of

secondary organic aerosol, Geophysical Research Letters, 34, 10.1029/2006gl027485, 2007.

Knote, C., Hodzic, A., and Jimenez, J. L.: The effect of dry and wet deposition of condensable vapors on secondary organic aerosols concentrations over the continental US, Atmos. Chem. Phys., 15, 1-18, 10.5194/acp-15-1-2015, 2015.

Koch, R., Knispel, R., Elend, M., Siese, M., and Zetzsch, C.: Consecutive reactions of aromatic-OH adducts with NO, NO2 and O-2: benzene, naphthalene, toluene, m- and p-xylene, hexamethylbenzene, phenol, m-cresol and aniline, Atmos. Chem. Phys., 7, 2057-2071, 10.5194/acp-7-2057-2007, 2007.

Krechmer, J. E., Groessl, M., Zhang, X., Junninen, H., Massoli, P., Lambe, A. T., Kimmel, J. R., Cubison, M. J., Graf, S., Lin, Y. H., Budisulistiorini, S. H., Zhang, H. F., Surratt, J. D., Knochenmuss, R., Jayne, J. T., Worsnop, D. R., Jimenez, J. L., and Canagaratna, M. R.: Ion mobility spectrometry-mass spectrometry (IMS-MS) for on- and offline analysis of atmospheric gas and aerosol species, Atmos. Meas. Tech., 9, 3245-3262, 10.5194/amt-9-3245-2016, 2016.

Kroll, J. H., Ng, N. L., Murphy, S. M., Flagan, R. C., and Seinfeld, J. H.: Secondary organic aerosol formation from isoprene photooxidation under high-NOx conditions, Geophysical Research Letters, 32, 4, 10.1029/2005gl023637, 2005.

Kroll, J. H., Ng, N. L., Murphy, S. M., Flagan, R. C., and Seinfeld, J. H.: Secondary organic aerosol formation from isoprene photooxidation, Environ. Sci. Technol., 40, 1869-1877, 10.1021/es0524301, 2006.

Kulmala, M., Suni, T., Lehtinen, K. E. J., Dal Maso, M., Boy, M., Reissell, A., Rannik, U., Aalto, P., Keronen, P., Hakola, H., Back, J. B., Hoffmann, T., Vesala, T., and Hari, P.: A new feedback mechanism linking forests, aerosols, and climate, Atmos. Chem. Phys., 4, 557-562, 10.5194/acp-4-557-2004, 2004.

Kulmala, M., Lehtinen, K. E. J., and Laaksonen, A.: Cluster activation theory as an explanation of the linear dependence between formation rate of 3nm particles and sulphuric acid concentration, Atmos. Chem. Phys., 6, 787-793, 2006.

Lamarque, J. F., Bond, T. C., Eyring, V., Granier, C., Heil, A., Klimont, Z., Lee, D., Liousse, C., Mieville, A., Owen, B., Schultz, M. G., Shindell, D., Smith, S. J., Stehfest, E., Van Aardenne, J., Cooper, O. R., Kainuma, M., Mahowald, N., McConnell, J. R., Naik, V., Riahi, K., and van Vuuren, D. P.: Historical (1850-2000) gridded anthropogenic and biomass burning emissions of reactive gases and aerosols: methodology and application, Atmos. Chem. Phys., 10, 7017-7039, 10.5194/acp-10-7017-2010, 2010.

Lamarque, J. F., Kyle, G. P., Meinshausen, M., Riahi, K., Smith, S. J., van Vuuren, D. P., Conley, A. J., and Vitt, F.: Global and regional evolution of short-lived radiatively-active gases and aerosols in the Representative Concentration Pathways, Climatic Change, 109, 191-212, 10.1007/s10584-011-0155-0, 2011.

Lathiere, J., Hauglustaine, D. A., De Noblet-Ducoudre, N., Krinner, G., and Folberth, G. A.: Past and future changes in biogenic volatile organic compound emissions simulated with a global dynamic vegetation model, Geophysical Research Letters, 32, 10.1029/2005gl024164, 2005.

Lee, A., Goldstein, A. H., Kroll, J. H., Ng, N. L., Varutbangkul, V., Flagan, R. C., and Seinfeld, J. H.: Gas-phase products and secondary aerosol yields from the photooxidation of 16 different terpenes, J. Geophys. Res.-Atmos., 111, 10.1029/2006jd007050, 2006.

Lee, J. D., Whalley, L. K., Heard, D. E., Stone, D., Dunmore, R. E., Hamilton, J. F., Young, D. E., Allan, J. D., Laufs, S., and Kleffmann, J.: Detailed budget analysis of HONO in central London reveals a missing daytime source, Atmos. Chem. Phys., 16, 2747-2764, 10.5194/acp-16-2747-2016, 2016.

Lee, S., Kim, H. K., Yan, B., Cobb, C. E., Hennigan, C., Nichols, S., Chamber, M., Edgerton, E. S., Jansen, J. J., Hu, Y. T., Zheng, M., Weber, R.

J., and Russell, A. G.: Diagnosis of aged prescribed burning plumes impacting an urban area, Environ. Sci. Technol., 42, 1438-1444, 10.1021/es7023059, 2008.

Lelieveld, J., Gromov, S., Pozzer, A., and Taraborrelli, D.: Global tropospheric hydroxyl distribution, budget and reactivity, Atmos. Chem. Phys., 16, 12477-12493, 10.5194/acp-16-12477-2016, 2016.

Levis, S., Foley, J. A., and Pollard, D.: Potential high-latitude vegetation feedbacks on CO2-induced climate change, Geophysical Research Letters, 26, 747-750, 10.1029/1999gl900107, 1999.

Li, J. L., Zhang, M. G., Wu, F. K., Sun, Y. L., and Tang, G. G.: Assessment of the impacts of aromatic VOC emissions and yields of SOA on SOA concentrations with the air quality model RAMS-CMAQ, Atmos. Environ., 158, 105-115, 10.1016/j.atmosenv.2017.03.035, 2017a.

Li, L. J., Tang, P., Nakao, S., and Cocker, D. R.: Impact of molecular structure on secondary organic aerosol formation from aromatic hydrocarbon photooxidation under low-NOx conditions, Atmos. Chem. Phys., 16, 10793-10808, 10.5194/acp-16-10793-2016, 2016.

Li, L. J., Qi, L., and Cocker, D. R.: Contribution of methyl group to secondary organic aerosol formation from aromatic hydrocarbon photooxidation, Atmos. Environ., 151, 133-139, 10.1016/j.atmosenv.2016.11.064, 2017b.

Liao, H., Chen, W.-T., and Seinfeld, J. H.: Role of climate change in global predictions of future tropospheric ozone and aerosols, J. Geophys. Res.-Atmos., 111, 10.1029/2005jd006852, 2006a.

Liao, H., Chen, W. T., and Seinfeld, J. H.: Role of climate change in global predictions of future tropospheric ozone and aerosols, J. Geophys. Res.-Atmos., 111, 10.1029/2005jd006852, 2006b.

Lin, G., Penner, J. E., Sillman, S., Taraborrelli, D., and Lelieveld, J.: Global modeling of SOA formation from dicarbonyls, epoxides, organic nitrates and peroxides, Atmos. Chem. Phys., 12, 4743-4774, 10.5194/acp-12-4743-2012, 2012.

Lin, G., Sillman, S., Penner, J. E., and Ito, A.: Global modeling of SOA: the use of different mechanisms for aqueous-phase formation, Atmos. Chem. Phys., 14, 5451-5475, 10.5194/acp-14-5451-2014, 2014.

Lin, G. X., Penner, J. E., and Zhou, C.: How will SOA change in the future?, Geophysical Research Letters, 43, 1718-1726, 10.1002/2015gl067137, 2016.

Lin, Y. H., Zhang, H. F., Pye, H. O. T., Zhang, Z. F., Marth, W. J., Park, S., Arashiro, M., Cui, T. Q., Budisulistiorini, H., Sexton, K. G., Vizuete, W., Xie, Y., Luecken, D. J., Piletic, I. R., Edney, E. O., Bartolotti, L. J., Gold, A., and Surratt, J. D.: Epoxide as a precursor to secondary organic aerosol formation from isoprene photooxidation in the presence of nitrogen oxides, Proceedings of the National Academy of Sciences of the United States of America, 110, 6718-6723, 10.1073/pnas.1221150110, 2013.

Llorens, L., Llusia, J., Murchie, E. H., Penuelas, J., and Beerling, D. J.: Monoterpene emissions and photoinhibition of "living fossil" trees grown under CO2 enrichment in a simulated Cretaceous polar environment, Journal of Geophysical Research-Biogeosciences, 114, 10.1029/2008jg000802, 2009.

Lockwood, A. L., Shepson, P. B., Fiddler, M. N., and Alaghmand, M.: Isoprene nitrates: preparation, separation, identification, yields, and atmospheric chemistry, Atmos. Chem. Phys., 10, 6169-6178, 10.5194/acp-10-6169-2010, 2010.

Lopez-Hilfiker, F. D., Mohr, C., D'Ambro, E. L., Lutz, A., Riedel, T. P., Gaston, C. J., Iyer, S., Zhang, Z., Gold, A., Surratt, J. D., Lee, B. H., Kurten, T., Hu, W. W., Jimenez, J., Hallquist, M., and Thornton, J. A.: Molecular Composition and Volatility of Organic Aerosol in the Southeastern US: Implications for IEPDX Derived SOA, Environ. Sci. Technol., 50, 2200-2209, 10.1021/acs.est.5b04769, 2016.

Loreto, F., and Schnitzler, J. P.: Abiotic stresses and induced BVOCs, Trends in Plant Science, 15, 154-166, 10.1016/j.tplants.2009.12.006, 2010.

Loveland, T. R., Reed, B. C., Brown, J. F., Ohlen, D. O., Zhu, Z., Yang, L., and Merchant, J. W.: Development of a global land cover characteristics database and IGBP DISCover from 1 km AVHRR data, Int. J. Remote Sens., 21, 1303-1330, 10.1080/014311600210191, 2000.

Mann, G. W., Carslaw, K. S., Spracklen, D. V., Ridley, D. A., Manktelow, P. T., Chipperfield, M. P., Pickering, S. J., and Johnson, C. E.: Description and evaluation of GLOMAP-mode: a modal global aerosol microphysics model for the UKCA composition-climate model, Geoscientific Model Development, 3, 519-551, 10.5194/gmd-3-519-2010, 2010.

Mann, G. W., Carslaw, K. S., Reddington, C. L., Pringle, K. J., Schulz, M., Asmi, A., Spracklen, D. V., Ridley, D. A., Woodhouse, M. T., Lee, L. A., Zhang, K., Ghan, S. J., Easter, R. C., Liu, X., Stier, P., Lee, Y. H., Adams, P. J., Tost, H., Lelieveld, J., Bauer, S. E., Tsigaridis, K., van Noije, T. P. C., Strunk, A., Vignati, E., Bellouin, N., Dalvi, M., Johnson, C. E., Bergman, T., Kokkola, H., von Salzen, K., Yu, F., Luo, G., Petzold, A., Heintzenberg, J., Clarke, A., Ogren, A., Gras, J., Baltensperger, U., Kaminski, U., Jennings, S. G., O'Dowd, C. D., Harrison, R. M., Beddows, D. C. S., Kulmala, M., Viisanen, Y., Ulevicius, V., Mihalopoulos, N., Zdimal, V., Fiebig, M., Hansson, H. C., Swietlicki, E., and Henzing, J. S.: Intercomparison and evaluation of global aerosol microphysical properties among AeroCom models of a range of complexity, Atmos. Chem. Phys., 14, 4679-4713, 10.5194/acp-14-4679-2014, 2014.

Marais, E. A., Jacob, D. J., Jimenez, J. L., Campuzano-Jost, P., Day, D. A., Hu, W., Krechmer, J., Zhu, L., Kim, P. S., Miller, C. C., Fisher, J. A., Travis, K., Yu, K., Hanisco, T. F., Wolfe, G. M., Arkinson, H. L., Pye, H. O. T., Froyd, K. D., Liao, J., and McNeill, V. F.: Aqueous-phase mechanism for secondary organic aerosol formation from isoprene: application to the southeast United States and co-benefit of SO2 emission controls, Atmos. Chem. Phys., 16, 1603-1618, 10.5194/acp-16-1603-2016, 2016.

Martin, S. T., Andreae, M. O., Althausen, D., Artaxo, P., Baars, H., Borrmann, S., Chen, Q., Farmer, D. K., Guenther, A., Gunthe, S. S.,

Jimenez, J. L., Karl, T., Longo, K., Manzi, A., Muller, T., Pauliquevis, T., Petters, M. D., Prenni, A. J., Poschl, U., Rizzo, L. V., Schneider, J., Smith, J. N., Swietlicki, E., Tota, J., Wang, J., Wiedensohler, A., and Zorn, S. R.: An overview of the Amazonian Aerosol Characterization Experiment 2008 (AMAZE-08), Atmos. Chem. Phys., 10, 11415-11438, 10.5194/acp-10-11415-2010, 2010.

May, A. A., Levin, E. J. T., Hennigan, C. J., Riipinen, I., Lee, T., Collett, J. L., Jimenez, J. L., Kreidenweis, S. M., and Robinson, A. L.: Gas-particle partitioning of primary organic aerosol emissions: 3. Biomass burning, J. Geophys. Res.-Atmos., 118, 11327-11338, 10.1002/jgrd.50828, 2013a.

May, A. A., Presto, A. A., Hennigan, C. J., Nguyen, N. T., Gordon, T. D., and Robinson, A. L.: Gas-Particle Partitioning of Primary Organic Aerosol Emissions: (2) Diesel Vehicles, Environ. Sci. Technol., 47, 8288-8296, 10.1021/es400782j, 2013b.

May, A. A., Presto, A. A., Hennigan, C. J., Nguyen, N. T., Gordon, T. D., and Robinson, A. L.: Gas-particle partitioning of primary organic aerosol emissions: (1) Gasoline vehicle exhaust, Atmos. Environ., 77, 128-139, 10.1016/j.atmosenv.2013.04.060, 2013c.

May, A. A., Nguyen, N. T., Presto, A. A., Gordon, T. D., Lipsky, E. M., Karve, M., Gutierrez, A., Robertson, W. H., Zhang, M., Brandow, C., Chang, O., Chen, S. Y., Cicero-Fernandez, P., Dinkins, L., Fuentes, M., Huang, S. M., Ling, R., Long, J., Maddox, C., Massetti, J., McCauley, E., Miguel, A., Na, K., Ong, R., Pang, Y. B., Rieger, P., Sax, T., Truong, T., Vo, T., Chattopadhyay, S., Maldonado, H., Maricq, M. M., and Robinson, A. L.: Gas- and particle-phase primary emissions from in-use, on-road gasoline and diesel vehicles, Atmos. Environ., 88, 247-260, 10.1016/j.atmosenv.2014.01.046, 2014.

McNeill, V. F., Woo, J. L., Kim, D. D., Schwier, A. N., Wannell, N. J., Sumner, A. J., and Barakat, J. M.: Aqueous-Phase Secondary Organic

Aerosol and Organosulfate Formation in Atmospheric Aerosols: A Modeling Study, Environ. Sci. Technol., 46, 8075-8081, 10.1021/es3002986, 2012.

Mercado, L. M., Bellouin, N., Sitch, S., Boucher, O., Huntingford, C., Wild, M., and Cox, P. M.: Impact of changes in diffuse radiation on the global land carbon sink, Nature, 458, 1014-U1087, 10.1038/nature07949, 2009.

Mohr, C., DeCarlo, P. F., Heringa, M. F., Chirico, R., Slowik, J. G., Richter, R., Reche, C., Alastuey, A., Querol, X., Seco, R., Penuelas, J., Jimenez, J. L., Crippa, M., Zimmermann, R., Baltensperger, U., and Prevot, A. S. H.: Identification and quantification of organic aerosol from cooking and other sources in Barcelona using aerosol mass spectrometer data, Atmos. Chem. Phys., 12, 1649-1665, 10.5194/acp-12-1649-2012, 2012.

Monson, R. K., Trahan, N., Rosenstiel, T. N., Veres, P., Moore, D., Wilkinson, M., Norby, R. J., Volder, A., Tjoelker, M. G., Briske, D. D., Karnosky, D. F., and Fall, R.: Isoprene emission from terrestrial ecosystems in response to global change: minding the gap between models and observations, Philosophical Transactions of the Royal Society a-Mathematical Physical and Engineering Sciences, 365, 1677-1695, 10.1098/rsta.2007.2038, 2007.

Moore, R. M., Oram, D. E., and Penkett, S. A.: PRODUCTION OF ISOPRENE BY MARINE-PHYTOPLANKTON CULTURES, Geophysical Research Letters, 21, 2507-2510, 10.1029/94gl02363, 1994.

Morgan, W. T., Allan, J. D., Bower, K. N., Highwood, E. J., Liu, D., McMeeking, G. R., Northway, M. J., Williams, P. I., Krejci, R., and Coe, H.: Airborne measurements of the spatial distribution of aerosol chemical composition across Europe and evolution of the organic fraction, Atmos. Chem. Phys., 10, 4065-4083, 10.5194/acp-10-4065-2010, 2010.

Morgenstern, O., Braesicke, P., O'Connor, F. M., Bushell, A. C., Johnson, C. E., Osprey, S. M., and Pyle, J. A.: Evaluation of the new UKCA climate-composition model - Part 1: The stratosphere, Geoscientific Model Development, 2, 43-57, 10.5194/gmd-2-43-2009, 2009.

Myhre, G., Samset, B. H., Schulz, M., Balkanski, Y., Bauer, S., Berntsen, T. K., Bian, H., Bellouin, N., Chin, M., Diehl, T., Easter, R. C., Feichter, J., Ghan, S. J., Hauglustaine, D., Iversen, T., Kinne, S., Kirkevag, A., Lamarque, J. F., Lin, G., Liu, X., Lund, M. T., Luo, G., Ma, X., van Noije, T., Penner, J. E., Rasch, P. J., Ruiz, A., Seland, O., Skeie, R. B., Stier, P., Takemura, T., Tsigaridis, K., Wang, P., Wang, Z., Xu, L., Yu, H., Yu, F., Yoon, J. H., Zhang, K., Zhang, H., and Zhou, C.: Radiative forcing of the direct aerosol effect from AeroCom Phase II simulations, Atmos. Chem. Phys., 13, 1853-1877, 10.5194/acp-13-1853-2013, 2013.

Myriokefalitakis, S., Vignati, E., Tsigaridis, K., Papadimas, C., Sciare, J., Mihalopoulos, N., Facchini, M. C., Rinaldi, M., Dentener, F. J., Ceburnis, D., Hatzianastasiou, N., O'Dowd, C. D., van Weele, M., and Kanakidou, M.: Global Modeling of the Oceanic Source of Organic Aerosols, Advances in Meteorology, 10.1155/2010/939171, 2010.

Neu, J. L., Prather, M. J., and Penner, J. E.: Global atmospheric chemistry: Integrating over fractional cloud cover, J. Geophys. Res.-Atmos., 112, 10.1029/2006jd008007, 2007.

Ng, N. L., Kroll, J. H., Keywood, M. D., Bahreini, R., Varutbangkul, V., Flagan, R. C., Seinfeld, J. H., Lee, A., and Goldstein, A. H.: Contribution of first- versus second-generation products to secondary organic aerosols formed in the oxidation of biogenic hydrocarbons, Environ. Sci. Technol., 40, 2283-2297, 10.1021/es052269u, 2006.

Ng, N. L., Chhabra, P. S., Chan, A. W. H., Surratt, J. D., Kroll, J. H., Kwan, A. J., McCabe, D. C., Wennberg, P. O., Sorooshian, A., Murphy, S. M., Dalleska, N. F., Flagan, R. C., and Seinfeld, J. H.: Effect of NOx level on secondary organic aerosol (SOA) formation from the photooxidation of terpenes, Atmos. Chem. Phys., 7, 5159-5174, 10.5194/acp-7-5159-2007, 2007a.

Ng, N. L., Kroll, J. H., Chan, A. W. H., Chhabra, P. S., Flagan, R. C., and Seinfeld, J. H.: Secondary organic aerosol formation from m-xylene, toluene, and benzene, Atmos. Chem. Phys., 7, 3909-3922, 2007b.

Ng, N. L., Kwan, A. J., Surratt, J. D., Chan, A. W. H., Chhabra, P. S., Sorooshian, A., Pye, H. O. T., Crounse, J. D., Wennberg, P. O., Flagan, R. C., and Seinfeld, J. H.: Secondary organic aerosol (SOA) formation from reaction of isoprene with nitrate radicals (NO3), Atmos. Chem. Phys., 8, 4117-4140, 2008.

Nguyen, T. B., Crounse, J. D., Teng, A. P., Clair, J. M. S., Paulot, F., Wolfe, G. M., and Wennberg, P. O.: Rapid deposition of oxidized biogenic compounds to a temperate forest, Proceedings of the National Academy of Sciences of the United States of America, 112, E392-E401, 10.1073/pnas.1418702112, 2015.

Nguyen, T. L., Vereecken, L., and Peeters, J.: HOx Regeneration in the Oxidation of Isoprene III: Theoretical Study of the key Isomerisation of the Z-delta-hydroxy-peroxy Isoprene Radicals, ChemPhysChem, 11, 3996-4001, 10.1002/cphc.201000480, 2010.

Niinemets, U., Arneth, A., Kuhn, U., Monson, R. K., Penuelas, J., and Staudt, M.: The emission factor of volatile isoprenoids: stress, acclimation, and developmental responses, Biogeosciences, 7, 2203-2223, 10.5194/bg-7-2203-2010, 2010.

Noziere, B., Barnes, I., and Becker, K. H.: Product study and mechanisms of the reactions of alpha-pinene and of pinonaldehyde with OH radicals, J. Geophys. Res.-Atmos., 104, 23645-23656, 10.1029/1999jd900778, 1999.

O'Connor, F. M., Johnson, C. E., Morgenstern, O., Abraham, N. L., Braesicke, P., Dalvi, M., Folberth, G. A., Sanderson, M. G., Telford, P. J., Voulgarakis, A., Young, P. J., Zeng, G., Collins, W. J., and Pyle, J. A.: Evaluation of the new UKCA climate-composition model - Part 2: The Troposphere, Geoscientific Model Development, 7, 41-91, 10.5194/gmd-7-41-2014, 2014.

Odum, J. R., Hoffmann, T., Bowman, F., Collins, D., Flagan, R. C., and Seinfeld, J. H.: Gas/particle partitioning and secondary organic aerosol yields, Environ. Sci. Technol., 30, 2580-2585, 10.1021/es950943+, 1996.

Odum, J. R., Jungkamp, T. P. W., Griffin, R. J., Flagan, R. C., and Seinfeld, J. H.: The atmospheric aerosol-forming potential of whole gasoline vapor, Science, 276, 96-99, 10.1126/science.276.5309.96, 1997.

Pacifico, F., Harrison, S. P., Jones, C. D., Arneth, A., Sitch, S., Weedon, G. P., Barkley, M. P., Palmer, P. I., Serca, D., Potosnak, M., Fu, T. M., Goldstein, A., Bai, J., and Schurgers, G.: Evaluation of a photosynthesis-based biogenic isoprene emission scheme in JULES and simulation of isoprene emissions under present-day climate conditions, Atmos. Chem. Phys., 11, 4371-4389, 10.5194/acp-11-4371-2011, 2011.

Pacifico, F., Folberth, G. A., Jones, C. D., Harrison, S. P., and Collins, W. J.: Sensitivity of biogenic isoprene emissions to past, present, and future environmental conditions and implications for atmospheric chemistry, J. Geophys. Res.-Atmos., 117, 10.1029/2012jd018276, 2012.

Pajunoja, A., Lambe, A. T., Hakala, J., Rastak, N., Cummings, M. J., Brogan, J. F., Hao, L. Q., Paramonov, M., Hong, J., Prisle, N. L., Malila, J., Romakkaniemi, S., Lehtinen, K. E. J., Laaksonen, A., Kulmala, M., Massoli, P., Onasch, T. B., Donahue, N. M., Riipinen, I., Davidovits, P., Worsnop, D. R., Petaja, T., and Virtanen, A.: Adsorptive uptake of water by semisolid secondary organic aerosols, Geophysical Research Letters, 42, 3063-3068, 10.1002/2015gl063142, 2015.

Pandis, S. N., Paulson, S. E., Seinfeld, J. H., and Flagan, R. C.: AEROSOL FORMATION IN THE PHOTOOXIDATION OF ISOPRENE AND BETA-PINENE, Atmospheric Environment Part a-General Topics, 25, 997-1008, 10.1016/0960-1686(91)90141-s, 1991.

Pankow, J. F.: AN ABSORPTION-MODEL OF THE GAS AEROSOL PARTITIONING INVOLVED IN THE FORMATION OF SECONDARY ORGANIC AEROSOL, Atmos. Environ., 28, 189-193, 10.1016/1352-2310(94)90094-9, 1994.

Pankow, J. F., and Asher, W. E.: SIMPOL.1: a simple group contribution method for predicting vapor pressures and enthalpies of

vaporization of multifunctional organic compounds, Atmos. Chem. Phys., 8, 2773-2796, 10.5194/acp-8-2773-2008, 2008.

Paulot, F., Crounse, J. D., Kjaergaard, H. G., Kurten, A., St Clair, J. M., Seinfeld, J. H., and Wennberg, P. O.: Unexpected Epoxide Formation in the Gas-Phase Photooxidation of Isoprene, Science, 325, 730-733, 10.1126/science.1172910, 2009.

Peeters, J., Nguyen, T. L., and Vereecken, L.: HOx radical regeneration in the oxidation of isoprene, Phys. Chem. Chem. Phys., 11, 5935-5939, 10.1039/b908511d, 2009.

Peeters, J., and Nguyen, T. L.: Unusually Fast 1,6-H Shifts of Enolic Hydrogens in Peroxy Radicals: Formation of the First-Generation C-2 and C-3 Carbonyls in the Oxidation of Isoprene, Journal of Physical Chemistry A, 116, 6134-6141, 10.1021/jp211447q, 2012.

Peng, J. L., Li, M., Zhang, P., Gong, S. Y., Zhong, M. A., Wu, M. H., Zheng, M., Chen, C. H., Wang, H. L., and Lou, S. R.: Investigation of the sources and seasonal variations of secondary organic aerosols in PM2.5 in Shanghai with organic tracers, Atmos. Environ., 79, 614-622, 10.1016/j.atmosenv.2013.07.022, 2013.

Penner, J. E., Atherton, C. S., Dignon, J., Ghan, S. J., Walton, J. J., and Hameed, S.: TROPOSPHERIC NITROGEN - A 3-DIMENSIONAL STUDY OF SOURCES, DISTRIBUTIONS, AND DEPOSITION, J. Geophys. Res.-Atmos., 96, 959-990, 10.1029/90jd02228, 1991.

Pfrang, C., Shiraiwa, M., and Poschl, U.: Chemical ageing and transformation of diffusivity in semi-solid multi-component organic aerosol particles, Atmos. Chem. Phys., 11, 7343-7354, 10.5194/acp-11-7343-2011, 2011.

Poschl, U., von Kuhlmann, R., Poisson, N., and Crutzen, P. J.: Development and intercomparison of condensed isoprene oxidation mechanisms for global atmospheric modeling, J. Atmos. Chem., 37, 29-52, 10.1023/a:1006391009798, 2000.

Possell, M., Hewitt, C. N., and Beerling, D. J.: The effects of glacial atmospheric CO2 concentrations and climate on isoprene emissions by vascular plants, Global Change Biology, 11, 60-69, 10.1111/j.1365-2486.2004.00889.x, 2005.

Price, C., and Rind, D.: A SIMPLE LIGHTNING PARAMETERIZATION FOR CALCULATING GLOBAL LIGHTNING DISTRIBUTIONS, J. Geophys. Res.-Atmos., 97, 9919-9933, 10.1029/92jd00719, 1992.

Pye, H. O. T., and Seinfeld, J. H.: A global perspective on aerosol from low-volatility organic compounds, Atmos. Chem. Phys., 10, 4377-4401, 10.5194/acp-10-4377-2010, 2010.

Rastak, N., Pajunoja, A., Navarro, J. C. A., Ma, J., Song, M., Partridge, D. G., Kirkevag, A., Leong, Y., Hu, W. W., Taylor, N. F., Lambe, A., Cerully, K., Bougiatioti, A., Liu, P., Krejci, R., Petaja, T., Percival, C., Davidovits, P., Worsnop, D. R., Ekman, A. M. L., Nenes, A., Martin, S., Jimenez, J. L., Collins, D. R., Topping, D. O., Bertram, A. K., Zuend, A., Virtanen, A., and Riipinen, I.: Microphysical explanation of the RH-dependent water affinity of biogenic organic aerosol and its importance for climate, Geophysical Research Letters, 44, 5167-5177, 10.1002/2017gl073056, 2017.

Riahi, K., Rao, S., Krey, V., Cho, C. H., Chirkov, V., Fischer, G., Kindermann, G., Nakicenovic, N., and Rafaj, P.: RCP 8.5-A scenario of comparatively high greenhouse gas emissions, Climatic Change, 109, 33-57, 10.1007/s10584-011-0149-y, 2011.

Riipinen, I., Pierce, J. R., Yli-Juuti, T., Nieminen, T., Hakkinen, S., Ehn, M., Junninen, H., Lehtipalo, K., Petaja, T., Slowik, J., Chang, R., Shantz, N. C., Abbatt, J., Leaitch, W. R., Kerminen, V. M., Worsnop, D. R., Pandis, S. N., Donahue, N. M., and Kulmala, M.: Organic condensation: a vital link connecting aerosol formation to cloud condensation nuclei (CCN) concentrations, Atmos. Chem. Phys., 11, 3865-3878, 10.5194/acp-11-3865-2011, 2011.

Riipinen, I., Yli-Juuti, T., Pierce, J. R., Petaja, T., Worsnop, D. R., Kulmala, M., and Donahue, N. M.: The contribution of organics to atmospheric nanoparticle growth, Nature Geoscience, 5, 453-458, 10.1038/ngeo1499, 2012.

Robinson, A. L., Donahue, N. M., Shrivastava, M. K., Weitkamp, E. A., Sage, A. M., Grieshop, A. P., Lane, T. E., Pierce, J. R., and Pandis, S. N.: Rethinking organic aerosols: Semivolatile emissions and photochemical aging, Science, 315, 1259-1262, 10.1126/science.1133061, 2007.

Robinson, A. L., Grieshop, A. P., Donahue, N. M., and Hunt, S. W.: Updating the Conceptual Model for Fine Particle Mass Emissions from Combustion Systems, Journal of the Air & Waste Management Association, 60, 1204-1222, 10.3155/1047-3289.60.10.1204, 2010.

Robinson, N. H., Allan, J. D., Trembath, J. A., Rosenberg, P. D., Allen, G., and Coe, H.: The lofting of Western Pacific regional aerosol by island thermodynamics as observed around Borneo, Atmos. Chem. Phys., 12, 5963-5983, 10.5194/acp-12-5963-2012, 2012.

Rosenkranz, M., Pugh, T. A. M., Schnitzler, J. P., and Arneth, A.: Effect of land-use change and management on biogenic volatile organic compound emissions - selecting climate-smart cultivars, Plant Cell and Environment, 38, 1896-1912, 10.1111/pce.12453, 2015.

Rosenstiel, T. N., Potosnak, M. J., Griffin, K. L., Fall, R., and Monson, R. K.: Increased CO2 uncouples growth from isoprene emission in an agriforest ecosystem, Nature, 421, 256-259, 10.1038/nature01312, 2003.

Rossignol, S., Aregahegn, K. Z., Tinel, L., Fine, L., Noziere, B., and George, C.: Glyoxal Induced Atmospheric Photosensitized Chemistry Leading to Organic Aerosol Growth, Environ. Sci. Technol., 48, 3218-3227, 10.1021/es405581g, 2014.

Safieddine, S. A., Heald, C. L., and Henderson, B. H.: The global nonmethane reactive organic carbon budget: A modeling perspective, Geophysical Research Letters, 44, 3897-3906, 10.1002/2017gl072602, 2017.

Sanderson, M. G., Jones, C. D., Collins, W. J., Johnson, C. E., and Derwent, R. G.: Effect of climate change on isoprene emissions and surface ozone levels, Geophysical Research Letters, 30, 10.1029/2003gl017642, 2003.

Sareen, N., Carlton, A. G., Surratt, J. D., Gold, A., Lee, B., Lopez-Hilfiker, F. D., Mohr, C., Thornton, J. A., Zhang, Z. F., Lim, Y. B., and Turpin, B. J.: Identifying precursors and aqueous organic aerosol formation pathways during the SOAS campaign, Atmos. Chem. Phys., 16, 14409-14420, 10.5194/acp-16-14409-2016, 2016.

Sarrafzadeh, M., Wildt, J., Pullinen, I., Springer, M., Kleist, E., Tillmann, R., Schmitt, S. H., Wu, C., Mentel, T. F., Zhao, D. F., Hastie, D. R., and Kiendler-Scharr, A.: Impact of NOx and OH on secondary organic aerosol formation from beta-pinene photooxidation, Atmos. Chem. Phys., 16, 11237-11248, 10.5194/acp-16-11237-2016, 2016.

Schurgers, G., Arneth, A., and Hickler, T.: Effect of climate-driven changes in species composition on regional emission capacities of biogenic compounds, J. Geophys. Res.-Atmos., 116, 10.1029/2011jd016278, 2011.

Schwantes, R. H., Schilling, K. A., McVay, R. C., Lignell, H., Coggon, M. M., Zhang, X., Wennberg, P. O., and Seinfeld, J. H.: Formation of highly oxygenated low-volatility products from cresol oxidation, Atmos. Chem. Phys., 17, 3453-3474, 10.5194/acp-17-3453-2017, 2017.

Scott, C. E., Rap, A., Spracklen, D. V., Forster, P. M., Carslaw, K. S., Mann, G. W., Pringle, K. J., Kivekas, N., Kulmala, M., Lihavainen, H., and Tunved, P.: The direct and indirect radiative effects of biogenic secondary organic aerosol, Atmos. Chem. Phys., 14, 447-470, 10.5194/acp-14-447-2014, 2014.

Scott, C. E., Spracklen, D. V., Pierce, J. R., Riipinen, I., D'Andrea, S. D., Rap, A., Carslaw, K. S., Forster, P. M., Artaxo, P., Kulmala, M., Rizzo, L. V., Swietlicki, E., Mann, G. W., and Pringle, K. J.: Impact of gas-to-particle partitioning approaches on the simulated radiative effects of biogenic

secondary organic aerosol, Atmos. Chem. Phys., 15, 12989-13001, 10.5194/acp-15-12989-2015, 2015.

Scott, C. E., Arnold, S. R., Monks, S. A., Asmi, A., Paasonen, P., and Spracklen, D. V.: Substantial large-scale feedbacks between natural aerosols and climate, Nature Geoscience, 11, 44-+, 10.1038/s41561-017-0020-5, 2018.

Shaw, S. L., Chisholm, S. W., and Prinn, R. G.: Isoprene production by Prochlorococcus, a marine cyanobacterium, and other phytoplankton, Marine Chemistry, 80, 227-245, 10.1016/s0304-4203(02)00101-9, 2003.

Shrivastava, M., Easter, R. C., Liu, X. H., Zelenyuk, A., Singh, B., Zhang, K., Ma, P. L., Chand, D., Ghan, S., Jimenez, J. L., Zhang, Q., Fast, J., Rasch, P. J., and Tiitta, P.: Global transformation and fate of SOA: Implications of low-volatility SOA and gas-phase fragmentation reactions, J. Geophys. Res.-Atmos., 120, 4169-4195, 10.1002/2014jd022563, 2015.

Shrivastava, M., Cappa, C. D., Fan, J. W., Goldstein, A. H., Guenther, A. B., Jimenez, J. L., Kuang, C., Laskin, A., Martin, S. T., Ng, N. L., Petaja, T., Pierce, J. R., Rasch, P. J., Roldin, P., Seinfeld, J. H., Shilling, J., Smith, J. N., Thornton, J. A., Volkamer, R., Wang, J., Worsnop, D. R., Zaveri, R. A., Zelenyuk, A., and Zhang, Q.: Recent advances in understanding secondary organic aerosol: Implications for global climate forcing, Rev. Geophys., 55, 509-559, 10.1002/2016rg000540, 2017.

Shrivastava, M. K., Lane, T. E., Donahue, N. M., Pandis, S. N., and Robinson, A. L.: Effects of gas particle partitioning and aging of primary emissions on urban and regional organic aerosol concentrations, J. Geophys. Res.-Atmos., 113, 10.1029/2007jd009735, 2008.

Slinn, W. G. N.: PREDICTIONS FOR PARTICLE DEPOSITION TO VEGETATIVE CANOPIES, Atmos. Environ., 16, 1785-1794, 10.1016/0004-6981(82)90271-2, 1982.

Song, C., Na, K. S., and Cocker, D. R.: Impact of the hydrocarbon to NOx ratio on secondary organic aerosol formation, Environ. Sci. Technol., 39, 3143-3149, 10.1021/es0493244, 2005.

Spracklen, D. V., Pringle, K. J., Carslaw, K. S., Chipperfield, M. P., and Mann, G. W.: A global off-line model of size-resolved aerosol microphysics: II. Identification of key uncertainties, Atmos. Chem. Phys., 5, 3233-3250, 2005a.

Spracklen, D. V., Pringle, K. J., Carslaw, K. S., Chipperfield, M. P., and Mann, G. W.: A global off-line model of size-resolved aerosol microphysics: I. Model development and prediction of aerosol properties, Atmos. Chem. Phys., 5, 2227-2252, 2005b.

Spracklen, D. V., Carslaw, K. S., Merikanto, J., Mann, G. W., Reddington, C. L., Pickering, S., Ogren, J. A., Andrews, E., Baltensperger, U., Weingartner, E., Boy, M., Kulmala, M., Laakso, L., Lihavainen, H., Kivekas, N., Komppula, M., Mihalopoulos, N., Kouvarakis, G., Jennings, S. G., O'Dowd, C., Birmili, W., Wiedensohler, A., Weller, R., Gras, J., Laj, P., Sellegri, K., Bonn, B., Krejci, R., Laaksonen, A., Hamed, A., Minikin, A., Harrison, R. M., Talbot, R., and Sun, J.: Explaining global surface aerosol number concentrations in terms of primary emissions and particle formation, Atmos. Chem. Phys., 10, 4775-4793, 10.5194/acp-10-4775-2010, 2010.

Spracklen, D. V., Jimenez, J. L., Carslaw, K. S., Worsnop, D. R., Evans, M. J., Mann, G. W., Zhang, Q., Canagaratna, M. R., Allan, J., Coe, H., McFiggans, G., Rap, A., and Forster, P.: Aerosol mass spectrometer constraint on the global secondary organic aerosol budget, Atmos. Chem. Phys., 11, 12109-12136, 10.5194/acp-11-12109-2011, 2011.

Squire, O. J., Archibald, A. T., Abraham, N. L., Beerling, D. J., Hewitt, C. N., Lathiere, J., Pike, R. C., Telford, P. J., and Pyle, J. A.: Influence of future climate and cropland expansion on isoprene emissions and tropospheric ozone, Atmos. Chem. Phys., 14, 1011-1024, 10.5194/acp-14-1011-2014, 2014.

Squire, O. J., Archibald, A. T., Griffiths, P. T., Jenkin, M. E., Smith, D., and Pyle, J. A.: Influence of isoprene chemical mechanism on modelled changes in tropospheric ozone due to climate and land use over the 21st

century, Atmos. Chem. Phys., 15, 5123-5143, 10.5194/acp-15-5123-2015, 2015.

Stockwell, C. E., Veres, P. R., Williams, J., and Yokelson, R. J.: Characterization of biomass burning emissions from cooking fires, peat, crop residue, and other fuels with high-resolution proton-transfer-reaction time-of-flight mass spectrometry, Atmos. Chem. Phys., 15, 845-865, 10.5194/acp-15-845-2015, 2015.

Stone, D., Whalley, L. K., and Heard, D. E.: Tropospheric OH and HO2 radicals: field measurements and model comparisons, Chem. Soc. Rev., 41, 6348-6404, 10.1039/c2cs35140d, 2012.

Surratt, J. D., Chan, A. W. H., Eddingsaas, N. C., Chan, M. N., Loza, C. L., Kwan, A. J., Hersey, S. P., Flagan, R. C., Wennberg, P. O., and Seinfeld, J. H.: Reactive intermediates revealed in secondary organic aerosol formation from isoprene, Proceedings of the National Academy of Sciences of the United States of America, 107, 6640-6645, 10.1073/pnas.0911114107, 2010.

Swinnert.Jw, Linnenbo.Vj, and Lamontag.Ra: OCEAN . A NATURAL SOURCE OF CARBON MONOXIDE, Science, 167, 984-&, 10.1126/science.167.3920.984, 1970.

Tao, Z. N., and Jain, A. K.: Modeling of global biogenic emissions for key indirect greenhouse gases and their response to atmospheric CO2 increases and changes in land cover and climate, J. Geophys. Res.-Atmos., 110, 10.1029/2005jd005874, 2005.

Tasoglou, A., and Pandis, S. N.: Formation and chemical aging of secondary organic aerosol during the beta-caryophyllene oxidation, Atmos. Chem. Phys., 15, 6035-6046, 10.5194/acp-15-6035-2015, 2015.

Tiitta, P., Vakkari, V., Croteau, P., Beukes, J. P., van Zyl, P. G., Josipovic, M., Venter, A. D., Jaars, K., Pienaar, J. J., Ng, N. L., Canagaratna, M. R., Jayne, J. T., Kerminen, V. M., Kokkola, H., Kulmala, M., Laaksonen, A., Worsnop, D. R., and Laakso, L.: Chemical composition, main sources

and temporal variability of PM1 aerosols in southern African grassland, Atmos. Chem. Phys., 14, 1909-1927, 10.5194/acp-14-1909-2014, 2014.

Tsigaridis, K., and Kanakidou, M.: Global modelling of secondary organic aerosol in the troposphere: a sensitivity analysis, Atmos. Chem. Phys., 3, 1849-1869, 2003.

Tsigaridis, K., and Kanakidou, M.: Secondary organic aerosol importance in the future atmosphere, Atmos. Environ., 41, 4682-4692, 10.1016/j.atmosenv.2007.03.045, 2007.

Tsigaridis, K., Daskalakis, N., Kanakidou, M., Adams, P. J., Artaxo, P., Bahadur, R., Balkanski, Y., Bauer, S. E., Bellouin, N., Benedetti, A., Bergman, T., Berntsen, T. K., Beukes, J. P., Bian, H., Carslaw, K. S., Chin, M., Curci, G., Diehl, T., Easter, R. C., Ghan, S. J., Gong, S. L., Hodzic, A., Hoyle, C. R., Iversen, T., Jathar, S., Jimenez, J. L., Kaiser, J. W., Kirkevag, A., Koch, D., Kokkola, H., Lee, Y. H., Lin, G., Liu, X., Luo, G., Ma, X., Mann, G. W., Mihalopoulos, N., Morcrette, J. J., Muller, J. F., Myhre, G., Myriokefalitakis, S., Ng, N. L., O'Donnell, D., Penner, J. E., Pozzoli, L., Pringle, K. J., Russell, L. M., Schulz, M., Sciare, J., Seland, O., Shindell, D. T., Sillman, S., Skeie, R. B., Spracklen, D., Stavrakou, T., Steenrod, S. D., Takemura, T., Tiitta, P., Tilmes, S., Tost, H., van Noije, T., van Zyl, P. G., von Salzen, K., Yu, F., Wang, Z., Wang, Z., Zaveri, R. A., Zhang, H., Zhang, K., Zhang, Q., and Zhang, X.: The AeroCom evaluation and intercomparison of organic aerosol in global models, Atmos. Chem. Phys., 14, 10845-10895, 10.5194/acp-14-10845-2014, 2014.

Tsimpidi, A. P., Karydis, V. A., Zavala, M., Lei, W., Molina, L., Ulbrich, I. M., Jimenez, J. L., and Pandis, S. N.: Evaluation of the volatility basis-set approach for the simulation of organic aerosol formation in the Mexico City metropolitan area, Atmos. Chem. Phys., 10, 525-546, 2010.

Tsimpidi, A. P., Karydis, V. A., Pandis, S. N., and Lelieveld, J.: Global combustion sources of organic aerosols: model comparison with 84 AMS factor-analysis data sets, Atmos. Chem. Phys., 16, 8939-8962, 10.5194/acp-16-8939-2016, 2016.

Unger, N.: Human land-use-driven reduction of forest volatiles cools global climate, Nature Climate Change, 4, 907-910, 10.1038/nclimate2347, 2014.

Utembe, S. R., Cooke, M. C., Archibald, A. T., Shallcross, D. E., Derwent, R. G., and Jenkin, M. E.: Simulating secondary organic aerosol in a 3-D Lagrangian chemistry transport model using the reduced Common Representative Intermediates mechanism (CRI v2-R5), Atmos. Environ., 45, 1604-1614, 10.1016/j.atmosenv.2010.11.046, 2011.

Vaden, T. D., Imre, D., Beranek, J., Shrivastava, M., and Zelenyuk, A.: Evaporation kinetics and phase of laboratory and ambient secondary organic aerosol, Proceedings of the National Academy of Sciences of the United States of America, 108, 2190-2195, 10.1073/pnas.1013391108, 2011.

Valverde-Canossa, J., Ganzeveld, L., Rappengluck, B., Steinbrecher, R., Klemm, O., Schuster, G., and Moortgat, G. K.: First measurements of H2O2 and organic peroxides surface fluxes by the relaxed eddy-accumulation technique, Atmos. Environ., 40, S55-S67, 10.1016/j.atmosenv.2006.03.038, 2006.

van der Gon, H., Bergstrom, R., Fountoukis, C., Johansson, C., Pandis, S. N., Simpson, D., and Visschedijk, A. J. H.: Particulate emissions from residential wood combustion in Europe revised estimates and an evaluation, Atmos. Chem. Phys., 15, 6503-6519, 10.5194/acp-15-6503-2015, 2015.

van der Werf, G. R., Randerson, J. T., Giglio, L., Collatz, G. J., Mu, M., Kasibhatla, P. S., Morton, D. C., DeFries, R. S., Jin, Y., and van Leeuwen, T. T.: Global fire emissions and the contribution of deforestation, savanna, forest, agricultural, and peat fires (1997-2009), Atmos. Chem. Phys., 10, 11707-11735, 10.5194/acp-10-11707-2010, 2010.

Virtanen, A., Joutsensaari, J., Koop, T., Kannosto, J., Yli-Pirila, P., Leskinen, J., Makela, J. M., Holopainen, J. K., Poschl, U., Kulmala, M., Worsnop, D. R., and Laaksonen, A.: An amorphous solid state of biogenic

secondary organic aerosol particles, Nature, 467, 824-827, 10.1038/nature09455, 2010.

Volkamer, R., Martini, F. S., Molina, L. T., Salcedo, D., Jimenez, J. L., and Molina, M. J.: A missing sink for gas-phase glyoxal in Mexico City: Formation of secondary organic aerosol, Geophysical Research Letters, 34, 5, 10.1029/2007gl030752, 2007.

Von Schneidemesser, E., Zhou, J. B., Stone, E. A., Schauer, J. J., Shpund, J., Brenner, S., Qasrawi, R., Abdeen, Z., and Sarnat, J. A.: Spatial Variability of Carbonaceous Aerosol Concentrations in East and West Jerusalem, Environ. Sci. Technol., 44, 1911-1917, 10.1021/es9014025, 2010.

Voulgarakis, A., Naik, V., Lamarque, J. F., Shindell, D. T., Young, P. J., Prather, M. J., Wild, O., Field, R. D., Bergmann, D., Cameron-Smith, P., Cionni, I., Collins, W. J., Dalsoren, S. B., Doherty, R. M., Eyring, V., Faluvegi, G., Folberth, G. A., Horowitz, L. W., Josse, B., MacKenzie, I. A., Nagashima, T., Plummer, D. A., Righi, M., Rumbold, S. T., Stevenson, D. S., Strode, S. A., Sudo, K., Szopa, S., and Zeng, G.: Analysis of present day and future OH and methane lifetime in the ACCMIP simulations, Atmos. Chem. Phys., 13, 2563-2587, 10.5194/acp-13-2563-2013, 2013.

Walters, D. N., Williams, K. D., Boutle, I. A., Bushell, A. C., Edwards, J. M., Field, P. R., Lock, A. P., Morcrette, C. J., Stratton, R. A., Wilkinson, J. M., Willett, M. R., Bellouin, N., Bodas-Salcedo, A., Brooks, M. E., Copsey, D., Earnshaw, P. D., Hardiman, S. C., Harris, C. M., Levine, R. C., MacLachlan, C., Manners, J. C., Martin, G. M., Milton, S. F., Palmer, M. D., Roberts, M. J., Rodriguez, J. M., Tennant, W. J., and Vidale, P. L.: The Met Office Unified Model Global Atmosphere 4.0 and JULES Global Land 4.0 configurations, Geoscientific Model Development, 7, 361-386, 10.5194/gmd-7-361-2014, 2014.

Walton, J. J., Maccracken, M. C., and Ghan, S. J.: A GLOBAL-SCALE LAGRANGIAN TRACE SPECIES MODEL OF TRANSPORT,

TRANSFORMATION, AND REMOVAL PROCESSES, J. Geophys. Res.-Atmos., 93, 8339-8354, 10.1029/JD093iD07p08339, 1988.

Wang, L., Khalizov, A. F., Zheng, J., Xu, W., Ma, Y., Lal, V., and Zhang, R. Y.: Atmospheric nanoparticles formed from heterogeneous reactions of organics, Nature Geoscience, 3, 238-242, 10.1038/ngeo778, 2010.

Wang, Q., Jacob, D. J., Fisher, J. A., Mao, J., Leibensperger, E. M., Carouge, C. C., Le Sager, P., Kondo, Y., Jimenez, J. L., Cubison, M. J., and Doherty, S. J.: Sources of carbonaceous aerosols and deposited black carbon in the Arctic in winter-spring: implications for radiative forcing, Atmos. Chem. Phys., 11, 12453-12473, 10.5194/acp-11-12453-2011, 2011.

Wesely, M. L.: PARAMETERIZATION OF SURFACE RESISTANCES TO GASEOUS DRY DEPOSITION IN REGIONAL-SCALE NUMERICAL-MODELS, Atmos. Environ., 23, 1293-1304, 10.1016/0004-6981(89)90153-4, 1989.

White, S. J., Jamie, I. M., and Angove, D. E.: Chemical characterisation of semi-volatile and aerosol compounds from the photooxidation of toluene and NOx, Atmos. Environ., 83, 237-244, 10.1016/j.atmosenv.2013.11.023, 2014.

WHO: Review of Evidence on Health Aspects of Air Pollution – REVIHAAP Project: Final Technical Report 2013.

Winter, B., and Chylek, P.: Contribution of sea salt aerosol to the planetary clear-sky albedo, Tellus Series B-Chemical and Physical Meteorology, 49, 72-79, 10.1034/j.1600-0889.49.issue1.5.x, 1997.

Winterhalter, R., Herrmann, F., Kanawati, B., Nguyen, T. L., Peeters, J., Vereecken, L., and Moortgat, G. K.: The gas-phase ozonolysis of beta-caryophyllene (C15H24). Part I: an experimental study, Phys. Chem. Chem. Phys., 11, 4152-4172, 10.1039/b817824k, 2009.

Woodward, S.: Modeling the atmospheric life cycle and radiative impact of mineral dust in the Hadley Centre climate model, J. Geophys. Res.-Atmos., 106, 18155-18166, 10.1029/2000jd900795, 2001.

Wu, S., Mickley, L. J., Kaplan, J. O., and Jacob, D. J.: Impacts of changes in land use and land cover on atmospheric chemistry and air quality over the 21st century, Atmos. Chem. Phys., 12, 1597-1609, 10.5194/acp-12-1597-2012, 2012.

Yassaa, N., Peeken, I., Zollner, E., Bluhm, K., Arnold, S., Spracklen, D., and Williams, J.: Evidence for marine production of monoterpenes, Environ. Chem., 5, 391-401, 10.1071/en08047, 2008.

Yienger, J. J., and Levy, H.: EMPIRICAL-MODEL OF GLOBAL SOIL-BIOGENIC NOX EMISSIONS, J. Geophys. Res.-Atmos., 100, 11447-11464, 10.1029/95jd00370, 1995.

Yokelson, R. J., Burling, I. R., Gilman, J. B., Warneke, C., Stockwell, C. E., de Gouw, J., Akagi, S. K., Urbanski, S. P., Veres, P., Roberts, J. M., Kuster, W. C., Reardon, J., Griffith, D. W. T., Johnson, T. J., Hosseini, S., Miller, J. W., Cocker, D. R., Jung, H., and Weise, D. R.: Coupling field and laboratory measurements to estimate the emission factors of identified and unidentified trace gases for prescribed fires, Atmos. Chem. Phys., 13, 89-116, 10.5194/acp-13-89-2013, 2013.

Young, P. J., Arneth, A., Schurgers, G., Zeng, G., and Pyle, J. A.: The CO2 inhibition of terrestrial isoprene emission significantly affects future ozone projections, Atmos. Chem. Phys., 9, 2793-2803, 10.5194/acp-9-2793-2009, 2009.

Young, P. J., Naik, V., Fiore, A. M., Gaudel, A., Guo, J., Lin, M. Y., Neu, J. L., Parrish, D. D., Rieder, H. E., Schnell, J. L., Tilmes, S., Wild, O., Zhang, L., Ziemke, J., Brandt, J., Delcloo, A., Doherty, R. M., Geels, C., Hegglin, M. I., Hu, L., Im, U., Kumar, R., Luhar, A., Murray, L., Plummer, D., Rodriguez, J., Saiz-Lopez, A., Schultz, M. G., Woodhouse, M. T., and Zeng, G.: Tropospheric Ozone Assessment Report: Assessment of global-scale model performance for global and regional ozone distributions, variability, and trends, Elementa-Science of the Anthropocene, 6, 10.1525/elementa.265, 2018.

Zhang, K., O'Donnell, D., Kazil, J., Stier, P., Kinne, S., Lohmann, U., Ferrachat, S., Croft, B., Quaas, J., Wan, H., Rast, S., and Feichter, J.: The global aerosol-climate model ECHAM-HAM, version 2: sensitivity to improvements in process representations, Atmos. Chem. Phys., 12, 8911-8949, 10.5194/acp-12-8911-2012, 2012.

Zhang, Q., Jimenez, J. L., Canagaratna, M. R., Allan, J. D., Coe, H., Ulbrich, I., Alfarra, M. R., Takami, A., Middlebrook, A. M., Sun, Y. L., Dzepina, K., Dunlea, E., Docherty, K., DeCarlo, P. F., Salcedo, D., Onasch, T., Jayne, J. T., Miyoshi, T., Shimono, A., Hatakeyama, S., Takegawa, N., Kondo, Y., Schneider, J., Drewnick, F., Borrmann, S., Weimer, S., Demerjian, K., Williams, P., Bower, K., Bahreini, R., Cottrell, L., Griffin, R. J., Rautiainen, J., Sun, J. Y., Zhang, Y. M., and Worsnop, D. R.: Ubiquity and dominance of oxygenated species in organic aerosols in anthropogenically-influenced Northern Hemisphere midlatitudes, Geophysical Research Letters, 34, 6, 10.1029/2007gl029979, 2007.

Zhang, R. Y., Suh, I., Zhao, J., Zhang, D., Fortner, E. C., Tie, X. X., Molina, L. T., and Molina, M. J.: Atmospheric new particle formation enhanced by organic acids, Science, 304, 1487-1490, 10.1126/science.1095139, 2004.

Zhang, X., Cappa, C. D., Jathar, S. H., McVay, R. C., Ensberg, J. J., Kleeman, M. J., and Seinfeld, J. H.: Influence of vapor wall loss in laboratory chambers on yields of secondary organic aerosol, Proceedings of the National Academy of Sciences of the United States of America, 111, 5802-5807, 10.1073/pnas.1404727111, 2014.

Zhao, Y. L., Hennigan, C. J., May, A. A., Tkacik, D. S., de Gouw, J. A., Gilman, J. B., Kuster, W. C., Borbon, A., and Robinson, A. L.: Intermediate-Volatility Organic Compounds: A Large Source of Secondary Organic Aerosol, Environ. Sci. Technol., 48, 13743-13750, 10.1021/es5035188, 2014.

Zhao, Y. L., Nguyen, N. T., Presto, A. A., Hennigan, C. J., May, A. A., and Robinson, A. L.: Intermediate Volatility Organic Compound Emissions

from On-Road Diesel Vehicles: Chemical Composition, Emission Factors, and Estimated Secondary Organic Aerosol Production, Environ. Sci. Technol., 49, 11516-11526, 10.1021/acs.est.3b02841, 2015.